Investigating the Transurothelial Delivery of Therapeutic Agents

A thesis submitted for the degree of
Philosophiae Doctor in Cardiff University

By

Nicholas Alexander Williams

May 2015

Cardiff School of Pharmacy
and Pharmaceutical Sciences
Cardiff University

Declaration

This work has not been submitted in substance for any other degree or award at this or any other university or place of learning; nor is being submitted concurrently in candidature for any degree or other award.

Signed:  (candidate) Date: 15th May 2015

STATEMENT 1

This thesis is being submitted in partial fulfillment of the requirements for the degree of PhD.

Signed:  (candidate) Date: 15th May 2015

STATEMENT 2

This thesis is the result of my own independent work / investigation, except where otherwise stated. Other sources are acknowledged by explicit references. The views expressed are my own.

Signed:  (candidate) Date: 15th May 2015

STATEMENT 3

I hereby give consent for my thesis, if accepted, to be available for photocopying and for inter - library loans **after expiry of a bar on access previously approved by the Academic Standards & Quality Committee.**

Signed:  (candidate) Date: 15th May 2015

Acknowledgements

I would first like to thank my supervisors, Dr Chris Allender, Professor Mark Gumbleton, Dr Jenna Bowen, and Mr Hrishi Joshi, for the encouragement, support and wisdom you have provided me with over the course of this project. As a mentor, Chris always put me first and the support I received from Jenna and himself was far above and beyond what is expected of supervisors. For your time, dedication and knowledge I am truly grateful.

I would also like to thank Boston Scientific and the Cardiff School of Pharmacy and Pharmaceutical Sciences, for funding this project. Dr Tim Harrah deserves a special mention for his kindness, support and the invaluable experience he afforded me whilst I was over in the US.

In addition, I would also like to express my gratitude to collaborators from outside of the department; Derek Scarborough for his impeccable histology work and Dr Yuri Anissimov for his help with mathematical modelling. A special thank you also goes to Dave Havard for providing me with an endless supply of pig bladders. Without his generosity this project would not have been possible. Dave is a lovely gentleman and someone who is totally dedicated in his own way to helping the progression of science; that said I am not sure I can forgive the fact that he nicknamed me '*Bladder Man*' on the first day we met and that ever since he has refused to use my Christian name.

A massive thank you goes to all of my fellow lab colleagues, Danielle, Jenna, Vibs, Ghaith, Adi and Ericka. I have had an amazing time working, and socialising, with each of them. This was a great lab and a fantastic place to spend 4 years.

Last, and most importantly, I would like to thank my family and Zein. I have worked tirelessly throughout this project and consequently have not dedicated them anywhere near the time and attention they deserve. Their patience, support and encouragement has been invaluable and without them this project would not have been completed. I love you all.

Summary

Intravesical drug delivery (IDD) offers a unique opportunity to target pathology of the lower urinary tract. High concentrations of drug can be delivered directly to the bladder with minimal systemic absorption. IDD has been used successfully to manage a range of conditions such as bladder cancer and overactive bladder and continues to be investigated for novel indications. Despite this the majority of IDD regimens remain empirically driven and as a result its potential largely unfulfilled.

This thesis developed and validated an *ex vivo* porcine model to investigate the transurothelial delivery and bladder wall distribution of drugs after topical application to the urothelium. Using the model, transurothelial permeability coefficients were determined and tissue layer specific bladder wall concentrations calculated for a range of clinically relevant drugs including ketorolac and oxybutynin. The results of these studies were used to inform on the viability of delivering these drugs intravesically *in vivo*. Additionally a computer – based pharmacokinetic model of IDD was developed using STELLA® modelling software. The model was used to investigate the key variables associated with IDD and suggest novel techniques and dosing concepts to improve its efficacy. For the first time, the relative permeability of the upper and lower urinary tract was investigated for a single drug. *Ex vivo* porcine ureteral urothelium was shown to be significantly more permeable to mitomycin C than that of the bladder. If translated into human, the more permeable urothelium may provide higher target tissue concentrations after local delivery and a significant opportunity to manage upper tract urothelial carcinoma conservatively.

This project developed novel *ex vivo* and *in silico* methods to investigate IDD. These techniques can be used to rationally inform on the design of new, or optimisation of existing, IDD regimens.

Table of Contents

List of Figures

List of Tables

List of Publications

The following publications resulted directly from work reported in this thesis:

Williams NA, Bowen JL, Al-Jayyoussi G, Gumbleton M, Allender CJ, Li J, *et al*. An *ex vivo* investigation into the transurothelial permeability and bladder wall distribution of the non - steroidal anti - inflammatory ketorolac. Molecular Pharmaceutics. 2014 March; 11(3): 673 – 82.

Williams NA, Lee KM, Bowen JL, Gumbleton M, Allender CJ, Harrah T, *et al*. Investigating detrusor muscle concentrations of oxybutynin after intravesical delivery in an *ex vivo* porcine model. Journal of Pharmaceutical Science. 2015 April; Ahead of print.

Williams NA, Barnard L, Bowen JL, Gumbleton M, Allender CJ, Harrah T, *et al*. Evidence of non - uniformity in urothelium barrier function between the upper and lower urinary tract. 2015 April; Manuscript submitted for publication.

The following publications resulted from studies carried out since the start of this thesis but are not directly related to work reported herein:

Loizidou EZ, Williams NA, Barrow DA, Eaton MJ, McCrory J, Evans SL, *et al*. Structural characterisation and transdermal delivery studies on sugar microneedles: Experimental and finite element modelling analyses. European Journal of Pharmaceutics and Biopharmaceutics. 2015 January; 89: 224 – 31.

List of Abbreviations

ACh	Acetylcholine
ACN	Acetonitrile
ANOVA	Analysis of variance
ATP	Adenosine triphosphate
AUC	Area under the curve
BAUS	British Association of Urological Surgeons
BCG	Bacillus Calmette – Guérin
BSC	Boston Scientific Corporation
Cmax	Peak drug concentrations
COX	Cyclooxygenase
DMSO	Dimethyl sulfoxide
EAU	European Association of Urology
EMDA	Electromotive drug administration
FCE	Finished consultant episodes
GAG	Glycosaminoglycan
H & E	Haematoxylin and eosin
HES	Hospital episode statistics
HPC	Hydroxypropylcellulose
HPLC	High performance liquid chromatography
IC / PBS	Interstitial cystitis / painful bladder syndrome
IC_{50}	Half maximal inhibitory concentration
ICC	Interstitial cells of Cajal
IDD	Intravesical drug delivery
LLOD	Lower limit of detection
LLOQ	Lower limit of quantification
LUTS	Lower urinary tract symptoms
MMC	Mitomycin C
MOA	Mechanism of action
MS	Mass spectrometry
NHU	Normal human urothelial cells
NMIBC	Non - muscle invasive bladder cancer
NSAID	Non - steroidal anti - inflammatory drug
OAB	Overactive bladder

OCT	Optimal cutting temperature medium
PK	Pharmacokinetic
PVR	Post – void residual
RCT	Randomised controlled trial
RNU	Radical nephroureterectomy
RPM	Revolutions per minute
SD	Standard deviation
SEM	Scanning electron microscopy
SEM	Standard error of the mean
SRD	Stent - related discomfort
STELLA	Structural Thinking Experimental Learning Laboratory with Animation
TEER	Transepithelial electrical resistance
TJ	Tight junction
UP	Uroplakin
UPEC	Uropathogenic *E. coli*
UTI	Urinary tract infection
UTUC	Upper - tract urothelial carcinoma
UV	Ultraviolet
Z0 – 1	Zonular occludin 1

Chapter One: General Introduction

1.1. The Urinary Bladder

Located behind the pubic symphysis in the pelvic cavity, the bladder is a hollow, distensible sac that provides a reservoir for urine prior to micturition (Figure 1.1). Collapsed when empty, it expands upon filling adopting a balloon - like shape as its capacity increases. The bladder is highly flexible and capable of stretching to hold large volumes of urine, whilst being able to contract and expel urine once a certain capacity is reached[1]. When fully distended, the adult human bladder has a maximum capacity of ~ 800 mls[2], however a strong urge to void is usually initiated at 25 - 50 % of maximum capacity beyond which voluntary control diminishes[2,3].

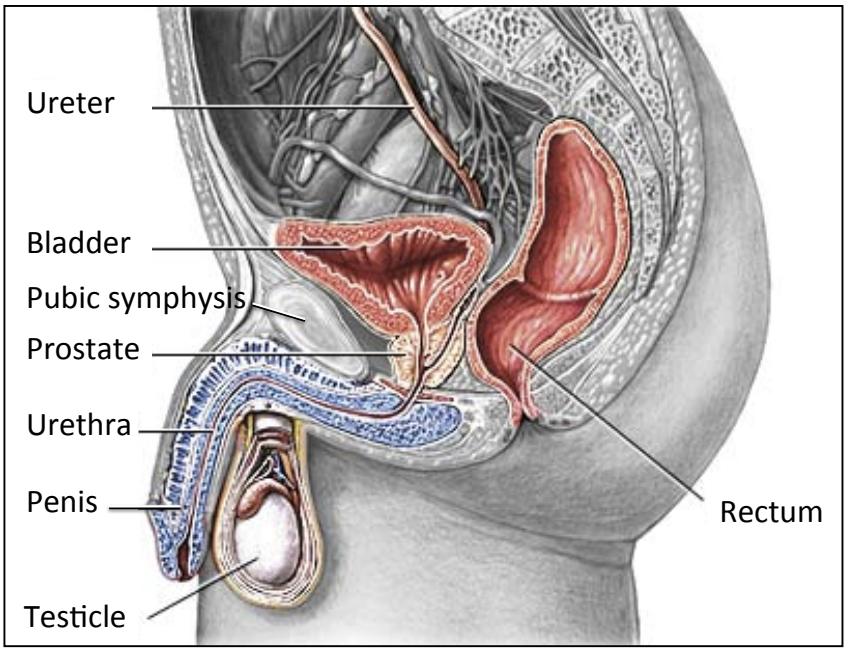

Figure 1.1. Anatomy of the male urinary tract. The bladder lies in the pelvic cavity between the rectum and the pubic symphysis. Figure adapted from Simon[4].

Urine contains harmful waste products such as urea and ammonia and electrolytes including sodium, potassium, calcium and chloride[5]. The reabsorption of such molecules can be associated with metabolic consequences such as hyperchloremic acidosis[6]. Fortunately, the structure of the bladder wall prevents the uncontrolled movement of substances back into the bloodstream.

1.1.1. Structure of the bladder wall

The bladder wall is comprised of a number of distinct layers: urothelium, lamina propria, detrusor muscle and adventitia / serosa (Figure 1.3)[7].

The urothelium forms the inner lining of the organ, separating the contents of the bladder lumen from the underlying bladder wall. It covers the entire luminal surface, transitioning to ureteral and proximal urethral urothelium at the ureteral and internal urethral orifices respectively[8]. Owing to the triangular shape formed between the ureteral and urethral openings, this region of the bladder base is known as the trigone (Figure 1.2). The thickness of the urothelium varies depending on the extent of bladder distension[9]. In the contracted bladder the human urothelium is ~ 5 – 7 cells thick, whilst in the distended state it can be as thin as 2 – 3 cells[10]. The urothelium is a highly specialised barrier to the movement of substances from the urine back into systemic circulation and is discussed further in section 1.1.2.

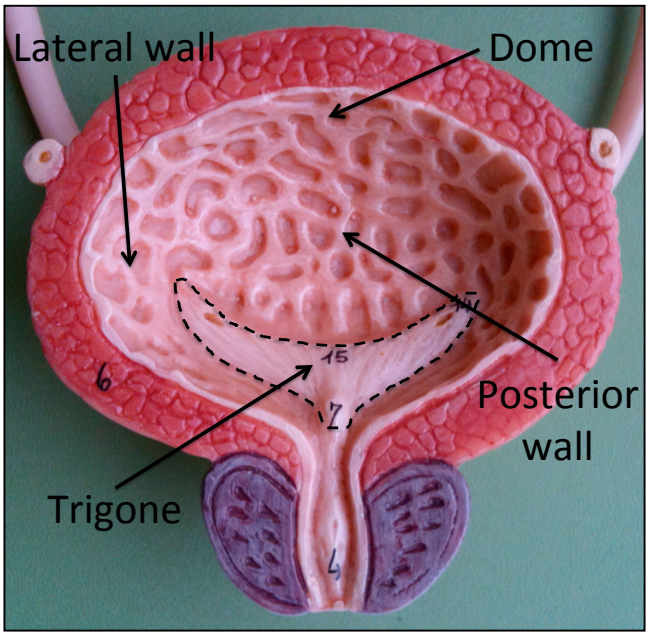

Figure 1.2. Anatomically, the interior of the bladder lumen is separated into the posterior wall, anterior wall (not shown), lateral walls, dome region and trigone[11]. The trigone is the triangular region of the bladder base, formed by the convergence of the ureteral and internal urethral orifices. Figure adapted from Webster[12].

The lamina propria lies directly below the urothelium and consists largely of connective tissue with blood vessels, lymphatics and small amounts of adipose tissue[10]. Intermittent wisps of smooth muscle (muscularis mucosa) are often found in the lamina propria[13], however these cells are discontinuous and distinguishable from the underlying detrusor layer.

The detrusor constitutes the thickest layer of the bladder wall and consists of inner longitudinal, circular and outer longitudinal layers of smooth muscle[10]. It is fundamental to the normal functioning of the bladder, remaining relaxed during filling and then contracting to expel urine during micturition[14].

The outermost serosal layer does not cover the entire bladder; it is only present on the top third of the organ forming part of the peritoneum[15]. Where there is no serosa, the connective tissue between the bladder and other organs merges and is termed the adventitia[15]. Additionally, a layer of perivesical fat surrounds the outside of the serosa and adventitia covering the entire exterior surface of the bladder[15]. Even amongst urological pathologists, different terminology is used to describe the microstructure of the bladder wall. Some advocate the use of terms such as 'submucosa' to describe the lower section of the lamina propria[15], whilst others classify all tissue between the urothelium and detrusor muscle as lamina propria[10]. Collectively the urothelium and lamina propria are referred to as the mucosal layer or mucosa[10].

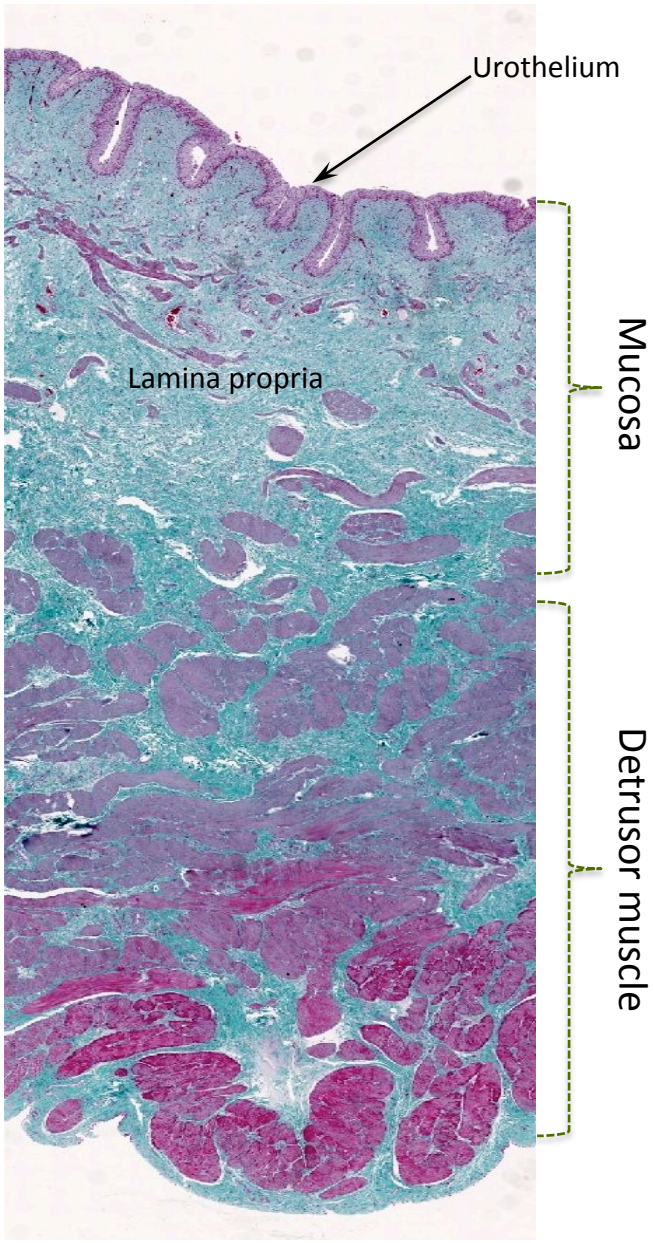

Figure 1.3. Cross section histology of porcine bladder wall stained with Masson's trichrome. Figure represents original work (Chapter 3, section 3.2.6).

1.1.2. Structure of the Urothelium

The urothelium is the principal barrier to the permeation of molecules into the bladder wall[16]. It is a highly differentiated, stratified epithelial layer that lines not only the bladder but also the apical surface of the renal pelvis, ureters and upper urethra[16]. The urothelium consists of three distinct layers; umbrella cells, intermediate cells and a basal layer[17,18]. The superficial umbrella cells line the apical surface of the bladder; they are the largest of the three cell types (diameter ~ 50 - 120 μm) and vary in diameter depending on the distension of the bladder. Below lie the intermediate cells (diameter ~ 20 μm) whilst the basal layer, consisting of germinal cells (diameter ~ 5 - 10 μm), lines the basolateral side of the urothelium[16]. Cell recycling involves progenitor basal cells migrating and differentiating into intermediate cells which in turn are partially differentiated forms of the distinct umbrella cells[19]. The intermediate and basal layers are unremarkable in morphology and investigations have shown that they pose no significant barrier to the movement of substances through the bladder wall[17,20,21]. Rather it is the umbrella cells that are responsible for the impermeability of the urothelium and they are highly differentiated to fit their role as the rate - limiting permeation barrier.

1.1.2.1. Umbrella Cells

Umbrella cells form a single layer of specialised cells lining the apical membrane of the urothelium. They are often multinucleated[22]. Dynamic in nature, they change shape in accordance with the filling state of the bladder, adopting a cuboidal form when the bladder is empty and an elongated squamous shape as the bladder fills[23]. This stretching can double the diameter of the cells and is thought to help the bladder achieve the required distension during filling[7]. The umbrella cells demonstrate distinct morphological features that increase the impermeability of the urothelium.

1.1.2.1.a. Uroplakin Plaques

The apical membrane of the umbrella cells is covered in scalloped shaped plaques that are separated by plasma membrane domains referred to as 'hinges'[24–26]. These polygonal plaques (~ 0.5 μm in diameter, 12 nm thick) are thought to cover ~ 90 % of the surface area of the umbrella cells[24]. The hinge membranes (~ 8 nm thick) surround the plaques in a mosaic pattern occupying the remaining ~ 10 % of the membrane surface area[16,27]. The membrane is referred to as an asymmetrical unit membrane because the plaques make the outer leaflet up to twice as thick as the inner leaflet[28]. The plaques are comprised of ~ 1,000 subunits, each made up of cell surface proteins known as uroplakins (UPs). Four major UPs (UPIa, UP1b, UPII and UPIII) have been identified[29–33]. UPs form heterodimers with one another, forming two sets of uroplakin pairs, UPIa / UPII and UP1b / UPIII (Figure 1.4)[34]. The formation of heterodimers marks the first step of UP assembly and is necessary for UPs to exit the endoplasmic reticulum[35]. Furthermore, the presence of both heterodimers is essential to correct assembly at the apical membrane. UPIII is an integral subunit to the formation of normal urothelial plaques and the subsequent generation of a fully functional urothelium[36,37]. Ablation of the UPIII gene results in the formation of smaller, less organised plaques[36,38]. Consequently the urothelium of UPIII knockout animals is more leaky and exhibits increased permeability to molecules such as water and urea[39]. The mechanism by which UP plaques contribute to urothelial barrier function is unclear, however it is hypothesised to centre on their highly ordered organisation at the apical membrane[36,39]. Such organisation allows dense packing of the plaques, protecting the bladder luminal surface from damage during distension[38,40].

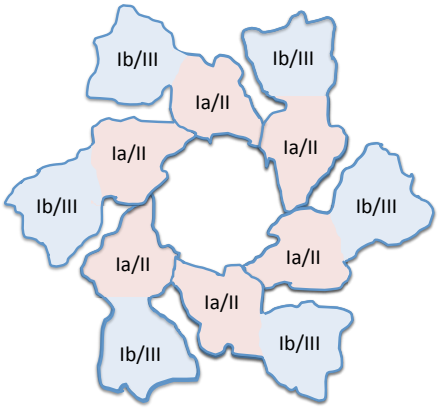

Figure 1.4. Schematic of an individual uroplakin subunit. UPIa forms a heterodimer with UPII, whilst UP1b forms a heterodimer with UPIII. Figure adapted from Sun *et al*[41].

UPs are thought to underlie the aetiology of bladder diseases which exhibit increased urothelial permeability such as interstitial cystitis / painful bladder syndrome (IC / PBS)[42]. Additionally, UPs may play a significant role in urinary tract infections (UTIs). Cystitis, a syndrome characterised by dysuria, urgency, frequency and lower abdominal pain, is usually caused by bacterial infection with uropathogenic *E. coli* (UPEC) being the most common causative pathogen[43]. UPEC expresses type 1 fimbrial FimH adhesin that facilitates adherence of the bacteria to the surface receptors of the umbrella cells (Figure 1.5)[44]. It has been elucidated that UPIa is the urothelial surface receptor for UPEC[44,45] and this docking marks the beginning of a cascade eventually resulting in internalisation of the bacteria into the umbrella cell[45,46]. Identifying intracellular bacteria in shed urothelial cells (Figure 1.6) has recently been shown beneficial in the diagnosis of latent UTIs in renal transplant recipients[47]. The FimH - mediated binding of UPEC to UPIa is integral to the pathogenesis of the bacteria as it provides a foothold to the urothelium, preventing them from being removed during micturition cycles[44]. Inhibiting this binding event may prove to be a useful strategy to treat bacterial cystitis and in the future might provide novel antibacterials for patients refractory to currently available treatment options.

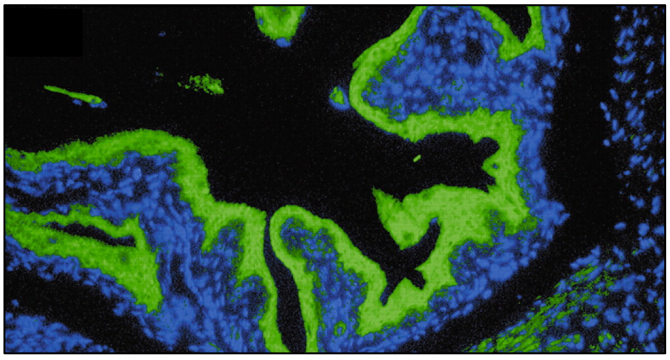

Figure 1.5. Selective binding of FimH (green) to murine umbrella cells (blue). Figure adapted from Zhou *et al*[44].

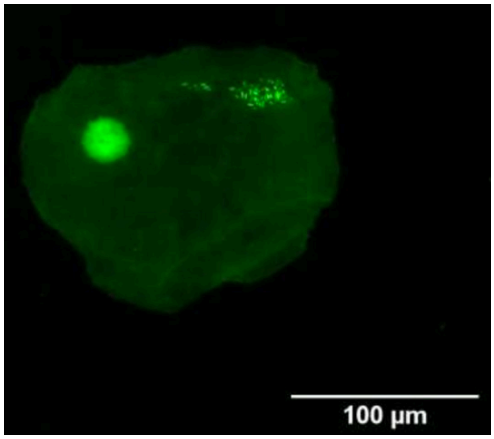

Figure 1.6. Intracellular bacteria identified in a shed urothelial cell from a renal transplant recipient. Figure adapted from Kelley *et al*[47].

1.1.2.1.b. Tight junctions

Adjacent umbrella cells are held together by tight junctions (TJ). TJs are composed of integral transmembrane proteins, such as occludin, junctional adhesion molecule and claudins that comprise the paracellular barrier[48]. Cytoplasmic proteins, such as zonular occludin 1 (ZO - 1), link the transmembrane proteins to the umbrella cell cytoskeleton (Figure 1.7)[49]. In addition to bringing structural integrity to the urothelium, TJs form a paracellular diffusion barrier to the movement of molecules between adjacent cells as well as an intramembrane diffusion barrier preventing the movement and mixing of intracellular components[48,50,51].

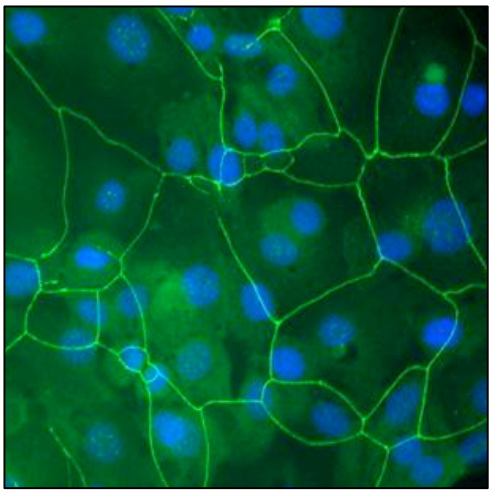

Figure 1.7. ZO - 1 labelling (fluorescent green) in human umbrella cell tight junctions. Figure adapted from Southgate and Baker[52].

1.1.2.1.c. Glycosaminoglycan (GAG) Layer

The impermeability of the urothelium is further augmented by a glycosaminoglycan (GAG) formed mucin layer that coats the luminal side of the umbrella cell membrane. GAGs are long, unbranched polysaccharides that form a thin hydrophilic layer on top of the umbrella cells[53–55]. The GAG layer protects the bladder wall from the permeation of irritant urinary substances (e.g. urea[56], potassium ions[57] and calcium ions[56]) and has a functional role in preventing UTIs by reducing bacterial adherence to the bladders luminal surface[58,59]. Studies have revealed that the GAG layer consists of heparan sulphate (~ 50 %), chondroitin sulphate (~ 30 %) and dermatan sulpate (~ 15 %)[60]. IC / PBS is associated with GAG deficiency[61] resulting in increased permeation of irritant potassium ions into the bladder wall[62–64] (Figure 1.8). Accordingly, GAG replenishment with agents such as chondroitin sulphate, heparin and pentosan polysulphate have become mainstay therapies for IC / PBS management[65,66].

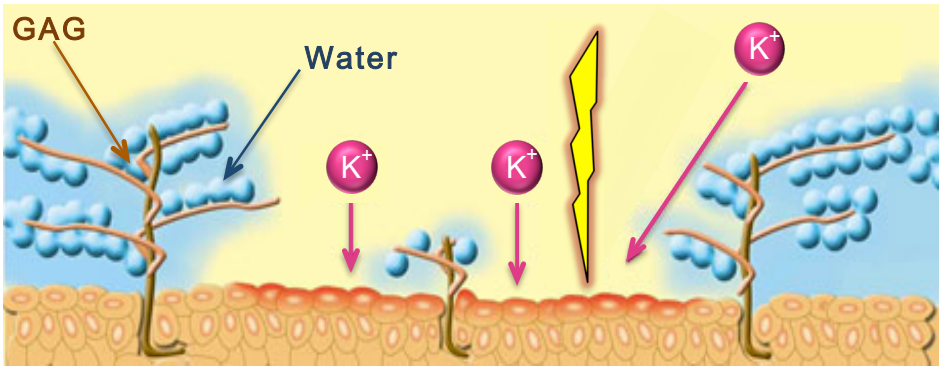

Figure 1.8. In IC / PBS, a deficiency in the protective GAG layer results in an increased exposure of irritant solutes such as potassium (K^+) to the urothelium, resulting in localised inflammation, irritation and pain. Figure adapted from Pohl Boskamp Ltd[67].

1.1.3. Permeability of the Urothelium

The combination of UPs, TJs and the GAG layer prevent the movement of unwanted substances from the urine back into the systemic circulation. The main mechanism by which molecules enter the bladder wall is passive permeability[7]; specifically, the passive diffusion of molecules across the urothelium down a concentration gradient. As with all epithelia there are two basic routes by which ions and solutes can move across the urothelium; paracellularly through the TJs of adjacent

umbrella cells and transcellularly moving over cell membranes through the cytoplasm and out the basal membrane[68].

The most common measure of ion permeability is transepithelial electrical resistance (TEER)[16]. TEER is considered a sensitive, well defined determinant of epithelial permeability and takes into account the overall resistance of the transcellular and paracellular routes[68,69]. The urothelium exhibits one of the highest recorded TEER values of any epithelia measured[16]. Frömter and Diamond collected TEER values for a wide range of epithelial tissues and using the trends observed grouped them into two categories; 'leaky' and 'tight'[70]. A resistance of ≥ 500 Ω cm^2 is indicative of a tight epithelium. Although there is significant inter - species variation (Table 1.1), the urothelium is undoubtedly a tight epithelia with greater TEER than others investigated such as rabbit ileum (115 Ω cm^2)[71] or even rat blood brain barrier (5,900 Ω cm^2)[72].

Urothelium origin	TEER (Ω cm^2)
Human (cultured cell line)[73]	3,000
Porcine (cultured cell line)[74]	7,000
Rabbit[75]	75,000 – 160,000
Feline[76]	310,000
Guinea pig[77]	3,000
Rat[78]	1,800

Table 1.1. Example TEER values for different species of urothelium.

1.2. Intravesical Drug Delivery (IDD)

1.2.1. Definition of IDD

The urethra allows for direct access to the bladder via a catheter. This presents significant opportunity to deliver high concentrations of drug directly to the bladder; such opportunities generally do not exist for other organs. Intravesical drug delivery (IDD) describes the local application of drug to the bladder lumen via the urethra. This is commonly achieved by formulating the drug as a solution and instilling the dose directly into the bladder through a urinary catheter[7] (Figure 1.9A). Post - instillation the catheter is removed and the patient asked to hold their bladder for a predefined period of time (usually 1 - 2 h). Once the instillation period is complete, the patient is able to urinate and void the instilled dose. The intravesical route is used to deliver a wide range of therapies and treat many different diseases of the bladder (Figure 1.9B). The majority of IDD treatments used clinically are for bladder cancer, IC / PBS and overactive bladder (OAB). This is reflected not only by current research (Figure 1.10) and clinical practice (Figure 1.11B), but also by the licensed intravesical therapies currently available (Figure 1.11A).

A

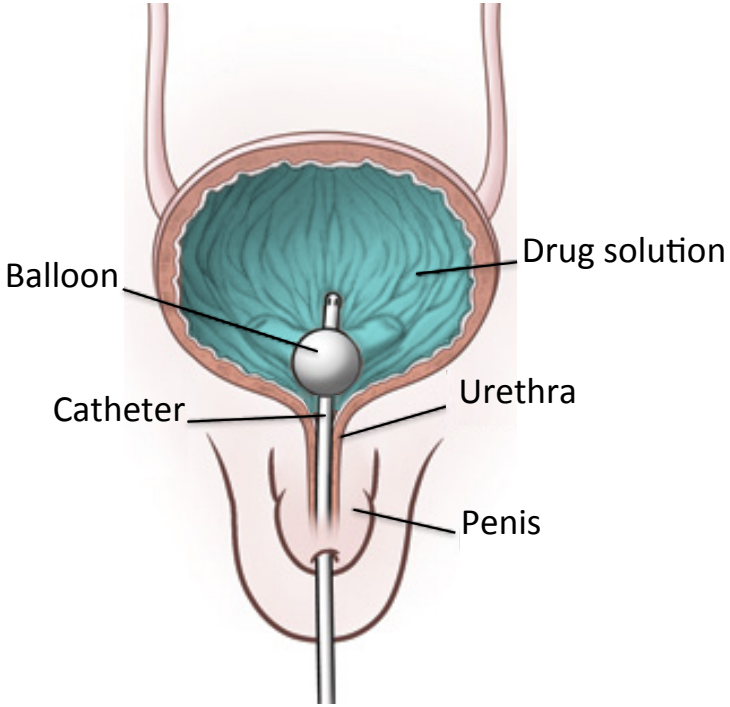

B

Bladder pathology	Intravesical agent
Bladder cancer	Bacillus Calmette - Guerin[79], mitomycin - C[80], gemcitabine[81], doxorubicin[82], cisplatin[83], paclitaxel[84], docetaxel[85], methotrexate[86], pirarubicin[87], epirubicin[88], pemetrexed[89], vinorelbine[90], capecitabine[91], thiotepa[92], 5 - fluorouracil[93], interferon[93], hydroxycamptothecin[94], valrubicin[95].
OAB	Oxybutynin[96], onabotulinumtoxin-a[97], abobotulinumtoxin - a[98], resiniferatoxin[99].
IC / PBS	Lidocaine[100], pentosan polysulphate[101], Bacillus Calmette - Guerin[102], sodium hyaluronate[103], heparin[104], chondroitin sulfate[105], dimethyl sulfoxide (DMSO)[66], resiniferatoxin[106], capsaicin[107], triamcinolone[108].
Ureteral stent - related pain	Ketorolac[109], oxybutynin[109], lidocaine[109].
UTI	Gentamicin[110], amikacin[111], tobramycin[112], amphotericin B[113], neomycin[114], cefalotin[115], noxythiolin[116], trimethoprim[117], sulfamethoxazole[117], heparin[118], hyaluronic acid[119], chondroitin sulfate[119].

Figure 1.9. A) Schematic depicting the process of IDD in a male patient. Drug solution is instilled directly into the bladder through a urinary catheter. Figure adapted from Krames Staywell patient education[120]. B) Examples and indications of drugs that have been delivered intravesically.

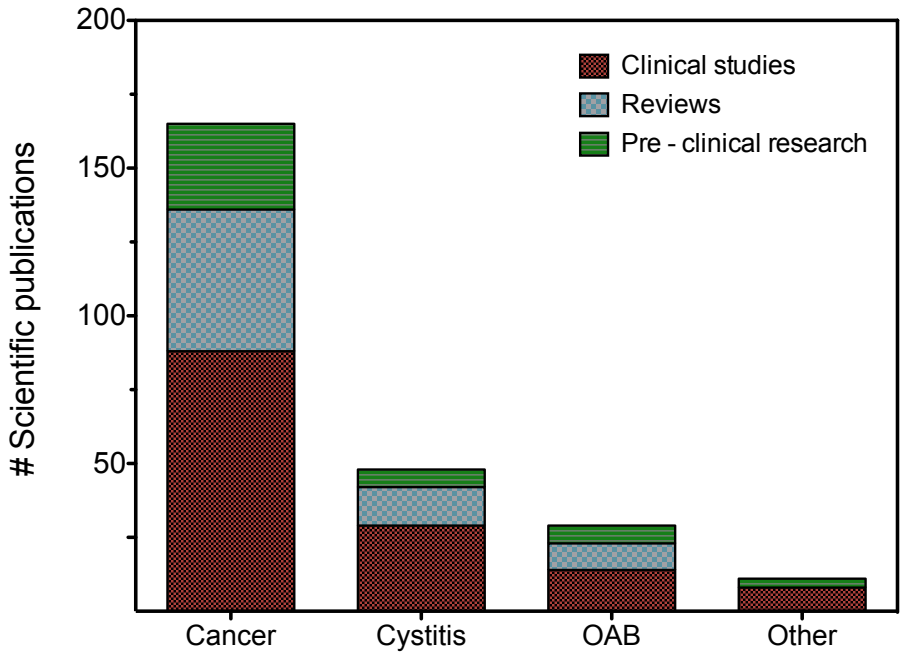

Figure 1.10. The number of IDD - related scientific publications published between 2012 and 2014. Data was obtained by searching Pubmed using the key words 'intravesical' + 'drug'. The search was limited to articles published between 01/01/2012 and 31/12/2013. The search yielded 371 articles, of which 109 were excluded on the basis of relevance. Articles were then stratified into four groups: bladder cancer ('Cancer'), 'Cystitis', overactive bladder ('OAB') or 'Other' depending on their relevant therapeutic area. Cancer, cystitis and OAB included all varieties of bladder cancer, cystitis and bladder dysfunction respectively. All articles outside of these parameters were grouped into 'Other' and this included UTIs, local analgesia, bladder spasm and haematuria. Articles were then further stratified into 'Pre - clinical research', 'Reviews' or 'Clinical studies'. Pre - clinical research included all *in vivo* and *in vitro* pre - human investigations. Reviews included all reviews, round - table discussions, treatment guidelines and patterns of practice. Clinical studies included all clinical trials, case - series, case reports, cohort studies and retrospective analysis.

A

Pathology	*Product*	*Active agent*	*Marketing authorisation holder*
Cancer	Mitomycin-C Kyowa®	Mitomycin-C (MMC)	ProStrakan Ltd
Cancer	ImmuCyst®	Bacillus Calmette-Guerin (BCG)	Alliance Pharmaceuticals Ltd
Cancer	Valstar®	Valrubicin	Endo Pharmaceuticals Ltd
Cancer	Doxorubicin (generic)	Doxorubicin	Actavis Ltd
Cancer	Thiotepa (generic)	Thiotepa	Boehringer Ingelheim Ltd
IC/PBS	Uracyst®	sodium chondroitin sulfate	Stellar Pharmaceuticals Inc
IC/PBS	Gepan®	sodium chondroitin sulfate	Pohl Boskamp Ltd
IC/PBS	iAluril®	sodium hyaluronate + chondroitin sulfate	Aspire Pharmaceuticals Ltd
IC/PBS	Hyacyst®	sodium hyaluronate	Syner-Med Ltd
IC/PBS	Cystistat®	sodium hyaluronate	Bioniche Life Sciences Inc
OAB	BOTOX®	Onabotulinumtoxin-a	Allergan Ltd
OAB	Dysport®	Abobotulinumtoxin-a	Ipsen Ltd

B

2012 - 2013, NHS England Hospital episode statistics (HES)

Pathology	*# FCEs*	*Intravesical treatments*
Cancer	99,522	70,294*
IC / PBS	10,605	
OAB	7,865	

Figure 1.11. A) List of licensed intravesical therapies currently available in the UK. B) Number of finished consultant episodes (FCEs) where the primary diagnosis was bladder cancer, IC / PBS or OAB in England NHS trusts between 2012 and 2013[121,122]. There were 70,294 intravesical treatments administered in England NHS trusts between 2012 and 2013[121,122]. * Stratified data for the indication of treatment was not available.

1.2.2. Advantages of IDD

IDD has a number of advantages, the most significant of which is targeted drug delivery[123]. High concentrations of drug can be delivered directly to the luminal surface of the bladder wall[7]. For specific pathologies, such as superficial bladder cancer, this is the site of action of the drug[124]. For other indications the target may be deeper in the bladder wall within the lamina propria or detrusor muscle layers[125]. In these instances the topical application of high concentrations of drug should favour transurothelial permeation and the subsequent accumulation of drug in these layers. Compared to IDD, the bladder wall bioavailability of systemically delivered drugs is small and large doses are often required to deliver effective concentrations[7]. Furthermore, systemic absorption after IDD is minimal and consequently adverse - effect profiles are highly favourable compared to systemic therapy[123]. Additional advantages relate to the anatomy and accessibility of the bladder[126]. IDD is minimally invasive; the bladder can be accessed directly through the urethra without surgery. Therapy therefore can be conducted in outpatient clinics minimising morbidity / mortality risks to the patient and negating the need for overnight hospital admission. Additionally, an instilled dose can be immediately removed if necessary. If a patient has a local allergic reaction to an instilled drug solution, the bladder can be instantly drained and subsequently flushed with saline. The same cannot be said for systemically - introduced targeted delivery strategies[127] or even organ - targeted injections[128]. IDD is also highly flexible; instillation volumes, concentrations and durations can be tailored to suit a particular therapy, indication or even patient.

1.2.3. Disadvantages of IDD

Despite its advantages, IDD has several inherent limitations. Even in the diseased state, the urothelium has evolved to prevent the movement of small molecules back into the bloodstream and hence its permeability to drugs is low[7]. Subsequently, although high concentrations of drug may be introduced to the bladder surface, concentrations achievable beyond the urothelium are usually low and often subtherapeutic[126]. Several normal physiological processes associated with the urinary tract hinder IDD. Urine produced by the kidneys is constantly draining into the bladder diluting the instilled drug solution. At a normal urine

production rate (~1 ml min^{-1} [129]), a 30 ml instillation of drug will have decreased in concentration by at least 50 % after only 30 min. Furthermore, the bladder has limited capacity and voiding excretes the entire dose. This limited residence time means that a constant concentration gradient across the bladder wall can only be maintained for a limited period of time. Because it requires catheterization, IDD is impractical as a long – term therapy. Unless the patient practices intermittent or permanent catheterization, frequent IDD dosing is inconvenient. This is highlighted by the fact that with the exception of bladder cancer, IDD is a secondary treatment option initiated only subsequent to failed oral management[130]. As IDD requires catheterization, it also increases the risk of UTIs and bleeding[131,132]. Finally, although perhaps not an inherent limitation, a significant pitfall of IDD is the way in which regimens are designed and implemented. The majority of IDD regimens are empirically driven, with minimal scientific, clinical or physiological understanding underpinning treatment design. Examples include poor choice of instillation volume[109], arbitrary instillation times[133] and dosing concentrations derived without knowledge of resulting target bladder wall drug concentrations[109]. As a result IDD remains poorly understood and its potential unfulfilled.

1.2.4. Advancements in IDD

Considering the barrier function of the urothelium restricts the penetration of drug into the bladder wall, one way to improve IDD is to minimize TEER. This has been approached in two ways: physical methods to perturb barrier function and the use of chemical permeation enhancers[7]. The most commonly exploited physical method is iontophoresis (also referred to as Electromotive Drug Administration (EMDA)), a form of electrophoresis that describes the administration of water - soluble drugs across a membrane barrier under the influence of an electric field[134,135]. With regard to the bladder, the application of a small electrical current temporarily disrupts the electrochemical gradient either side of the luminal membrane increasing the passive diffusion of drug molecules through the urothelium and into the bladder wall[7]. Intravesical EMDA has been investigated for several drugs including mitomycin - C (MMC)[136], oxybutynin[137], lidocaine[138] and hyaluronic acid[103] with significantly increased permeation rates shown versus passive diffusion. Subsequently, improved clinical outcomes have been achieved

uptake of drug into the bladder wall[138–140]. Chemical permeation enhancers such as dimethyl sulfoxide (DMSO) and protamine sulfate interact chemically with the urothelium to disrupt its barrier function[7]. Chemical enhancers have been used to improve the delivery of anti - cancer drugs such as doxorubicin and cisplatin into the bladder wall[7,134].

In addition to physical and chemical enhancement, several groups have sought to increase the efficiency of IDD by modulating the release, absorption and retention characteristics of drugs using advanced formulations such as liposomes[141], nanoparticles[142], hydrogels[143] and mucoadhesive polymers[144]. Such formulations have shown potential in the management of IC / PBS[97,145], bladder cancer[146–148] and cystitis - induced incontinence[143]. An additional approach (discussed further in Chapter 2) is the development of intravesical medical devices. Such devices include drug - eluting ureteral stents, which are formulated to release drug over long periods of time (usually days or weeks) and have shown promise in the treatment of stent - related discomfort[149] and UTIs[150–152]. Recently Taris Biomedical® developed a continuous lidocaine - releasing intravesical system (LiRIS®) for the treatment of IC / PBS[153]. LiRIS® is currently in phase II clinical trials (correct for 01.11.2014) with phase I results suggesting the system is well tolerated and produces clinically significant improvements that are maintained for several months after device removal[154]. If approved, LiRIS® will be the first drug - releasing device approved for IDD.

Recently, the first IDD specialty pharmaceutical (spec pharma) company has emerged. TheraCoat Ltd specialise in IDD solutions for bladder cancer, IC / PBS and OAB. Their patented, thermosensitive hydrogel technology (TCGel®) adheres to the urothelium providing the sustained, controlled release of drug over the designated treatment period[155]. The company have completed safety and tolerability studies of a MMC - TCGel formulation for bladder cancer[156] and are currently recruiting participants for similar studies in IC / PBS[157] and OAB[158]. The emergence of IDD spec pharma stands testament to not only the clinical but also the commercial progression occurring in the IDD field.

1.3. Aims and Objectives of Thesis

1.3.1. Aims

The overarching aim of this project was to further understanding of the basic science underlying the IDD process and in doing so reduce the empiricism preventing this drug delivery strategy from realising its potential.

1.3.2. Objectives

The main objective was to develop an *ex vivo* porcine model of IDD and use this to investigate the transurothelial permeation and bladder wall distribution of clinically relevant drugs. Investigating the transurothelial permeation of existing or potential intravesical agents reveals crucial information about the target concentrations achievable in the bladder wall and subsequently the viability of delivering drugs in this manner. This bottom - up approach will lead to the design of more rational and ultimately efficient intravesical regimens.

1.4. Reference List

1. Yoshimura N, Chancellor MB. Urine transport, storage and emptying. In: (Hon WSMMM, editor. Campbell-Walsh Urology 10th Edition Review, 1e. 10th Revised edition edition. Philadelphia, PA: Elsevier Saunders; 2011. p. 329–35.

2. Tortora GJ, Derrickson BH. Principles of Anatomy and Physiology. 12th ed. John Wiley & Sons; 2008.

3. Wyndaele JJ, Wachter SD. Cystometrical Sensory Data from a Normal Population: Comparison of Two Groups of Young Healthy Volunteers Examined with 5 Years Interval. Eur Urol. 2002 Jul;42(1):34–8.

4. Simon H. Enlarged Prostate: In-Depth Report. The New York Times [Internet]. New York, NY, USA; 2013 Sep 20 [cited 2014 Aug 19]; Available from: http://www.nytimes.com/health/guides/disease/enlarged-prostate/background.html

5. Kirchmann H, Pettersson S. Human urine - Chemical composition and fertilizer use efficiency. Fertil Res. 1994 Jan 1;40(2):149–54.

6. Austin JC. Long-term risks of bladder augmentation in pediatric patients. Curr Opin Urol. 2008 Jul;18(4):408–12.

7. GuhaSarkar S, Banerjee R. Intravesical drug delivery: Challenges, current status, opportunities and novel strategies. J Controlled Release. 2010 Dec 1;148(2):147–59.

8. Urethra: Normal Structure. Urologic Pathology. Third. Lippincott Williams & Wilkins; 2009.

9. Reuter, V. The Urothelial Tract: Renal pelvis, ureter, urinary bladder and urethra. In: Sternberg SS, Mills SE, Carter D, editors. Sternberg's Diagnostic Surgical Pathology. Fourth. Lippincott Williams & Wilkins; 2004. p. 2035–82.

10. Chaux A. Normal Bladder Histology [Internet]. PathologyOutlines. 2011 [cited 2014 Aug 19]. Available from: http://www.pathologyoutlines.com / topic /bladderhistology.html

11. National Cancer Institute. SEER Training: Bladder Coding Guidelines [Internet]. National Cancer Institute: SEER. 2013 [cited 2014 Aug 24]. Available from: http://seer.cancer.gov/archive/manuals/2010/AppendixC/bladder/coding_guidelines.pdf

12. Webster S. Anatomy of the bladder [Internet]. Dont be a salmon. 2009 [cited 2014 Aug 24]. Available from: http://www.dontbeasalmon.net/archives/2009/12/week-114-anatom.html

13. Ro JY, Ayala AG, el-Naggar A. Muscularis mucosa of urinary bladder. Importance for staging and treatment. Am J Surg Pathol. 1987 Sep;11(9):668–73.

14. Fry CH, Meng E, Young JS. The physiological function of lower urinary tract smooth muscle. Auton Neurosci Basic Clin. 2010 Apr 19;154(1-2):3–13.

15. Scientific Applications International Corporation. Bladder Cancer: Advanced abstracting [Internet]. Centre for Disease Control and Prevention. 2012 [cited 2014 Aug 19]. Available from: http://www.cdc.gov/cancer/npcr/training/nets/module10/

16. Lewis SA. Everything you wanted to know about the bladder epithelium but were afraid to ask. Am J Physiol Renal Physiol. 2000;278(6):F867.

17. Walker BE. Electron microscopic observations on transitional epithelium of the mouse urinary bladder. J Ultrastruct Res. 1960 Jun;3(4):345–61.

18. Richter WR, Moize SM. Electron microscopic observations on the collapsed and distended mammalian urinary bladder (transitional epithelium). J Ultrastruct Res. 1963 Aug;9(1-2):1–9.

19. Martin BF. Cell replacement and differentiation in transitional epithelium: a histological and autoradiographic study of the guinea-pig bladder and ureter. J Anat. 1972;112(Pt 3):433.

20. Peter S. The junctional connections between the cells of the urinary bladder in the rat. Cell Tissue Res. 1978;187(3):439–48.

21. Lewis SA, Eaton DC, Diamond JM. The mechanism of Na+ transport by rabbit urinary bladder. J Membr Biol. 1976 Aug 27;28(1):41–70.

22. Palaoro LA, Guerra F, Angeleri A, Palamas M, Melba S-S, Rocher AE. Urothelial cells in smears from cervix uteri. J Cytol. 2012;29(1):41–4.

23. Khandelwal P, Abraham SN, Apodaca G. Cell biology and physiology of the uroepithelium. Am J Physiol Renal Physiol. 2009 Dec;297(6):F1477–501.

24. Porter KR, Kenyon K, Badenhausen S. Specializations of the unit membrane. Protoplasma. 1967;63(1):262–74.

25. Hicks RM. The fine structure of the transitional epithelium of rat ureter. J Cell Biol. 1965;26(1):25.

26. Hicks RM, Ketterer B. Hexagonal Lattice of Subunits in the Thick Luminal Membrane of the Rat Urinary Bladder. Nature. 1969 Dec 27;224(5226):1304–5.

27. Walz T, Haner M, Wu XR, Henn C, Engel A, Sun TT, et al. Towards the molecular architecture of the asymmetric unit membrane of the mammalian urinary bladder epithelium: a closed“ twisted ribbon” structure. J Mol Biol. 1995;248(5):887–900.

28. Sun T-T, Zhao H, Provet J, Aebi U, Wu X-R. Formation of asymmetric unit membrane during urothelial differentiation. Mol Biol Rep. 1996 Mar 1;23(1):3–11.

29. Wu XR, Sun TT. Molecular cloning of a 47 kDa tissue-specific and differentiation-dependent urothelial cell surface glycoprotein. J Cell Sci. 1993 Sep;106 (Pt 1):31–43.

30. Wu XR, Lin JH, Walz T, Häner M, Yu J, Aebi U, et al. Mammalian uroplakins. A group of highly conserved urothelial differentiation-related membrane proteins. J Biol Chem. 1994 May 6;269(18):13716–24.

31. Yu J, Lin JH, Wu XR, Sun TT. Uroplakins Ia and Ib, two major differentiation products of bladder epithelium, belong to a family of four transmembrane domain (4TM) proteins. J Cell Biol. 1994 Apr;125(1):171–82.

32. Deng F-M, Liang F-X, Tu L, Resing KA, Hu P, Supino M, et al. Uroplakin IIIb, a urothelial differentiation marker, dimerizes with uroplakin Ib as an early step of urothelial plaque assembly. J Cell Biol. 2002 Nov 25;159(4):685–94.

33. Lin JH, Wu XR, Kreibich G, Sun TT. Precursor sequence, processing, and urothelium-specific expression of a major 15-kDa protein subunit of asymmetric unit membrane. J Biol Chem. 1994 Jan 21;269(3):1775–84.

34. Wu XR, Medina JJ, Sun TT. Selective interactions of UPIa and UPIb, two members of the transmembrane 4 superfamily, with distinct single transmembrane-domained proteins in differentiated urothelial cells. J Biol Chem. 1995 Dec 15;270(50):29752–9.

35. Tu L, Sun T-T, Kreibich G. Specific heterodimer formation is a prerequisite for uroplakins to exit from the endoplasmic reticulum. Mol Biol Cell. 2002 Dec;13(12):4221–30.

36. Hu P, Deng FM, Liang FX, Hu CM, Auerbach AB, Shapiro E, et al. Ablation of uroplakin III gene results in small urothelial plaques, urothelial leakage, and vesicoureteral reflux. J Cell Biol. 2000 Nov 27;151(5):961–72.

37. Liang F-X, Bosland MC, Huang H, Romih R, Baptiste S, Deng F-M, et al. Cellular basis of urothelial squamous metaplasia. J Cell Biol. 2005 Dec 5;171(5):835–44.

38. Kong XT, Deng FM, Hu P, Liang FX, Zhou G, Auerbach AB, et al. Roles of uroplakins in plaque formation, umbrella cell enlargement, and urinary tract diseases. J Cell Biol. 2004;167(6):1195.

39. Hu P, Meyers S, Liang F-X, Deng F-M, Kachar B, Zeidel ML, et al. Role of membrane proteins in permeability barrier function: uroplakin ablation elevates urothelial permeability. Am J Physiol Renal Physiol. 2002 Dec;283(6):F1200–7.

40. Staehelin LA, Chlapowski FJ, Bonneville MA. Lumenal plasma membrane of the urinary bladder. J Cell Biol. 1972;53(1):73.

41. Sun T-T. Altered phenotype of cultured urothelial and other stratified epithelial cells: implications for wound healing. Am J Physiol Renal Physiol. 2006 Jul 1;291(1):F9–21.

42. Wu X-R, Kong X-P, Pellicer A, Kreibich G, Sun T-T. Uroplakins in urothelial biology, function, and disease. Kidney Int. 2009 Jun;75(11):1153–65.

43. Schaeffer AJ, Schaeffer EM. Infections of the urinary tract. In: Wein AJ, Kavoussi LR, Novick AC, Partin AW, Peters CA, editors. Campbell-Walsh Urology: Expert Consult Premium Edition. 10th edition. Philadelphia, PA: Saunders; 2011.

44. Zhou G, Mo WJ, Sebbel P, Min G, Neubert TA, Glockshuber R, et al. Uroplakin Ia is the urothelial receptor for uropathogenic Escherichia coli: evidence from in vitro FimH binding. J Cell Sci. 2001 Nov;114(Pt 22):4095–103.

45. Wu XR, Sun TT, Medina JJ. In vitro binding of type 1-fimbriated Escherichia coli to uroplakins Ia and Ib: relation to urinary tract infections. Proc Natl Acad Sci U S A. 1996 Sep 3;93(18):9630–5.

46. Kreft ME, Jezernik K, Kreft M, Romih R. Apical plasma membrane traffic in superficial cells of bladder urothelium. Ann N Y Acad Sci. 2009 Jan;1152:18–29.

47. Kelley SP, Courtneidge HR, Birch RE, Contreras-Sanz A, Kelly MC, Durodie J, et al. Urinary ATP and visualization of intracellular bacteria: a superior diagnostic marker for recurrent UTI in renal transplant recipients? SpringerPlus [Internet]. 2014 Apr 23 [cited 2015 Apr 4];3. Available from: http://www.ncbi.nlm.nih.gov/pmc/articles/PMC4022969/

48. Matter K, Balda MS. Signalling to and from tight junctions. Nat Rev Mol Cell Biol. 2003 Mar;4(3):225–37.

49. Varley CL, Garthwaite MAE, Cross W, Hinley J, Trejdosiewicz LK, Southgate J. PPARgamma-regulated tight junction development during human urothelial cytodifferentiation. J Cell Physiol. 2006 Aug;208(2):407–17.

50. Birder LA, de Groat WC. Mechanisms of Disease: involvement of the urothelium in bladder dysfunction. Nat Clin Pract Urol. 2007 Jan;4(1):46–54.

51. Acharya P, Beckel J, Ruiz WG, Wang E, Rojas R, Birder L, et al. Distribution of the tight junction proteins ZO-1, occludin, and claudin-4,-8, and-12 in bladder epithelium. Am J Physiol Renal Physiol. 2004;287(2):F305.

52. Southgate J, Baker D, Glover A. Immunohistochemistry services [Internet]. Histotech. 2012 [cited 2014 Aug 25]. Available from: http://www-users.york.ac.uk/~biol32/histotech/AboutUs.html

53. Poggi MM, Johnstone PA., Conner RJ. Glycosaminoglycan content of human bladders: a method of analysis using cold-cup biopsies. Urol Oncol. 2000 Sep;5(5):234–7.

54. Soler R, Bruschini H, Martins JR, Dreyfuss JL, Camara NO, Alves MT, et al. Urinary glycosaminoglycans as biomarker for urothelial injury: is it possible to discriminate damage from recovery? Urology. 2008;72(4):937–42.

55. Parsons CL, Lilly JD, Stein P. Epithelial dysfunction in nonbacterial cystitis (interstitial cystitis). J Urol. 1991 Apr;145(4):732–5.

56. Parsons CL, Boychuk D, Jones S, Hurst R, Callahan H. Bladder surface glycosaminoglycans: an epithelial permeability barrier. J Urol. 1990 Jan;143(1):139–42.

57. Parsons CL, Greenberger M, Gabal L, Bidair M, Barme G. The role of urinary potassium in the pathogenesis and diagnosis of interstitial cystitis. J Urol. 1998 Jun;159(6):1862–6; discussion 1866–7.

58. Parsons CL, Greenspan C, Mulholland SG. The primary antibacterial defense mechanism of the bladder. Invest Urol. 1975 Jul;13(1):72–8.

59. Parsons CL, Greenspan C, Moore SW, Mulholland SG. Role of surface mucin in primary antibacterial defense of bladder. Urology. 1977;9(1):48–52.

60. Hurst RE, Zebrowski R. Identification of proteoglycans present at high density on bovine and human bladder luminal surface. J Urol. 1994 Nov;152(5 Pt 1):1641–5.

61. Hurst RE, Roy JB, Min KW, Veltri RW, Marley G, Patton K, et al. A deficit of chondroitin sulfate proteoglycans on the bladder uroepithelium in interstitial cystitis. Urology. 1996 Nov;48(5):817–21.

62. Buffington CA, Woodworth BE. Excretion of fluorescein in the urine of women with interstitial cystitis. J Urol. 1997 Sep;158(3 Pt 1):786–9.

63. Parsons CL, Zupkas P, Parsons JK. Intravesical potassium sensitivity in patients with interstitial cystitis and urethral syndrome. Urology. 2001 Mar;57(3):428–32; discussion 432–3.

64. Parsons CL. The role of the urinary epithelium in the pathogenesis of interstitial cystitis/prostatitis/urethritis. Urology. 2007 Apr;69(4 Suppl):9–16.

65. Kurth KH, Parsons CL. The interstitial cystitis syndrome: intravesical and oral treatment. Eur Urol Suppl. 2003;2(4):2–9.

66. Dellis A, Papatsoris AG. Intravesical treatment of bladder pain syndrome/interstitial cystitis: from the conventional regimens to the novel botulinum toxin injections. Expert Opin Investig Drugs. 2014 Jun;23(6):751–7.

67. Pohl Boskamp Ltd. How does Gepan instill work? [Internet]. Pohl Boskamp. 2014 [cited 2014 Aug 24]. Available from: http://produkte.pohl-boskamp.de/en/products/Gepan_instill_therapy/77074/

68. Lewis SA. Epithelial electrophysiology. In: Wills NK, Reuss L, Lewis SA, editors. Epithelial transport: a guide to methods and experimental analysis. London: Chapman & Hall; 1996. p. 93–117.

69. Hicks RM. The mammalian urinary bladder: an accommodating organ. Biol Rev Camb Philos Soc. 1975 May;50(2):215–46.

70. Fromter E, Diamond J. Route of passive ion permeation in epithelia. Nature. 1972;235(53):9–13.

71. Anderson JM, Itallie CMV. Physiology and Function of the Tight Junction. Cold Spring Harb Perspect Biol. 2009 Aug 1;1(2).

72. Butt AM, Jones HC, Abbott NJ. Electrical resistance across the blood-brain barrier in anaesthetized rats: a developmental study. J Physiol. 1990 Oct;429:47–62.

73. Cross WR, Eardley I, Leese HJ, Southgate J. A biomimetic tissue from cultured normal human urothelial cells: analysis of physiological function. Am J Physiol Renal Physiol. 2005 Aug;289(2):F459–68.

74. Turner AM, Subramaniam R, Thomas DFM, Southgate J. Generation of a functional, differentiated porcine urothelial tissue in vitro. Eur Urol. 2008 Dec;54(6):1423–32.

75. Lewis SA, Diamond JM. Na+ transport by rabbit urinary bladder, a tight epithelium. J Membr Biol. 1976;28(1):1–40.

76. Lavelle JP, Meyers SA, Ruiz WG, Buffington CAT, Zeidel ML, Apodaca G. Urothelial pathophysiological changes in feline interstitial cystitis: a human model. Am J Physiol Renal Physiol. 2000 Apr 1;278(4):F540–53.

77. Lavelle JP, Apodaca G, Meyers SA, Ruiz WG, Zeidel ML. Disruption of guinea pig urinary bladder permeability barrier in noninfectious cystitis. Am J Physiol. 1998 Jan;274(1 Pt 2):F205–14.

78. Apodaca G, Kiss S, Ruiz W, Meyers S, Zeidel M, Birder L. Disruption of bladder epithelium barrier function after spinal cord injury. Am J Physiol Renal Physiol. 2003 May;284(5):F966–76.

79. Schellhammer PF, Kaplan MH, Pinsky CM, Whitmore Jr WF. Study of local and systemic effects of intravesical BCG. Urology. 1975;6(5):562–7.

80. Tolley DA, Parmar MK, Grigor KM, Lallemand G, Benyon LL, Fellows J, et al. The effect of intravesical mitomycin C on recurrence of newly diagnosed superficial bladder cancer: a further report with 7 years of follow up. J Urol. 1996 Apr;155(4):1233–8.

81. Shelley MD, Jones G, Cleves A, Wilt TJ, Mason MD, Kynaston HG. Intravesical gemcitabine therapy for non-muscle invasive bladder cancer (NMIBC): a systematic review. BJU Int. 2012 Feb;109(4):496–505.

82. Chai M, Wientjes MG, Badalament RA, Burgers JK, Au JL. Pharmacokinetics of intravesical doxorubicin in superficial bladder cancer patients. J Urol. 1994;152(2):374–8.

83. Blumenreich MS, Needles B, Yagoda A, Sogani P, Grabstald H, Whitmore WF Jr. Intravesical cisplatin for superficial bladder tumors. Cancer. 1982 Sep 1;50(5):863–5.

84. Hadaschik BA, ter Borg MG, Jackson J, Sowery RD, So AI, Burt HM, et al. Paclitaxel and cisplatin as intravesical agents against non-muscle-invasive bladder cancer. BJU Int. 2008 Jun;101(11):1347–55.

85. Laudano MA, Barlow LJ, Murphy AM, Petrylak DP, Desai M, Benson MC, et al. Long-term clinical outcomes of a phase I trial of intravesical docetaxel in the management of non-muscle-invasive bladder cancer refractory to standard intravesical therapy. Urology. 2010 Jan;75(1):134–7.

86. Smith G, Theodorou C, Field G, Hargreave TB, Chisholm GD. Intravesical methotrexate in the treatment of superficial bladder cancer. Br J Urol. 1984 Dec;56(6):663–7.

87. Li N, Ye Z, Na Y, CUA THP® Immediate Instillations Study Group. Efficacy of immediate instillation combined with regular instillations of pirarubicin for Ta and T1 transitional cell bladder cancer after transurethral resection: a prospective, randomized, multicenter study. Chin Med J (Engl). 2013;126(15):2805–9.

88. Berrum-Svennung I, Granfors T, Jahnson S, Boman H, Holmäng S. A single instillation of epirubicin after transurethral resection of bladder tumors prevents only small recurrences. J Urol. 2008;179(1):101–6.

89. Hendricksen K, Moonen PMJ, van der Heijden AG, Molkenboer-Kuenen J, Hulsbergen-van de Kaa CA, Witjes JA. Potential and toxicity of intravesical pemetrexed: a preclinical study in pigs. Clin Cancer Res. 2006 Apr 15;12(8):2597–601.

90. Bonfil RD, Russo DM, Schmilovich AJ, Garcia-Palazzo IB. Intravesical therapy with vinorelbine tartrate: antitumor activity in orthotopic murine cell carcinoma of the bladder. J Urol. 1997 Sep;158(3 Pt 1):912–5.

91. Matsushima H, Kawabe K, Fujime M, Kitamura T, Homma Y, Kishi H, et al. Treatment of patients with superficial bladder cancer by intravesical instillation of anticancer drugs plus oral chemotherapy following TUR-Bt: a randomized controlled trial. Oncol Rep. 2002 Apr;9(2):283–8.

92. Fallah F, Fallah M, Sajadi Nia RS. Thiotepa versus Bacille Calmette-Guérin in Non-Muscle Invasive Bladder Cancer. Curr Urol. 2013 Jan;6(3):160–4.

93. Hugosson J, Bergdahl S, Carlsson G, Frösing R, Norlén L, Gustavsson B. Effects of intravesical instillation of 5-fluorouracil and interferon in patients with recurrent superficial urinary bladder carcinoma. A clinical and pharmacodynamic study. Scand J Urol Nephrol. 1997 Aug;31(4):343–7.

94. Chen S-Y, DU L-D, Zhang Y-H. Pilot study of intravesical instillation of two new generation anthracycline antibiotics in prevention of superficial bladder cancer recurrence. Chin Med J (Engl). 2010 Dec;123(23):3422–6.

95. Patterson AL, Greenberg RE, Weems L, Bahnson R, Wajsman Z, Israel M, et al. Pilot study of the tolerability and toxicity of intravesical valrubicin immediately after transurethral resection of superficial bladder cancer. Urology. 2000;56(2):232–5.

96. Weese DL, Roskamp DA, Leach GE, Zimmern PE. Intravesical oxybutynin chloride: experience with 42 patients. Urology. 1993 Jun;41(6):527–30.

97. Chuang Y-C, Kaufmann JH, Chancellor DD, Chancellor MB, Kuo H-C. Bladder instillation of liposome encapsulated onabotulinumtoxina improves overactive bladder symptoms: a prospective, multicenter, double-blind, randomized trial. J Urol. 2014 Dec;192(6):1743–9.

98. Blackburn SC, Jones C, Bedoya S, Steinbrecher HA, Malone PS, Griffin SJ. Intravesical botulinum type-A toxin (Dysport®) in the treatment of idiopathic detrusor overactivity in children. J Pediatr Urol. 2013 Dec;9(6 Pt A):750–3.

99. Kuo H-C. Multiple intravesical instillation of low-dose resiniferatoxin is effective in the treatment of detrusor overactivity refractory to anticholinergics. BJU Int. 2005 May;95(7):1023–7.

100. Aoyagi T. Intravesical Non-Alkalinized Lidocaine Instillation for Interstitial Cystitis/Bladder Pain Syndrome Patients. Open J Urol. 2012;02(04):223–6.

101. Davis EL, El Khoudary SR, Talbott EO, Davis J, Regan LJ. Safety and efficacy of the use of intravesical and oral pentosan polysulfate sodium for interstitial cystitis: a randomized double-blind clinical trial. J Urol. 2008 Jan;179(1):177–85.

102. Aghamir SM., Mohseni MG, Arasteh S. Intravesical bacillus Calmette-Guerin for treatment of refractory interstitial cystitis. Urol J. 2009;4(1):18–23.

103. Gülpınar O, Haliloğlu AH, Gökce Mİ, Arıkan N. Instillation of Hyaluronic Acid via Electromotive Drug Administration Can Improve the Efficacy of Treatment in Patients With Interstitial Cystitis/Painful Bladder Syndrome: A Randomized Prospective Study. Korean J Urol. 2014 May;55(5):354–9.

104. Generali JA, Cada DJ. Intravesical heparin: interstitial cystitis (painful bladder syndrome). Hosp Pharm. 2013 Nov;48(10):822–4.

105. Thakkinstian A, Nickel JC. Efficacy of intravesical chondroitin sulphate in treatment of interstitial cystitis/bladder pain syndrome (IC/BPS): Individual patient data (IPD) meta-analytical approach. Can Urol Assoc J. 2013 Jun;7(5-6):195–200.

106. Peng C-H, Kuo H-C. Multiple intravesical instillations of low-dose resiniferatoxin in the treatment of refractory interstitial cystitis. Urol Int. 2007;78(1):78–81.

107. Lazzeri M, Beneforti P, Benaim G, Maggi CA, Lecci A, Turini D. Intravesical capsaicin for treatment of severe bladder pain: a randomized placebo controlled study. J Urol. 1996;156(3):947–52.

108. Gafni-Kane A, Botros SM, Du H, Sand RI, Sand PK. Measuring the success of combined intravesical dimethyl sulfoxide and triamcinolone for treatment of bladder pain syndrome/interstitial cystitis. Int Urogynecology J. 2013 Feb;24(2):303–11.

109. Beiko D, Watterson J, Knudsen B, others. A double-blinded prospective randomized controlled trial assessing the safety and efficacy of intravesical agents for ureteral stent symptoms following extracorporeal shockwave lithotripsy. J Endourol. 2004;18(8):723–30.

110. Van Nieuwkoop C, den Exter PL, Elzevier HW, den Hartigh J, van Dissel JT. Intravesical gentamicin for recurrent urinary tract infection in patients with intermittent bladder catheterisation. Int J Antimicrob Agents. 2010 Dec;36(6):485–90.

111. Salehipour M, Salahi H, Fathikalajahi A, Mohammadian R, Emadmarvasti V, Bahador A, et al. Is perioperative intravesically applied antibiotic solution effective in the prophylaxis of urinary tract infections after renal transplantation? Urol Int. 2010;85(1):66–9.

112. Wood GC, Chapman JL, Boucher BA, Mueller EW, Fabian TC, Croce MA. Tobramycin bladder irrigation for treating a urinary tract infection in a critically ill patient. Ann Pharmacother. 2004 Aug;38(7-8):1318–9.

113. Trinh T, Simonian J, Vigil S, Chin D, Bidair M. Continuous versus intermittent bladder irrigation of amphotericin B for the treatment of candiduria. J Urol. 1995 Dec;154(6):2032–4.

114. De Jong TP, Donckerwolcke RA, Boemers TM. Neomycin toxicity in bladder irrigation. J Urol. 1993 Oct;150(4):1199.

115. Salmela K, Eklund B, Kyllönen L, Isoniemi H, Korsbäck C, Höckerstedt K, et al. The effect of intravesically applied antibiotic solution in the prophylaxis of infectious complications of renal transplantation. Transpl Int. 1990 May;3(1):12–4.

116. Jones MA, Hasan A. Controlled trial of intravesical noxythiolin in the prevention of infection following outflow tract surgery. Br J Urol. 1988 Oct;62(4):311–4.

117. Hachen HJ. Bladder instillations with trimethoprim-sulfamethoxazole in the treatment of urinary infection. Chemotherapy. 1978;24(1):55–60.

118. Ablove T, Patankar M, Seo S. Prevention of recurrent urinary tract infections by intravesical administration of heparin: a pilot study. Ther Adv Urol. 2013 Dec;5(6):303–9.

119. Damiano R, Quarto G, Bava I, Ucciero G, De Domenico R, Palumbo MI, et al. Prevention of Recurrent Urinary Tract Infections by Intravesical Administration of Hyaluronic Acid and Chondroitin Sulphate: A Placebo-Controlled Randomised Trial. Eur Urol. 2011 Apr;59(4):645–51.

120. Staywell K. HealthcareSheets: When your child needs a Foley catheter [Internet]. Princeton Healthcare System. 2014 [cited 2014 Aug 25]. Available from: http://princetonhcs.kramesonline.com/HealthSheets/3,S,89291

121. The NHS Information Centre for Health and Social Care. Hospital Episode Statistics, Admitted Patient Care, England 2012-2013 [Internet]. 2013 [cited

2014 Aug 22]. Available from: http://www.hscic.gov.uk/article/2021/Website-Search?productid=13264&q=urolithiasis&sort=Relevance&size=10&page=1&area=both#top

122. The NHS Information Centre for Health and Social Care. Hospital Episode Statistics, Hospital Outpatient Activity, England 2012-2013 [Internet]. 2013 [cited 2014 Aug 22]. Available from: http://www.hscic.gov.uk/article/2021/Website-Search?productid=13264&q=urolithiasis&sort=Relevance&size=10&page=1&area=both#top

123. Shen Z, Shen T, Wientjes MG, O'Donnell MA, Au JL. Intravesical treatments of bladder cancer: review. Pharm Res. 2008;25(7):1500–10.

124. Fang J-Y, Huang Z-R. Intravesical drug delivery into the bladder to treat cancers. Curr Drug Deliv. 2009 Jul;6(3):227–37.

125. Goldman HB. Long-term outcome of the use of intravesical botulinum toxin for the treatment of overactive bladder (OAB). BJU Int. 2013 Jan;111(1):8.

126. Hsu C-C, Chuang Y-C, Chancellor MB. Intravesical drug delivery for dysfunctional bladder. Int J Urol. 2013 Jun;20(6):552–62.

127. Tiwari G, Tiwari R, Sriwastawa B, Bhati L, Pandey S, Pandey P, et al. Drug delivery systems: An updated review. Int J Pharm Investig. 2012;2(1):2–11.

128. Topaloglu S, Ozturk MH. Chemoembolization for neuroendocrine liver metastasis. Hepatogastroenterology. 2014 Apr;61(130):398–404.

129. Helms JR. Urinalysis and Renal Clearance. Mathematics for Medical and Clinical Laboratory Professionals. 1st ed. Cengage Learning; 2008. p. 193–202.

130. Buyse G, Waldeck K, Verpoorten C, Björk H, Casaer P, Andersson KE. Intravesical oxybutynin for neurogenic bladder dysfunction: less systemic side effects due to reduced first pass metabolism. J Urol. 1998 Sep;160(3 Pt 1):892–6.

131. Nicolle LE. Catheter associated urinary tract infections. Antimicrob Resist Infect Control. 2014;3:23.

132. Miletic, M N. Intra-vesical therapy (bladder instillation therapy) for interstitial cystitis: patient information [Internet]. University Hospitals Birmingham NHS Foundation Trust. 2010. Available from: http://www.uhb.nhs.uk/pdf/PiBladderInstillation.pdf

133. Shirley SW, Stewart BH, Mirelman S. Dimethyl sulfoxide in treatment of inflammatory genitourinary disorders. Urology. 1978 Mar;11(3):215–20.

134. Giannantoni A, Di Stasi SM, Chancellor MB, Costantini E, Porena M. New frontiers in intravesical therapies and drug delivery. Eur Urol. 2006 Dec;50(6):1183–93; discussion 1193.

135. Marwah H, Garg T, Goyal AK, Rath G. Permeation enhancer strategies in transdermal drug delivery. Drug Deliv. 2014 Jul 9;1–15.

136. Di Stasi SM, Giannantoni A, Stephen RL, Capelli G, Navarra P, Massoud R, et al. Intravesical electromotive mitomycin C versus passive transport mitomycin C for high risk superficial bladder cancer: a prospective randomized study. J Urol. 2003;170(3):777–82.

137. Di Stasi SM, Giannantoni A, Navarra P, Capelli G, Storti L, Porena M, et al. Intravesical oxybutynin: mode of action assessed by passive diffusion and electromotive administration with pharmacokinetics of oxybutynin and N-desethyl oxybutynin. J Urol. 2001;166(6):2232–6.

138. Jewett MA, Valiquette L, Sampson HA, Katz J, Fradet Y, Redelmeier DA. Electromotive drug administration of lidocaine as an alternative anesthesia for transurethral surgery. J Urol. 1999 Feb;161(2):482–5.

139. Di Stasi SM, Giannantoni A, Giurioli A, Valenti M, Zampa G, Storti L, et al. Sequential BCG and electromotive mitomycin versus BCG alone for high-risk superficial bladder cancer: a randomised controlled trial. Lancet Oncol. 2006 Jan;7(1):43–51.

140. Di Stasi SM, Giannantoni A, Vespasiani G, Navarra P, Capelli G, Massoud R, et al. Intravesical electromotive administration of oxybutynin in patients with detrusor hyperreflexia unresponsive to standard anticholinergic regimens. J Urol. 2001;165(2):491–8.

141. Tyagi P, Chancellor MB, Li Z, De Groat WC, Yoshimura N, Fraser MO, et al. Urodynamic and immunohistochemical evaluation of intravesical capsaicin delivery using thermosensitive hydrogel and liposomes. J Urol. 2004 Jan;171(1):483–9.

142. Mugabe C, Matsui Y, So AI, Gleave ME, Baker JHE, Minchinton AI, et al. In vivo evaluation of mucoadhesive nanoparticulate docetaxel for intravesical treatment of non-muscle-invasive bladder cancer. Clin Cancer Res. 2011 May 1;17(9):2788–98.

143. Tyagi P, Li Z, Chancellor M, De Groat WC, Yoshimura N, Huang L. Sustained intravesical drug delivery using thermosensitive hydrogel. Pharm Res. 2004 May;21(5):832–7.

144. Zaharoff DA, Hoffman BS, Hooper HB, Benjamin CJ, Khurana KK, Hance KW, et al. Intravesical immunotherapy of superficial bladder cancer with chitosan/interleukin-12. Cancer Res. 2009 Aug 1;69(15):6192–9.

145. Chuang Y-C, Lee W-C, Lee W-C, Chiang P-H. Intravesical liposome versus oral pentosan polysulfate for interstitial cystitis/painful bladder syndrome. J Urol. 2009 Oct;182(4):1393–400.

146. Chang L-C, Wu S-C, Tsai J-W, Yu T-J, Tsai T-R. Optimization of epirubicin nanoparticles using experimental design for enhanced intravesical drug delivery. Int J Pharm. 2009 Jul 6;376(1-2):195–203.

147. Leakakos T, Ji C, Lawson G, Peterson C, Goodwin S. Intravesical administration of doxorubicin to swine bladder using magnetically targeted carriers. Cancer Chemother Pharmacol. 2003 Jun;51(6):445–50.

148. Eroğlu M, Irmak S, Acar A, Denkbaş EB. Design and evaluation of a mucoadhesive therapeutic agent delivery system for postoperative

chemotherapy in superficial bladder cancer. Int J Pharm. 2002 Mar 20;235(1-2):51–9.

149. Krambeck AE, Walsh RS, Denstedt JD, Preminger GM, Li J, Evans JC, et al. A novel drug eluting ureteral stent: a prospective, randomized, multicenter clinical trial to evaluate the safety and effectiveness of a ketorolac loaded ureteral stent. J Urol. 2010;183(3):1037–43.

150. Cadieux PA, Chew BH, Knudsen BE, Dejong K, Rowe E, Reid G, et al. Triclosan loaded ureteral stents decrease proteus mirabilis 296 infection in a rabbit urinary tract infection model. J Urol. 2006 Jun;175(6):2331–5.

151. Cadieux PA, Chew BH, Nott L, Seney S, Elwood CN, Wignall GR, et al. Use of triclosan-eluting ureteral stents in patients with long-term stents. J Endourol. 2009 Jul;23(7):1187–94.

152. Mendez-Probst CE, Goneau LW, MacDonald KW, Nott L, Seney S, Elwood CN, et al. The use of triclosan eluting stents effectively reduces ureteral stent symptoms: a prospective randomized trial. BJU Int. 2012 Sep;110(5):749–54.

153. Lee H, Cima MJ. An intravesical device for the sustained delivery of lidocaine to the bladder. J Control Release. 2011 Jan 20;149(2):133–9.

154. Nickel JC, Jain P, Shore N, Anderson J, Giesing D, Lee H, et al. Continuous intravesical lidocaine treatment for interstitial cystitis/bladder pain syndrome: safety and efficacy of a new drug delivery device. Sci Transl Med. 2012 Jul 18;4(143):143ra100.

155. TheraCoat Ltd. TheraCoat technology overview [Internet]. TheraCoat, Therapeutic Coatings. 2012 [cited 2014 Aug 23]. Available from: http://theracoat.com/technology/

156. TheraCoat Ltd. An Open Label Study Evaluating Short Term Safety and Tolerability of Patients With muscle invasive bladder cancer-for Intravesical Instillation Mitomycin c Mixed With Disposable Device Which Prevents Drug Drainage Out of the Patient's Bladder [Internet]. National Library of Medicine (US); 2013 [cited 2013 Aug 23]. Available from:

http://clinicaltrials.gov/ct2/show/NCT01648010?term=TheraCoat+Ltd&rank=1. NLM Identifier: NCT01648010.

157. TheraCoat Ltd. Pilot Study Evaluating Efficacy and Safety of Intravesical Instillations of Botulinum Toxin in TC-3 Gel in Interstitial Cystitis Patients [Internet]. National Library of Medicine (US); 2014 [cited 2013 Aug 23]. Available from: http://clinicaltrials.gov/ct2/show/NCT01997983?term=TheraCoat+Ltd&rank=3. NLM Identifier: NCT01997983

158. TheraCoat Ltd. Pilot Study Evaluating Safety and Efficacy of Intravesical Instillations of Botulinum Toxin in TC-3 Gel in OAB Patients [Internet]. National Library of Medicine (US); 2014 [cited 2013 Aug 23]. Available from: http://clinicaltrials.gov/ct2/show/NCT02179099?term=TheraCoat+Ltd&rank=2. NLM Identifier: NCT02179099

159. Escobar PF, Haber G-P, Kaouk J, Kroh M, Chalikonda S, Falcone T. Single-port surgery: laboratory experience with the daVinci single-site platform. JSLS. 2011 Jun;15(2):136–41.

160. Tunc L, Resorlu B, Unsal A, Oguz U, Diri A, Gozen AS, et al. In vivo Porcine Model for Practicing Retrograde Intrarenal Surgery. Urol Int. 2013 Aug 6;

161. Crowe R, Burnstock G. A histochemical and immunohistochemical study of the autonomic innervation of the lower urinary tract of the female pig. Is the pig a good model for the human bladder and urethra? J Urol. 1989 Feb;141(2):414–22.

162. Sibley G. An experimental model of detrusor instability in the obstructed pig. Br J Urol. 1985;57(3):292–8.

163. Kumar V, Chapple CC, Chess-Williams R. Characteristics of adenosine triphosphatase release from porcine and human normal bladder. J Urol. 2004;172(2):744–7.

164. Williams NA, Bowen JL, Al-Jayyoussi G, Gumbleton M, Allender CJ, Li J, et al. An ex Vivo Investigation into the Transurothelial Permeability and Bladder Wall

Distribution of the Nonsteroidal Anti-Inflammatory Ketorolac. Mol Pharm. 2014 Feb 6;

165. Lose G, Nørgaard JP. Intravesical oxybutynin for treating incontinence resulting from an overactive detrusor. BJU Int. 2001 Jun;87(9):767–73.

166. Ploeg M, Aben KKH, Kiemeney LA. The present and future burden of urinary bladder cancer in the world. World J Urol. 2009 Jun;27(3):289–93.

167. Raman JD, Messer J, Sielatycki JA, Hollenbeak CS. Incidence and survival of patients with carcinoma of the ureter and renal pelvis in the USA, 1973-2005. BJU Int. 2011 Apr;107(7):1059–64.

168. Aboumarzouk OM, Somani B, Ahmad S, Nabi G, Townell N, Kata SG. Mitomycin C instillation following ureterorenoscopic laser ablation of upper urinary tract carcinoma. Urol Ann. 2013 Jul;5(3):184–9.

169. Keeley FX Jr, Bagley DH. Adjuvant mitomycin C following endoscopic treatment of upper tract transitional cell carcinoma. J Urol. 1997 Dec;158(6):2074–7.

170. Eastham JA, Huffman JL. Technique of mitomycin C instillation in the treatment of upper urinary tract urothelial tumors. J Urol. 1993 Aug;150(2 Pt 1):324–5.

Chapter Two: Development of an Ex Vivo Model for Investigating the Transurothelial Permeability and Bladder Wall Distribution of Therapeutic Agents

2.1. Introduction

2.1.1. Relevant Prologue: Boston Scientific collaboration

Ureteral stents are thin, flexible, hollow tubes that are placed in the ureter between the kidney and the bladder[1]. In contemporary urological practice, the most commonly used stent is the double - J or double - pigtail variety[2] (the two names are used interchangeably) (Figure 2.1A). Double - J stents are specially designed to form a 'J' shape at either end of the device. Once inserted, these ends form coils in the kidney and bladder preventing displacement of the stent[3] (Figure 2.1B).

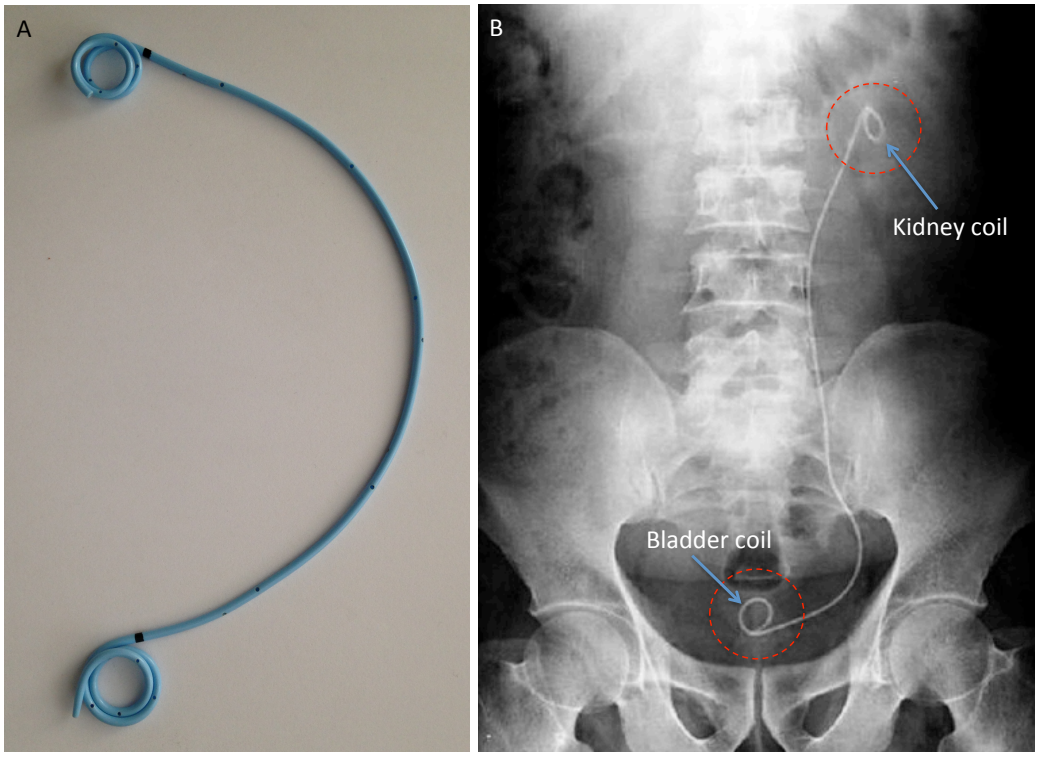

Figure 2.1. Double - J ureteral stent out of the packet (A) and *in situ* as viewed on x - ray (B)[4].

Inserted after a wide range of procedures, ureteral stents aid urine drainage by relieving or preventing obstruction of the upper urinary tract[1]. Specifically, they passively dilate the ureter allowing urine to drain through the centre and around the outside of the device[5]. Stents may remain indwelling for several weeks or even months at a time[6], and although effective, their use is associated with a wide range of morbidities often leading to a reduced quality of life for the patient[7]. Since their

envisagement in the 19th century[8], stent design has advanced considerably. Developments have focused on producing more tolerable stents by using softer biomaterials[9,10], varying the stent size[11] and shape[12] and designing novel biodegradable stents[13]. Despite this, their use continues to be associated with significant patient morbidity[14,15]. Stent - related discomfort (SRD) remains one of the most problematic adverse effects with occurrence rates as high as 80 %[16]. Patients commonly report SRD as pain in the suprapubic, flank area (side to middle of the back)[17]. Its exact aetiology remains unknown, with pain varying in site of presentation and intensity. For some patients, stents have to be removed prematurely such is the level of discomfort[18]. The pharmacological management of SRD has traditionally lacked a sufficiently strong evidence base with no consensus on the effectiveness of non - steroidal anti – inflammatories (NSAIDs), antimuscarinics, anaesthetics or alpha - blockers, all of which only provide partial symptomatic relief[19].

Boston Scientific Corporation (BSC), who co - sponsored this project, is a global medical device manufacturer who currently occupies a significant portion of the ureteral stent market[20]. The collaboration between BSC and this research group arose as a result of BSC's unsuccessful attempt to develop a drug - eluting ureteral stent known as the Lexington™ stent (Lexington™ stent, Boston Scientific, Natick, MA, USA)[21]. By providing localised, controlled release of drug at the very site of stent placement, Lexington™ was designed to reduce SRD and in doing so make up for the shortcomings of oral therapies. Early drug - selection studies, based on intravesical efficacy, highlighted ketorolac tromethamine as the lead candidate for incorporation into the stent[22]. Alternative agents, such as intravesical oxybutynin chloride and intravesical alkaline - buffered lidocaine hydrochloride, were found to be less efficacious[22]. Ketorolac is a non – selective NSAID that is particularly effective in the management of post - surgical pain (Figure 2.2) [23].

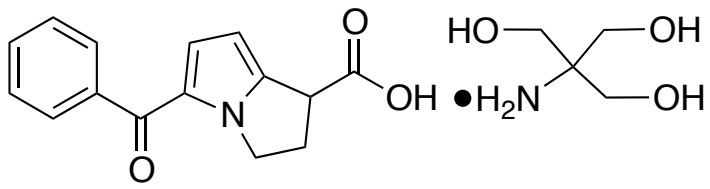

$C_{19}H_{24}N_2O_6$
MWt – 376.41 g mol^{-1}

Figure 2.2. Chemical structure of ketorolac tromethamine

A pre - clinical safety study demonstrated Lexington™ to be safe, with low systemic absorption of ketorolac and no indication of local urinary tract inflammation or ulceration in any of the test animals[24]. Subsequently, BSC rolled out a prospective, double - blind, randomised controlled trial (RCT) evaluating the efficacy of Lexington™ against a control stent after uteroscopy[21]. Surprisingly the Lexington™ stent provided no clinical benefit over the control group with suggestions that further studies with higher drug concentrations were likely required.

2.1.2. The paucity of basic science underlying IDD regimens

As a result of the Lexington™ study, BSC believed that a new, bottom - up approach was required if the ketorolac - eluting stent was to be successful. Although pre - clinical studies suggested intravesical ketorolac to be effective in SRD[22], there was no knowledge of bladder wall concentrations achieved. It is difficult to establish required stent – loading and drug – elution rates without knowledge of the target bladder wall concentrations desired. This example is not unique, the empirical nature of IDD is recognised by key opinion leaders in both the clinical[25–27] and scientific[28] remit and is evident in the majority of IDD regimens. A good illustration of this concerns the intravesical delivery of Bacillus Calmette – Guerin (BCG) for non - muscle invasive bladder cancer (NMIBC). Originally, the dose was determined to be 120 mg as this dose was tolerated when administered intradermally[29]. Furthermore, instillations were given once a week for 6 weeks because BCG came packaged in 6 vials and adverse events lasted less than a week[25,29]. Intravesical BCG has been used clinically since 1976 and remains first -

line pharmacotherapy for NMIBC[30], however the optimum dose is unknown and the mechanism of action poorly understood[25].

So despite having been used for a number of decades, IDD regimens, such as the one BSC used to identify Ketorolac, remain largely empirical. Consequently little is known of target tissue concentrations achievable or ultimately the viability of delivering drugs locally to the urinary tract. *In vivo* data remains limited due to the difficulty in obtaining bladder tissue concentrations in human and animal subjects. Intravesical pharmacokinetic (PK) studies have been carried out for several drugs including MMC[31], doxorubicin[32], gemcitabine[33] and oxybutynin[34]. While such investigations reveal valuable information concerning systemic drug levels, they rarely elucidate concentrations achieved in the bladder wall or urine. Consequently IDD regimens are largely based on clinical outcomes such as tolerability or perceived benefit. Although such qualitative end points are clinically useful, quantitative data on urothelial permeability and bladder wall tissue distribution is equally important when predicting the usefulness of local drug delivery approaches. BSC believed fundamental research investigating the transurothelial permeability of ketorolac would help ascertain whether bladder wall concentrations achieved after local delivery are sufficient to justify incorporation into a drug - eluting ureteral stent.

2.1.3. Methods to investigate transurothelial delivery

Considering what has been discussed, it is important to review some of the techniques that have been used to investigate the transurothelial delivery and bladder wall distribution of drugs.

2.1.3.1. In vivo studies

In vivo, bladder wall penetration after IDD has been investigated in mice[35], rats[36] and larger animals such as rabbits[37], dogs[38,39] and pigs[40–43]. The urinary tract of larger animals, such as pigs, is anatomically closer in structure and size to man[44] and subsequently offers significant advantages over smaller species in pre - clinical studies. Pig bladders can hold ~ 500 ml of urine[45] (similar to the human bladder[46]) whereas the maximum capacity of the mouse and rat bladder is ~ 0.15 and ~1 ml respectively[47]. Accordingly when conducting pre - clinical studies of potential IDD regimens, pharmaceutical companies generally use pigs[43,48,49]. Studies are

designed to mimic human IDD regimens. Animals receive instillations (~ 50 ml[49]) through a urinary catheter and the drug solution is maintained in the bladder for the desired instillation period (usually ~ 1 - 2 h[48,49]) prior to bladder draining. Note only female pigs are used as the shape of the porcine penis makes urethral catheterisation difficult if not impossible[50]. Blood samples are usually taken periodically after instillation and urine collected upon bladder drainage[48].

Interestingly, two studies (from the same research group) have investigated bladder wall concentrations after IDD in humans[51,52]. Ethical approval was obtained to give intravesical instillations to radical cystectomy patients prior to the start of their surgery. Radical cystectomy is a surgical procedure used in bladder cancer to remove the whole of the bladder and nearby lymph nodes[53]. Such studies are extremely rare, would likely be impossible to obtain ethical approval for in the present day and as such have been included for completeness rather than relevance to current *in vivo* techniques.

By their nature, *in vivo* studies encompass all the attributes associated with a living animal. For IDD the major advantages are dilution of the instilled dose by urine and systemic clearance of drug from the bladder wall. *In vivo* studies in large animals are the gold standard model of IDD and if designed correctly can yield a plethora of data including urine pharmacokinetics, bladder wall drug concentrations and systemic levels of drug achieved after treatment[40]. That said, bladder wall concentrations are often neglected in favour of focusing on local bladder toxicology and systemic PK[48,49]. Furthermore these studies are extremely costly (~ $15,000 per pig, Tim Harrah, personal communication, June 20th, 2013) and as such are typically only carried out when phase 1 human studies are anticipated. Consequently the majority of early - stage research into transurothelial delivery is investigated *in vitro* or *ex vivo*.

2.1.3.2. In vitro / ex vivo studies

2.1.3.2.a. Cell culture systems

Although not used to investigate delivery across the urothelium, cell culture has been used to investigate the uptake of chemotherapeutics into target urothelial cells[54,55]. The most commonly used system is immortalised human urothelial cell

cultures[56], although normal human urothelial cells (NHU) are also used[57]. A significant limitation from a drug delivery point of view is the barrier function provided by these systems. The immortalization process appears to prevent normal cellular differentiation and subsequently the urothelial cells do not develop a functional barrier[58]. NHU are superior to immortalized systems and, when cultured on permeable membrane supports, can form an apparently functional or 'biomimetic urothelium' exhibiting significant barrier functionality (TEER values of > 3 kΩ cm^2)[59]. Additionally, seeding onto these permeable membranes allows the modelling of systemic and intravesical drug exposure by addition of the compound the basal or apical chamber respectively[58]. Although cell culture systems provide a useful tool to investigate urothelial - drug interactions, they are less valuable in terms of drug delivery studies. Such systems represent isolated urothelium and do not therefore permit investigations of drug distribution into other layers of the bladder wall. When investigating IDD, distribution of drug into the different layers of the bladder wall is essential as bladder wall targets may reside in tissue layers below the urothelium (Section 1.2.2).

2.1.3.2.b. *Ex vivo* bladder tissue

Ex vivo, bladder wall penetration after local application to the urothelium has been investigated using rabbit[60], porcine[61] and human[62] bladder tissue. Although whole bladder models have been reported[63,64], the majority of studies use sections of *ex vivo* bladder tissue loaded into diffusion apparatus[61,65–68]. Typically drug solution is applied to the bladder surface and removed after a predefined period of time representative of the intravesical instillation period[67]. Unlike urothelial cell culture systems, full thickness sections of bladder tissue allow determination of drug concentrations throughout the bladder wall. An established technique to do this is concentration - depth profiling where bladder tissue exposed to drug is sectioned parallel to the urothelial surface all the way down to the serosal side of the tissue[61]. This, in combination with knowledge of tissue - layer depths, allows quantitation of drug in the different layers of the bladder wall and has been used to investigate the IDD of agents such as paclitaxel[66] and docetaxel[67].

Ex vivo studies, while more feasible than *in vivo* work, are inherently limited by the absence of systemic drug clearance and processes such as urine dilution and periodic voiding which are fundamental to IDD[28] (Section 1.2.3). To date, no

studies have sought to incorporate allowances for these processes into *ex vivo* studies. Furthermore many of the investigations reported have done little to verify the suitability of the *ex vivo* urothelial barrier as a model for transurothelial permeation[61,65,69,70]. In terms of apparatus, examples include the use of diffusion cells without a receiver chamber to supply the tissue with buffer[69,70], whilst experimentally basic histological studies are often relied on to demonstrate urothelial barrier function[62]. A recent study used de - frosted porcine bladder tissue to investigate transurothelial delivery; histological analysis showed abnormal looking tissue with minimal evidence of an intact urothelium[71].

2.1.4. Aims and Objectives of Chapter Two

The overall aim of this section of work was to develop an *ex vivo* model facilitating investigation of the transurothelial permeability and bladder wall distribution of drugs after their local application to the urothelium.

The key objectives were:

1. To design an *ex vivo*, diffusion cell setup to investigate the transurothelial permeability of drugs into bladder tissue

2. To validate the viability and appropriateness of the *ex vivo* porcine tissue by investigating markers of permeability, measuring TEER and examining the urothelial surface using scanning electron microscopy.

3. To investigate the transurothelial permeation of Ketorolac tromethamine and evaluate target drug concentrations achieved in the bladder wall.

2.2. Materials and Methods

2.2.1. Materials

All chemicals were purchased from Sigma - Aldrich, Poole, UK and were used as received unless otherwise stated. All organic solvents were of HPLC grade and were obtained from Fisher Scientific, Loughborough, UK unless otherwise stated.

2.2.2. Analysis of propranolol hydrochloride

Propranolol hydrochloride was analysed by high – performance liquid chromatography (HPLC) using a Thermo Scientific HPLC automated system fitted with a Kromasil, 5 μm, C18, 250 mm x 4.6 mm i.d column (Sigma - Aldrich, Poole, UK). The mobile phase consisted of 70 % acetonitrile (ACN) : 30 % sodium dodecyl sulfate (10 mM), disodium hydrogen phosphate (10 mM) adjusted to pH 2.3 with phosphoric acid. UV detection was set at 290 nm. The injection volume was 20 μl and flow rate 1 ml min^{-1}.

2.2.3. Analysis of sodium fluorescein

Sodium fluorescein was analysed by fluorescence (Fluostar Optima microplate reader, BMG Labtech GmbH, Ortenburg, Germany). The excitation and emission wavelengths were set at 485 nm and 520 nm respectively.

2.2.4. Analysis of ketorolac tromethamine

Ketorolac was analysed by HPLC (2.2.2). The mobile phase consisted of 60 % 0.02 M phosphate buffer (adjusted to pH 3.5 with phosphoric acid) : 40 % ACN. UV detection was set at 315 nm. The injection volume was 20 μl and flow rate 1 ml min^{-1}.

2.2.5. Bladder tissue preparation

Porcine bladders from pigs weighing 70 - 90 kg, were obtained fresh from a local abattoir within five min of excision and transported in ice - cold oxygenated Krebs - Henseleit buffer (Krebs buffer, composition: NaCl 118.3 mM, $NaHCO_3$ 25 mM, $CaCl_2$ 2.5 mM, $MgSO_4$ 1.2 mM, KCl 4.7 mM, KH_2PO_4 1.2 mM and D - glucose 11 mM, pH 7.4). Bladders were filled and drained with 37 °C saline to remove any residual urine. Using a scalpel, excess perivesical fat was trimmed away and a vertical incision made along the length of the bladder. Tissue sections (~ 2 cm^2) from the posterior wall, lateral walls and dome area of the bladder (Figure 1.2) were loaded into glass Franz - type diffusion cells (Figure 2.3, average exposed tissue area 1.32 cm^2, custom - made, UK) with the urothelium facing upwards. Care was taken to avoid contact with the urothelial surface and a metal clamp was used to secure the tissue between the donor and receiver chambers of the apparatus. The receiver compartment was filled with oxygenated Krebs buffer and equilibrated at 37 °C for 30 min with a micro - stirrer bar providing continuous stirring. A solution of the drug was pipetted into the donor chamber (on to the urothelial surface), which was covered with a glass disc to prevent evaporative loss. The sampling arm was capped and the cells placed in to a thermostatically controlled water bath at 37 °C.

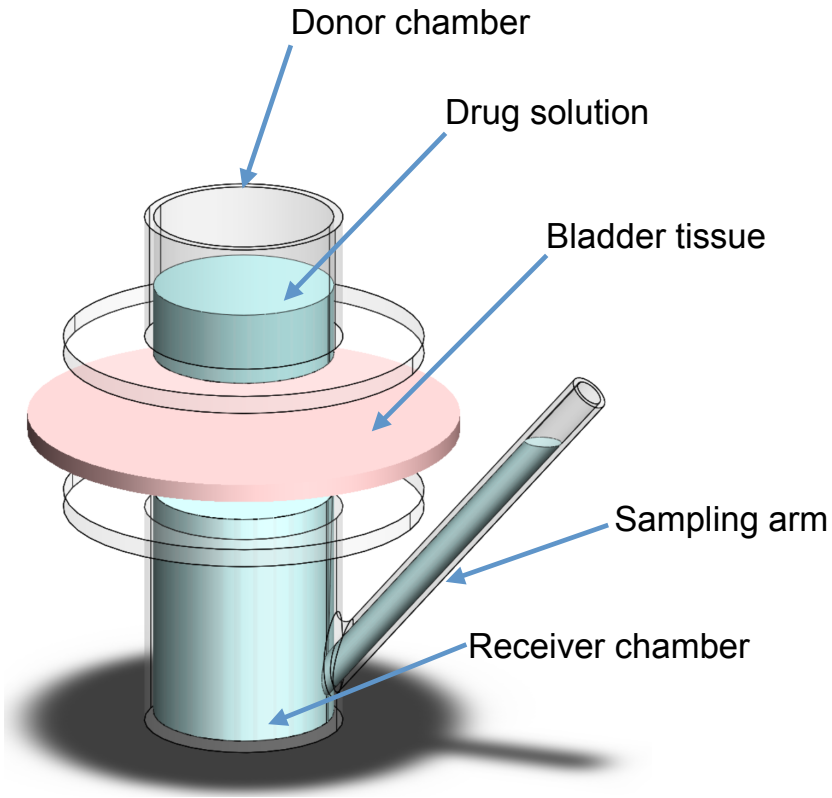

Figure 2.3. Schematic of the custom built Franz - type diffusion cell loaded with porcine bladder tissue.

2.2.6. Confirmation of tissue viability

2.2.6.1. Investigating markers of permeability

The viability of the bladder tissue was evaluated in an assay investigating the co - permeation of propranolol hydrochloride and sodium fluorescein. A 500 µl aliquot of a saline solution containing 1 mM propranolol hydrochloride and 0.1 mM sodium fluorescein was added to the donor chamber of the Franz - type cell. At fixed time points (0.5, 1.5, 3.5 and 6.5 h), the contents of the receiver and donor chambers were collected and the bladder tissue removed.

Prior to removal with a cork borer, the area of tissue in contact with the drug was rinsed 3 x 1 ml with saline to remove any surface - adsorbed drug and the urothelium and lamina propria (mucosa) carefully separated from the underlying detrusor muscle by cutting along the natural plane of division with a scalpel (Figure 2.4). Tissue sections were then weighed, homogenised (Precellys®24, Bertin Technologies Inc, Bordeaux, France) and drug extracted in 1 ml of mobile phase (section 2.2.2) for 36 h with 10 min sonication per sample. Samples were then centrifuged for 5 min (7,000 RPM, 2,680 g) and the supernatant isolated for analysis.

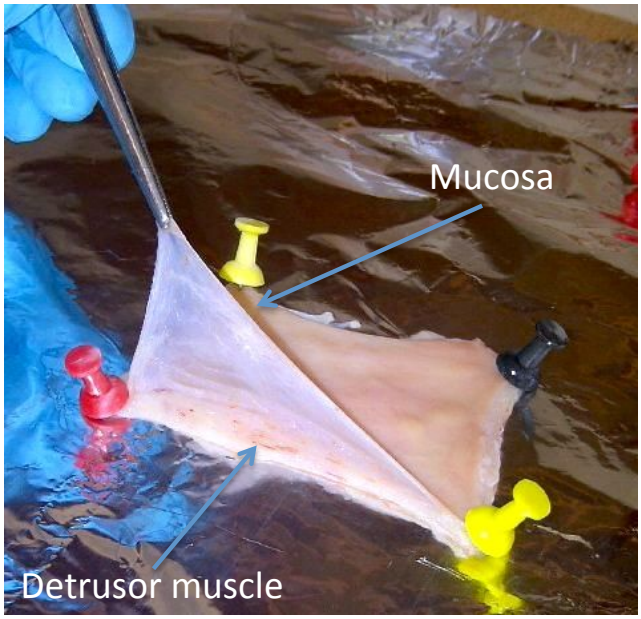

Figure 2.4. Separation of porcine mucosa from the underlying detrusor muscle.

Accurate separation of the bladder mucosa from the underlying detrusor muscle was confirmed histologically. The mucosa was removed from one half of a bladder section, leaving the other half as full thickness bladder wall. Tissue samples were fixed to cork mounts with optimal cutting temperature medium (OCT) (Tissue - Tek™, CRYO - OCT Compound, Fisher Scientific UK Ltd, Leicestershire, England) and snap frozen between two metal plates using liquid nitrogen. Samples were sectioned at 10 μm using a cryostat (Leica CM3050 S, Leica Microsystems, Buckinghamshire, England). Sections were then stained with haematoxylin - eosin (H & E) and examined by light microscopy.

2.2.6.2. Transepithelial electrical resistance (TEER)

The integrity of urothelial, paracellular tight junctions (TJs) was investigated by measuring TEER across the bladder mucosa over 2.5 h. The urothelium and lamina propria was carefully removed and a 1 cm^2 section mounted into an Ussing chamber (NaviCyte vertical multichannel Ussing chambers, Warner Instruments, Hamden, CT, USA). The mucosal chamber was filled with 4 ml of either normal saline or ketorolac 1.1 mg ml^{-1} in saline, whilst the serosal chamber was filled with 4 ml of oxygenated Krebs buffer. The Ussing chambers were maintained at 37 °C and after a 10 min equilibration period, TEER across the mucosa measured at 15 min intervals. TEER was measured using a multi - channel voltage – current clamp (EC - 800 single channel, Warner Instruments, Hamden, CT, USA). The Ussing chambers were equipped with two pairs of Ag / AgCl electrodes, for measuring potential difference (V) and for passing current (I). The experiments were performed under open circuit conditions, whereby the current was set to zero and the natural transepithelial potential difference could be observed. Electrical resistance was determined according to Ohm's law (R = V / I). The TEER value at time zero was taken to be the baseline reading, from which the percentage change was calculated. TEER was calculated as the net electrical resistance of the mucosa multiplied by the apparent exposed tissue area of the Ussing chamber (0.12 cm^2). Percentage change from baseline TEER was compared for the saline and ketorolac groups. All statistical analysis was performed using GraphPad Prism version 6.0c (GraphPad Software, Inc, San Diego, California, USA). Unpaired t - tests were used for all comparisons.

2.2.6.3. Scanning electron microscopy (SEM)

To further confirm the integrity of the urothelial barrier under experimental conditions, bladder tissue was examined by scanning electron microscopy (SEM). Bladder sections were loaded into Franz - type diffusion cells and 500 μl of normal saline (negative control), ketorolac 1.1 mg ml^{-1} in saline (test agent) or protamine sulfate 10 mg ml^{-1} in saline (positive control) added to the donor chamber. After 90 min the contents of the donor chamber was discarded, the urothelial surface subjected to 3 x 1 ml saline rinses and the tissue sample removed. An additional sample, fixed on - site at the abattoir immediately post – excision of the bladder (approximately 5 min after slaughter), was examined as a control. Sections of tissue (~ 2 cm^2) were carefully cut without touching the urothelial surface and fixed in a solution of 4 % formaldehyde and 0.2 % glutaraldehyde in 0.1 M phosphate buffer for 24 h at room temperature. Following washing with distilled water (2 x 60 min), tissue samples were dehydrated in isopropyl alcohol solutions of increasing concentrations (50 – 100 %) before undergoing chemical drying in 100 % hexamethyldisilazane. Samples were then sputter - coated with gold (Emscope sputter coater, Emscope, Ashford, Kent, UK) before SEM examination (5 kV, Jeol JSM 840A, Tokyo, Japan). Images were acquired with an ADDA 2 image grabber and processed using Scandium analysis software (Soft Imaging System GmbH, Münster, Germany).

2.2.7. Evaluation of the delivery of ketorolac to the bladder wall

2.2.7.1. Permeation of ketorolac across the urothelium

Franz - type cells were assembled as described (Section 2.2.5) and a 500 μl aliquot of a 1.1 mg ml^{-1} ketorolac solution (in normal saline) applied to the donor chamber. At fixed time points (0.5, 1, 2, 3.5 and 5 h), the contents of the receiver and donor chambers were collected and the tissue sample removed. The tissue was rinsed 3 x 1 ml with saline and ketorolac extracted in 1 ml of mobile phase (Section 2.2.6.1). Drug was quantified using HPLC (Section 2.2.4).

2.2.7.2. Distribution of ketorolac into the bladder wall

Franz - type cells were assembled as described (Section 2.2.5) and a 500 μl aliquot of a 1.1 mg ml^{-1} ketorolac solution (in normal saline) applied to the donor

chamber. After 90 min the Franz - type cells were dismantled, the donor and receiver compartments collected and the urothelial surface rinsed 3 x 1 ml with saline. The area of drug contact was isolated, immediately snap frozen between two metal plates using liquid nitrogen, fixed to cork mounts with OCT and the tissue sectioned using a cryostat (Section 2.2.6.1). Care was taken to ensure OCT was only present on the serosal side of the tissue. Samples were serially sectioned parallel to the urothelial surface at 50 μm thickness and sections collected in pre - weighed 1.5 ml eppendorf tubes. Tissue sections between 0 and 200 μm (urothelium) were collected individually for analysis. Groups of five 50 μm tissue sections between 200 and 1,200 μm (lamina propria) and ten tissue sections between 1,200 and 3,200 μm (detrusor muscle) were collected and pooled prior to analysis. For pooled samples, tissue depths were expressed as the midpoint depth of the sections. Tissue sections were then weighed, extracted in 500 μl mobile phase for 24 h and drug quantified using HPLC (Section 2.2.4). Average tissue concentrations achieved in the urothelium, lamina propria, detrusor muscle and whole bladder wall were calculated by dividing the total amount of drug recovered by the total weight of tissue in that layer.

2.3. Results and Discussion

2.3.1. Using ex vivo porcine bladder tissue

When designing an *ex vivo* model, fresh human tissue is the gold standard tissue upon which to carry out investigations. For certain organs, such as human skin, obtaining fresh samples is feasible owing to the steady supply of surgical excess tissue[72]. Unfortunately the same is not true for human bladder tissue. Statistics published by the British Association of Urological Surgeons (BAUS) reported that only 743 cystectomies, across 45 health centres in England, Scotland and Wales were performed in 2012[73]. Such a low procedure rate, an average of less than two cystectomies per health centre per month, would not yield an adequate supply of human bladders for this research project. Considering this, pig bladders were chosen.

Porcine bladder tissue was a natural choice owing to the long history of pigs being used as animal models in urology[74–76]. A number of studies have reported the physiology of the porcine urinary tract to be similar to that of humans[45,77,78]. Anatomically, the porcine urinary tract is a good representation of man[79] and for several decades anaesthetised pigs have been, and continue to be, used for urological surgical training[44,80]. Histological analysis has shown parallels between the structure and composition of the porcine and human bladder wall; both comprise an ordered layering of urothelium, lamina propria, detrusor muscle and adventitia[81–83]. An additional advantage of procuring abattoir - derived porcine tissue concerns ethical approval. As none of the animals at an abattoir are killed for experimental reasons, ethical approval is not required.

2.3.2. Confirmation of tissue viability

2.3.2.1. Tissue procurement and transportation

The ability to obtain fresh tissue was considered essential to this project. Porcine bladders were obtained immediately at the time of excision, the total warm ischemic time between killing the animal and bladder retrieval was consistently under 10 min. Bladders were transported from the abattoir in oxygenated Krebs buffer[84]. Krebs is a balanced salt solution used to maintain tissue at a physiological pH and ensure intracellular and extracellular osmotic balance[85]. It was a logical choice based on its extensive use in *ex vivo* full bladder[86,87] and isolated bladder tissue studies[66,67,88,89].

Buffer was made fresh for each experiment and was cooled such that the temperature during bladder transportation was ~ 4 °C. Cooling prevents hypoxic injury by reducing cellular metabolism and therefore the oxygen requirements of the organ[90]. The van't Hoff - Arrhenius law states that the rate of a biochemical reaction is halved for each 10 °C decrease in temperature[91] and data obtained from perfused rat livers has shown oxygen requirements to be significantly reduced at lower temperatures compared to 37 °C[90]. Such cooling techniques are used in organ transplantation, where hypothermia remains the principal method of maintaining organ viability during ischaemic transfer from donor to recipient[90]. In addition to cooling, the Krebs buffer was bubbled with carbogen (95 % O_2, 5 % CO_2) to provide oxygen for the bladder tissue. Prior to oxygenation the buffer was

chilled, as oxygen solubility is higher at lower water temperatures[92]. Consistent with other reported Krebs recipes[86,89,93], the buffer was modified by the addition of glucose to provide an energy source for cell maintenance.

2.3.2.2. Investigating markers of permeability

Whilst the literature suggested that gross bladder viability should be maintained under the conditions described[66,86] (Section 2.3.2.1), there was uncertainty as to how the urothelial barrier function would be affected by bladder excision, transport and experimentation. In addition to preventing the significant permeation of molecules, a functional barrier would be expected to differentiate between molecules that permeate paracellularly and those that permeate transcellularly[94]. Sodium fluorescein and propranolol hydrochloride are recognised paracellular and transcellular markers respectively[95,96]. In this study the two compounds were used to evaluate the integrity of the urothelial barrier over 6.5 h.

2.3.2.2.a. Analysis of sodium fluorescein and propranolol hydrochloride

Sodium fluorescein was analysed by fluorescence (Section 2.2.3). The lower limit of detection (LLOD) and quantification (LLOQ), calculated as 3 and 10 - fold the signal to noise ratio, was 4.12 nM and 13.73 nM respectively. Propranolol hydrochloride was quantified by HPLC (Section 2.2.2). The LLOD and LLOQ was 0.15 μM and 0.5 μM respectively. Quantitation was calculated using an external standard solution ranging in concentration from 0.001 to 10 μM for sodium fluorescein and 0.05 to 100 μM for propranolol hydrochloride. Calibration curves (response plotted against external standard concentration) were run in triplicate to ensure reproducibility and showed high linearity across the expected analyte concentration range (Figure 2.5).

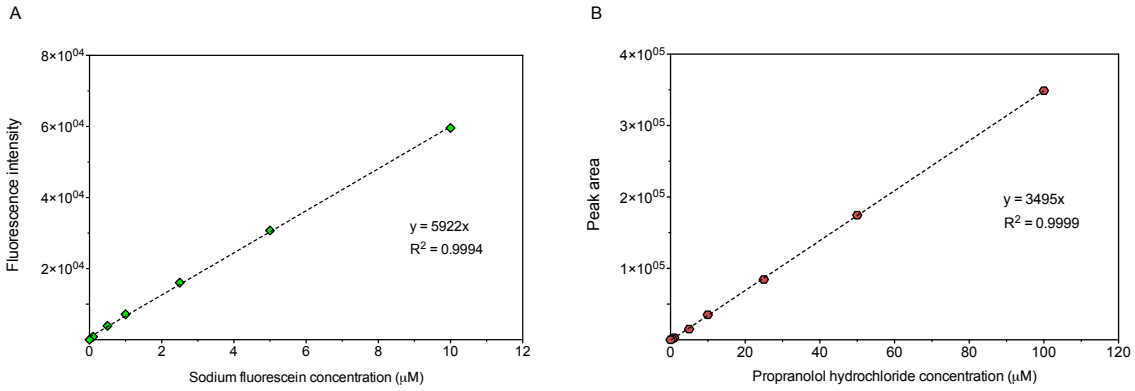

Figure 2.5. External standard calibration curves for sodium fluorescein (A) and propranolol hydrochloride (B).

2.3.2.2.b. Permeation of sodium fluorescein and propranolol hydrochloride into the bladder wall

Figure 2.6A shows the amount of each marker permeated across the mucosa over time, normalised to the surface area of the urothelium. This was calculated by summing the amount of drug extracted from the detrusor muscle and any drug recovered from the receiver compartment. Figure 2.6B shows the successful removal of the mucosa (urothelium and lamina propria (U and LP)) leaving the underlying detrusor muscle (M). Apparent permeability coefficients (K_p), calculated by normalising the transurothelial flux to the concentration of drug applied to the urothelium at time zero, were 5.1 x 10^{-6} cm s^{-1} and 1.3 x 10^{-6} cm s^{-1} for propranolol hydrochloride and sodium fluorescein respectively. Over 6.5 h the permeation rate of both molecules was constant, indicative of little change in the tissue's behaviour. Furthermore the calculated K_p values were distinct and, although there are no directly comparable figures available in the literature, in the same range as those reported for other small molecules such as urea (5.1 x 10^{-05} cm s^{-1})[97] and ammonia (6.4 x 10^{-05} cm s^{-1})[97].

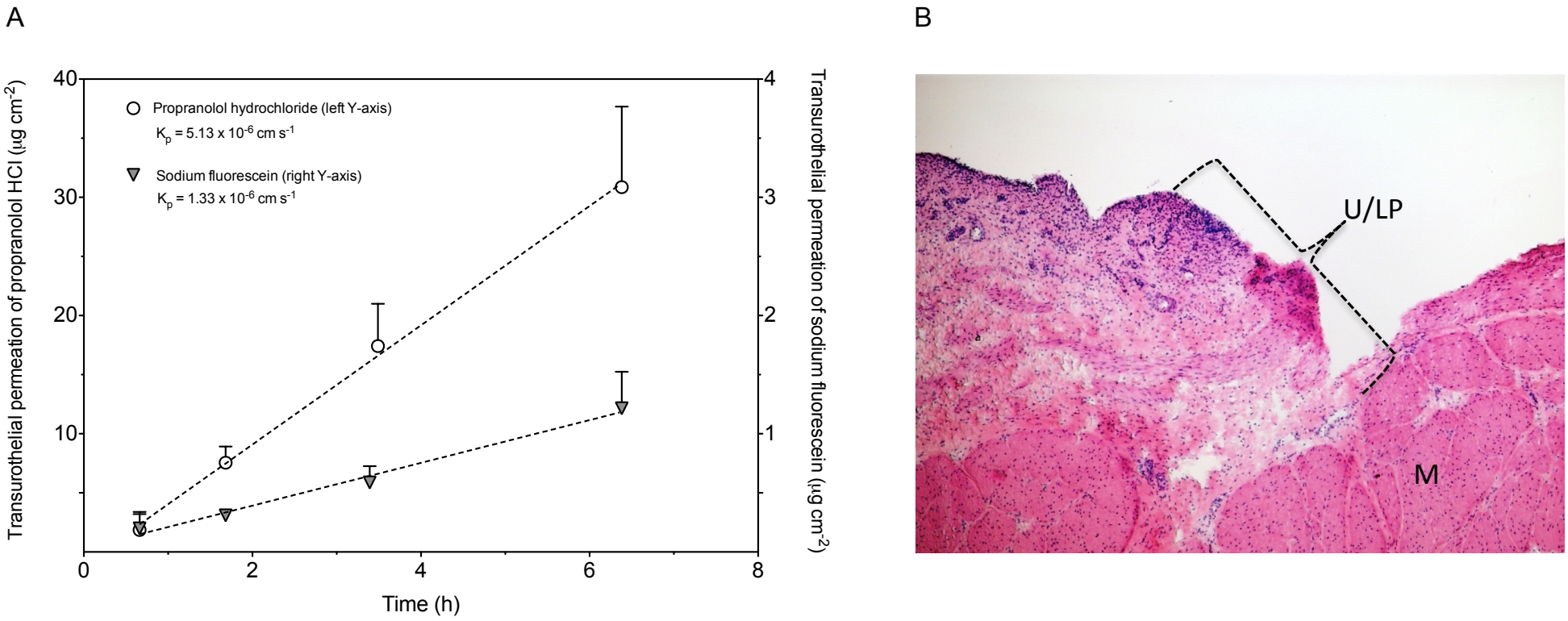

Figure 2.6. (A) Permeation profile of 0.1 mM sodium fluorescein and 1 mM propranolol hydrochloride across porcine mucosa. Permeability coefficients (K_p, cm s^{-1}) were calculated by normalising the flux (J, µg cm^{-2} s^{-1}) to the dosing concentration. (n = 6 tissue samples from 2 bladders ± SD). (B) Photomicrograph of H & E stained bladder wall with the mucosa excised from half the section (400 x). U / LP – urothelium and lamina propria (mucosa), M – detrusor muscle.

2.3.2.3. Transepithelial electrical resistance (TEER)

TEER is an established method of investigating the paracellular permeability of the urothelium[98–100]. By assessing the resistance across bladder mucosa, the maintenance of umbrella cell TJs crucial to the barrier function of the urothelium can be evaluated. Absolute TEER and deviation from baseline TEER across the bladder mucosa was investigated after the application of saline (negative control) and ketorolac to the urothelium (Figure 2.7). At time zero, average TEER values were 8.3 and 7.8 kΩ cm^2 for the saline and ketorolac samples respectively; indicative of tight epithelia[101]. Although not previously reported for *ex vivo* porcine bladder, these values are comparable to those in the literature for fully functional *in vitro* human (3.0 kΩ cm^2)[59] and porcine (6.7 kΩ cm^2)[102] urothelium. TEER values decreased marginally with time and at the end of the experiment (2.5 h) mucosa exposed to saline and ketorolac exhibited 77 and 78 % of baseline TEER respectively. This decrease was within range of what can be expected for *ex vivo* experiments such as this. There was no significant difference in relative or absolute TEER reduction between samples exposed to saline or ketorolac at any timepoint investigated ($p > 0.05$, calculated by unpaired t - test). In agreement with these observations *ex vivo* rat bladder tissue has been shown to retain transurothelial barrier function for several hours post excision[99].

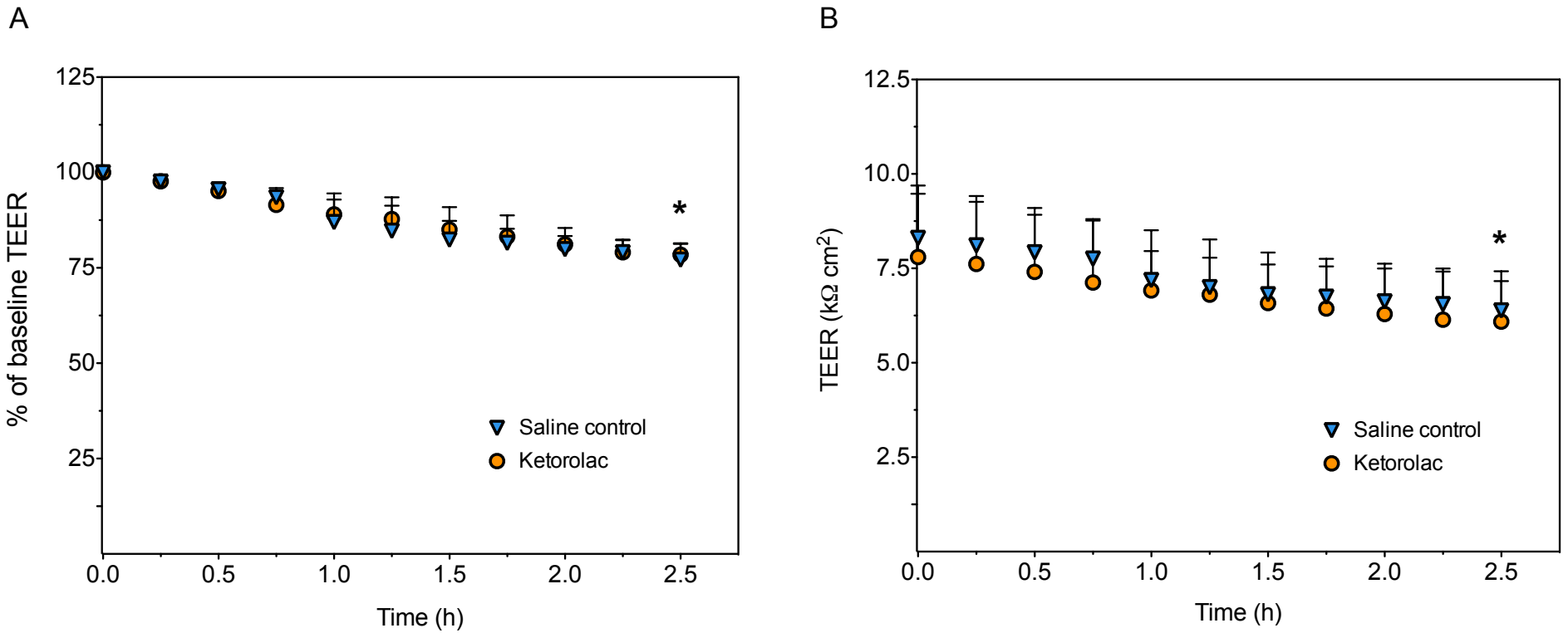

Figure 2.7. Percentage (A) and absolute (B) decrease in transepithelial electrical resistance (TEER) across *ex vivo* porcine bladder mucosa exposed to saline or ketorolac. There was no significant difference in percentage or absolute TEER reduction at any timepoint (*p > 0.05 at 2.5 h, calculated using unpaired t - test). (n = 4 bladders ± SD).

2.3.2.4. Scanning electron microscopy (SEM)

In addition to alterations in TJ integrity, an increase in permeability may result from epithelial cell loss[100]. SEM was used to microscopically examine the urothelial surface of the *ex vivo* porcine bladder tissue (Figure 2.8). Tissue exposed to saline (negative control) and ketorolac displayed normal surface morphology with no evidence of significant damage. Scallop - shaped, polygonal umbrella cells with intact tight junctions were evident and closely resembled that reported by others (Figure 2.9A)[103–105]. The morphology of the saline and ketorolac samples (Figure 2.8C - D and E - F respectively) did not differ from the control tissue fixed on - site at the abattoir (Figure 2.8A - B). Protamine sulfate was used as a positive control (Figure 2.8G - H) as it has been shown to cause immediate umbrella cell sloughing accompanied by a significant decrease in TEER across the urothelium[103]. Close examination of the urothelium exposed to protamine (Figure 2.9B) showed a significant loss of integrity, evidenced by widened TJs, extensive cell lysis and the apparent shedding of the umbrella cell's apical membrane.

In combination, results of paracellular permeation, TEER and SEM analysis suggested the *ex vivo* porcine bladder tissue was appropriate for use in our studies. This is in agreement with others who have used *ex vivo* porcine bladder tissue in a similar manner for similar lengths of time[66,67,69].

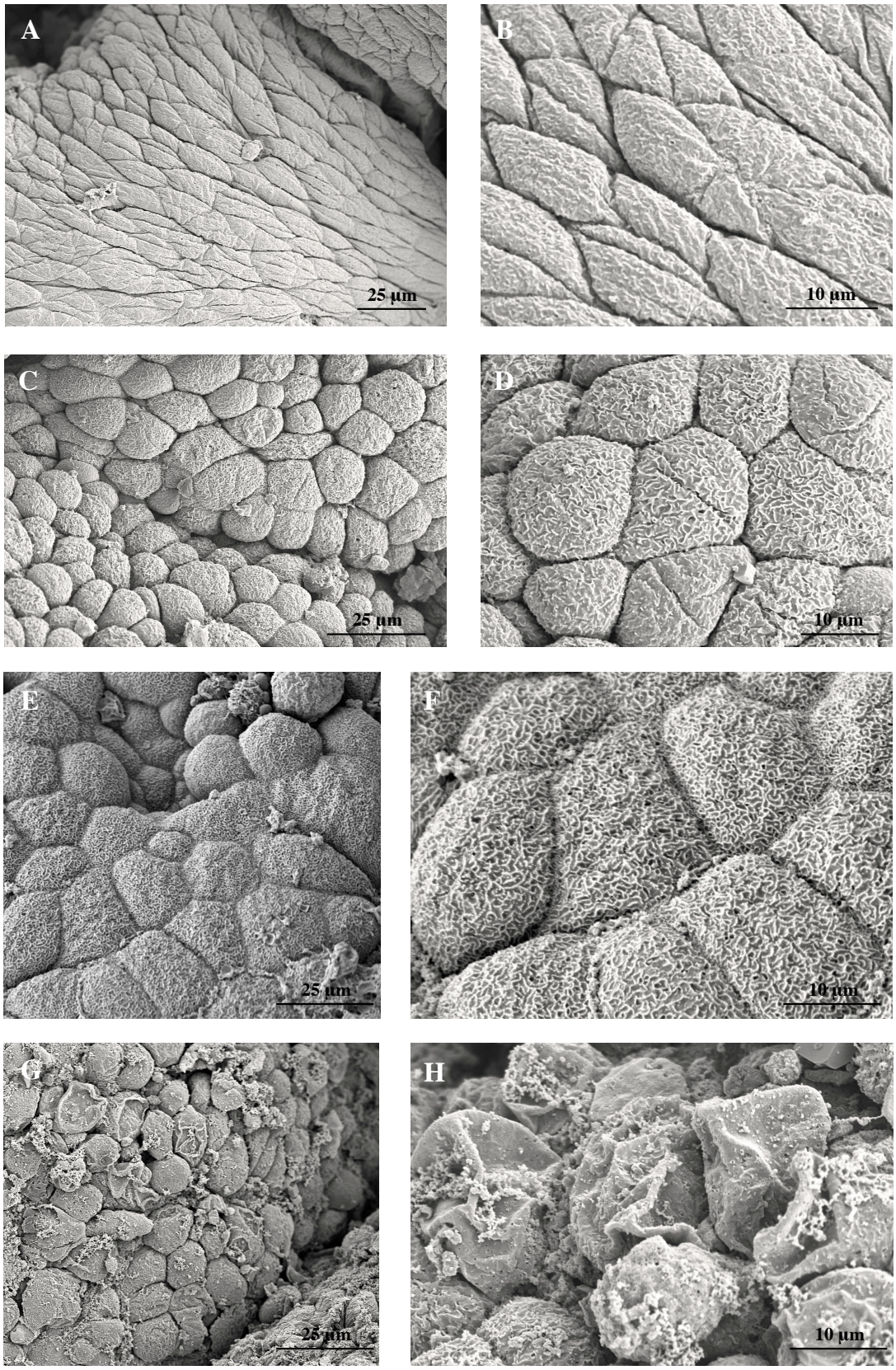

Figure 2.8. SEM of *ex vivo* porcine bladder tissue. Control samples fixed on - site at the abattoir within 5 min of excision (A and B). Samples loaded In Franz - type diffusion cells and exposed to saline (C and D), 1.1 mg ml^{-1} ketorolac (E and F) and 10 mg ml^{-1} protamine sulfate (G and H) for 90 min.

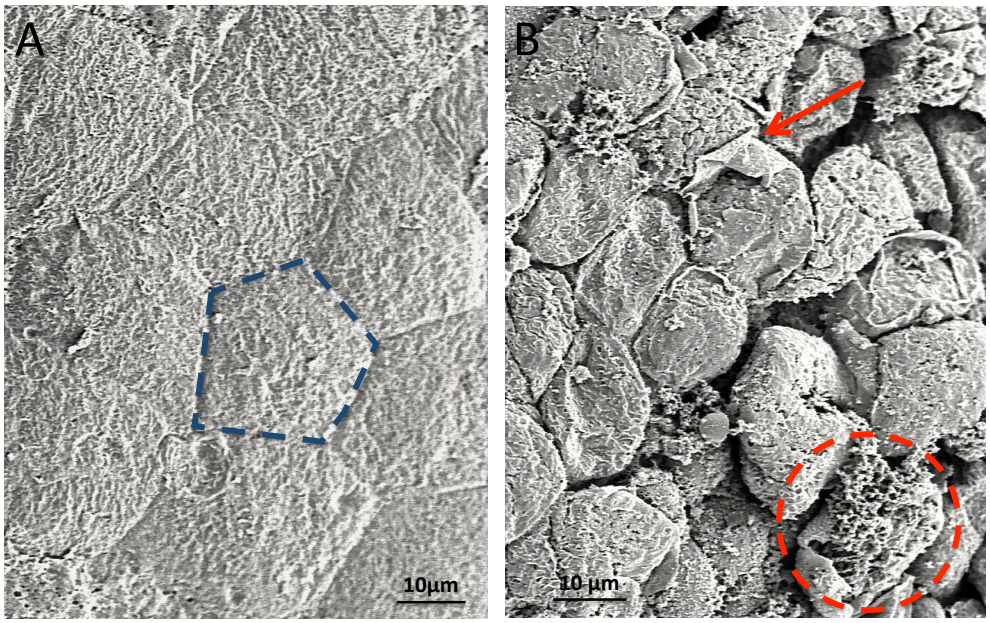

Figure 2.9. A closer look at SEM micrographs of *ex vivo* porcine bladder tissue loaded into Franz - type diffusion cells and treated with 1.1 mg ml^{-1} ketorolac (A) and 10 mg ml^{-1} protamine sulfate (B) for 90 min. Tissue exposed to ketorolac displayed normal tissue morphology with exemplar polygonal umbrella cells (traced blue for clarity). Umbrella cell membrane shedding (red arrow) and whole cell lysis (red circle) was evident in the protamine group.

2.3.3. Evaluation of the delivery of ketorolac to the bladder wall

Ketorolac, although not commonly used in the UK, has an established role in reducing post - operative pain in the US[106] and has been shown effective in the relief of renal, ureteral and bladder pain[107–109]. BSC's decision to use ketorolac in the Lexington™ stent was the result of a clinical study evaluating the effectiveness of localised, intravesical therapies to reduce ureteral SRD[22]. They found that an intravesical solution of ketorolac (1.1 mg ml^{-1}) caused a significant reduction in SRD when compared to the control instillation (0.9 % saline). While this provides an opportunity for developing more advanced local delivery techniques such as the Lexington™ stent, its translation into effective patient management will undoubtedly benefit from an understanding of the rate and extent of delivery of ketorolac into the bladder wall. By gathering information regarding the barrier properties of the urothelium and investigating, in quantitative terms, ketorolac delivery, we can begin to make predictions about the viability of delivering ketorolac intravesically and the bladder tissue concentrations necessary to bring

about a therapeutic effect. We chose therefore to use a 1.1 mg ml^{-1} ketorolac solution in our *ex vivo* studies.

2.3.3.1 Analysis of ketorolac tromethamine

HPLC analysis of ketorolac produced narrow, near symmetrical peaks eluting at a stable retention time (Figure 2.11). Analyte quantitation (based on peak area) was calculated using an external standard solution ranging in concentration from 0.0011 to 11 μg ml^{-1} (Figure 2.10). Calibration curves were run in triplicate to ensure reproducibility and showed high linearity across the expected analyte concentration range. The LLOD and LLOQ was 0.0173 and 0.0575 μg ml^{-1} respectively. There was minimal analyte peak interference in the homogenised bladder tissue and background noise was low enabling good precision around the LLOQ (Figure 2.11C).

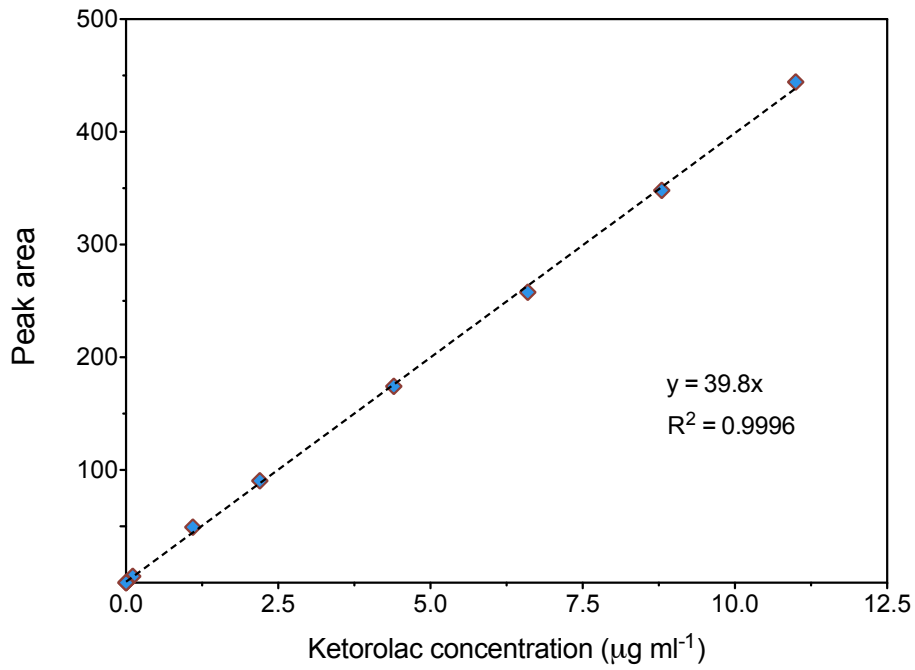

Figure 2.10. External standard calibration curve used in the HPLC analysis of ketorolac.

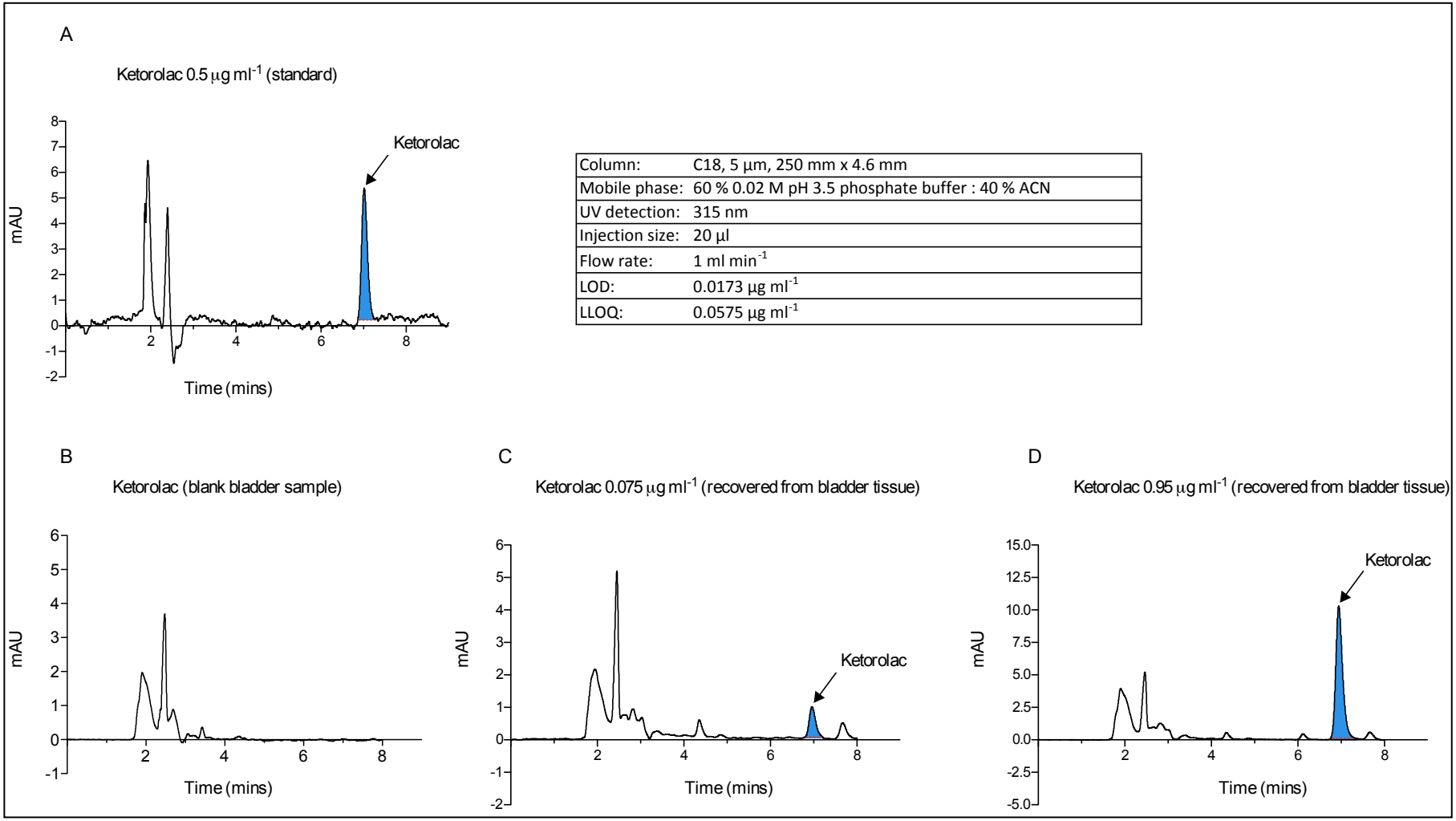

Figure 2.11. Example HPLC chromatograms showing the analysis of a calibration standard (A), blank tissue sample (B), tissue recovery near the LLOQ (C) and higher concentration tissue recovery (D) of ketorolac.

2.3.3.2 Permeation of ketorolac across the urothelium

In section 2.2.6.1, where the permeation of sodium fluorescein and propranolol hydrochloride was investigated, the mucosa was separated from the detrusor muscle prior to drug determination. The amount permeated across the mucosa was then calculated by summing drug extracted from the detrusor muscle and receiver compartment. This was a precautionary measure to ensure no surface - adsorbed drug was included in permeability calculations. In this experiment the two layers were not separated. Rather the amount permeated was calculated by summing drug extracted from the entire tissue and receiver compartment. This was a case of experimental improvement; studies showed that after several saline rinses of the urothelial surface, any remaining surface - adsorbed drug was within the standard deviation (SD) of the drug extracted from the tissue (Figure 2.12). Therefore any drug extracted from the tissue following the saline rinse was considered to have permeated the urothelium making the separation step unnecessary. After the third saline rinse, the amount of drug extracted (0.1 % of the applied dose) was more than 10 fold smaller than the SD of that extracted from the tissue (1.3 % of the applied dose). Additional washes resulted in similar values suggesting at this point drug may be drawn out of the umbrella cells. Considering this, a 3 x 1 ml saline rinse protocol was considered sufficient for the removal of surface - adsorbed drug.

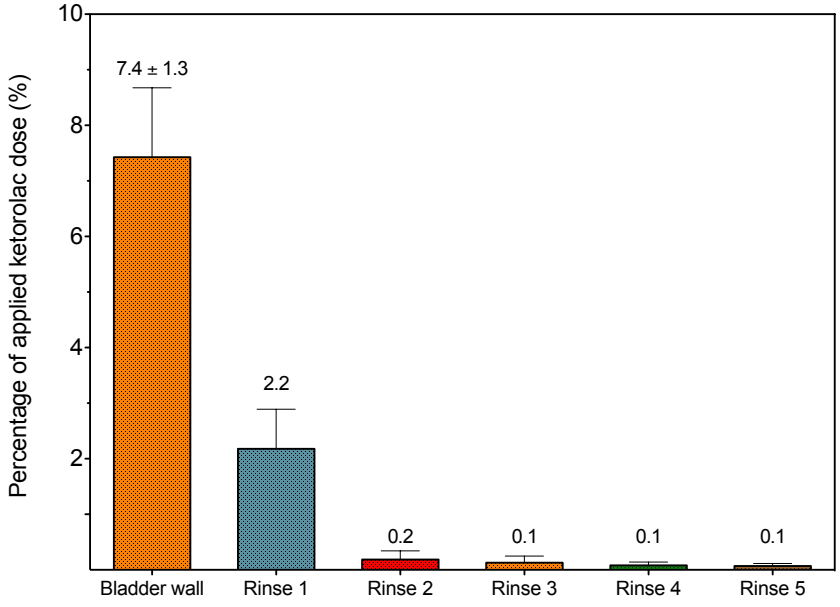

Figure 2.12. Percentage of applied ketorolac dose recovered from a 5 h application of a 0.5 ml aliquot of 1.1 mg ml^{-1} ketorolac solution according to the methods described in section 2.2.7.1. (n = 10 tissue samples from 2 bladders ± SD).

Figure 2.13A shows that ketorolac was capable of permeating across the urothelium. Drug permeated in a linear fashion and after 5 h approximately 60 μg cm^{-2} of ketorolac had permeated into the bladder wall. An apparent transurothelial K_p value of 2.63 x 10^{-6} cm s^{-1} was calculated by normalising the flux to the concentration applied to the donor chamber at time zero. Results of mass balance analysis showed good recovery of drug from the Franz - cell apparatus with an average 95.2 % of the applied ketorolac dose recovered per sample (Figure 2.13B). Over the 5 h experiment the majority of drug remained in the donor chamber, whilst the amount accumulating in the bladder tissue increased steadily with time. Drug was only present in the receiver compartment for the 5 h time point, constituting ~ 0.2 % of the applied ketorolac dose.

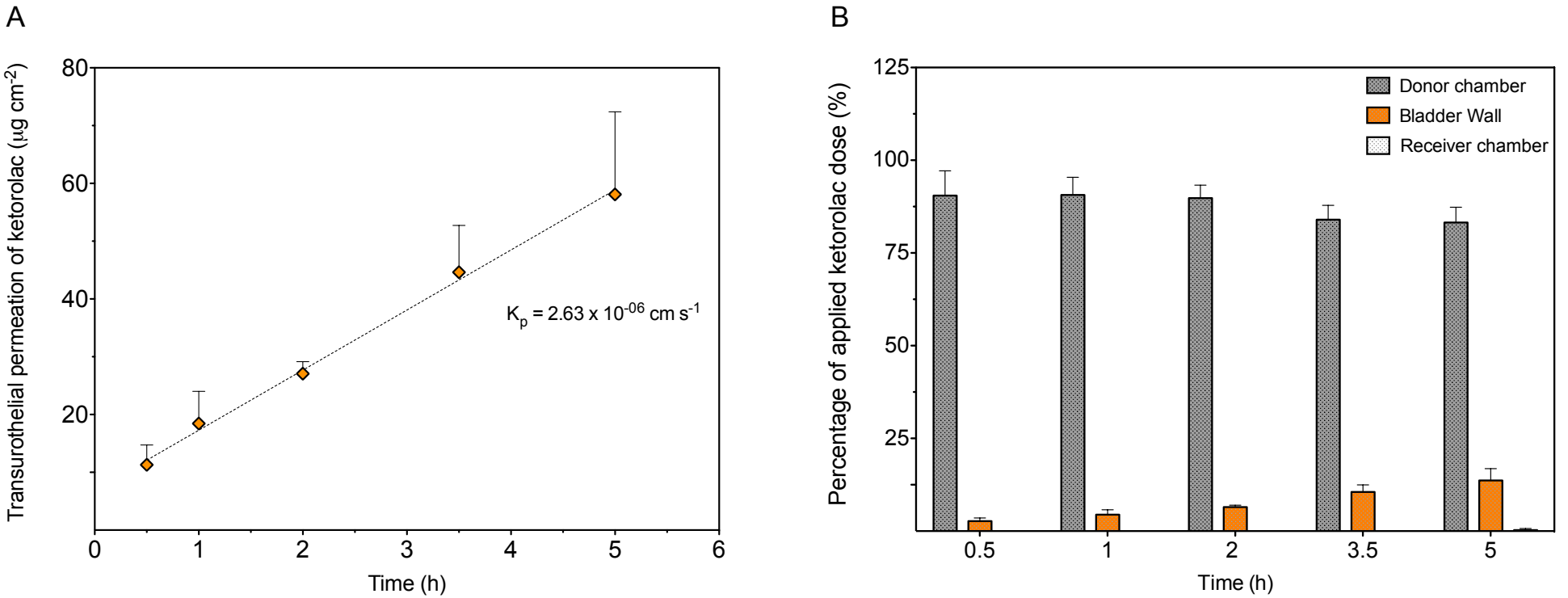

Figure 2.13. (A) Permeation profile of 1.1 mg ml^{-1} ketorolac across porcine bladder urothelium, permeability coefficients (K_p, cm s^{-1}) were calculated by normalising the flux (J, µg cm^{-2} s^{-1}) to the dosing concentration. (B) Mass balance analysis of the recovery of ketorolac from the Franz - type cell setup per sampling timepoint. (n = 4 tissue samples from 2 bladders ± SD).

2.3.3.2 Distribution of ketorolac into the bladder wall

According to the mean urination time reported in the BSC intravesical study[22], ketorolac would have been voided from the bladder after ~ 90 min. Given this, an endpoint of 90 min was chosen in this study. To understand the distribution of ketorolac into the different layers of the bladder wall, a concentration - depth profile was constructed (Figure 2.14A). Tissue - layer depths for porcine bladder wall were based on those reported in the literature[66]. Drug concentrations declined with tissue depth with average concentrations of 400, 141 and 21 μg g^{-1} achieved in the urothelium, lamina propria and detrusor muscle respectively (Figure 2.14B). In agreement with others who have performed similar studies on *ex vivo* porcine bladder, our distribution study shows a linear decrease in drug concentration over the urothelium, followed by an exponential decrease in concentration over the lamina propria and detrusor muscle[66,69]. After 90 min the average concentration in the whole bladder wall was calculated to be 87 μg g^{-1} (Figure 2.14B).

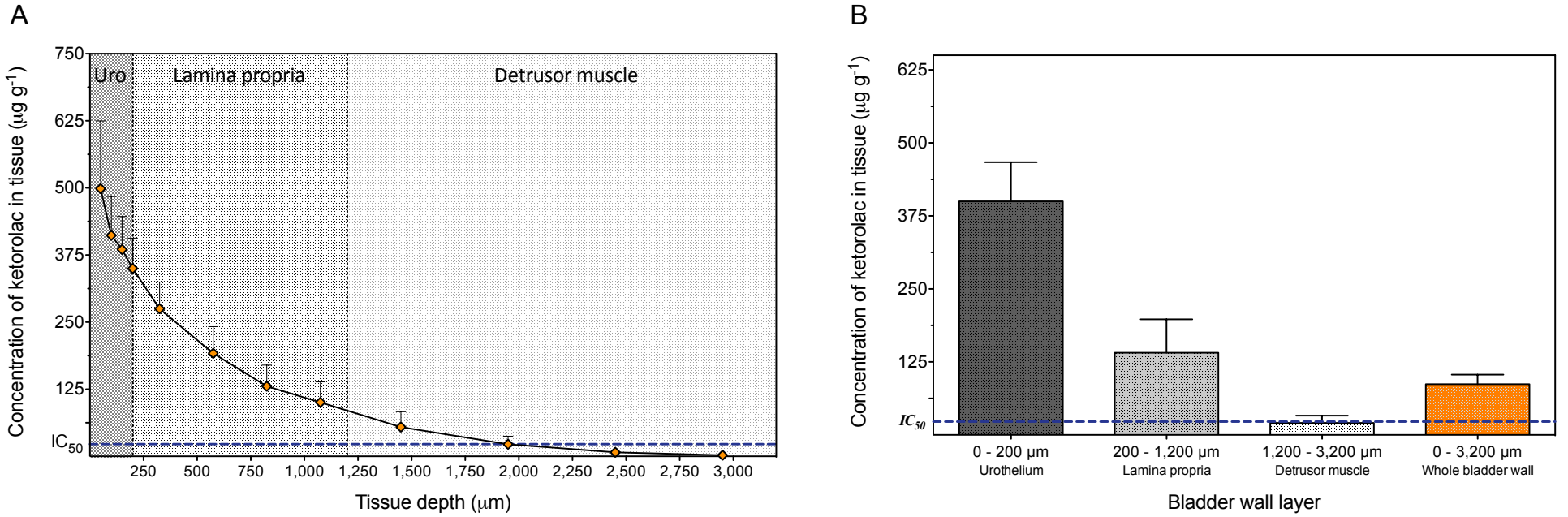

Figure 2.14. (A) Concentration - depth profile of ketorolac into porcine bladder wall after 90 min. For pooled samples, tissue depths were expressed as the midpoint depth of the sections. IC_{50} represents the top - end value reported at COX - 1 and COX - 2 for ketorolac[110]. (B) Corresponding average ketorolac concentrations achieved in the urothelium (0 - 200 μm), lamina propria (200 – 1,200 μm), detrusor muscle (1,200 – 3,200 μm) and whole bladder wall (0 – 3,200 μm) after 90 min (B). (n = 5 bladders ± SD).

Although the exact aetiology of SRD is unclear, one proposed theory is that the bladder coil rubs against the urothelium resulting in irritation, inflammation, spasm and pain[111]. BSC conducted an in - house porcine study (details confidential) that stipulated the unilateral placement of a double - J ureteral stent for 72 h. Necropsy findings provide a good example of the urothelial irritation caused by the ureteral stent (Figure 2.15). Prostaglandins have been shown to produce contractions of isolated detrusor muscle *in vitro* and *in vivo*[112] and their synthesis can be initiated by urothelial damage[113]. Blocking prostaglandin synthesis with indomethacin, a non - selective cyclooxygenase (COX) inhibitor, has recently been shown to decrease acetylcholine - mediated autonomic contractions in the isolated bladder[114]. In addition, afferent C - fibres terminating in the urothelium and lamina propria are known to respond to prostaglandins released (from cells in the urothelium and lamina propria) in response to injury[115]; suggesting the possibility that, by inhibiting mediators released from urothelial and lamina propria cells, intravesically delivered ketorolac may provide pain relief in part via modulation of sensory pathways. The NSAID ketorolac non - selectively inhibits COX - 1 and COX - 2, the enzymes responsible for the production of prostaglandins and has been shown to inhibit ureteral contractility *in vitro*[116]. It follows that by reducing inflammation and spasm, ketorolac has the potential to be beneficial in reducing SRD.

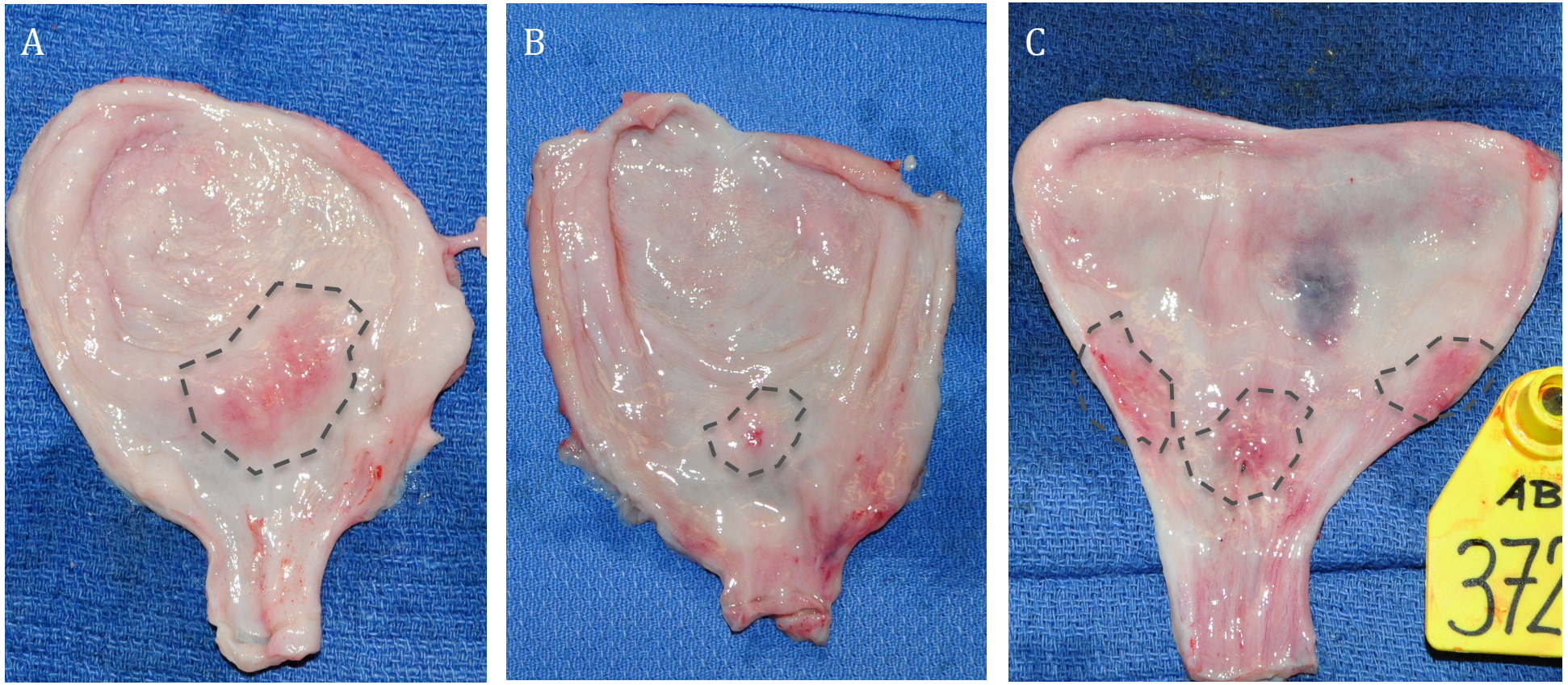

Figure 2.15. Necropsy examination of porcine bladders from three test animals 72 h post placement of a ureteral stent (A - C). Irritation and associated erythema near the ureteral orifice, where the distal coil of the ureteral stent resides, is highlighted.

The production of prostaglandins within the bladder wall is well established with synthesis occurring not only in the detrusor muscle but also within the urothelium and lamina propria[117–119], all of these regions can therefore be taken to be targets for the IDD of ketorolac. After 90 min the total concentration in these target regions was 87 μg g^{-1}. The reported potency of ketorolac, in terms of IC_{50} values, varies widely with top end values of 31.5 and 60.5 μM for COX - 1 and COX - 2 respectively[110]. Taking the average bladder wall concentration of 87 μg g^{-1} and making the assumption that 1 g of bladder tissue has a volume of ~ 1 cm^3, a target bladder wall concentration of 231.1 μM was achieved after 90 min. This equates to a predictive ketorolac concentration of at least seven times the IC_{50} for COX - 1 and three and a half times the IC_{50} for COX - 2 at the site of action (Figure 2.14B), suggesting that levels of ketorolac in the bladder wall could indeed be sufficient to provide an anti - inflammatory effect.

It is important to point out however that these studies are *ex vivo* and therefore have inherent limitations. Systemic clearance and dilution of the intravesical instillation by urine are notably absent in our model. As shall be discussed later in this thesis, these processes can have significant effects on the delivery of drug into the bladder wall. Subsequently, concentrations achieved in these *ex vivo* studies likely overestimate the *in vivo* situation.

2.4. Conclusions

This chapter described and validated an *ex vivo* porcine bladder tissue model for studying the barrier properties of the urothelium and investigating, in quantitative terms, drug delivery into the bladder wall. Using this model the transurothelial permeation of the NSAID ketorolac was studied and its delivery into the different layers of the bladder wall investigated. Fundamental studies such as these can be used to inform on the viability of delivering drugs intravesically *in vivo*. The data suggest that, in the *ex vivo* setting, the levels of ketorolac delivered to the bladder wall following local application to the urothelium would be pharmacodynamically appropriate to provide an anti - inflammatory effect. In practice local delivery strategies to the urinary tract are largely guided by clinical outcome, with little

outcome, with little information available on target drug concentrations. Investigations such as those described here yield quantitative *ex vivo* data that can be used to rationally design new transurothelial drug delivery strategies and optimise existing intravesical drug regimens.

2.5. Reference List

1. Yachia D, Paterson PJ. Stenting the Urinary System. 2nd ed. London; New York: CRC Press; 2004.

2. Chew BH, Knudsen BE, Denstedt JD. The use of stents in contemporary urology. Curr Opin Urol. 2004 Mar;14(2):111–5.

3. Finney RP. Experience with new double J ureteral catheter stent. J Urol. 1978 Dec;120(6):678–81.

4. Hegde P, Giridhar V, Natarajan K. Migration of forgotten stent into renal pelvis. Indian J Urol. 2011;27(2):282.

5. Siggers JH, Waters S, Wattis J, Cummings L. Flow dynamics in a stented ureter. Math Med Biol. 2009 Mar;26(1):1–24.

6. Joshi HB, Keeley Jr FX, Timoney AG. Having a Ureteric Stent - What to Expect and How to Manage [Internet]. Bristol Urological Institute. 2000 [cited 2014 Aug 28]. Available from: http://www.bui.ac.uk/PatientInfo/ureterstent.html

7. Joshi HB, Stainthorpe A, MacDonagh R, Keeley F, others. Indwelling ureteral stents: evaluation of symptoms, quality of life and utility. J Urol. 2003;169(3):1065–9.

8. Uthappa MC, Cowan NC. Retrograde or antegrade double-pigtail stent placement for malignant ureteric obstruction? Clin Radiol. 2005 May;60(5):608–12.

9. Lennon G, Thornhill J, Sweeney P, Grainger R, McDermott T, Butler M. “Firm” versus “soft” double pigtail ureteric stents: a randomised blind comparative trial. Eur Urol. 1995;28(1):1–5.

10. Joshi HB, Chitale S, Nagarajan M, Irving S, Browning A, Biyani C, et al. A prospective randomized single-blind comparison of ureteral stents composed of firm and soft polymer. J Urol. 2005;174(6):2303–6.

11. Erturk E, Sessions A, Joseph JV. Impact of ureteral stent diameter on symptoms and tolerability. J Endourol. 2003;17(2):59–62.

12. Dunn MD, Portis AJ, Kahn SA, Yan Y, Shalhav AL, Elbahnasy AM, et al. Clinical effectiveness of new stent design: randomized single-blind comparison of tail and double-pigtail stents. J Endourol. 2000;14(2):195–202.

13. Chew BH, Lange D, Paterson RF, Hendlin K, Monga M, Clinkscales KW, et al. Next generation biodegradable ureteral stent in a Yucatan pig model. J Urol. 2010;183(2):765–71.

14. Pengfei S, Yutao L, Jie Y, Wuran W, Yi D, Hao Z, et al. The results of ureteral stenting after ureteroscopic lithotripsy for ureteral calculi: a systematic review and meta-analysis. J Urol. 2011 Nov;186(5):1904–9.

15. Leibovici D, Cooper A, Lindner A, Ostrowsky R, Kleinmann J, Velikanov S, et al. Ureteral stents: morbidity and impact on quality of life. Isr Med Assoc J. 2005 Aug;7(8):491–4.

16. Joshi HB, Okeke A, Newns N, Keeley Jr F, Timoney A. Characterization of urinary symptoms in patients with ureteral stents. Urology. 2002;59(4):511–6.

17. Dyer RB, Chen MY, Zagoria RJ, Regan JD, Hood CG, Kavanagh PV. Complications of Ureteral Stent Placement. RadioGraphics. 2002 Sep 1;22(5):1005–22.

18. Saltzman B. Ureteral stents. Indications, variations, and complications. Urol Clin North Am. 1988 Aug;15(3):481–91.

19. Miyaoka R, Monga M. Ureteral stent discomfort: Etiology and management. Indian J Urol. 2009;25(4):455–60.

20. Life Science Intelligence. U.S. Markets for non-vascular stents: Market analysis for 2011-2014 [Internet]. Huntington Beach, CA; 2011 [cited 2014 Jul 20] p. 140. Available from: https://www.lifescienceintelligence.com/market-reports-page.php?id=A255

21. Krambeck AE, Walsh RS, Denstedt JD, Preminger GM, Li J, Evans JC, et al. A novel drug eluting ureteral stent: a prospective, randomized, multicenter clinical trial to evaluate the safety and effectiveness of a ketorolac loaded ureteral stent. J Urol. 2010;183(3):1037–43.

22. Beiko D, Watterson J, Knudsen B, others. A double-blinded prospective randomized controlled trial assessing the safety and efficacy of intravesical agents for ureteral stent symptoms following extracorporeal shockwave lithotripsy. J Endourol. 2004;18(8):723–30.

23. Buckley MM, Brogden RN. Ketorolac. A review of its pharmacodynamic and pharmacokinetic properties, and therapeutic potential. Drugs. 1990 Jan;39(1):86–109.

24. Chew BH, Davoudi H, Li J, Denstedt JD. An In Vivo Porcine Evaluation of the Safety, Bioavailability, and Tissue Penetration of a Ketorolac Drug-Eluting Ureteral Stent Designed to Improve Comfort. J Endourol. 2010;24(6):1023–9.

25. Madbouly K. Intravesical bacillus Calmette-Guerin for bladder cancer: What is known? What is not? What is next? Urol Ann. 2013;5(2):108–9.

26. Zargar H, Aning J, Ischia J, So A, Black P. Optimizing intravesical mitomycin C therapy in non-muscle-invasive bladder cancer. Nat Rev Urol. 2014 Apr;11(4):220–30.

27. Colombo R, Rocchini L, Suardi N, Benigni F, Colciago G, Bettiga A, et al. Neoadjuvant short-term intensive intravesical mitomycin C regimen compared with weekly schedule for low-grade recurrent non-muscle-invasive bladder cancer: preliminary results of a randomised phase 2 study. Eur Urol. 2012 Nov;62(5):797–802.

28. Wientjes MG, Badalament RA, Au JL. Use of pharmacologic data and computer simulations to design an efficacy trial of intravesical mitomycin C therapy for superficial bladder cancer. Cancer Chemother Pharmacol. 1993;32(4):255–62.

29. Morales A, Eidinger D, Bruce AW. Intracavitary Bacillus Calmette-Guerin in the treatment of superficial bladder tumors. J Urol. 1976 Aug;116(2):180–3.

30. Babjuk M, Burger M, Zigeuner R, Shariat SF, van Rhijn BWG, Compérat E, et al. EAU guidelines on non-muscle-invasive urothelial carcinoma of the bladder: update 2013. Eur Urol. 2013 Oct;64(4):639–53.

31. Maffezzini M, Campodonico F, Manuputty EE, Puntoni M, Martelli A, Marini V, et al. Systemic absorption and pharmacokinetics of single-dose early intravesical mitomycin C after transurethral resection of non-muscle-invasive bladder cancer. Urology. 2013 Aug;82(2):400–4.

32. Chai M, Wientjes MG, Badalament RA, Burgers JK, Au JL. Pharmacokinetics of intravesical doxorubicin in superficial bladder cancer patients. J Urol. 1994;152(2):374–8.

33. Witjes JA, van der Heijden AG, Vriesema JLJ, Peters GJ, Laan A, Schalken JA. Intravesical gemcitabine: a phase 1 and pharmacokinetic study. Eur Urol. 2004 Feb;45(2):182–6.

34. Krause P, Fuhr U, Schnitker J, Albrecht U, Stein R, Rubenwolf P. Pharmacokinetics of intravesical versus oral oxybutynin in healthy adults: results of an open label, randomized, prospective clinical study. J Urol. 2013 Nov;190(5):1791–7.

35. Hsieh J-T, Zhou J, Gore C, Zimmern P. R11, a novel cell-permeable peptide, as an intravesical delivery vehicle. BJU Int. 2011 Nov;108(10):1666–71.

36. Hwang T-L, Fang C-L, Chen C-H, Fang J-Y. Permeation enhancer-containing water-in-oil nanoemulsions as carriers for intravesical cisplatin delivery. Pharm Res. 2009 Oct;26(10):2314–23.

37. Lee H, Cima MJ. An intravesical device for the sustained delivery of lidocaine to the bladder. J Control Release. 2011 Jan 20;149(2):133–9.

38. Song D, Wientjes MG, Au JL. Bladder tissue pharmacokinetics of intravesical taxol. Cancer Chemother Pharmacol. 1997;40(4):285–92.

39. Lu Z, Yeh T-K, Wang J, Chen L, Lyness G, Xin Y, et al. Paclitaxel gelatin nanoparticles for intravesical bladder cancer therapy. J Urol. 2011 Apr;185(4):1478–83.

40. Leakakos T, Ji C, Lawson G, Peterson C, Goodwin S. Intravesical administration of doxorubicin to swine bladder using magnetically targeted carriers. Cancer Chemother Pharmacol. 2003 Jun;51(6):445–50.

41. Baranowska-Kortylewicz J, Dalrymple GV, Harrison KA, Holdeman KP, Sharp JG, Cohen SM, et al. On the safety of 5-[125I]iodo-2'-deoxyuridine--Preclinical evaluation in swine. Acta Oncol. 1996;35(7):925–33.

42. Harrison KA, Dalrymple GV, Baranowska-Kortylewicz J, Holdeman KP, Schneiderman MH, Lieberman RP, et al. Radiolabeled iododeoxyuridine: safety evaluation. J Nucl Med. 1996 Apr;37(4 Suppl):13S – 16S.

43. Arentsen HC, Hulsbergen-Van de Kaa CA, Jansen CFJ, Maj R, Leoni LM, Oosterwijk E, et al. Pharmacokinetics and toxicity of intravesical TMX-101: a preclinical study in pigs. BJU Int. 2011 Oct;108(7):1210–4.

44. Tunc L, Resorlu B, Unsal A, Oguz U, Diri A, Gozen AS, et al. In vivo porcine model for practicing retrograde intrarenal surgery. Urol Int. 2014;92(1):64–7.

45. Sibley G. An experimental model of detrusor instability in the obstructed pig. Br J Urol. 1985;57(3):292–8.

46. Tortora GJ, Derrickson BH. Principles of Anatomy and Physiology. 12th ed. John Wiley & Sons; 2008.

47. Andersson K-E, Arner A. Urinary bladder contraction and relaxation: physiology and pathophysiology. Physiol Rev. 2004 Jul;84(3):935–86.

48. Hendricksen K, Moonen PMJ, van der Heijden AG, Molkenboer-Kuenen J, Hulsbergen-van de Kaa CA, Witjes JA. Potential and toxicity of intravesical pemetrexed: a preclinical study in pigs. Clin Cancer Res. 2006 Apr 15;12(8):2597–601.

49. Witjes JA, Vriesema JLJ, van der Heijden AG, Peters GJ, Schalken JA. Pharmacokinetics of intravesical gemcitabine: a preclinical study in pigs. Eur Urol. 2003 Nov;44(5):615–9.

50. Swindle MM. Urinary System and Adrenal Glands. Swine in the Laboratory: surgery, anesthesia, imaging, and experimental techniques. 2nd ed. Florida: CRC Press; 2007.

51. Wientjes MG, Badalament RA, Au JL. Penetration of intravesical doxorubicin in human bladders. Cancer Chemother Pharmacol. 1996;37(6):539–46.

52. Wientjes MG, Badalament RA, Wang RC, Hassan F, Au JL. Penetration of mitomycin C in human bladder. Cancer Res. 1993;53(14):3314.

53. Steinberg PL, Ghavamian R. Robotic-assisted radical cystectomy: current technique and outcomes. Expert Rev Anticancer Ther. 2012 Jul;12(7):913–7.

54. Bolenz C, Trojan L, Gabriel U, Honeck P, Wendt-Nordahl G, Schaaf A, et al. Cellular uptake and ex vivo urothelial penetration by oligodeoxynucleotides for optimizing treatment of transitional cell carcinoma. Anal Quant Cytol. 2008 Oct;30(5):265–73.

55. Bilensoy E, Sarisozen C, Esendağlı G, Doğan AL, Aktaş Y, Şen M, et al. Intravesical cationic nanoparticles of chitosan and polycaprolactone for the delivery of Mitomycin C to bladder tumors. Int J Pharm. 2009 Apr 17;371(1–2):170–6.

56. Perrone RD, Johns C, Grubman SA, Moy E, Lee DW, Alroy J, et al. Immortalized human bladder cell line exhibits amiloride-sensitive sodium absorption. Am J Physiol. 1996 Jan;270(1 Pt 2):F148–53.

57. Huygens A, Kamuhabwa AR, Roskams T, van Cleynenbreugel B, van Poppel H, de Witte PAM. Permeation of hypericin in spheroids composed of different grade transitional cell carcinoma cell lines and normal human urothelial cells. J Urol. 2005 Jul;174(1):69–72.

58. Baker SC, Shabir S, Southgate J. Biomimetic urothelial tissue models for the in vitro evaluation of barrier physiology and bladder drug efficacy. Mol Pharm. 2014 Jul 7;11(7):1964–70.

59. Cross WR, Eardley I, Leese HJ, Southgate J. A biomimetic tissue from cultured normal human urothelial cells: analysis of physiological function. Am J Physiol Renal Physiol. 2005 Aug;289(2):F459–68.

60. Negrete HO, Lavelle JP, Berg J, Lewis SA, Zeidel ML. Permeability properties of the intact mammalian bladder epithelium. Am J Physiol Renal Physiol. 1996;271(4):F886.

61. Kerec M, Švigelj V, Bogataj M, Mrhar A. The enhancement of pipemidic acid permeation into the pig urinary bladder wall. Int J Pharm. 2002 Jun 20;240(1-2):33–6.

62. Di Stasi SM, Giannantoni A, Massoud R, Cortese C, Vespasiani G, Micali F. Electromotive administration of oxybutynin into the human bladder wall. J Urol. 1997 Jul;158(1):228–33.

63. Tammela T, Wein AJ, Monson FC, Levin RM. Urothelial permeability of the isolated whole bladder. Neurourol Urodyn. 1993;12(1):39–47.

64. Tringali G, Lisi L, Bettella F, Renier D, Di Stasi SM, Navarra P. The in vitro rabbit whole bladder as a model to investigate the urothelial transport of anticancer agents The ONCOFID-P paradigm. Pharmacol Res. 2008 Dec;58(5-6):340–3.

65. Grabnar I, Bogataj M, Mrhar A. Influence of chitosan and polycarbophil on permeation of a model hydrophilic drug into the urinary bladder wall. Int J Pharm. 2003;256(1-2):167–73.

66. Tsallas A, Jackson J, Burt H. The uptake of paclitaxel and docetaxel into ex vivo porcine bladder tissue from polymeric micelle formulations. Cancer Chemother Pharmacol. 2011 Aug;68(2):431–44.

67. Mugabe C, Raven PA, Fazli L, Baker JHE, Jackson JK, Liggins RT, et al. Tissue uptake of docetaxel loaded hydrophobically derivatized hyperbranched

polyglycerols and their effects on the morphology of the bladder urothelium. Biomaterials. 2012 Jan;33(2):692–703.

68. Stasi SMD, Giannantoni A, Navarra P, Massoud R, Zavaglia D, Bertucci P, et al. The stability of lidocaine and epinephrine solutions exposed to electric current and comparative administration rates of the two drugs into pig bladder wall. Urol Res. 2003 Jul 1;31(3):169–76.

69. Kerec M, Bogataj M, Veranic P, Mrhar A. Permeability of pig urinary bladder wall: the effect of chitosan and the role of calcium. Eur J Pharm. 2005 May;25(1):113–21.

70. Kos MK, Bogataj M, Veranic P, Mrhar A. Permeability of pig urinary bladder wall: time and concentration dependent effect of chitosan. Biol Pharm Bull. 2006 Aug;29(8):1685–91.

71. Moch C, Salmon D, Rodríguez Armesto L, Colombel M, Pivot C, Pirot F. Bladder tissue permeability and transport modelling of intravesical alum, lidocaine hydrochloride, methylprednisolone hemisuccinate and mitomycin C. Int J Pharm. 2014 Apr 10;464(1-2):91–103.

72. Tissue Solutions Ltd. Fresh Human Tissues [Internet]. Tissue Solutions Ltd. 2012 [cited 2014 Aug 29]. Available from: http://www.tissue-solutions.com/prod_fresh.html

73. Fowler S. Analyses of Cystectomy Dataset for 2012. Section of Oncology. London: BAUS; 2013.

74. Tscholl R, Tettamanti F, Zingg E. Ileal substitute of ureter with reflux-plasty by terminal intussusception of bowel: animal experiments and clinical experience. Urology. 1977 Apr;9(4):385–9.

75. Coolsaet BL, van Mastrigt R, van Duyl WA, van Rees Vellinga F. Some influences of the contractile element on the visco-elastic properties of bladder wall strips. Eur Urol. 1978;4(6):450–6.

76. Van Mastrigt R, Griffiths DJ. Contractility of the urinary bladder. Urol Int. 1979;34(6):410–20.

77. Crowe R, Burnstock G. A histochemical and immunohistochemical study of the autonomic innervation of the lower urinary tract of the female pig. Is the pig a good model for the human bladder and urethra? J Urol. 1989 Feb;141(2):414–22.

78. Bridgewater M, MacNeil H, Brading A. Regulation of tone in pig urethral smooth muscle. J Urol. 1993;150(1):223–8.

79. Ciprian P, Bogdan F, Ona V, Costin N. Training Model in Laparoscopic Urologic Surgery - Laparoscopic Cure of Bladder Injuries in Pig Animal Models. Med Connect. 2012 Mar;25(1):1–11.

80. Escobar PF, Haber G-P, Kaouk J, Kroh M, Chalikonda S, Falcone T. Single-port surgery: laboratory experience with the daVinci single-site platform. JSLS. 2011 Jun;15(2):136–41.

81. Dixon JS, Gosling JA. Histology and fine structure of the muscularis mucosae of the human urinary bladder. J Anat. 1983 Mar;136(Pt 2):265–71.

82. Teufl F, Dammann F, Wehrmann M. In vitro study of morphology of the bladder wall using MR tomography at 1.0 Tesla: correlation with histology. RöFo. 1997 May;166(5):406–10.

83. Narumi Y, Kadota T, Inoue E, Kuriyama K, Horinouchi T, Kasai K, et al. Bladder wall morphology: in vitro MR imaging-histopathologic correlation. Radiology. 1993 Apr;187(1):151–5.

84. Krebs HA, Henseleit K. Untersuchungen uber die Harnstoffbildung im Tierkörper. Hoppe-Seyler´s Z Für Physiol Chem. 1932 Jan;210(1-2):33–66.

85. HiMedia Laboratories Ltd. Krebs-Ringer Bicarbonate Buffer, Product Code TS1097 [Internet]. Mumbai, India; 2013 [cited 2013 Aug 20]. Available from: http://himedialabs.com/TD/TS1097.pdf

86. Dittrich R, Beckmann MW, Maake C, Oppelt PG, Mueller A, Mueller S, et al. The extracorporeal perfusion of the female pig detrusor as an experimental model for the study of bladder contractility. Neurourol Urodyn. 2007;26(7):1024–9.

87. Parsons BA, Drake MJ, Gammie A, Fry CH, Vahabi B. The validation of a functional, isolated pig bladder model for physiological experimentation. Front Pharmacol. 2012;3(52):1–8.

88. Pick DL, Shelkovnikov S, Canvasser N, Louie MK, Tongson-Ignacio J, McDougall EM, et al. First prize: Chitosan and the urothelial barrier: effects on ureteral intraluminal drug penetration and peristalsis. J Endourol Endourol Soc. 2011 Mar;25(3):385–90.

89. Rivera L, Brading AF. The role of Ca2+ influx and intracellular Ca2+ release in the muscarinic-mediated contraction of mammalian urinary bladder smooth muscle. BJU Int. 2006 Oct;98(4):868–75.

90. Guibert EE, Petrenko AY, Balaban CL, Somov AY, Rodriguez JV, Fuller BJ. Organ Preservation: Current Concepts and New Strategies for the Next Decade. Transfus Med Hemotherapy. 2011 Apr;38(2):125–42.

91. Scaravilli V, Bonacina D, Citerio G. Rewarming: facts and myths from the systemic perspective. Crit Care. 2012 Jun 7;16(Suppl 2):A25.

92. Wise DL, Houghton G. Solubilities and diffusivities of oxygen in hemolyzed human blood solutions. Biophys J. 1969 Jan;9(1):36–53.

93. Sigma-Aldrich Company Ltd. Krebs-Henseleit Buffer, Product Number K3753 [Internet]. Dorset, England; 2007 [cited 2013 Aug 20]. Available from: http://www.sigmaaldrich.com/etc/medialib/docs/Sigma/Product_Information_Sheet/1/k3753pis.Par.0001.File.tmp/k3753pis.pdf

94. Lewis SA. Epithelial electrophysiology. In: Wills NK, Reuss L, Lewis SA, editors. Epithelial transport: a guide to methods and experimental analysis. London: Chapman & Hall; 1996. p. 93–117.

95. Hermanns MI, Unger RE, Kehe K, Peters K, Kirkpatrick CJ. Lung epithelial cell lines in coculture with human pulmonary microvascular endothelial cells: development of an alveolo-capillary barrier in vitro. Lab Invest. 2004;84(6):736–52.

96. Walgren RA, Walle UK, Walle T. Transport of quercetin and its glucosides across human intestinal epithelial Caco-2 cells. Biochem Pharmacol. 1998;55(10):1721–7.

97. Sugasi S, Lesbros Y, Bisson I, Zhang YY, Kucera P, Frey P. In vitro engineering of human stratified urothelium: analysis of its morphology and function. J Urol. 2000;164(3):951–7.

98. Janssen DAW, van Wijk XMR, Jansen KCFJ, van Kuppevelt TH, Heesakkers JPFA, Schalken JA. The distribution and function of chondroitin sulfate and other sulfated glycosaminoglycans in the human bladder and their contribution to the protective bladder barrier. J Urol. 2013 Jan;189(1):336–42.

99. Erman A, Kerec Kos M, Žakelj S, Resnik N, Romih R, Veranič P. Correlative study of functional and structural regeneration of urothelium after chitosan-induced injury. Histochem Cell Biol. 2013 Nov;140(5):521–31.

100. Lewis SA, Berg JR, Kleine TJ. Modulation of epithelial permeability by extracellular macromolecules. Physiol Rev. 1995 Jul;75(3):561–89.

101. Fromter E, Diamond J. Route of passive ion permeation in epithelia. Nature. 1972;235(53):9–13.

102. Turner AM, Subramaniam R, Thomas DFM, Southgate J. Generation of a functional, differentiated porcine urothelial tissue in vitro. Eur Urol. 2008 Dec;54(6):1423–32.

103. Lavelle J, Meyers S, Ramage R, Bastacky S, Doty D, Apodaca G, et al. Bladder permeability barrier: recovery from selective injury of surface epithelial cells. Am J Physiol Renal Physiol. 2002 Aug 1;283(2):F242–53.

104. Lavelle JP, Meyers SA, Ruiz WG, Buffington CAT, Zeidel ML, Apodaca G. Urothelial pathophysiological changes in feline interstitial cystitis: a human model. Am J Physiol Renal Physiol. 2000 Apr 1;278(4):F540–53.

105. Sun T-T. Altered phenotype of cultured urothelial and other stratified epithelial cells: implications for wound healing. Am J Physiol Renal Physiol. 2006 Jul 1;291(1):F9–21.

106. Redden RJ. Ketorolac tromethamine: an oral / injectable nonsteroidal anti-inflammatory for postoperative pain control. J Oral Maxillofac Surg. 1992 Dec;50(12):1310–3.

107. Miller OF, Bloom TL, Smith LJ, Mc Aleer IM, Kaplan GW, Kolon TF. Early hospital discharge for intravesical ureteroneocystostomy. J Urol. 2002;167(6):2556–9.

108. Routh JC, Graham DA, Nelson CP. Ketorolac is underutilized after ureteral reimplantation despite reduced hospital cost and reduced length of stay. Urology. 2010;76(1):9–13.

109. Stein A, Dov DB, Finkel B, Mecz Y, Kitzes R, Lurie A. Single-dose intramuscular ketorolac versus diclofenac for pain management in renal colic. Am J Emerg Med. 1996;14(4):385–7.

110. Laneuville O, Breuer DK, Dewitt DL, Hla T, Funk CD, Smith WL. Differential inhibition of human prostaglandin endoperoxide H synthases-1 and -2 by nonsteroidal anti-inflammatory drugs. J Pharmacol Exp Ther. 1994 Nov;271(2):927–34.

111. El-Nahas AR, El-Assmy AM, Shoma AM, Eraky I, El-Kenawy MR, El-Kappany HA. Self-retaining ureteral stents: analysis of factors responsible for patients' discomfort. J Endourol. 2006 Jan;20(1):33–7.

112. Bultitude MI, Hills NH, Shuttleworth KE. Clinical and experimental studies on the action of prostaglandins and their synthesis inhibitors on detrusor muscle in vitro and in vivo. Br J Urol. 1976;48(7):631–7.

113. Rahnama'i MS, van Koeveringe GA, Essers PB, de Wachter SGG, de Vente J, van Kerrebroeck PE, et al. Prostaglandin Receptor EP1 and EP2 Site in Guinea Pig Bladder Urothelium and Lamina Propria. J Urol. 2010 Mar;183(3):1241–7.

114. Rahnama'i MS, van Koeveringe GA, van Kerrebroeck PEV, de Wachter SGG. The effect of indomethacin on the muscarinic induced contractions in the isolated normal guinea pig urinary bladder. BMC Urol. 2013;13:8.

115. Birder LA. Nervous network for lower urinary tract function. Int J Urol. 2013 Jan;20(1):4–12.

116. Wen CC, Coyle TLC, Jerde TJ, Nakada SY. Ketorolac effectively inhibits ureteral contractility in vitro. J Endourol. 2008 Apr;22(4):739–42.

117. Abrams PH, Sykes JA, Rose AJ, Rogers AF. The synthesis and release of prostaglandins by human urinary bladder muscle in vitro. Invest Urol. 1979 Mar;16(5):346–8.

118. Kasakov LN, Vlaskovska MV. Profile of prostaglandins generated in the detrusor muscle of rat urinary bladder: effects of adenosine triphosphate and adenosine. Eur J Pharmacol. 1985 Jul 31;113(3):431–6.

119. Jeremy JY, Mikhailidis DP, Dandona P. The rat urinary bladder produces prostacyclin as well as other prostaglandins. Prostaglandins Leukot Med. 1984 Nov;16(2):235–48.

Chapter Three: *Investigating the Transurothelial Permeation and Bladder Wall Distribution of Oxybutynin*

3.1. Introduction

3.1.1. Oxybutynin

Oxybutynin is an antispasmodic, non - specific antimuscarinic agent which exhibits local anaesthetic properties on the bladder wall[1]. Administered as a racemate of the R - and S - isomers, oxybutynin is a tertiary amine with a molecular weight of 357 g mol^{-1} [2,3] (Figure 3.1). Pharmacologically it competitively antagonises the M_1, M_2 and M_3 subtypes of the muscarinic acetylcholine (ACh) receptor[4]. Oxybutynin's primary indication is the treatment of overactive bladder (OAB), for which it remains the most widely prescribed drug worldwide[5].

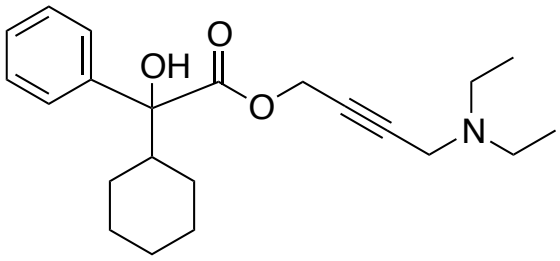

Figure 3.1. Chemical structure of oxybutynin

3.1.2. Overactive bladder (OAB)

OAB is a condition described by a collection of lower urinary tract symptoms (LUTS). LUTS are classified as either storage or voiding in origin[6]. In OAB, symptoms typically include urgency, with or without urge incontinence, often with frequency and nocturia, in the absence of proven infection or other obvious pathology[7–9]; it is therefore best described as a storage condition. OAB is a chronic disorder, affecting approximately 17 % of men and women over the age of forty[10]. It significantly affects quality of life[8], with symptoms having a profound affect on social behaviour, physical activity and psychological wellbeing[8]. In combination with behavioural therapies such as pelvic floor muscle training and fluid management, first - line pharmacotherapy is treatment with antimuscarinics[11]. The last decade has seen significant advancement in our understanding of the

mechanism of action (MOA) by which antimuscarinics improve OAB symptoms[12]. Traditional dogma was based on the understanding of nervous control of detrusor muscle contraction[13]. Accordingly, an overview of bladder detrusor neurology is necessary.

3.1.3. Neural control of the detrusor muscle

3.1.3.1. Parasympathetic control

Bladder voiding is initiated by contraction of the detrusor muscle, a process mediated by the parasympathetic system. Preganglionic neurons originating in sacral spinal cord segments S2 - S4 travel in the pelvic nerve and synapse with postganglionic fibres in the pelvic plexus and bladder wall[14]. Transmission to postganglionic fibres is cholinergic and mediated through nicotinic receptors[14]. Postganglionic fibres, if not already present, travel to the bladder wall where excitatory parasympathetic innervation causes the detrusor to contract. Cholinergic transmission is mediated through M_3 muscarinic receptors, whilst non - cholinergic transmission is mediated by adenosine triphosphate (ATP) at P2X purinergic receptors. It is ACh however that is the principal parasympathetic neurotransmitter in the detrusor[14].

3.1.3.2. Sympathetic control

Relaxation of the bladder detrusor muscle, which is essential during filling, is regulated by the sympathetic system. Sympathetic innervation of the bladder originates in the lower thoracic and upper lumbar segments of the spinal cord (T10 - L2)[14]. Preganglionic axons synapse with postganglionic fibres in the inferior mesenteric ganglia and pelvic plexus. Postganglionic neurons travel in the hypogastric and pelvic nerves to the detrusor muscle, where innervation causes relaxation mediated predominantly through β_3 - adrenoceptors and to a lesser extent β_2 - adrenoceptors[15].

3.1.3.3. Afferent pathways

The afferent division of the peripheral nervous system is responsible for transmitting sensory information. Bladder afferent pathways initiate the micturition reflex and are essential to the normal functioning of the organ. In response to filling, afferent fibres are excited by mechanical (e.g. bladder wall

stretch, torsion, increased intravesical pressure) and chemical (e.g. ATP, ACh) stimuli[16]. Afferent fibres in the urinary tract travel in three sets of nerves to the central nervous system, the most important for micturition being the pelvic nerve[17]. Myelinated Aδ and unmyelinated C - fibres are activated by mechanoreceptors in the bladder wall that relay sensory information to second - order neurons in the dorsal horn of the spinal cord[14]. Aδ fibres are involved in normal micturition, whilst C - fibres are typically associated with painful sensations[18]. From the spinal cord, sensory information is conveyed to higher centres in the periaqueductal gray area of the midbrain, which itself receives input from several forebrain structures (hypothalamus, amygdala and orbital - medial prefrontal cortex)[14]. These structures participate in limbic networks that evaluate certain risks and emotional significance. In the context of bladder voiding this may include whether it is safe and socially appropriate for an individual to urinate[15].

3.1.3.4. Bladder filling and voiding

The neural pathways controlling bladder filling and voiding operate according to an on - off switch mechanism. When bladder volume is low or moderate, micturition is inhibited because sympathetic activity is greater than parasympathetic activity, i.e., the 'switch' is off[19].

This voiding 'switch' can be turned on involuntarily (autonomic, referred to as reflexly) or voluntarily (somatic)[14]. In the autonomic pathway increased afferent firing from mechanoreceptors in the bladder wall at the micturition threshold reverses the overall efferent signal; parasympathetic activity increases, while sympathetic decreases. This results in relaxation of the internal urethral sphincter followed shortly by contraction of the bladder detrusor, an increase in bladder luminal pressure and urination[14].

3.1.4. Signalling in the urothelium and lamina propria

Nervous innervation extends beyond the detrusor muscle with evidence of unmyelinated C - fibres located in the lamina propria at close proximity to the urothelium[20–23]. These nerve fibres can synthesise a number of neurotransmitters and express a wide range of receptors including muscarinic and purinergic receptors[24–26]. In addition, they are known to respond to mediators released from

cells in response to inflammation, injury and ischaemia including prostaglandins, serotonin and ATP[23].

There is now considerable evidence that cells in the urothelium and lamina propria can modulate, and be modulated by these sensory pathways[23,27]. Urothelial cells express a variety of receptors and ion channels allowing them to be modulated by mechanical and chemical inputs from a variety of sources[27–31]. In addition to muscarinic receptors (Section 3.1.5.3)[32–36], examples include nicotinic receptors[37], purinergic receptors[38–40] and adrenoceptors[41,42]. Suggested mechanical inputs include changes in intravesical pressure and tension / torsion in the bladder wall during filling. Chemical inputs include factors found in the urine such as epidermal growth factor or mediators such as ACh, adenosine and noradrenaline released from sympathetic nerve terminals, inflammatory cells and blood vessels[23,27]. These inputs can cause various outputs from the urothelium such as the secretion of ATP, ACh, prostaglandins, prostacyclin, nitric oxide and cytokines[23]. It is believed that through paracrine signalling these outputs allow functional processes to occur in nearby and underlying cells and that this propagation can be enhanced by a number of stimuli including stretch of the bladder wall and states of pathological disease[23,43–45].

3.1.5. Distribution of muscarinic receptors in the bladder wall

Five subtypes of muscarinic receptors (M_1 - M_5) have been cloned and pharmacologically characterised[46] and although all are expressed in the bladder wall, population density and subtype varies depending of the tissue layer in question.

3.1.5.1. Detrusor muscle

At the protein level, immunoprecipitation and radioligand binding studies have shown the human detrusor to express the M_1, M_2 and M_3 but not the M_4 or M_5 subtypes[35,47–49]. In terms of population density the M_2 subtype predominates over the M_3 and M_1 subtypes representing ~ 70 %, 20 – 30 % and 10 % of the muscarinic receptor population respectively[35,47]. However, in all species investigated, it is the relatively minor population of M_3 receptors that mediate direct detrusor contractile responses[49].

3.1.5.2. Lamina propria

The lamina propria contains a population of cells with similar morphology to the interstitial cells of Cajal (ICC) of the gastrointestinal tract[50]. ICCs are found throughout the lamina propria, including just below the urothelium, and have been shown to form connections with afferent nerves[51]. The function of the ICCs in the bladder is unclear. It has been suggested that they may play a role in sensory pathways, acting to regulate the contractile activity of detrusor[49]. There is also evidence that ICC cell expression is up - regulated in bladder pathology such as OAB[50]. Immunostaining has shown ICCs of the human bladder to express both M_2 and M_3 receptors[36].

3.1.5.3. Urothelium

All five subtypes of the muscarinic receptor are expressed by the human urothelium[32,33,35,52]. Like the detrusor, at the protein level the M_2 subtype appears to be the most highly expressed[33,35]. Expression is urothelial cell layer dependent. In human urothelium M_2 receptors are found exclusively in the umbrella cells, whilst M_1 receptors are located solely in the lower basal layer[33]. Conversely, the M_3, M_4 and M_5 subtypes are expressed throughout the urothelium[33].

3.1.6. The mechanism of action of antimuscarinics in OAB

Traditionally, storage LUTS were believed to result from abnormal, involuntary detrusor contractions during the bladder filling (detrusor overactivity)[53]. Since antimuscarinics are effective in treating such symptoms and are established to be beneficial in OAB[54], their MOA was believed to be antagonism of the M_3 muscarinic receptors in the detrusor muscle and subsequent inhibition of these involuntary contractions[13,55].

However significant evidence now suggests this may not be the case and the MOA of antimuscarinics has come under scrutiny[56–58]. Although it is well established that antimuscarinics reduce the symptoms associated with OAB[59], whether this is brought about by an inhibition in parasympathetic mediated detrusor contraction is unclear[56,57]. Finney *et al* conducted a review of all articles containing cystometric data for both storage and voiding phases in OAB patients before and after antimuscarinic therapy[57]. They found that although antimuscarinics significantly

improved the storage symptoms associated with OAB, they did not cause a significant reduction in detrusor muscle contraction. In agreement, although at high doses antimuscarinics can inhibit detrusor contraction during voiding and as such cause retention, the likelihood of this occurring at clinical doses is low[12,60]. Some have made the point that the common antimuscarinics prescribed for OAB such as oxybutynin, tolteradine and solifenacin are competitive antagonists and therefore their effectiveness should be reduced during times of significant ACh release, such as during micturition[57]. During bladder filling the parasympathetic switch is off (there is no parasympathetic outflow form spinal cord / no activity in the parasympathetic nerves innervating the detrusor) and post - junctional muscarinic receptors in the detrusor are presumably inactive[17]. Therefore the ability of antimuscarinics to improve storage symptoms is unlikely to be explained exclusively by antagonism of the parasympathetic - controlled, ACh - activated M_3 receptors of the detrusor[61].

3.1.6.1. Afferent mechanisms of antimuscarinic drugs

Kim *et al* investigated the possibility that antimuscarinic agents improve OAB symptoms by inhibiting sensory pathways[62]. When instilled intravesically at a concentration of 0.167 mg ml^{-1}, oxybutynin significantly increased bladder capacity, intercontraction interval and pressure threshold (indicators of bladder storage function) without decreasing detrusor contractility in the normal rat bladder[62]. Instillations were retained for short periods of time (~ 30 min) and cystometric effects observed immediately after emptying. The authors therefore attributed the effects of oxybutynin to a local action on muscarinic receptors in the urothelium or lamina propria rather than the underlying detrusor muscle[62]. The MOA was suggested to be desensitisation of afferent C - fibres. This agrees with previous work showing that intravesical oxybutynin desensitises C - fibre afferents in the rat bladder[1]. In a different study Iijima *et al* showed that systemic administration of the M_3 antagonist darifenacin reduced afferent activity induced by bladder filling in the normal bladder[63].

There is evidence that in patients with OAB, the M_2 and M_3 receptors on the suburothelial ICCs exhibit increased immunoreactivity[36,50]. This increased immunoreactivity has been correlated with patient urgency, suggesting a role for these receptors in the underlying aetiology of urgency[13,36]. Although the

parasympathetic switch is off during filling, the bladder exhibits spontaneous (myogenic) contractions of the detrusor[12]. This is believed to be reinforced by neuronal and non - neuronal mediators and helps the bladder exhibit tone during filling[64–66]. It is suggested that this myogenic activity can modulate afferent signals[65] and that in OAB these signals may be enhanced[12,67]. In addition to the detrusor, it has recently been shown that isolated porcine mucosa exhibits spontaneous phasic contractile activity that is increased during stretch[68]. Contractions appear to be ACh mediated through M_3 muscarinic receptors and clinically used antimuscarinics were shown to depress this activity[68].

Evidence suggests therefore that in OAB, antimuscarinics might elicit their effects not by decreasing direct contractility of the detrusor muscle, but rather by modifying afferent mechanisms in the storage phase[12,69].

3.1.6.2. Pharmacology underlying bladder afferent pathways

The pharmacology underlying afferent modulation in OAB is thought to centre on two intertwined mediators; ATP and ACh (Figure 3.2). During filling, stretch of the bladder wall results in ATP release from urothelial cells[70–72]. The concentration of ATP in voided urine correlates strongly with voided volume, suggesting ATP is released in an incremental fashion in response to bladder wall stretch[73]. In comparison to the normal bladder, ATP release is significantly increased in detrusor overactivity[74] and interstitial cystitis / painful bladder syndrome[75,76] suggesting a functional role in bladder pathology. ATP released from the urothelium can directly activate afferents in the mucosa through P2X3 receptors, resulting in the increased firing associated with bladder filling[16,72,77,78]. ATP can also activate purinergic receptors (P2X[79] or P2Y[80]) on ICCs, indirectly activating closely associated afferent nerves[81–83] and subsequently amplifying afferent firing during bladder filling[84,85].

The urothelium is also capable of synthesising ACh[86,87] and bladder stretch is associated with non - neuronal ACh release from the urothelium[88,89]. OAB seems to be associated with an increased release of ACh during the storage phase suggesting the mediator contributes to the pathophysiology of the disorder[12]. Interestingly basal and stretch - induced urothelial ACh release increases with age and is significantly higher in those aged > 65 years[86]. It is unclear whether muscarinic

receptor expression or function changes with age[12], however it would appear clinical response to antimuscarinics does not differ in older patients[90,91]. Up regulation of urothelial muscarinic receptors appears to be involved in the aetiology of bladder disorders[92,93]. However, despite some evidence that mucosal M_2 and M_3 receptor functionality is altered in OAB[36], no consistent changes in muscarinic receptor function have been attributed to the condition[12].

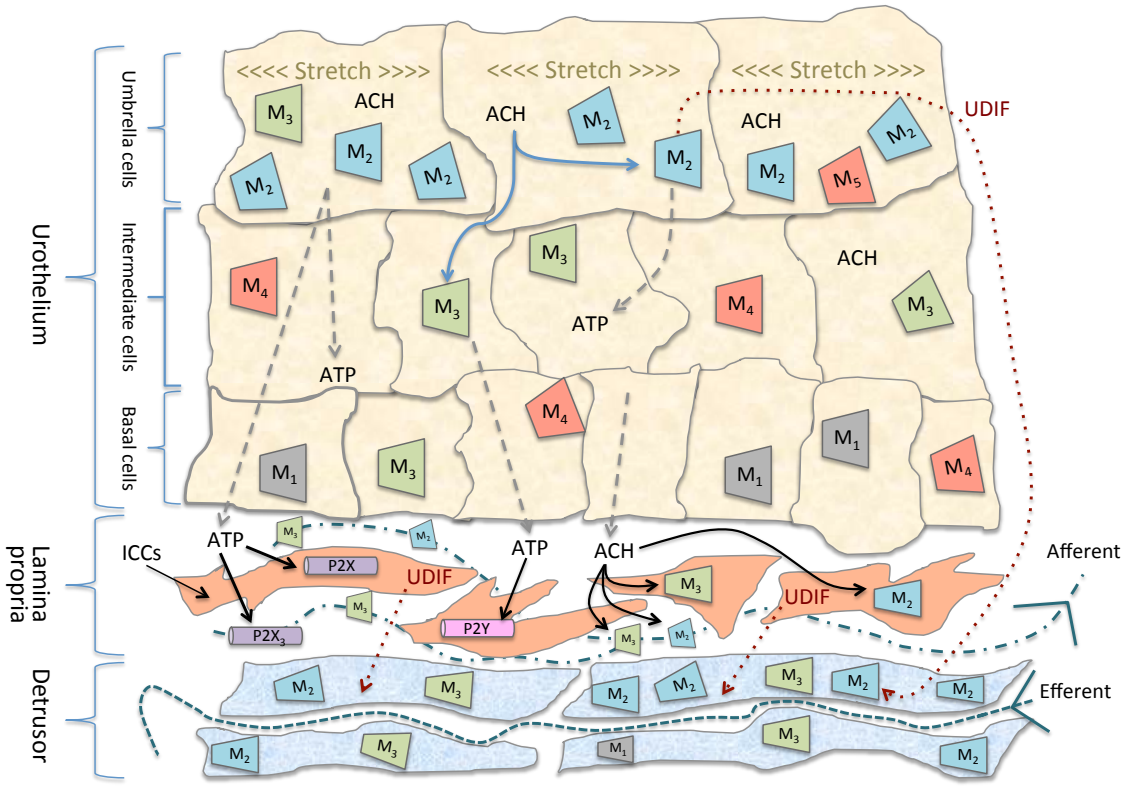

Figure 3.2. The suggested mechanism of cholinergic signalling in the bladder wall and proposed MOA of antimuscarinics in modulating afferent activity. Figure adapted from Mansfield et al[13].

Intravesical administration of muscarinic agonists has been shown to increase afferent excitability *in vivo*[62,94,95]. These effects were attributed to muscarinic receptor activation and the subsequent ATP - mediated activation of purinergic receptors on afferent nerves. The location of these muscarinic receptors was believed to be the urothelium or underlying lamina propria[62,95]. In agreement, antimuscarinics have been shown to inhibit bladder afferent excitation. Systemically administered oxybutynin inhibits Aδ and C - fibre afferent firing during bladder filling[72] and long term administration is associated with decreased afferent nerve activity[96]. Antimuscarinics are thought to improve bladder capacity by inhibiting C - fibre afferents; intravesical tolteradine increased bladder capacity in non - resiniferatoxin pre - treated rats, but had no effect in those that had received the C - fibre desensitising toxin[97]. In addition intravesical oxybutynin significantly reduced bladder C - fibre afferent response to intravesical pressure and volume[1]. Kullmann *et al* found activation of muscarinic receptors located in the apical cells of the urothelium leads to modulation of afferent C - fibres which in turn alters the frequency of reflex voiding[95]. Yokoyama showed that intravesically induced hydrodistention of the bladder leads to increased intravesical concentrations of urothelial-released ATP and that antimuscarinics significantly suppressed this increase[98]. Indeed it has recently been confirmed that M_2 and M_3 muscarinic receptor antagonism inhibits stretch - induced ATP release from the bladder mucosa, further suggesting urothelial muscarinic receptor involvement in the MOA of antimuscarinics in bladder pathology[99]. In addition to the urothelium, the M_2 - M_4 subtypes of muscarinic receptor are found on bladder afferent nerves[100]; raising the possibility that ACh (like ATP) may directly activate afferent nerves in the mucosa[101]. Interestingly, activation of M_2 receptors in the bladder urothelium by the muscarinic agonist carbachol leads to release of 'urothelial derived inhibitory factor' (UDIF), which directly inhibits detrusor muscle contractions[102–105].

The exact MOA through which antimuscarinics inhibit afferent firing in the bladder wall is still uncertain. However the evidence strongly suggests mucosal muscarinic receptors are integral to the process. Based on the pharmacology elicited, a MOA has been suggested (Figure 3.2)[12,13,101]. During filling the bladder wall stretches and releases ATP and ACh. ACh may activate muscarinic receptors in the

urothelium leading to the release of more ATP[95,99]. ATP and ACh can modulate afferents indirectly through activation of purinergic and muscarinic receptors on ICCs. In addition ATP and ACh can activate afferent nerves directly through P2X3 and M_2 / M_3 receptors located on afferent nerves. Afferent firing then initiates the micturition reflex and / or enhances the spontaneous (myogenic) contractile activity of the detrusor which occurs during filling[13]. Therefore the MOA of antimuscarinics in OAB is believed to be the competitive antagonism of the mucosal muscarinic receptors, although the exact location of these targets (urothelium, suburothelial ICCs, suburothelial afferent nerves) is unknown. It is postulated that after oral administration, antimuscarinics reach the mucosa through the plexus of blood vessels located in the lamina propria or via drug excreted in the active form in the urine[13,106].

Therefore on the basis of growing evidence suggesting the antagonism of muscarinic receptors in the bladder mucosa is the MOA for antimuscarinics in OAB, it would seem probable that locally delivered drug might lead to improved clinical outcomes.

3.1.7. Clinical use of Intravesical oxybutynin

Although oral antimuscarinics are first - line pharmacotherapy for OAB, for some patients they are unsuitable either due to insufficient suppression of detrusor overactivity[12] (up to 45 % of patients discontinue treatment owing to a lack of efficacy[107]) or the experience of significant adverse effects such as dry mouth, constipation and blurred vision[108–110]. For such patients, conservative management with intravesical oxybutynin is an option[108]. In the late 1980's Kato *et al* documented the first investigation into the IDD of oxybutynin using an *in vitro* rabbit bladder model[111]. They suggested that the local delivery of antimuscarinics might be advantageous in the treatment of neurogenic bladder, especially for patients already managed by clean intermittent catheterisation. Since then a wealth of evidence has documented intravesical oxybutynin to be not only highly efficacious in increasing mean bladder capacity and decreasing mean maximum filling pressure, but also to be well tolerated and associated with less adverse effects than its oral counterpart[112–124]. Although more commonly reported in neurogenic patients, the efficacy of intravesical oxybutynin extends also to the non

- neurogenic population[125–127]. In most reports intravesical oxybutynin is administered in doses between 0.2 and 0.6 mg kg^{-1} day^{-1} divided over two or three instillations[108,128]. Tolerability studies have shown this can be further increased to 0.9 mg kg^{-1} day^{-1} without causing toxicity[124].

The mechanism underlying the improved adverse effect profile of intravesical oxybutynin compared to oral delivery is well understood. When administered orally, oxybutynin undergoes rapid hepatic metabolism into its major oxidative metabolites N – desethyl - oxybutynin and oxybutynin N - oxide (Figure 3.3)[129]. The reduced adverse effects of intravesical oxybutynin are attributed to reduced first - pass metabolism and subsequently lower systemic levels of N – desethyl - oxybutynin[122,129]. Subsequently significant work has focused on post - intravesical pharmacokinetics and the systemic levels of oxybutynin and N – desethyl - oxybutynin achieved[128–132]. However to our knowledge only one study has investigated bladder wall concentrations achieved after the local application of oxybutynin to the urothelium[133]. Furthermore results from this study detailed only average, rather than tissue - layer specific, drug concentrations for the bladder wall. Given the development in the understanding of the MOA, it would seem pertinent to investigate the concentrations of oxybutynin achieved in the different layers of the bladder wall.

This chapter reports a more detailed analysis of oxybutynin concentrations achieved in the urothelium, lamina propria and detrusor muscle after intravesical delivery to *ex vivo* porcine bladder. Crucially dilution by urine from the kidneys is accounted for.

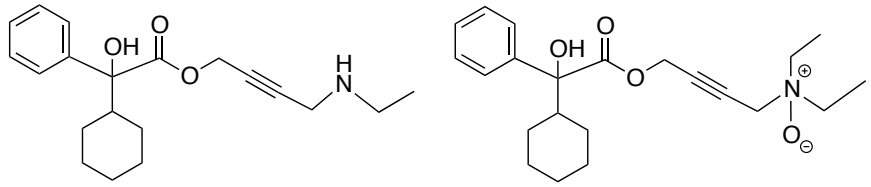

A B

Figure 3.3. The chemical structures of N – desethyl - oxybutynin (A) and oxybutynin – N - oxide (B).

3.1.8. Aims and Objectives of Chapter Three

The overall aim of this section of work was to investigate the transurothelial permeability and bladder wall distribution of oxybutynin chloride after intravesical delivery in an *ex vivo* setting.

The key objectives were:

1. To investigate the bladder wall permeability of oxybutynin and generate an apparent transurothelial K_P value using the Franz - type diffusion apparatus.

2. To investigate the tissue - layer specific concentrations of oxybutynin achieved in the bladder wall after intravesical delivery of a clinically relevant dose.

3. To incorporate urine dilution into the *ex vivo* IDD studies and investigate the effect this has on drug concentrations achieved in the bladder wall.

3.2. Materials and methods

3.2.1. Materials

All chemicals were purchased from Sigma - Aldrich, Poole, UK and were used as received unless otherwise stated. All organic solvents were of HPLC grade and were obtained from Fisher Scientific, Loughborough, UK unless otherwise stated.

3.2.2. Analysis of oxybutynin chloride

Oxybutynin was quantified using a Quattro liquid chromatography - tandem mass spectrometer (Waters, Elstree, Herts, UK) coupled to a Thermo Spectra System using a HPLC column (Section 2.2.2). The mobile phase consisted of 50 % aqueous formic acid (0.1 %) : 50 % ACN. The injection volume was 10 μl and flow rate 0.4 ml min^{-1}. Positive ion mass spectrometry was used for the detection, with single ion monitoring for the parent ion between 357.5 and 358.5 m / z.

3.2.3. Bladder tissue preparation

Porcine bladder tissue was prepared as previously described (Section 2.2.5). To one group of bladder tissue samples the urothelium was removed prior to loading in the Franz - type diffusion cells (urothelium denuded group). The other group were untreated (intact urothelium group).

3.2.3.1. Removal of the urothelium

After cutting the bladder tissue into sections, a cotton swab was rolled across the entire surface of the urothelium. Following this an additional cotton swab, this time dipped in Krebs, was used to gently wipe the urothelial surface. The tissue was then gently rinsed with Krebs to remove any debrided urothelial cells.

3.2.4. Permeation of oxybutynin across the urothelium

Bladder tissue sections were loaded in Franz - type cells (Section 2.2.5) and a 750 μl aliquot of oxybutynin chloride (0.167 mg ml^{-1} in deionised water) applied to the donor chamber. At fixed time points (20, 40 and 60 min) the Franz - type cells were disassembled (Section 2.2.7.1). Tissue samples were immediately snap frozen, fixed with OCT and sectioned using a cryostat (Section 2.2.7.2). Tissue

sections between 0 and 250 μm (urothelium) were collected individually for analysis. Four tissue sections between 250 and 1,050 μm (upper lamina propria) and 10 sections between 1,050 and 1,550 μm (lower lamina propria) were collected and pooled for analysis. Similarly ten tissue sections between 1,550 and 3,550 μm (detrusor muscle) were collected and pooled for analysis. The slight difference between tissue layer depths compared to the ketorolac study (Section 2.2.7.2) was based on histological analysis of the bladder samples used in this study (Section 3.2.6). The decision to collate 10 sections for the lower lamina propria was the result of preliminary experiments (in rare cases drug concentrations approached the LLOD when collating only four sections).

Drug was extracted in 0.75 ml mobile phase (Section 2.2.6.1) and the amount of oxybutynin in the bladder wall at each time point quantified using HPLC - MS (Section 3.2.2). Average tissue concentrations achieved in the urothelium, lamina propria and detrusor muscle were determined as described (Section 2.2.7.2).

3.2.5. Intravesical instillation of oxybutynin

Ex vivo porcine bladders were prepared as described (Section 2.2.5), however this time bladders were not cut open. Working in a shallow bed of Krebs, both ureteral orifices were sutured (0.5 cm apical to the serosal side of the bladder) and using an open - ended ureteral catheter (5 Fr, 70 cm, Cook medical Inc, Bloomington, IN, USA) 30 ml of oxybutynin chloride solution (0.167 mg ml^{-1} in deionised water) instilled into the bladder through the urethra. Care was taken to avoid contact with the urothelial surface and post - instillation the urethra sutured around the catheter prior to its retraction. Bladders were submerged in oxygenated Krebs and maintained at 37 °C in a waterbath (Figure 3.4). To one group of bladders, the ureteral catheter remained *in situ* and 37 °C artificial urine (composition: NaCl 105.5 mM, NaH_2PO_4 3.2 mM, $Na_3C_6H_5O_72H_2O$ 3.2 mM, $MgSO_4$ 3.9 mM, $CaCl_2$ 4.0 mM, Na_2SO_4 17 mM, KCl 64 mM, $Na_2C_2O_4$ 0.3 mM and $NaNO_3$ 1.0 mM, pH 5.8[134]) was introduced at a rate of 10 ml every 10 min for the duration of the experiment. After 60 min bladders were removed, emptied and opened with a vertical incision along the length of the organ. Samples of bladder wall from areas of drug contact were excised, sectioned and drug extracted and quantified as described (Section 3.2.4).

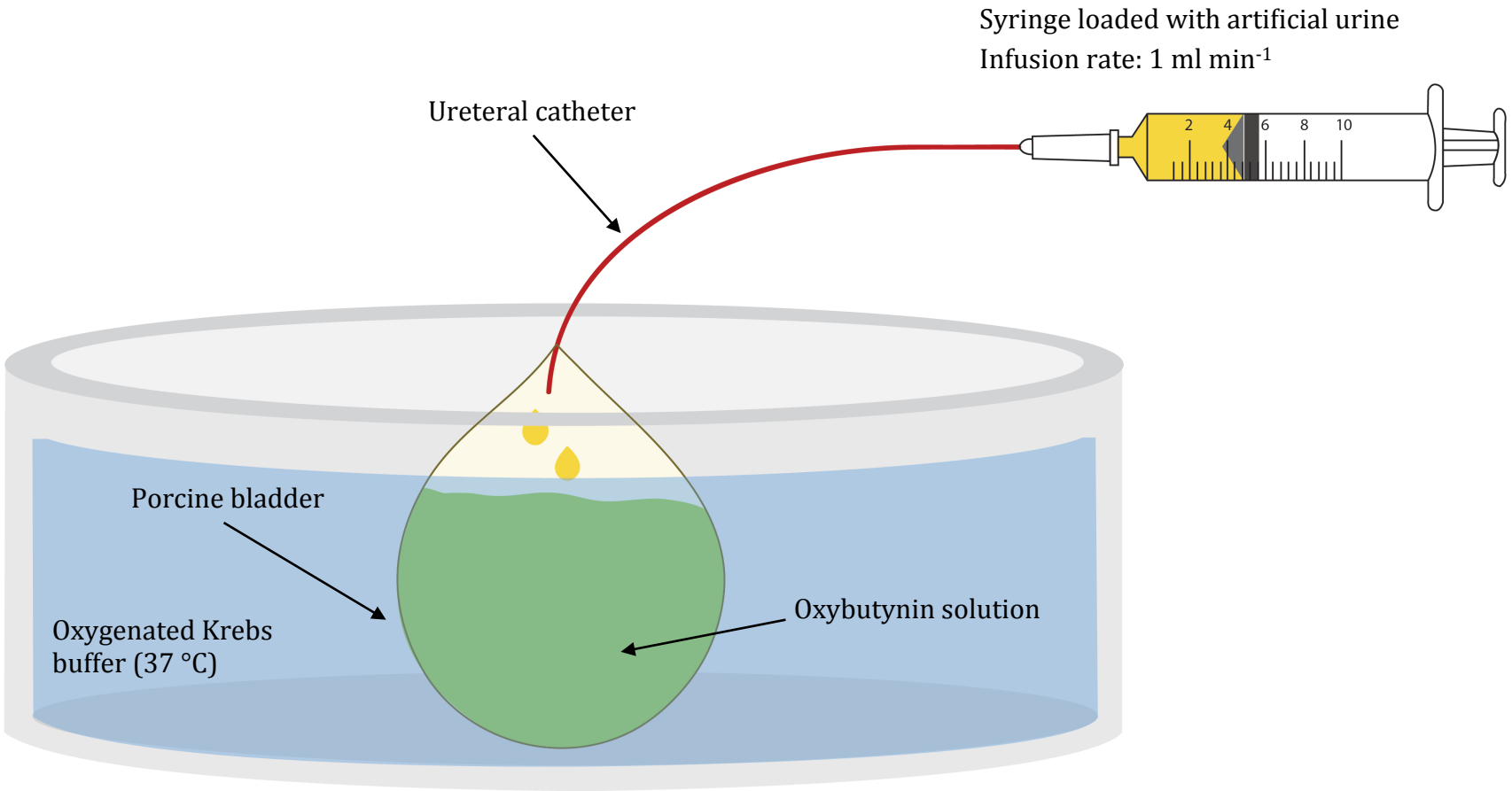

Figure 3.4. Schematic of the whole bladder setup used to investigate the intravesical instillation of oxybutynin.

3.2.6. Histology

Samples of bladder tissue were taken from: *A.*) bladders excised immediately post - sacrifice on - site at the abattoir, *B.*) bladders exposed to 60 min of oxybutynin instillation and *C.*) bladders before and after urothelial removal. Sections were fixed in 4 % buffered formaldehyde (Fisher Scientific UK Ltd, Leicestershire, England) for 48 h at room temperature. Tissues were embedded in paraffin, sectioned at 10 μm thickness and stained with Masson's trichrome prior to examination under light microscopy (Table 3.1).

Step	Slide treatment	Time (min)
1	Xylene	3
2	Xylene	3
3	100 % alcohol	2
4	100 % alcohol	2
5	95 % alcohol	2
6	70 % alcohol	2
7	Running tap water	3
8	Iron alum	5
9	Running tap water	2
10	Mayer's haematoxylin	5
11	Running tap water	5
12	Ponceau Fuchsin	5
13	Running tap water	1
14	Phosphomolybdic acid (1 %)	4
15	Light Green SF Yellowish	2
16	Running tap water	1
17	Acetic acid (1 %)	2
18	Running tap water	1
19	95 % alcohol	2
20	100 % alcohol	2
21	100 % alcohol	2
22	Xylene	3
23	Xylene	3

Table 3.1. Stepwise description of the Masson's trichrome staining protocol.

3.2.7. Statistical analysis

All statistical analysis was performed using GraphPad Prism version 6.0c (GraphPad Software, Inc, San Diego, California, USA). Unpaired t - tests were used for all comparisons.

3.3. Results and Discussion

It is well established that intravesical oxybutynin is beneficial for the treatment of OAB in patients refractory to oral treatment[112–124], although the MOA remains unclear[12]. Furthermore, the last decade has seen significant advancement, and a major change in direction, regarding our understanding of the MOA of antimuscarincs as a whole. Originally believed to act by inhibiting M_3 muscarinic receptors in the detrusor muscle and subsequently preventing involuntary bladder contractions during filling, there is now significant evidence that antimuscarinics activate muscarinic receptors at the urothelial and / or suburothelial level to modulate the afferent arc of the micturition cycle[12,13,57]. This hypothesis may explain the increased effectiveness of intravesical oxybutynin considering relatively high concentrations of drug are presented to the urothelium in comparison to the low bladder bioavailability after oral dosing. Considering this, bladder wall concentrations achieved after intravesical delivery of oxybutynin are valuable in ascertaining target concentrations necessary to modulate sensory pathways. Additionally, quantifying drug concentrations in the different layers of the bladder wall may provide more information regarding the site of action of antimuscarinics. A recurring limitation to understanding the pharmacological site of action of antimuscarinics has been not knowing the depth of penetration of drug after direct application to the urothelium[58,62,133,135]. This is particularly relevant to antimuscarinics as studies have shown muscarinic receptor subtype distribution to vary depending on the cell layer of the urothelium (Section 3.5.1.3)[33]. Concentration - depth profiling (Section 2.3.3.2) is becoming an established technique to quantify drug disposition in the bladder wall and has been used to investigate the local delivery of chemotherapeutics[136,137]. Such studies have not been carried out for antimuscarinics. This chapter aimed to quantify

concentrations of oxybutynin achieved in the different layers of the bladder wall following intravesical administration.

Intravesical oxybutynin is usually administered in doses ranging between 0.2 and 0.6 mg kg^{-1} day^{-1} (Section 3.1.7)[108,128]. Unfortunately, translating this dose into an instillation concentration was difficult. There is no suitable, commercially available intravesical oxybutynin solution and subsequently clinicians have improvised their own instillations. A range of preparation techniques (crushing oxybutynin tablets[112,114], formulating solutions from pure oxybutynin chloride salt[123,138]), concentrations (ranging from 0.05[139] to 1 mg ml^{-1} [128]) and vehicles (water[117,140–143], 0.9 % saline[114,122], 0.45 % saline[131,139], 0.1 % hyaluronic acid[144], 1 % hydroxypropylcellulose (HPC)[145,146]) have been used (Table 3.2). In their review of intravesical oxybutynin, Lose and Nergaard commented that most investigators crush and dissolve a single 5 mg oxybutynin chloride tablet in 30 ml of distilled water (making a 0.167 mg ml^{-1} solution)[127]. Despite the range of concentrations reported, many groups have used this or similar[112,130,147]. Accordingly a 0.167 mg ml^{-1} solution was used in this study. Like many intravesical therapies oxybutynin is commonly instilled for ~ 1 h[148,149]. Given this a 60 min endpoint was chosen.

Dose (mg kg^{-1})	Dose (mg)	Vehicle	Volume (ml)	Concentration (mg ml^{-1})	Reference
NR	5	Saline	20, 30	0.25, 0.167	[112]
0.1, 0.2, 0.3	5, 10, 15	Saline	20	0.25, 0.5, 0.75	[124]
0.1 - 0.2	*NR*	Water	10	*NR*	[143]
NR	5, 15	Saline	100	0.05, 0.15	[131,139]
NR	5	Water	30	0.167	[130]
0.2	5	Water	10	0.5	[138]
NR	10	Saline	10	1	[128]
NR	5	1 % HPC	10	0.5	[145]

Table 3.2. Examples of different intravesical oxybutynin solutions used clinically (NR – not reported).

3.3.1. Analysis of oxybutynin chloride

Oxybutynin was quantified by HPLC - MS (Section 3.2.2). The LLOD and LLOQ was 0.9 and 3 ng ml^{-1} respectively. Quantitation was calculated using an external standard solution (Section 2.3.3.1) ranging in concentration from 0.0017 to 1.7 μg ml^{-1}. Calibration curves showed high linearity across the expected analyte concentration range (Figure 3.5). MS analysis of drug in homogenised bladder tissue significantly reduced background noise otherwise present in UV analysis (Figure 3.6A) enabling good precision around the LLOQ (Figure 3.6B).

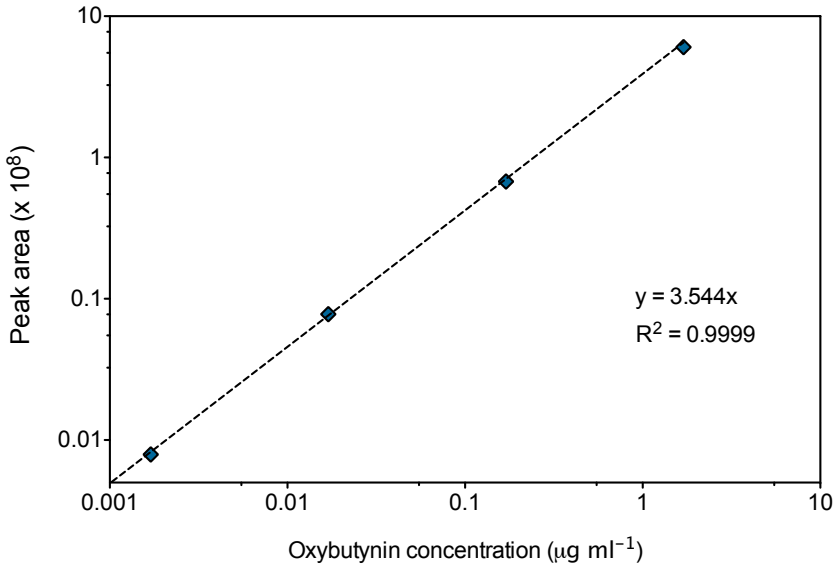

Figure 3.5. Example of an external standard calibration curve used in the HPLC - MS analysis of oxybutynin chloride.

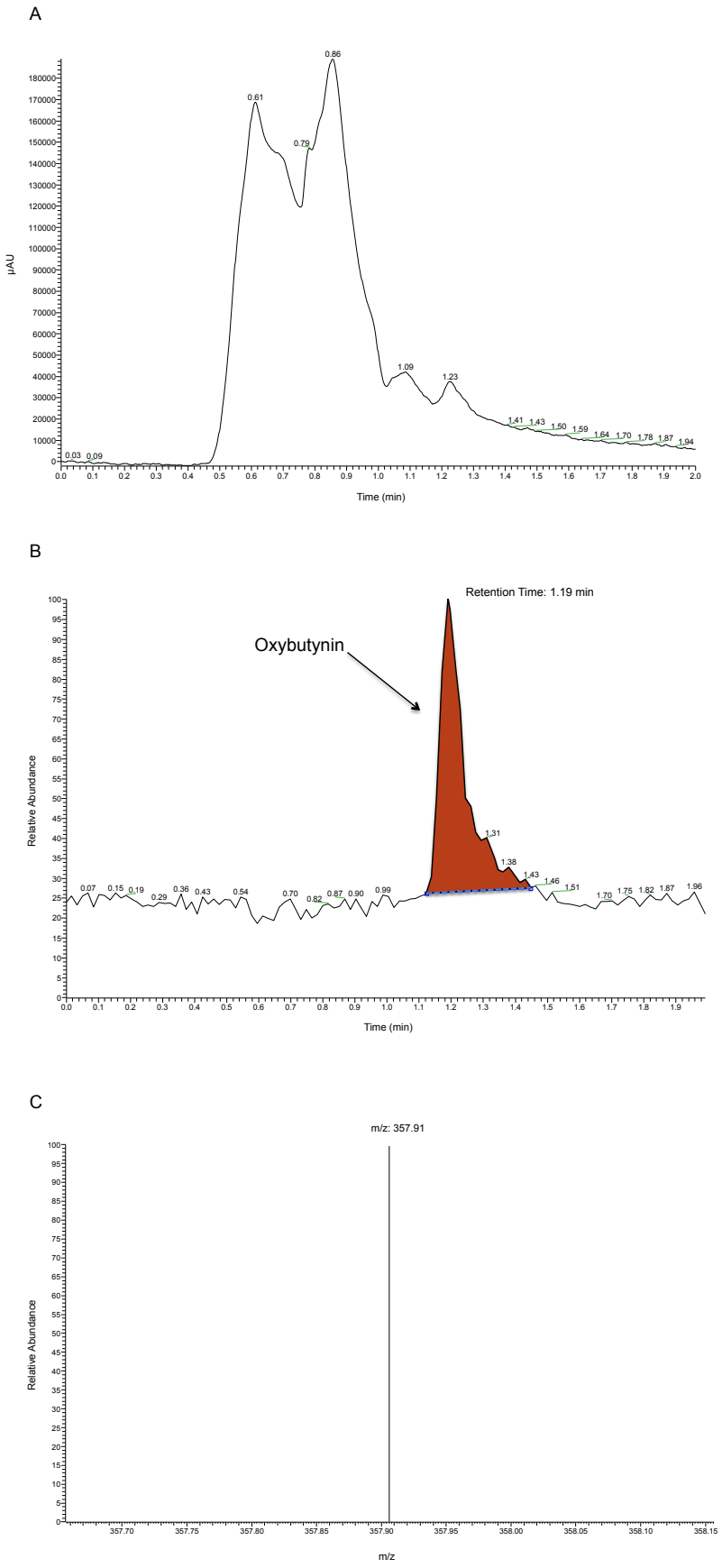

Figure 3.6. Representative UV (A) and relative abundance (B and C) traces from the HPLC - MS analysis of oxybutynin chloride (~ 5 ng ml^{-1}).

3.3.2. Evaluation of the delivery of oxybutynin to the bladder wall

3.3.2.1. Permeation of oxybutynin across the urothelium

Over the 60 min investigated, oxybutynin permeated into the bladder wall in a linear fashion with an apparent K_p value of 1.36 x 10^{-05} cm s^{-1} (Figure 3.7A). Mass balance studies showed that on average 94 % of the applied oxybutynin dose was recovered per diffusion cell with > 90 % recovered from the donor chamber (Figure 3.7B). Concentrations achieved in the urothelium, lamina propria and detrusor muscle generally increased with time with the exception being the slight decrease between the 40 and 60 min timepoints in the lamina propria layer (Figure 3.8A). Oxybutynin concentrations in the detrusor muscle (more clearly visible in Figure 3.8B) were 0.27, 0.82 and 1.77 μg g^{-1} after 20, 40 and 60 min respectively.

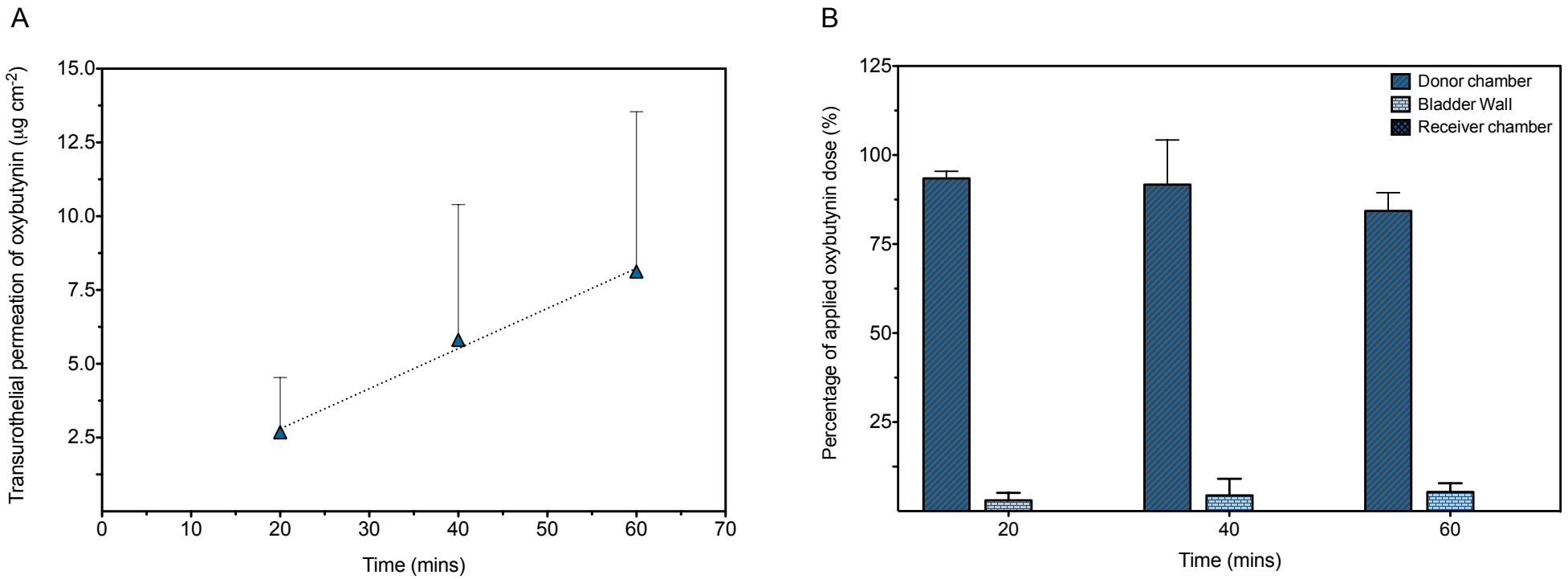

Figure 3.7. Results of the oxybutynin chloride transurothelial permeation study. A) Transurothelial permeation of oxybutynin into the bladder wall over 60 min. An apparent Kp of 1.36 x 10^{-05} cm s^{-1} was calculated by normalising the flux (J, µg cm^{-2} s^{-1}) to the dosing concentration (167 µg ml^{-1}). B) Mass balance analysis showing the percentage recovery of oxybutynin from the Franz - type cell apparatus per sampling timepoint. (n = 4 bladders ± SD).

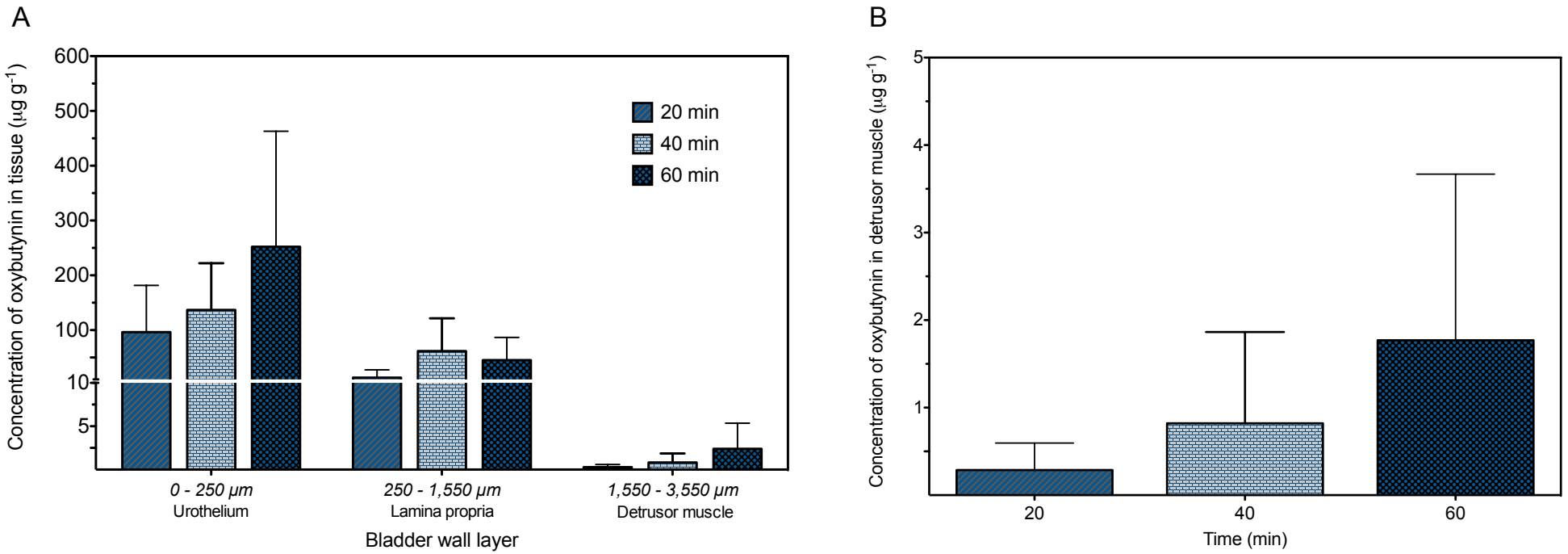

Figure 3.8. Results of the oxybutynin chloride transurothelial permeation study continued. A) Average oxybutynin concentrations achieved in the urothelium, lamina propria and detrusor muscle after 20, 40 and 60 min. B) Average oxybutynin concentrations achieved in the detrusor muscle after 20, 40 and 60 min. (n = 4 bladders ± SD).

Di Stasi *et al* investigated the overall bladder wall concentration achieved after the application of oxybutynin to *ex vivo* human bladder tissue[133]. In comparison to this work, the study used a lower concentration of oxybutynin (45 μg ml^{-1}) and drug was applied for a shorter period of time (15 min). Consequently direct comparisons to overall drug concentrations achieved in the bladder wall are of little value. However Di Stasi *et al* do report an apparent transurothelial flux and from this an apparent transurothelial K_p value can be derived according to the equation

$$k_P = \frac{J}{\Delta C}$$

where K_P is the apparent transurothelial permeability coefficient (cm s^{-1}), J is the apparent transurothelial flux (mg cm^{-2} s^{-1}) and ΔC is the dosing concentration of oxybutynin applied to the donor chamber of the diffusion apparatus at time zero.

K_p values are more comparable than tissue concentrations or flux values as they are normalised to the concentration of oxybutynin applied to the urothelium. From a reported flux value of 0.16 μg cm^{-2} min^{-1}, an apparent transurothelial K_p value of 5.93 x 10^{-05} cm s^{-1} was determined. This is higher than the Kp value determined in this study (1.36 x 10^{-05} cm s^{-1}, Figure 3.7A). Using their K_P value, a simulation was created to display the predicted permeation of oxybutynin in the Di Stasi study compared to this study had the concentration applied to the urothelium been the same (0.167 mg ml^{-1}) (Figure 3.9). The predicted profile helps visualise the difference in permeation rate reported by the two studies.

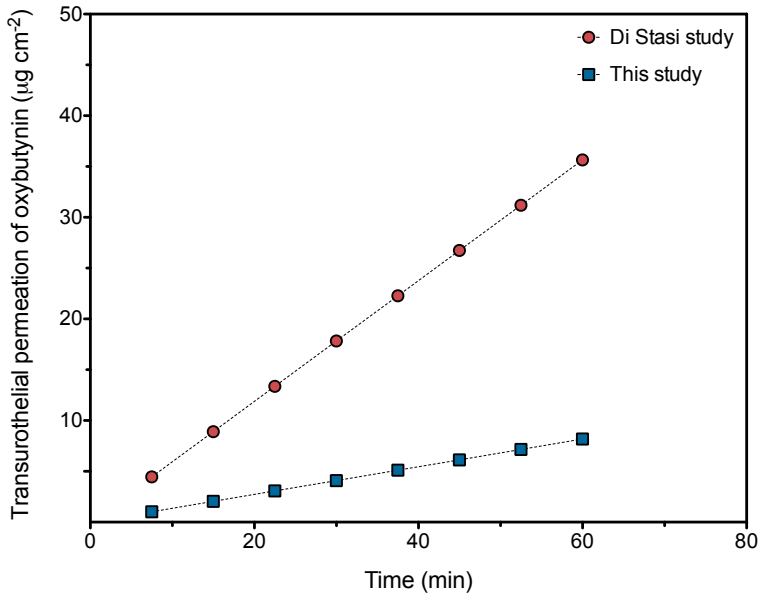

Figure 3.9. Predicted transurothelial permeation profiles of oxybutynin chloride over 60 min. Dosing concentration at time zero is assumed to be 0.167 mg ml^{-1} for both studies. Apparent transurothelial K_P values were calculated experimentally for this work (Figure 3.7A) and extracted from the literature for Di Stasi et al[133].

A possible explanation for the disparity in the values reported concerns the integrity of the urothelial barrier. Histological analysis of their *ex vivo* bladder tissue shows an eroded urothelium consisting of only basal cells and an absence of the superficial umbrella cells fundamental to barrier function (Figure 3.10). Although the value extracted from the Di Stasi study is > 4 fold greater than that determined in this study, they are 'similar' in that they are both markedly higher than that calculated for ketorolac (2.63 x 10^{-6} cm s^{-1}, Section 2.3.3.2). Interestingly in guinea pigs, oxybutynin has been shown to significantly increase bladder permeability to technetium compared to phosphate buffered saline (~ 5 fold increase in permeability)[150]. It is suggested that oxybutynin, a tertiary amine, increases permeability by inactivating the GAG layer in a similar fashion to the mechanism of the quaternary amine protamine. Disruption of the GAG layer could explain the high K_p value although it should be noted that the concentration of oxybutynin used in that study (5 mg ml^{-1}) was ~ 30 fold greater than this study (0.167 mg ml^{-1}).

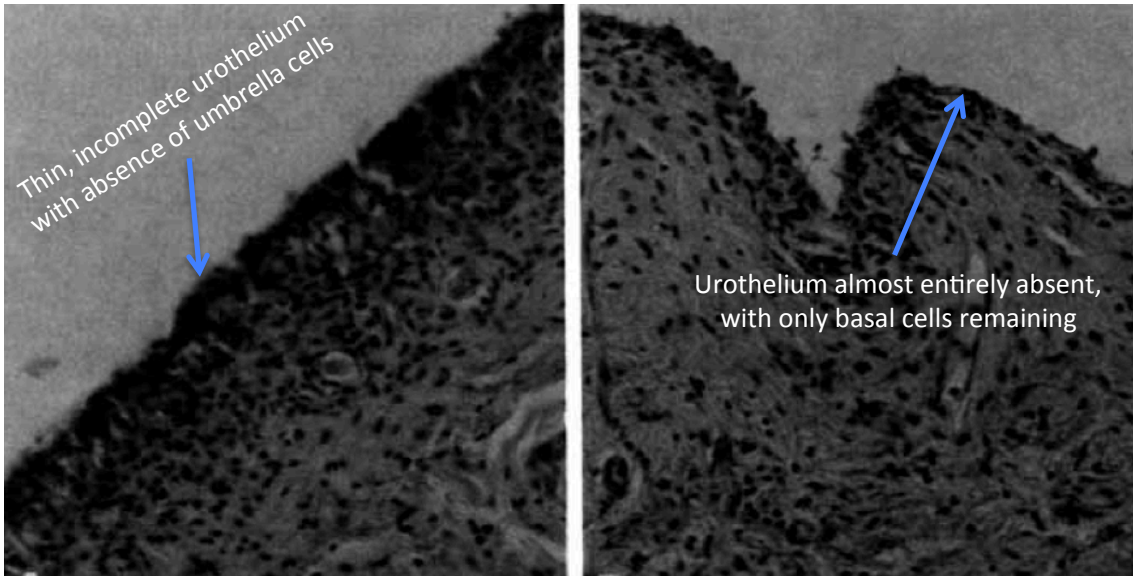

Figure 3.10. Photomicrographs adapted from Di Stasi *et al*[133]. Images show H & E stained mucosa of *ex vivo* human bladder tissue before (A) and after (B) 15 min exposure to oxybutynin chloride solution (45 μg ml^{-1}). The lack of an integral urothelium is evident even in the control sample (A).

In this chapter a new technique to selectively remove the urothelium was investigated. Histological analysis showed the urothelium was successful removed using a cotton swap (Figure 3.11B). In comparison to the same bladder tissue prior to removal (Figure 3.11A), the majority of the urothelium is absent with only basal cells remaining in the natural folds of the tissue layer. Despite urothelial removal, the lamina propria is still intact and of normal morphology. This technique was a modified version of one which has been shown effective in selectively removing rat urothelium[151]. Porcine urothelium is thicker than that of the rat[152] and therefore a more vigorous process was employed. Ideally no urothelial cells would be left intact after the process, however considering the natural folds of the urothelium this may be unrealistic. The cells that remained in the folds were characteristic of the lower, basal urothelial cells and not the superficial umbrella cells believed to be responsible for the barrier function of the urothelium. It is reasonable therefore to assume they provide a lesser barrier to that of an intact urothelium. Indeed this appears to be the case as urothelial removal resulted in a higher rate of permeation into the detrusor muscle, although this was not considered statistically significant (Figure 3.11D). Subsequently higher detrusor muscle concentrations of oxybutynin were achieved at each time point investigated (Figure 3.11C).

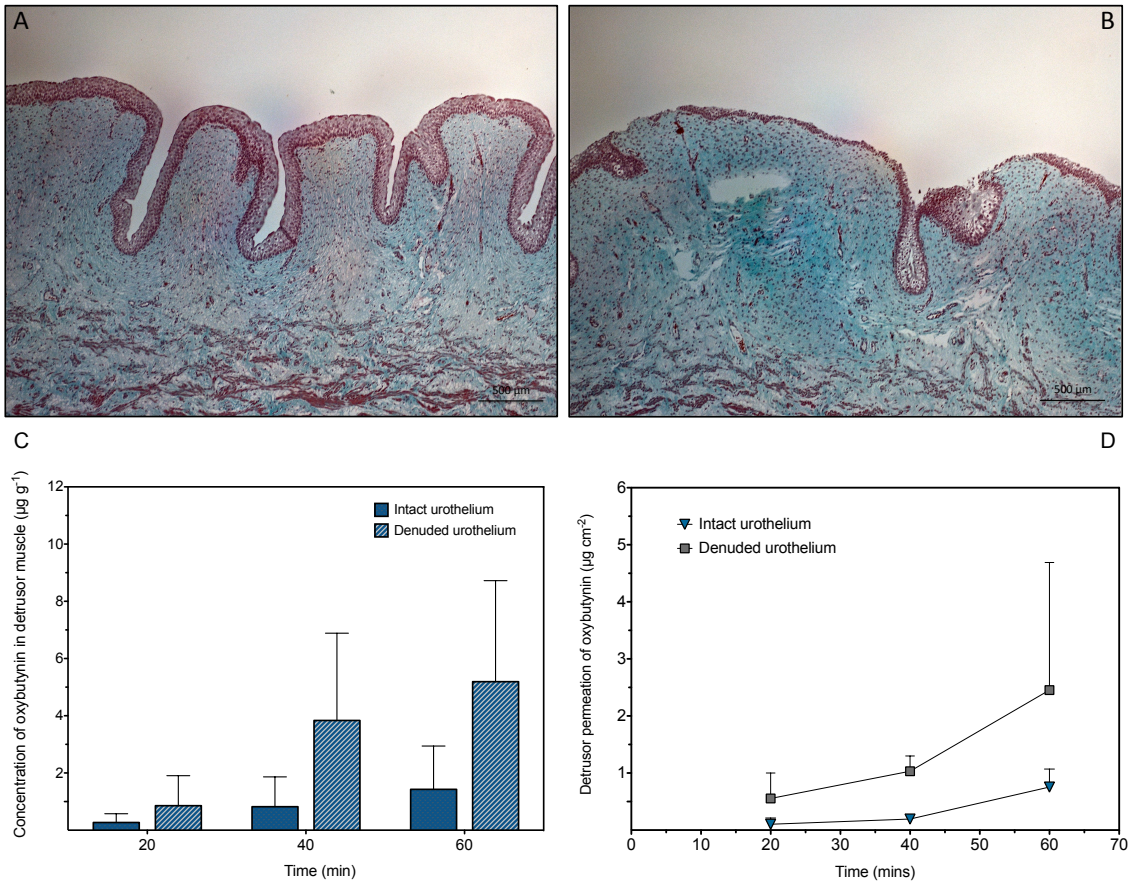

Figure 3.11. Photomicrograph of Masson's trichrome stained porcine bladder tissue before (A) and after (B) removal of the urothelium. Images A and B taken from the same bladder with 50 x magnification (scale bar represents 500 µm). C) Average oxybutynin concentrations achieved in the detrusor muscle of bladder tissue with and without the presence of an intact urothelium. D) Permeation of oxybutynin into the detrusor muscle after application to the surface of bladder tissue with and without the presence of an intact urothelium. (n = 4 bladders ± SD).

Although investigating detrusor concentrations in the denuded urothelium bladder may not have clinical relevance, it does provide a negative control for assessing the intactness of the urothelial barrier in our standard, urothelial intact samples. If there were damage to the urothelium in the non - denuded samples then you would not expect to see any difference in the rate of detrusor permeation or the concentrations achieved in this layer. Additionally histological validation of urothelial removal shows this to be a useful technique for removing porcine urothelium. Whilst this has been shown to be an effective technique in rats, groups using porcine bladder often resort to surgically removing the whole mucosa[102].

The advantage of the conservative technique used here is that an intact lamina propria remains (Figure 3.11B).

3.3.2.2. Intravesical instillation of oxybutynin

The intravesical delivery of oxybutynin was investigated in a whole bladder model. Whilst applying drug solution to the surface of bladder tissue sections (the Franz - cell setup) is a valid way of investigating urothelial permeability, it is not truly representative of IDD where urine production constantly dilutes the instilled dose. By using a whole bladder model we were able to incorporate this variable and additionally instil the same volume of drug solution used clinically (30 ml). Using a ureteral catheter, artificial urine was instilled at a rate of 10 ml every ten min (1ml min^{-1}) for the duration of the 60 min experiment. This is an accepted rate of human urine production[153]. Ideally urine would have been instilled every minute rather than every ten minutes, however this was not feasible with the experimental setup available. Future iterations could employ a pre - loaded syringe driver set at a rate of 1 ml min^{-1}. Artificial urine was prepared from an established recipe, which mirrors the salt content, pH and isotonicity of human urine[134].

Concentration - depth profiles (Figures 3.13 - 14) were typical of those generated for other drugs with the majority of drug sequestered in the superficial urothelium (Section 2.3.3.2)[154]. Bladder sectioning using the cryostat was consistent with no significant differences in average tissue layer weights between bladders instilled with standard or continually diluted with artificial urine oxybutynin solution ($p > 0.05$, Figure 3.12B).

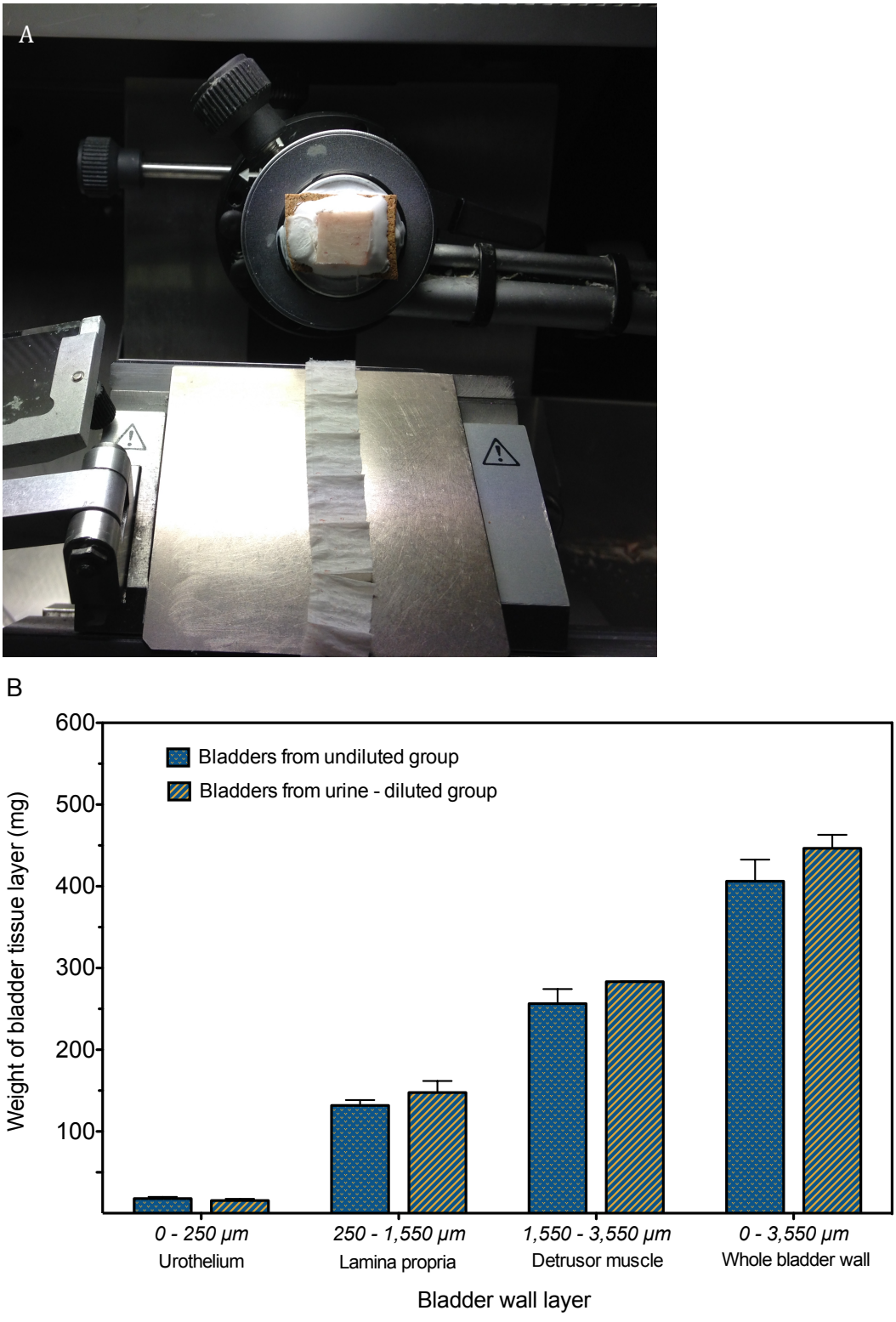

Figure 3.12. A) Representative photograph of the cryostat in use. In this example porcine bladder tissue is being sectioned at the detrusor muscle level. B) Mean total weights of bladder wall tissue layers sectioned from bladders instilled with standard and continually diluted with artificial urine oxybutynin solution. (n = 10 tissue samples from 2 bladders ± SD).

Average tissue concentrations of 298.7, 43.7, 0.93 and 25.8 μg g^{-1} were achieved in the urothelium, lamina propria, detrusor muscle and whole bladder wall respectively (Figure 3.15, blue bars). The introduction of a physiological rate of artificial urine had a significant effect on the penetration of oxybutynin into the bladder wall. In comparison to the standard oxybutynin solution, lower concentrations of 102.7, 23.8, 0.56 and 10.1 μg g^{-1} were achieved in the urothelium, lamina propria, detrusor muscle and whole bladder wall respectively ($p < 0.05$, Figure 3.15, yellow bars). Pharmacokinetic (PK) modelling of IDD has shown the production of urine decreases drug concentrations achieved in the bladder wall[154,155]. It is therefore an integral part of the IDD process. Despite this, it is a physiological variable frequently absent from studies and to date no other groups have incorporated it experimentally into *ex vivo* bladder permeability studies.

For both solutions, drug - tissue concentrations achieved in the urothelium and lamina propria but not the detrusor muscle were greater than reported IC_{50} values for oxybutynin in isolated detrusor muscle (2.27 μg g^{-1} [156], Figure 3.14); suggesting these concentrations are insufficient to significantly inhibit detrusor muscle contraction. This was the case at all depths of detrusor muscle investigated including sections located immediately beneath the lamina propria. This data suggests detrusor concentrations are not sufficient to justify an antimuscarinic MOA based exclusively on direct detrusor muscle inhibition. Furthermore, considering these studies are *ex vivo*, systemic drug clearance from the bladder wall is unaccounted for and therefore *in vivo* detrusor concentrations would likely be lower. These results agree with *in vivo* rat studies, which showed intravesical oxybutynin of the same concentration improved OAB symptoms without affecting detrusor muscle contractility[62].

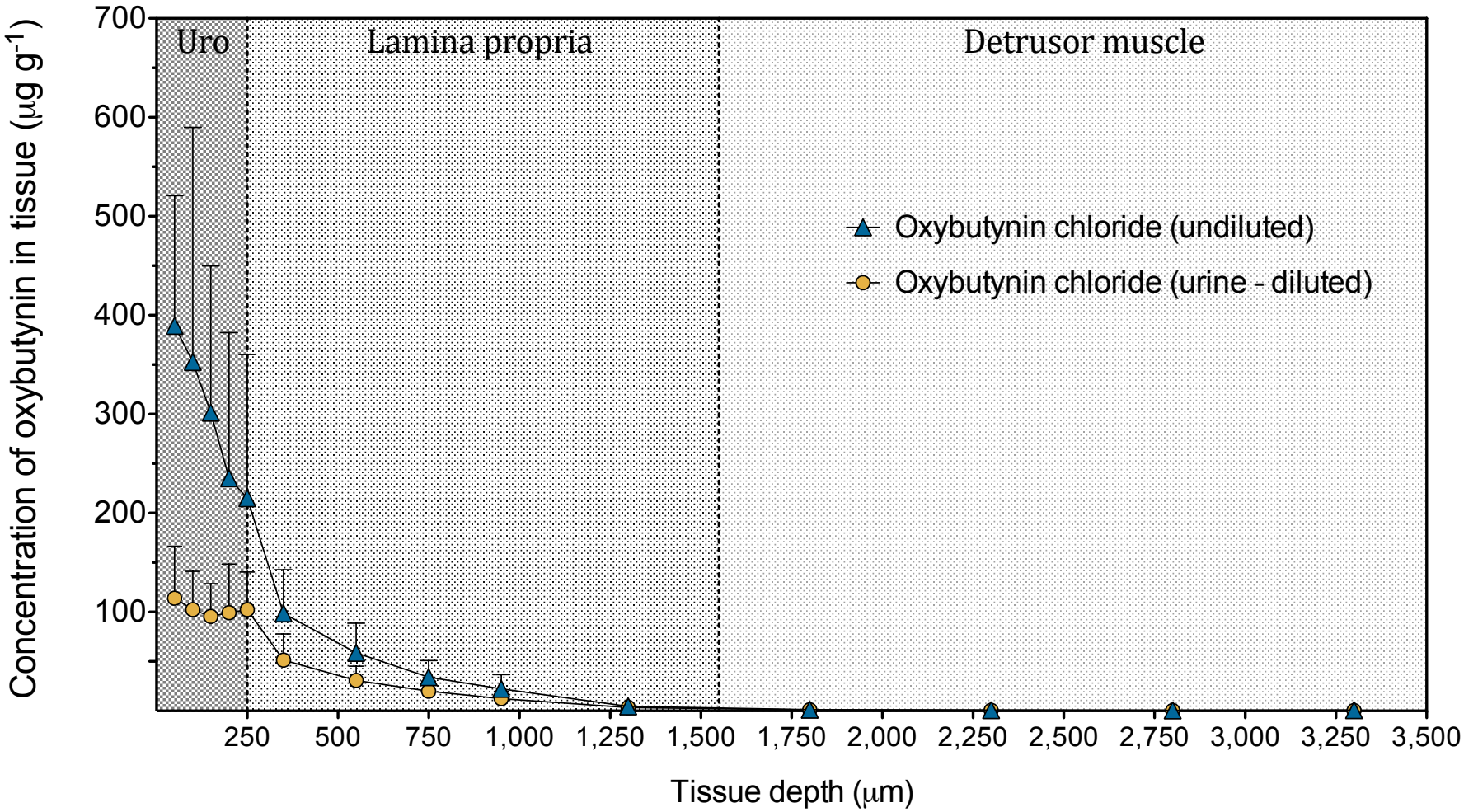

Figure 3.13. Concentration - depth profile showing concentrations of oxybutynin achieved in the bladder wall following 60 min instillation with undiluted or continually diluted with artificial urine oxybutynin solution. (n = 10 tissue samples from 2 bladders ± SD).

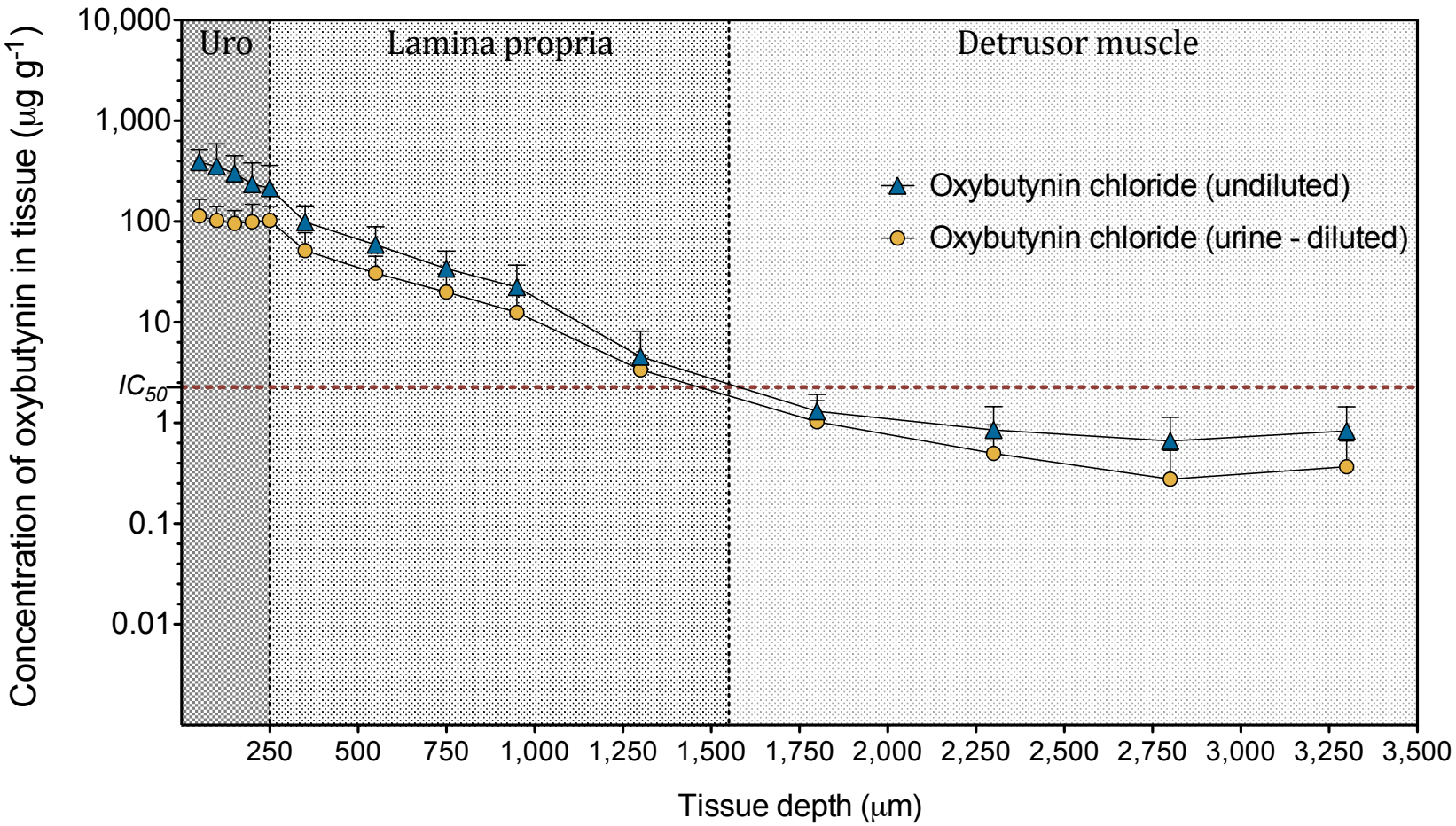

Figure 3.14. Log concentration - depth profile showing concentrations of oxybutynin achieved in the bladder wall following 60 min instillation with undiluted or continually diluted with artificial urine oxybutynin solution (same data as Figure 3.13). IC_{50} value for oxybutynin is included[156]. (n = 10 tissue samples from 2 bladders ± SD).

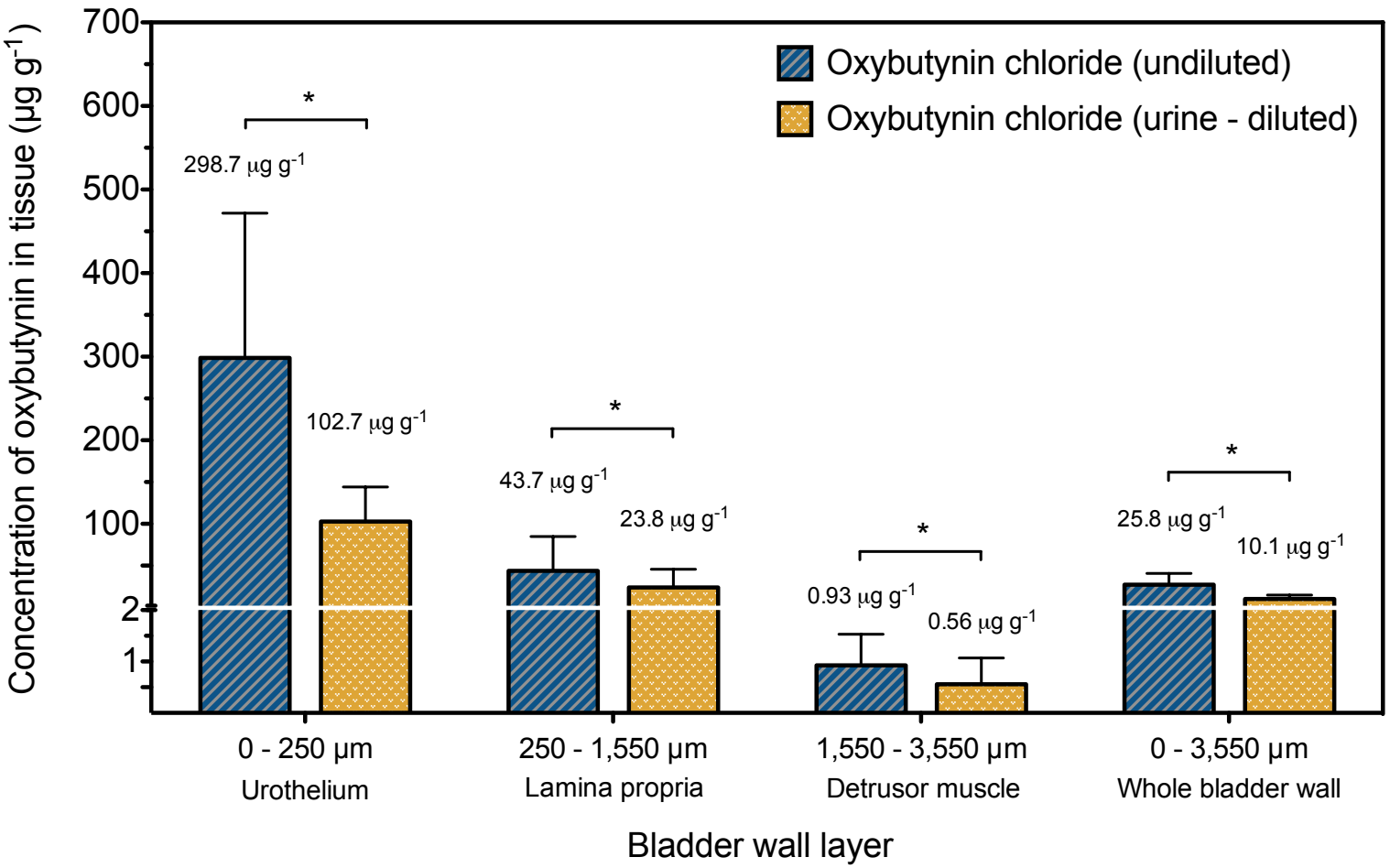

Figure 3.15. Average oxybutynin concentrations achieved in the different layers of the bladder wall following 60 min instillation with undiluted or continually diluted with artificial urine oxybutynin solution. (*$p < 0.05$, calculated by unpaired t – test, n = 10 tissue samples from 2 bladders ± SD).

3.3.2.3. Histology

Landau *et al* investigated the effects of intravesical oxybutynin on the morphology of the bladder wall using an *in vivo* rabbit model[157]. Oxybutynin (3.5 mg ml^{-1} in saline) was instilled daily and animals sacrificed at 1, 10 and 30 days. The authors did not specify how long instillations were retained in the bladder. Post - sacrifice, bladder tissue was examined under light microscopy and assessed for inflammation by a blinded pathologist. Intravesical oxybutynin caused no harmful local effects to the bladder tissue, with the mild inflammation observed attributed to the effects of daily catheterisation (as the same was observed in the control group).

To assess any effects oxybutynin may have had on the gross morphology of the *ex vivo* porcine bladder tissue, sections from bladders instilled with oxybutynin solution were stained with Masson's trichrome and compared to control samples excised immediately post – sacrifice (Figure 3.16). Masson's trichrome is a three - colour stain used to distinguish cellular layers (nuclei stain black, whilst cytoplasm, keratin and muscle cells stain pink) from surrounding connective tissue (collagen stains blue). Compared to a standard H & E technique, Masson's trichrome allows easy differentiation of the different bladder wall layers[158,159].

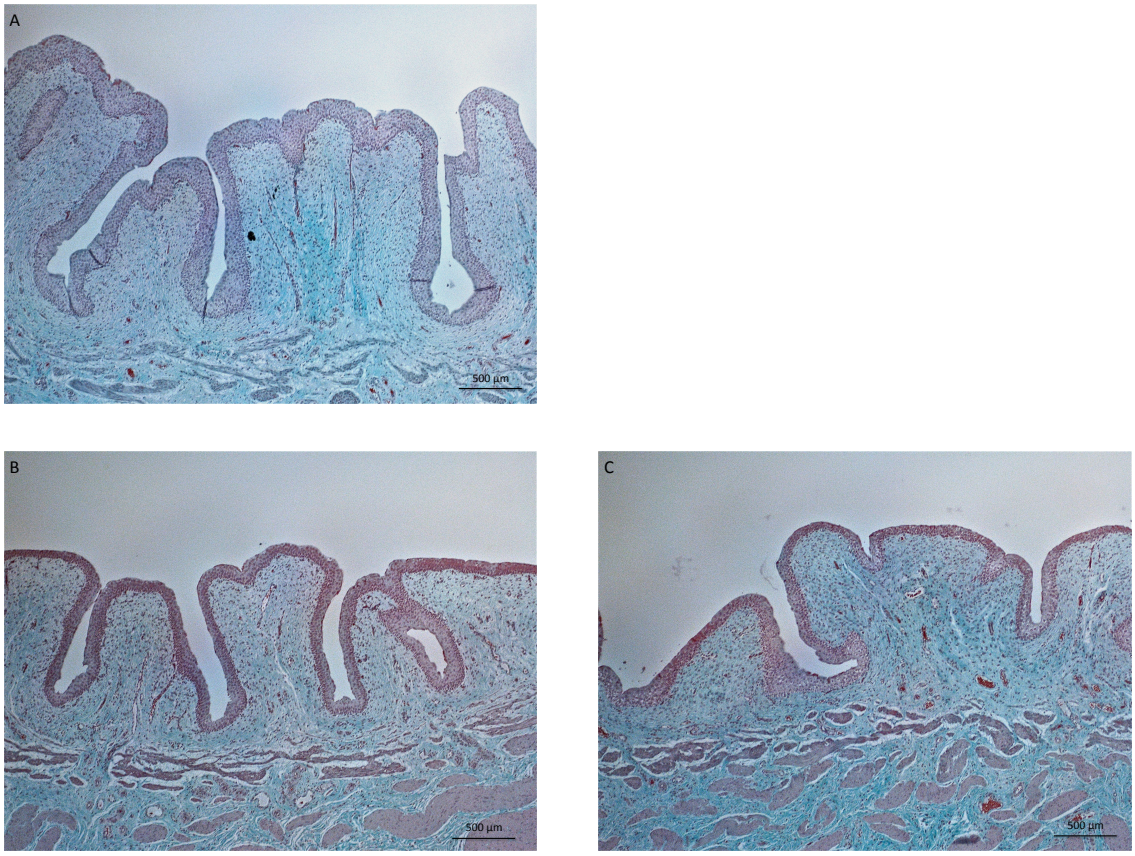

Figure 3.16. Photomicrographs of Masson's trichrome stained porcine bladder tissue taken from bladders excised immediately post - sacrifice (A), following 60 min instillation with standard (undiluted) oxybutynin solution (B) and following 60 min instillation with oxybutynin solution continually diluted with artificial urine (C). All images 50 x magnification (scale bar represents 500 µm).

In agreement with the aforementioned studies[157], the histological results of the *ex vivo* porcine bladder used in this study suggest no significant changes in the overall morphology of the tissue with intact, normal urothelium (pink) and lamina propria (blue) present in both the standard and urine diluted oxybutynin instillations (Figures 3.16B - C). Drug - treated sections are comparable to control sections taken on - site at the abattoir, immediately post - sacrifice of the animal (Figure 3.16A). The urothelium of the control bladder is slightly thicker than that of the drug - treated bladders, however it is well established that urothelial thickness varies not only between morphologically normal bladders of the same specie (the control section has to be taken from a different bladder to those used in the study) but also depending on bladder wall distension at the time of sectioning[160]. Additionally umbrella cells are present in photomicrographs of bladders instilled with oxybutynin solution (Figures 3.16B - C). In comparison to the histology

reported by Di Stasi *et al* (Figure 3.10)[133], the *ex vivo* bladder tissue used in this work displays a normal morphology with a complete, multi - cell layered urothelium.

3.4. Conclusions

This chapter aimed to increase our understanding of the concentrations of oxybutynin achieved in the bladder wall after intravesical delivery. A detailed analysis of drug concentrations achieved in the urothelium, lamina propria and detrusor muscle is provided. Oxybutynin permeated the bladder wall more readily than other drugs previously investigated. Abrading the urothelium with a cotton swab has been shown an effective way of selectively removing porcine urothelium and one that may be beneficial for future studies. For the first time, urine dilution has been incorporated into *ex vivo* permeability studies and its effect on concentrations achieved in the bladder wall shown. Concentration - depth profiles suggest oxybutynin concentrations achieved in the detrusor muscle after application of a clinically relevant intravesical dose are insufficient to directly inhibit bladder wall contraction. Consequently, these drug delivery studies add more weight to the growing argument that antimuscarincs exert their effects on the bladder wall through mechanisms other than direct detrusor inhibition. An inherent limitation of this study is that it did not concomitantly investigate detrusor muscle contractility with drug concentrations achieved in the bladder wall. We cannot therefore directly state that these concentrations are insufficient to inhibit detrusor muscle contraction. Ideally pharmacology groups will work hand in hand with drug delivery groups to achieve real time, functional concentration - depth profiles. This would elicit knowledge of *in vivo* tissue concentrations, and therefore information regarding site of action, necessary to modulate afferent activity in the bladder wall.

3.5. Reference List

1. De Wachter S, Wyndaele J-J. Intravesical oxybutynin: a local anesthetic effect on bladder C afferents. J Urol. 2003 May;169(5):1892–5.

2. Actavis Pharma Inc. SPC: Oxytrol [Internet]. 2013 [cited 2014 Jan 1]. Available from: http://www.actavis.com.au/NR/rdonlyres/2C1B73FC-BE23-41FC-81BA-9088F8DC2604/0/OXYTRO_PI.pdf

3. Patel R, Subrahmanyam EVS, Sharbaraya AR. Development and validation of new colorimetric method for the estimation of oxybutynin chloride in bulk and dosage form. J Chem Pharm Res. 2012;4(9):4324–51.

4. Abcam. Product data sheet: Oxybutynin hydrochloride ab142532 [Internet]. 2013 [cited 2014 Jan 1]. Available from: http://www.abcam.com/Oxybutynin-hydrochloride-ab142532.html

5. Jirschele K, Sand PK. Oxybutynin: past, present, and future. Int Urogynecology J. 2013 Apr;24(4):595–604.

6. Andersson KE. Storage and voiding symptoms: pathophysiologic aspects. Urology. 2003 Nov;62(5 Suppl 2):3–10.

7. Wein A. Symptom-based diagnosis of overactive bladder: an overview. Can Urol Assoc J. 2011 Oct;5(5 Suppl 2):S135–6.

8. Abrams P, Kelleher CJ, Kerr LA, Rogers RG. Overactive bladder significantly affects quality of life. Am J Manag Care. 2000 Jul;6(11 Suppl):S580–90.

9. Abrams P, Cardozo L, Fall M, Griffiths D, Rosier P, Ulmsten U, et al. The standardisation of terminology of lower urinary tract function: report from the Standardisation Sub-committee of the International Continence Society. Am J Obstet Gynecol. 2002 Jul;187(1):116–26.

10. Milsom I, Abrams P, Cardozo L, Roberts RG, Thüroff J, Wein AJ. How widespread are the symptoms of an overactive bladder and how are they

managed? A population-based prevalence study. BJU Int. 2001 Jun;87(9):760–6.

11. Gormley EA, Lightner DJ, Burgio KL, Chai TC, Clemens JQ, Culkin DJ, et al. Diagnosis and treatment of overactive bladder (non-neurogenic) in adults: AUA / SUFU guideline. J Urol. 2012 Dec;188(6 Suppl):2455–63.

12. Andersson K-E. Antimuscarinic mechanisms and the overactive detrusor: an update. Eur Urol. 2011 Mar;59(3):377–86.

13. Mansfield KJ. Muscarinic Receptor Antagonists, the Overactive Bladder and Efficacy against Urinary Urgency. Clin Med Insights Ther. 2010;(2):471–80.

14. De Groat WC. Neural control of the urinary bladder and sexual organs. In: Mathias CJ, Bannister R, editors. Autonomic failure. 4th ed. Oxford: Oxford University Press; 2001. p. 151–65.

15. Purves D. The Visceral Motor System: Autonomic Regulation of the Bladder. In: Augustine GJ, Fitzpatrick D, Hall WC, LaMantia A-S, White LE, Purves D, editors. Neuroscience. 5th ed. Sunderland, Mass.: Sinauer Associates; 2012. p. 470–4.

16. Rong W, Spyer KM, Burnstock G. Activation and sensitisation of low and high threshold afferent fibres mediated by P2X receptors in the mouse urinary bladder. J Physiol. 2002 Jun 1;541(Pt 2):591–600.

17. De Groat WC, Booth AM, Yoshimura N. Neurophysiology of micturition and its modification in animal models of human disease. In: Maggi CA, editor. Nervous control of the urogenital system. Chur, Switzerland; Langhorne, Pa.: Harwood Academic Publishers; 1993. p. 227–90.

18. Sengupta JN, Gebhart GF. Mechanosensitive properties of pelvic nerve afferent fibers innervating the urinary bladder of the rat. J Neurophysiol. 1994 Nov;72(5):2420–30.

19. Kandel ER, Schwartz JH, Jessell TM, Siegelbaum SA, Hudspeth AJ, editors. The Autonomic Motor System and the Hypothalamus. Principles of neural science. 5th ed. New York: McGraw-Hill Medical Publishing Division; 2011. p. 1067–8.

20. Gabella G, Davis C. Distribution of afferent axons in the bladder of rats. J Neurocytol. 1998 Mar;27(3):141–55.

21. Birder LA, Nakamura Y, Kiss S, Nealen ML, Barrick S, Kanai AJ, et al. Altered urinary bladder function in mice lacking the vanilloid receptor TRPV1. Nat Neurosci. 2002 Sep;5(9):856–60.

22. Grol S, van Koeveringe GA, de Vente J, van Kerrebroeck PEV, Gillespie JI. Regional differences in sensory innervation and suburothelial interstitial cells in the bladder neck and urethra. BJU Int. 2008 Sep;102(7):870–7.

23. Birder LA. Nervous network for lower urinary tract function. Int J Urol. 2013 Jan;20(1):4–12.

24. Cruz F, Dinis P. Resiniferatoxin and botulinum toxin type A for treatment of lower urinary tract symptoms. Neurourol Urodyn. 2007 Oct;26(6 Suppl):920–7.

25. Sánchez-Freire V, Blanchard MG, Burkhard FC, Kessler TM, Kellenberger S, Monastyrskaya K. Acid-sensing channels in human bladder: expression, function and alterations during bladder pain syndrome. J Urol. 2011 Oct;186(4):1509–16.

26. Ford AP. In pursuit of P2X3 antagonists: novel therapeutics for chronic pain and afferent sensitization. Purinergic Signal. 2012 Feb;8(Suppl 1):3–26.

27. Birder L, Andersson K-E. Urothelial signaling. Physiol Rev. 2013 Apr;93(2):653–80.

28. Apodaca G, Balestreire E, Birder LA. The uroepithelial-associated sensory web. Kidney Int. 2007 Nov;72(9):1057–64.

29. Birder LA, Ruggieri M, Takeda M, van Koeveringe G, Veltkamp SA, Korstanje C, et al. How does the urothelium affect bladder function in health and disease? Neurourol Urodyn. 2012 Mar;31(3):293–9.

30. Birder LA, de Groat WC. Mechanisms of Disease: involvement of the urothelium in bladder dysfunction. Nat Clin Pract Urol. 2007 Jan;4(1):46–54.

31. Khandelwal P, Abraham SN, Apodaca G. Cell biology and physiology of the uroepithelium. Am J Physiol Renal Physiol. 2009 Dec;297(6):F1477–501.

32. Arrighi N, Bodei S, Peroni A, Mirabella G, Zani D, Simeone C, et al. Detection of muscarinic receptor subtypes in human urinary bladder mucosa: age and gender-dependent modifications. Neurourol Urodyn. 2008;27(5):421–8.

33. Bschleipfer T, Schukowski K, Weidner W, Grando SA, Schwantes U, Kummer W, et al. Expression and distribution of cholinergic receptors in the human urothelium. Life Sci. 2007 May 30;80(24-25):2303–7.

34. Grol S, Essers PBM, van Koeveringe GA, Martinez-Martinez P, de Vente J, Gillespie JI. M(3) muscarinic receptor expression on suburothelial interstitial cells. BJU Int. 2009 Aug;104(3):398–405.

35. Mansfield KJ, Liu L, Mitchelson FJ, Moore KH, Millard RJ, Burcher E. Muscarinic receptor subtypes in human bladder detrusor and mucosa, studied by radioligand binding and quantitative competitive RT-PCR: changes in ageing. Br J Pharmacol. 2005 Apr;144(8):1089–99.

36. Mukerji G, Yiangou Y, Grogono J, Underwood J, Agarwal SK, Khullar V, et al. Localization of M2 and M3 muscarinic receptors in human bladder disorders and their clinical correlations. J Urol. 2006 Jul;176(1):367–73.

37. Beckel JM, Kanai A, Lee S-J, de Groat WC, Birder LA. Expression of functional nicotinic acetylcholine receptors in rat urinary bladder epithelial cells. Am J Physiol Renal Physiol. 2006 Jan;290(1):F103–10.

38. Burnstock G. Purine-mediated signalling in pain and visceral perception. Trends Pharmacol Sci. 2001 Apr;22(4):182–8.

39. Burnstock G. Purinergic signalling: past, present and future. Braz J Med Biol Res. 2009 Jan;42(1):3–8.

40. Chopra B, Gever J, Barrick SR, Hanna-Mitchell AT, Beckel JM, Ford AP, et al. Expression and function of rat urothelial P2Y receptors. Am J Physiol Renal Physiol. 2008 Apr;294(4):F821–9.

41. Moro C, Tajouri L, Chess-Williams R. Adrenoceptor function and expression in bladder urothelium and lamina propria. Urology. 2013 Jan;81(1):211.e1–7.

42. Birder LA, Nealen ML, Kiss S, de Groat WC, Caterina MJ, Wang E, et al. Beta-adrenoceptor agonists stimulate endothelial nitric oxide synthase in rat urinary bladder urothelial cells. J Neurosci. 2002 Sep 15;22(18):8063–70.

43. Ikeda Y, Fry C, Hayashi F, Stolz D, Griffiths D, Kanai A. Role of gap junctions in spontaneous activity of the rat bladder. Am J Physiol Renal Physiol. 2007 Oct;293(4):F1018–25.

44. Ikeda Y, Kanai A. Urotheliogenic modulation of intrinsic activity in spinal cord-transected rat bladders: role of mucosal muscarinic receptors. Am J Physiol Renal Physiol. 2008 Aug;295(2):F454–61.

45. Fry CH, Young JS, Jabr RI, McCarthy C, Ikeda Y, Kanai AJ. Modulation of spontaneous activity in the overactive bladder: the role of P2Y agonists. Am J Physiol Renal Physiol. 2012 Jun 1;302(11):F1447–54.

46. Caulfield MP, Birdsall NJ. International Union of Pharmacology. XVII. Classification of muscarinic acetylcholine receptors. Pharmacol Rev. 1998 Jun;50(2):279–90.

47. Wang P, Luthin GR, Ruggieri MR. Muscarinic acetylcholine receptor subtypes mediating urinary bladder contractility and coupling to GTP binding proteins. J Pharmacol Exp Ther. 1995 May;273(2):959–66.

48. Yamanishi T, Chapple CR, Yasuda K, Chess-Williams R. The role of M2-muscarinic receptors in mediating contraction of the pig urinary bladder in vitro. Br J Pharmacol. 2000;131(7):1482–8.

49. Sellers DJ, Chess-Williams R. Muscarinic agonists and antagonists: effects on the urinary bladder. Handb Exp Pharmacol. 2012;208:375–400.

50. McCloskey KD. Interstitial cells in the urinary bladder-localization and function. Neurourol Urodyn. 2010;29(1):82–7.

51. Davidson RA, McCloskey KD. Morphology and localization of interstitial cells in the guinea pig bladder: structural relationships with smooth muscle and neurons. J Urol. 2005 Apr;173(4):1385–90.

52. Tyagi S, Tyagi P, Van-le Suzy, Yoshimura N, Chancellor MB, de Miguel F. Qualitative and quantitative expression profile of muscarinic receptors in human urothelium and detrusor. J Urol. 2006 Oct;176(4 Pt 1):1673–8.

53. Yoshimura N. Lower urinary tract symptoms (LUTS) and bladder afferent activity. Neurourol Urodyn. 2007 Oct;26(6 Suppl):908–13.

54. Andersson K-E. Antimuscarinics for treatment of overactive bladder. Lancet Neurol. 2004 Jan;3(1):46–53.

55. De Groat WC, Yoshimura N. Mechanisms underlying the recovery of lower urinary tract function following spinal cord injury. Prog Brain Res. 2006;152:59–84.

56. Andersson K-E, Yoshida M. Antimuscarinics and the overactive detrusor-which is the main mechanism of action? Eur Urol. 2003 Jan;43(1):1–5.

57. Finney SM, Andersson K-E, Gillespie JI, Stewart LH. Antimuscarinic drugs in detrusor overactivity and the overactive bladder syndrome: motor or sensory actions? BJU Int. 2006 Sep;98(3):503–7.

58. Matsumoto Y, Miyazato M, Furuta A, Torimoto K, Hirao Y, Chancellor MB, et al. Differential roles of M2 and M3 muscarinic receptor subtypes in modulation of bladder afferent activity in rats. Urology. 2010 Apr;75(4):862–7.

59. Chapple CR, Khullar V, Gabriel Z, Muston D, Bitoun CE, Weinstein D. The effects of antimuscarinic treatments in overactive bladder: an update of a systematic review and meta-analysis. Eur Urol. 2008 Sep;54(3):543–62.

60. Abrams P, Kaplan S, De Koning Gans HJ, Millard R. Safety and tolerability of tolterodine for the treatment of overactive bladder in men with bladder outlet obstruction. J Urol. 2006 Mar;175(3 Pt 1):999–1004; discussion 1004.

61. Yu Y, de Groat WC. Effects of stimulation of muscarinic receptors on bladder afferent nerves in the in vitro bladder-pelvic afferent nerve preparation of the rat. Brain Res. 2010 Nov 18;1361:43–53.

62. Kim Y, Yoshimura N, Masuda H, de Miguel F, Chancellor MB. Antimuscarinic agents exhibit local inhibitory effects on muscarinic receptors in bladder-afferent pathways. Urology. 2005 Feb;65(2):238–42.

63. Iijima K, De Wachter S, Wyndaele J-J. Effects of the M3 receptor selective muscarinic antagonist darifenacin on bladder afferent activity of the rat pelvic nerve. Eur Urol. 2007 Sep;52(3):842–7.

64. Andersson K-E, Arner A. Urinary bladder contraction and relaxation: physiology and pathophysiology. Physiol Rev. 2004 Jul;84(3):935–86.

65. Gillespie JI, van Koeveringe GA, de Wachter SG, de Vente J. On the origins of the sensory output from the bladder: the concept of afferent noise. BJU Int. 2009 May;103(10):1324–33.

66. Gillespie JI. A developing view of the origins of urgency: the importance of animal models. BJU Int. 2005 Sep;96 Suppl 1:22–8.

67. Drake MJ, Harvey IJ, Gillespie JI, Van Duyl WA. Localized contractions in the normal human bladder and in urinary urgency. BJU Int. 2005 May;95(7):1002–5.

68. Moro C, Uchiyama J, Chess-Williams R. Urothelial/lamina propria spontaneous activity and the role of M3 muscarinic receptors in mediating rate responses to stretch and carbachol. Urology. 2011 Dec;78(6):1442.e9–15.

69. Reitz A. Editorial Comment on: Effects of the M3 Receptor Selective Muscarinic Antagonist Darifenacin on Bladder Afferent Activity of the Rat Pelvic Nerve. Eur Urol. 2007 Sep;52(3):848–9.

70. Ferguson DR, Kennedy I, Burton TJ. ATP is released from rabbit urinary bladder epithelial cells by hydrostatic pressure changes-a possible sensory mechanism? J Physiol. 1997 Dec 1;505 (Pt 2):503–11.

71. Yamaguchi O. Antimuscarinics and overactive bladder: other mechanism of action. Neurourol Urodyn. 2010;29(1):112–5.

72. De Laet K, De Wachter S, Wyndaele J-J. Systemic oxybutynin decreases afferent activity of the pelvic nerve of the rat: new insights into the working mechanism of antimuscarinics. Neurourol Urodyn. 2006;25(2):156–61.

73. Cheng Y, Mansfield KJ, Allen W, Walsh CA, Burcher E, Moore KH. Does adenosine triphosphate released into voided urodynamic fluid contribute to urgency signaling in women with bladder dysfunction? J Urol. 2010 Mar;183(3):1082–6.

74. Kumar V, Chapple CR, Rosario D, Tophill PR, Chess-Williams R. In vitro release of adenosine triphosphate from the urothelium of human bladders with detrusor overactivity, both neurogenic and idiopathic. Eur Urol. 2010 Jun;57(6):1087–92.

75. Kumar V, Chapple CR, Surprenant AM, Chess-Williams R. Enhanced adenosine triphosphate release from the urothelium of patients with painful bladder syndrome: a possible pathophysiological explanation. J Urol. 2007 Oct;178(4 Pt 1):1533–6.

76. Sun Y, Keay S, De Deyne PG, Chai TC. Augmented stretch activated adenosine triphosphate release from bladder uroepithelial cells in patients with interstitial cystitis. J Urol. 2001 Nov;166(5):1951–6.

77. Vlaskovska M, Kasakov L, Rong W, Bodin P, Bardini M, Cockayne DA, et al. P2X3 knock-out mice reveal a major sensory role for urothelially released ATP. J Neurosci. 2001 Aug 1;21(15):5670–7.

78. Cockayne DA, Hamilton SG, Zhu QM, Dunn PM, Zhong Y, Novakovic S, et al. Urinary bladder hyporeflexia and reduced pain-related behaviour in P2X3-deficient mice. Nature. 2000 Oct 26;407(6807):1011–5.

79. Liu F, Takahashi N, Yamaguchi O. Expression of P2X3 purinoceptors in suburothelial myofibroblasts of the normal human urinary bladder. Int J Urol. 2009 Jun;16(6):570–5.

80. Wu C, Sui GP, Fry CH. Purinergic regulation of guinea pig suburothelial myofibroblasts. J Physiol. 2004 Aug 15;559(Pt 1):231–43.

81. Fry CH, Ikeda Y, Harvey R, Wu C, Sui G-P. Control of bladder function by peripheral nerves: avenues for novel drug targets. Urology. 2004 Mar;63(3 Suppl 1):24–31.

82. Wiseman OJ, Fowler CJ, Landon DN. The role of the human bladder lamina propria myofibroblast. BJU Int. 2003 Jan;91(1):89–93.

83. Wiseman OJ, Brady CM, Hussain IF, Dasgupta P, Watt H, Fowler CJ, et al. The ultrastructure of bladder lamina propria nerves in healthy subjects and patients with detrusor hyperreflexia. J Urol. 2002 Nov;168(5):2040–5.

84. Brading AF, McCloskey KD. Mechanisms of Disease: specialized interstitial cells of the urinary tract-an assessment of current knowledge. Nat Clin Pract Urol. 2005 Nov;2(11):546–54.

85. Fry CH, Sui G-P, Kanai AJ, Wu C. The function of suburothelial myofibroblasts in the bladder. Neurourol Urodyn. 2007 Oct;26(6 Suppl):914–9.

86. Yoshida M, Miyamae K, Iwashita H, Otani M, Inadome A. Management of detrusor dysfunction in the elderly: changes in acetylcholine and adenosine triphosphate release during aging. Urology. 2004 Mar;63(3 Suppl 1):17–23.

87. Lips KS, Wunsch J, Zarghooni S, Bschleipfer T, Schukowski K, Weidner W, et al. Acetylcholine and molecular components of its synthesis and release machinery in the urothelium. Eur Urol. 2007 Apr;51(4):1042–53.

88. Yoshida M, Masunaga K, Satoji Y, Maeda Y, Nagata T, Inadome A. Basic and clinical aspects of non-neuronal acetylcholine: expression of non-neuronal acetylcholine in urothelium and its clinical significance. J Pharmacol Sci. 2008 Feb;106(2):193–8.

89. Hanna-Mitchell AT, Beckel JM, Barbadora S, Kanai AJ, de Groat WC, Birder LA. Non-neuronal acetylcholine and urinary bladder urothelium. Life Sci. 2007 May 30;80(24-25):2298–302.

90. Staskin DR. Overactive bladder in the elderly: a guide to pharmacological management. Drugs Aging. 2005;22(12):1013–28.

91. Wagg AS, Cardozo L, Chapple C, De Ridder D, Kelleher C, Kirby M, et al. Overactive bladder syndrome in older people. BJU Int. 2007 Mar;99(3):502–9.

92. Giglio D, Ryberg AT, To K, Delbro DS, Tobin G. Altered muscarinic receptor subtype expression and functional responses in cyclophosphamide induced cystitis in rats. Auton Neurosci Basic Clin. 2005 Oct 30;122(1-2):9–20.

93. Tong Y-C, Cheng J-T, Hsu C-T. Alterations of M(2)-muscarinic receptor protein and mRNA expression in the urothelium and muscle layer of the streptozotocin-induced diabetic rat urinary bladder. Neurosci Lett. 2006 Oct 9;406(3):216–21.

94. Kim Y, Yoshimura N, Masuda H, De Miguel F, Chancellor MB. Intravesical instillation of human urine after oral administration of trospium, tolterodine and oxybutynin in a rat model of detrusor overactivity. BJU Int. 2006 Feb;97(2):400–3.

95. Kullmann FA, Artim DE, Birder LA, de Groat WC. Activation of muscarinic receptors in rat bladder sensory pathways alters reflex bladder activity. J Neurosci. 2008 Feb 20;28(8):1977–87.

96. Haga N, Aikawa K, Shishido K, Takahashi N, Yanagida T, Yamaguchi O. Effect of long-term oxybutynin administration on c-Fos expression in spinal neurons: inhibition of antimuscarinics on bladder afferents in conscious rats. Urology. 2009 Jan;73(1):200–4.

97. Yokoyama O, Yusup A, Miwa Y, Oyama N, Aoki Y, Akino H. Effects of tolterodine on an overactive bladder depend on suppression of C-fiber bladder afferent activity in rats. J Urol. 2005 Nov;174(5):2032–6.

98. Yokoyama O, Tanaka I, Kusukawa N, Yamauchi H, Ito H, Aoki Y, et al. Antimuscarinics suppress adenosine triphosphate and prostaglandin E2 release from urothelium with potential improvement in detrusor overactivity in rats with cerebral infarction. J Urol. 2011 Jun;185(6):2392–7.

99. Young JS, Matharu R, Carew MA, Fry CH. Inhibition of stretching-evoked ATP release from bladder mucosa by anticholinergic agents. BJU Int. 2012 Oct;110(8 Pt B):E397–401.

100. Nandigama R, Bonitz M, Papadakis T, Schwantes U, Bschleipfer T, Kummer W. Muscarinic acetylcholine receptor subtypes expressed by mouse bladder afferent neurons. Neuroscience. 2010 Jul 14;168(3):842–50.

101. Andersson K-E. Detrusor myocyte activity and afferent signaling. Neurourol Urodyn. 2010;29(1):97–106.

102. Hawthorn MH, Chapple CR, Cock M, Chess-Williams R. Urothelium-derived inhibitory factor(s) influences on detrusor muscle contractility in vitro. Br J Pharmacol. 2000 Feb;129(3):416–9.

103. Templeman L, Chapple CR, Chess-Williams R. Urothelium derived inhibitory factor and cross-talk among receptors in the trigone of the bladder of the pig. J Urol. 2002 Feb;167(2 Pt 1):742–5.

104. Chaiyaprasithi B, Mang CF, Kilbinger H, Hohenfellner M. Inhibition of human detrusor contraction by a urothelium derived factor. J Urol. 2003 Nov;170(5):1897–900.

105. Scott R, Chapple C, Chess-Williams R. Which muscarinic receptor subtype causes the release of the urothelium derived inhibitory factor in the female pig bladder. Eur Urol Suppl. 2005 Mar;4(3):55.

106. Andersson K-E, Fullhase C, Soler R. Urothelial effects of oral agents for overactive bladder. Curr Urol Rep. 2008 Nov;9(6):459–64.

107. Sexton CC, Notte SM, Maroulis C, Dmochowski RR, Cardozo L, Subramanian D, et al. Persistence and adherence in the treatment of overactive bladder syndrome with anticholinergic therapy: a systematic review of the literature. Int J Clin Pract. 2011 May;65(5):567–85.

108. Verpoorten C, Buyse GM. The neurogenic bladder: medical treatment. Pediatr Nephrol Berl Ger. 2008 May;23(5):717–25.

109. Inoue S, Saito M, Honda M, Dimitriadis F, Takenaka A. Intravesical oxybutynin for neurogenic bladder in childen. Pediatr Ther. 2012;2(7).

110. Joint Formulary Committee. Section 7.4.2 Drugs for urinary frequency, enuresis and incontinence. British National Formulary. 66th ed. London, UK: Pharmaceutical Press; 2013. p. 1128.

111. Kato K, Kitada S, Chun A, Wein AJ, Levin RM. In vitro intravesical instillation of anticholinergic, antispasmodic and calcium blocking agents (rabbit whole bladder model). J Urol. 1989 Jun;141(6):1471–5.

112. Brendler CB, Radebaugh LC, Mohler JL. Topical oxybutynin chloride for relaxation of dysfunctional bladders. J Urol. 1989 Jun;141(6):1350–2.

113. Madersbacher H, Jilg G. Control of detrusor hyperreflexia by the intravesical instillation of oxybutynine hydrochloride. Paraplegia. 1991 Feb;29(2):84–90.

114. Greenfield SP, Fera M. The use of intravesical oxybutynin chloride in children with neurogenic bladder. J Urol. 1991 Aug;146(2 (Pt 2)):532–4.

115. Amarenco G, Adba MA, Kerdraon J. Value of intravesically instilled oxybutynin in refractory bladder hyperactivity. Study of 15 cases. Prog En Urol. 1992 Sep;2(4):660–3.

116. López Pereira P, Martínez MJ, Muguerza R, Jaureguizar E. Topical treatment with oxybutynin chloride in neurogenic incontinence. Cir Pediátrica. 1993 Jan;6(1):29–31.

117. Weese DL, Roskamp DA, Leach GE, Zimmern PE. Intravesical oxybutynin chloride: experience with 42 patients. Urology. 1993 Jun;41(6):527–30.

118. Prasad KV, Vaidyanathan S. Intravesical oxybutynin chloride and clean intermittent catheterisation in patients with neurogenic vesical dysfunction and decreased bladder capacity. Br J Urol. 1993 Nov;72(5 Pt 2):719–22.

119. O'Flynn KJ, Thomas DG. Intravesical instillation of oxybutynin hydrochloride for detrusor hyper-reflexia. Br J Urol. 1993 Nov;72(5 Pt 1):566–70.

120. Mizunaga M, Miyata M, Kaneko S, Yachiku S, Chiba K. Intravesical instillation of oxybutynin hydrochloride therapy for patients with a neuropathic bladder. Paraplegia. 1994 Jan;32(1):25–9.

121. Buyse G, Verpoorten C, Vereecken R, Casaer P. Treatment of neurogenic bladder dysfunction in infants and children with neurospinal dysraphism with clean intermittent catheterisation and optimized intravesical oxybutynin hydrochloride therapy. Eur J Pediatr Surg. 1995 Dec;5 Suppl 1:31–4.

122. Buyse G, Waldeck K, Verpoorten C, Björk H, Casaer P, Andersson KE. Intravesical oxybutynin for neurogenic bladder dysfunction: less systemic side effects due to reduced first pass metabolism. J Urol. 1998 Sep;160(3 Pt 1):892–6.

123. Buyse G, Verpoorten C, Vereecken R, Casaer P. Intravesical application of a stable oxybutynin solution improves therapeutic compliance and acceptance in children with neurogenic bladder dysfunction. J Urol. 1998 Sep;160(3 Pt 2):1084–7; discussion 1092.

124. Haferkamp A, Staehler G, Gerner HJ, Dörsam J. Dosage escalation of intravesical oxybutynin in the treatment of neurogenic bladder patients. Spinal Cord. 2000 Apr;38(4):250–4.

125. Enzelsberger H, Helmer H, Kurz C. Intravesical instillation of oxybutynin in women with idiopathic detrusor instability: a randomised trial. Br J Obstet Gynaecol. 1995 Nov;102(11):929–30.

126. Johansen JK, Lose G. Intravesical drug therapy in women with severe urge incontinence. Clinical experiences from a department of gynecology. Ugeskr Laeger. 1999 Nov 1;161(44):6052–5.

127. Lose G, Nørgaard JP. Intravesical oxybutynin for treating incontinence resulting from an overactive detrusor. BJU Int. 2001 Jun;87(9):767–73.

128. Krause P, Fuhr U, Schnitker J, Albrecht U, Stein R, Rubenwolf P. Pharmacokinetics of intravesical versus oral oxybutynin in healthy adults:

results of an open label, randomized, prospective clinical study. J Urol. 2013 Nov;190(5):1791–7.

129. Massad CA, Kogan BA, Trigo-Rocha FE. The pharmacokinetics of intravesical and oral oxybutynin chloride. J Urol. 1992 Aug;148(2 Pt 2):595–7.

130. Lehtoranta K, Tainio H, Lukkari-Lax E, Hakonen T, Tammela TLJ. Pharmacokinetics, efficacy, and safety of intravesical formulation of oxybutynin in patients with detrusor overactivity. Scand J Urol Nephrol. 2002 Feb;36(1):18–24.

131. Di Stasi SM, Giannantoni A, Navarra P, Capelli G, Storti L, Porena M, et al. Intravesical oxybutynin: mode of action assessed by passive diffusion and electromotive administration with pharmacokinetics of oxybutynin and N-desethyl oxybutynin. J Urol. 2001;166(6):2232–6.

132. Amark P, Eksborg S, Juneskans O, Bussman G, Palm C. Pharmacokinetics and effects of intravesical oxybutynin on the paediatric neurogenic bladder. Br J Urol. 1998 Dec;82(6):859–64.

133. Di Stasi SM, Giannantoni A, Massoud R, Cortese C, Vespasiani G, Micali F. Electromotive administration of oxybutynin into the human bladder wall. J Urol. 1997 Jul;158(1):228–33.

134. Shafat M, Rajakumar K, Syme H, Buchholz N, Knight MM. Stent encrustation in feline and human artificial urine: does the low molecular weight composition account for the difference? Urolithiasis. 2013 Nov;41(6):481–6.

135. Matsumoto Y, Miyazato M, Yokoyama H, Kita M, Hirao Y, Chancellor MB, et al. Role of M2 and M3 muscarinic acetylcholine receptor subtypes in activation of bladder afferent pathways in spinal cord injured rats. Urology. 2012 May;79(5):1184.e15–20.

136. Wientjes MG, Dalton JT, Badalament RA, Dasani BM, Drago JR, Au JL. A method to study drug concentration-depth profiles in tissues: mitomycin C in dog bladder wall. Pharm Res. 1991 Feb;8(2):168–73.

137. Tsallas A, Jackson J, Burt H. The uptake of paclitaxel and docetaxel into ex vivo porcine bladder tissue from polymeric micelle formulations. Cancer Chemother Pharmacol. 2011 Aug;68(2):431–44.

138. Guerra LA, Raju G, Milks J, Fang M, Pike J, Leonard M. Review of experience with intravesical oxybutynin at the Children's Hospital of Eastern Ontario. [Ottawa, Ontario, Canada: Department of Clinical Epidemiology and Community Health]: University of Ottawa; 2007.

139. Di Stasi SM, Giannantoni A, Vespasiani G, Navarra P, Capelli G, Massoud R, et al. Intravesical electromotive administration of oxybutynin in patients with detrusor hyperreflexia unresponsive to standard anticholinergic regimens. J Urol. 2001;165(2):491–8.

140. George J, Tharion G, Richar J, Macaden AS, Thomas R, Bhattacharji S. The effectiveness of intravesical oxybutynin, propantheline, and capsaicin in the management of neuropathic bladder following spinal cord injury. Sci World J. 2007;7:1683–90.

141. Palmer LS, Zebold K, Firlit CF, Kaplan WE. Complications of intravesical oxybutynin chloride therapy in the pediatric myelomeningocele population. J Urol. 1997 Feb;157(2):638–40.

142. Yokoyama O, Ishiura Y, Nakamura Y, Ohkawa M. The use of intravesical oxybutynin hydrochloride in patients with neurogenic bladder managed by intermittent catheterization. Hinyokika Kiyo. 1995 Jul;41(7):521–4.

143. Ferrara P, D'Aleo CM, Tarquini E, Salvatore S, Salvaggio E. Side-effects of oral or intravesical oxybutynin chloride in children with spina bifida. BJU Int. 2001 May;87(7):674–8.

144. Hanawa T, Tsuchiya C, Endo N, Hanawa K, Suzuki M, Suzuki T, et al. Formulation Study of Intravesical Oxybutynin Instillation Solution with Enhanced Retention in Bladder. Chem Pharm Bull (Tokyo). 2008;56(8):1073–6.

145. Saito M, Tabuchi F, Otsubo K, Miyagawa I. Treatment of overactive bladder with modified intravesical oxybutynin chloride. Neurourol Urodyn. 2000;19(6):683–8.

146. Hayashi A, Saito M, Okada S, Hanada T, Watanabe T, Satoh K, et al. Treatment with modified intravesical oxybutynin chloride for neurogenic bladder in children. J Pediatr Urol. 2007 Dec;3(6):438–42.

147. Fratta A, Bordenave J, Boissinot C, Le Grand J, Esquirol C, Radideau E, et al. Development of an intravesial oxybutynin chloride solution: from formulation to quality control. Ann Pharm Fr. 2005 Mar;63(2):162–6.

148. Mizunaga M, Miyata M, Kaneko S, Taniguchi N, Yachiku S, Chiba K, et al. Intravesical oxybutynin hydrochloride in the treatment of urge incontinence in the elderly. Nihon Hinyōkika Gakkai Zasshi. 1996 Jun;87(6):923–7.

149. Singh G, Thomas DG. Intravesical oxybutynin in patients with posterior rhizotomies and sacral anterior root stimulators. Neurourol Urodyn. 1995;14(1):65–71.

150. Ersay A, Demirtas OC. Intravesical oxybutynin affects bladder permeability. Int Urol Nephrol. 2001;32(3):359–61.

151. Munoz A, Gangitano DA, Smith CP, Boone TB, Somogyi GT. Removal of urothelium affects bladder contractility and release of ATP but not release of NO in rat urinary bladder. BMC Urol. 2010;10:10.

152. Romih R, Veranic P, Jezernik K. Actin filaments during terminal differentiation of urothelial cells in the rat urinary bladder. Histochem Cell Biol. 1999 Nov;112(5):375–80.

153. Helms JR. Urinalysis and Renal Clearance. Mathematics for Medical and Clinical Laboratory Professionals. 1st ed. Cengage Learning; 2008. p. 193–202.

154. Williams NA, Bowen JL, Al-Jayyoussi G, Gumbleton M, Allender CJ, Li J, et al. An ex vivo investigation into the transurothelial permeability and bladder wall distribution of the nonsteroidal anti-inflammatory ketorolac. Mol Pharm. 2014 Mar 3;11(3):673–82.

155. Wientjes MG, Badalament RA, Au JL. Use of pharmacologic data and computer simulations to design an efficacy trial of intravesical mitomycin C therapy for superficial bladder cancer. Cancer Chemother Pharmacol. 1993;32(4):255–62.

156. Wüst M, Averbeck B, Reif S, Bräter M, Ravens U. Different responses to drugs against overactive bladder in detrusor muscle of pig, guinea pig and mouse. Eur J Pharmacol. 2002 Nov 1;454(1):59–69.

157. Landau EH, Fung LC, Thorner PS, Mittelman MW, Jayanthi VR, Churchill BM, et al. Histologic studies of intravesical oxybutynin in the rabbit. J Urol. 1995 Jun;153(6):2022–4.

158. Burgos L, Encinas JL, García-Cabezas MÁ, Peiró JL, López-Santamaría M, Jaureguízar E. Bladder Changes After Several Coverage Modalities in the Surgically Induced Model of Myelomeningocele in Lambs. Actas Urol Esp. 2014 Feb;38(1):55–61.

159. Lepor H, Sunaryadi I, Hartanto V, Shapiro E. Quantitative morphometry of the adult human bladder. J Urol. 1992 Aug;148(2 Pt 1):414–7.

160. Cheng L, Bostwick DG, Lopez-Beltran A, Wiley InterScience (Online service). Bladder pathology. 1st ed. Hoboken, N.J.: Wiley-Blackwell; 2012.

Chapter Four: Development of a Computer - Based Pharmacokinetic Model of Intravesical Drug Delivery

4.1. Introduction

4.1.1. Introduction to STELLA® modelling software

STELLA® (Structural Thinking Experimental Learning Laboratory with Animation, Isee systems Inc, New Hampshire, USA) is a computer program that facilitates the mapping, modelling, simulation, and communication of dynamic processes[1]. It allows users to build dynamic models of complex systems. A system can be interpreted as a process or mechanism, the functioning of which depends on multiple parts working together. As these parts change over time, so does the functioning of the system. By embedding advanced mathematical equations behind simple, diagrammatical building blocks, STELLA® offers a practical way to study the underlying processes of complex systems. Once built, models can be used to investigate the contribution of different variables to the system as a whole. The human body is arguably the most complex system of all and certainly one about which a great deal remains unknown. It follows that STELLA® is well suited to PK modelling and has become a valuable resource for doing so[2]. Examples include investigating the effect of antibacterial doses on bacterial resistance[3], developing PK profiles of enteric coated tablets[4] and modelling ocular permeation[5,6]. In this chapter STELLA® was used to create a PK model of IDD.

4.1.2. Modelling IDD

Despite its common use, little work has been undertaken to maximise the potential of IDD. From a practical aspect IDD is a simple technique. The underlying pharmacokinetics however are complex, with many variables contributing to the overall process. This chapter documents the development of a PK model that investigates these variables. A greater understanding will yield more insight into how these variables can be manipulated to maximise the potential of IDD. The model combines equations from PK / diffusion theory, physiological variables and experimentally determined values.

4.1.3. Aims and Objectives of Chapter Four

The aim of this chapter was to develop a computer - based PK model of IDD.

The key objectives were:

1. To build a PK model using STELLA® that combines key physiological variables with experimentally determined values to predict:

    - Changes in bladder volume
    - Concentrations of drug in the urine
    - Drug concentration - depth profiles in the bladder wall

2. To validate model outputs using an independent PK model built using PYTHON™ coding language.

3. Use the model to optimise existing IDD regimens.

4.2. Methods

4.2.1. STELLA®

STELLA® models are built diagrammatically using building blocks, each having a specific purpose. 'Stocks' represent accumulation. For example, a stock may calculate the *collection of urine* in the bladder. Stock levels are controlled by 'flows'. Flows control the movement in and out of stocks, such as the *passage of urine* from the kidneys to the bladder. 'Converters' determine the rate at which flows alter stocks. Converters allow you to control how building blocks interact with one and other. They contain algebraic equations, input by the user, which allow variables to be calculated for a single point in time. For example, a converter will control the *rate at which urine collects* in the bladder. The frequency at which variables are calculated, known as the time - step (DT), is specified by the user. Changing the DT from 2 to 1 will double the rate at which calculations are performed. All model simulations in this work were performed with a DT value of 1 second.

4.2.2. Model construction

The PK model was constructed in a stepwise manner, with each step validated (Section 4.3) before advancing to the next. For clarity, STELLA® model schematics have been redrawn using Microsoft PowerPoint.

4.2.2.1. Step 1: Transfer of drug from bladder lumen into the bladder wall

The PK model was constructed as a multilayered diffusion model approximated by compartments[7] (Figure 4.1). The model was initially designed to describe drug transfer between compartments in terms of '*mass*' and later '*concentrations*'. A total of 18 compartments were used to describe; the bladder lumen (1 compartment), urothelium (5 compartments), lamina propria (5 compartments), detrusor muscle (6 compartments) and peritoneum (1 compartment) (Figure 4.2).

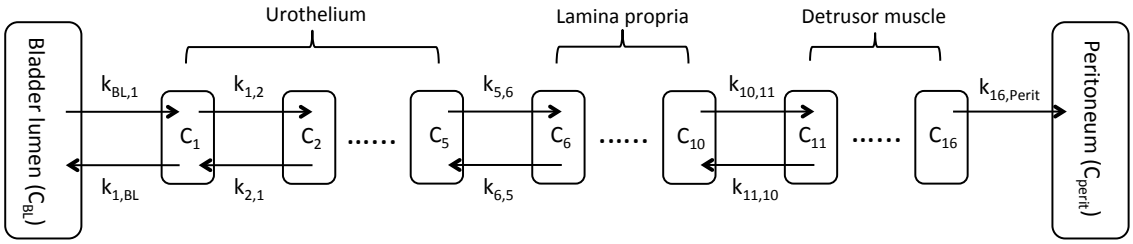

Figure 4.1. Schematic overview of the multilayered diffusion model. Drug is transferred between compartments according to equations 1 - 6. Drug is free to diffuse in both directions, e.g. C_1 to C_2 and C_2 to C_1 with the exception of the final detrusor muscle compartment (C_{16}) where movement is in the direction of the peritoneum (C_{perit}) only (sink conditions assumed). k is the drug transfer coefficient (s^{-1}) calculated according to equations 1 – 6.

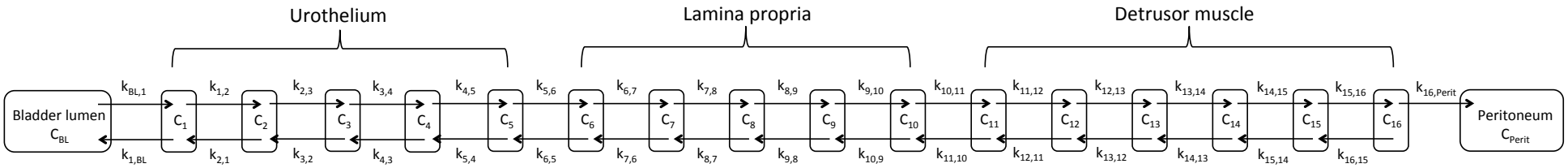

Figure 4.2. Full schematic of the multilayered, 18 - compartment diffusion model. The bladder lumen is represented by one compartment (C_{BL}), the urothelium by 5 compartments (C_1 - C_5), the lamina propria by 5 compartments (C_6 - C_{10}), the detrusor muscle by 6 compartments (C_{11} - C_{16}) and the peritoneum by one compartment (C_{Perit}). k is the drug transfer coefficient (s^{-1}) calculated according to equations 1 – 6.

Underlying equations

(i) Bladder lumen

At T = 0, all drug resides in the bladder lumen compartment (C_{BL}). Drug movement out of the bladder lumen and into the first compartment of the urothelium (C_1) is described by the equation

$$k_{BL,1} = \frac{K_{m1} \times D_1}{h_{BL}\left(\frac{h_1}{n_1}\right)} \qquad \text{where,} \qquad h_{BL} = \frac{V_{BL}}{A_{BL}} \tag{1}$$

where $k_{BL,1}$ is the transfer coefficient of drug into compartment C_1 (s^{-1}), K_{m1} is the partition coefficient of the drug between the urothelium and the bladder lumen (unitless), D_1 is the drug diffusion coefficient in the urothelium ($cm^2\ s^{-1}$), h_{BL} is the effective thickness of the bladder contents (cm), h_1 is the thickness of the urothelium (cm), n_1 the number of compartments in the urothelium, V_{BL} is bladder lumen volume (cm^3) and A_{BL} is the surface area of the bladder lumen (cm^2).

(ii) Urothelium

Drug transfer between compartments of the urothelium (C_1 - C_5, C_5 - $C_{BL,}$ bidirectional) is described by the equation

$$k_{i,i+1} or\ k_{i+1,i} = \frac{D_1}{\left(\frac{h_1}{n_1}\right)^2} \tag{2}$$

where $k_{i,i+1}$ is the transfer coefficient between adjacent urothelial compartments down the concentration gradient (e.g. C_2 to C_3) (s^{-1}) and $k_{i+1,i}$ is the transfer coefficient against the concentration gradient (e.g. C_3 to C_2, C_1 to C_{BL}) (s^{-1}).

At the urothelium / lamina propria boundary (C_5 to C_6), drug transfer into the first compartment of the lamina propria (C_6) is described by the equation

$$k_{5,6} = \frac{K_{m2}}{K_{m1}} \times \frac{D_2}{\left(\frac{h_1}{n_1}\right) \times \left(\frac{h_2}{n_2}\right)} \quad (3)$$

where $k_{5,6}$ is the transfer coefficient of drug from C_5 into C_6 (s^{-1}), K_{m2} is the partition coefficient of the drug between the lamina propria and the urothelium (unitless), D_2 is the drug diffusion coefficient in the lamina propria ($cm^2\ s^{-1}$), h_2 is the thickness of the lamina propria (cm) and n_2 is the number of compartments in the lamina propria.

(iii) Lamina propria

Drug transfer between compartments of the lamina propria (C_6 - C_{10}, C_{10} - C_5, bidirectional) is described by the equation

$$k_{i,i+1} or\ k_{i+1,i} = \frac{D_2}{\left(\frac{h_2}{n_2}\right)^2} \quad (4)$$

At the lamina propria / detrusor muscle boundary (C_{10} to C_{11}), drug transfer into the first compartment of the detrusor muscle (C_{11}) is described by the equation

$$k_{10,11} = \frac{K_{m3}}{K_{m2}} \times \frac{D_3}{\left(\frac{h_2}{n_2}\right) \times \left(\frac{h_3}{n_3 + 1}\right)} \quad (5)$$

where $k_{10,11}$ is the transfer coefficient of drug from C_{10} into C_{11} (s^{-1}), K_{m3} is the partition coefficient of the drug between the detrusor muscle and the lamina propria (unitless), D_3 is the drug diffusion coefficient in the detrusor muscle ($cm^2\ s^{-1}$), h_3 is the thickness of the detrusor muscle (cm) and n_3 is the number of compartments in the detrusor muscle.

(iv) Detrusor muscle

Drug transfer between compartments of the detrusor muscle (C_{11} - C_{16}, C_{16} - C_{10} bidirectional) is described by the equation

$$k_{i,i+1} or\ k_{i+1,i} = \frac{D_3}{\left(\frac{h_3}{(n_3+1)}\right)^2} \quad (6)$$

Drug transfer into the peritoneum at the detrusor muscle / peritoneum boundary (C_{16} to C_{Perit}) is also described by equation (6). In the peritoneum there is no drug transfer back into the detrusor muscle as sink conditions are assumed.

Geometric assumption

The bladder exists in pseudo spherical geometry. The outer layer of the bladder wall (represented by C_{16}) is further from the bladder lumen than the inner surface (represented by C_1) and as such has a greater surface area (Figure 4.3A). To allow easier modelling, the model treats the bladder as if it were in flat geometry (Figure 4.3B). Although the model allows the thickness of each layer (urothelium, lamina propria and detrusor muscle) to be varied (h_1 - h_3), the surface area of the different layers (A_{BL}) is assumed constant. The switch from spherical to flat geometry assumes bladder wall thickness to be small relative to the bladder lumen surface area. Consequently any differences between the surface area of the inner and outer bladder wall will be small, allowing easier modelling of the bladder. This assumption was investigated:

Consider a bladder with a maximum volume of 400 ml (a reasonable assumption seeing as the urge to void is usually initiated at ~300 – 400 ml[8]). Assuming the bladder to be spherical, the internal surface area can be calculated by the equation

$$A = 4\pi r^2 \qquad \text{where,} \qquad r = \left(3\frac{V}{4\pi}\right)^{\frac{1}{3}} \quad (7)$$

where A is the luminal surface area of the bladder (cm^2), r is the radius of the bladder lumen (cm) and V is the volume of the bladder lumen (cm^3).

Using equation 7 the internal bladder surface area is calculated to be 262.5 cm^2 and the radius 4.57 cm (Figure 4.3A). Bladder wall thickness is normally distributed around the bladder[9] and has been shown to be 0.335 cm on average[9]. Assuming a constant bladder wall thickness (regardless of luminal volume), the radius of the external surface of the bladder is calculated as 4.57 cm + 0.335 cm = 4.905 cm. The surface area of the outer surface of the bladder is therefore 302.3 cm^2 (Figure 4.3A). There is a 15.1 % difference in the surface area of the bladder at the inner and outermost surface. This difference was considered acceptable for the purpose of this model.

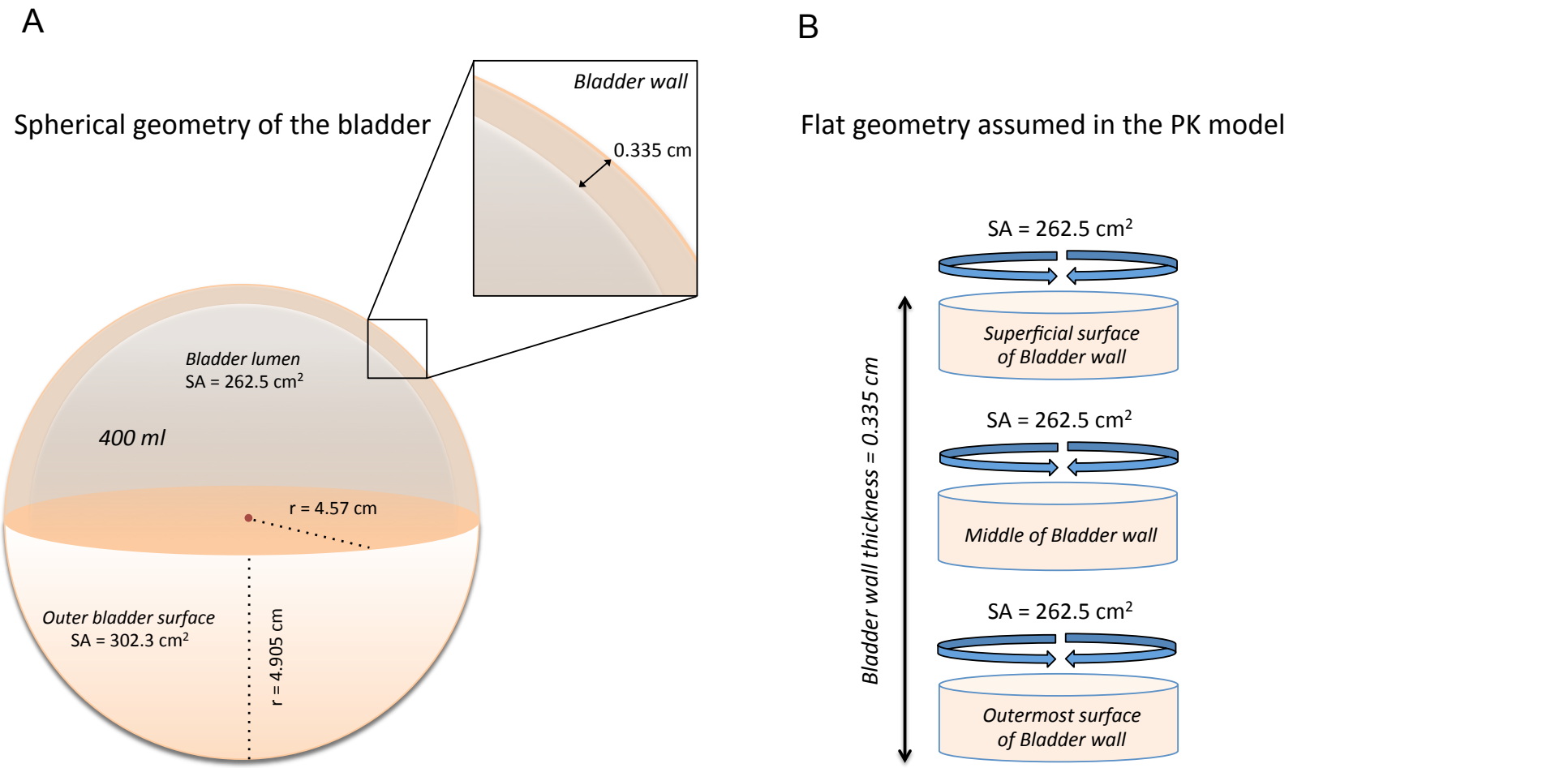

Figure 4.3. Comparing the spherical geometry of the bladder (A) with the flat geometry assumed in the multi - compartment PK model (B). With a luminal volume of 400 ml, the outer layer of the bladder has a greater surface area (302.3 cm^2) than the inner surface (262.5 cm^2) (A). Under the flat geometry assumption, this 15.1 % difference is ignored and all layers of the bladder wall are considered to have a constant surface area (B).

4.2.2.2. Step 2: Incorporating drug clearance from the bladder wall

Once in the bladder wall, drug is cleared into systemic circulation by capillaries. The microvascular architecture of the human bladder has been characterised in fine detail by corrosion casting and subsequent SEM analysis[10]. The bladder wall consists of two distinct capillary networks; the suburothelial capillaries located in the lamina propria and the muscular capillaries located in the detrusor. The urothelium does not contain a capillary network. Subsequently the PK model incorporates drug elimination from the lamina propria and detrusor muscle layers only (Figure 4.4). Eliminated drug collects in a separate compartment representing systemic circulation (C_{Blood}). The rate of drug elimination (k_{Elim}) is described by the equation

$$k_{Elim} = Q_B \times \rho \qquad (8)$$

where k_{Elim} is the elimination rate constant (s^{-1}), Q_B is blood flow rate per gram of bladder tissue (ml s^{-1} g^{-1}) and ρ is the density of bladder tissue (assumed to be 1 g ml^{-1}). The model assumes clearance to be solely blood flow limited and does not consider capillary resistance to the partitioning of drug into the bloodstream[7].

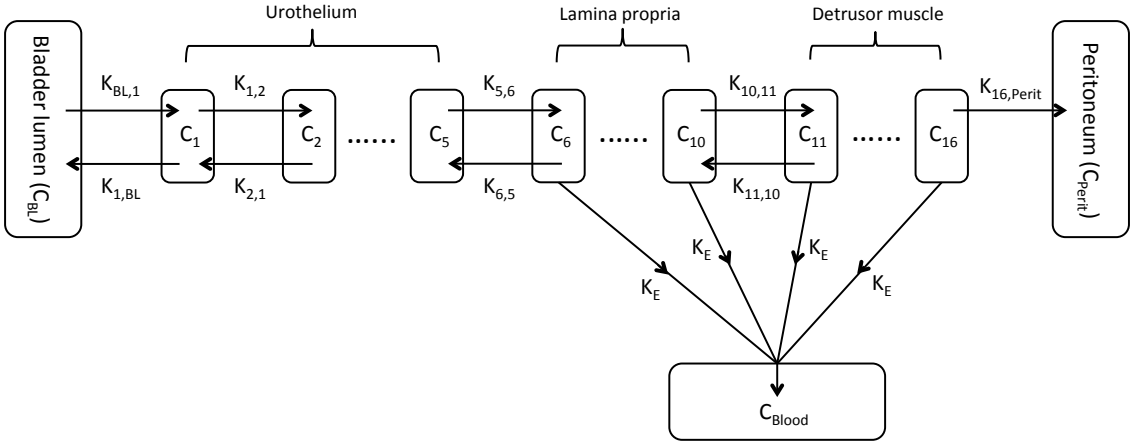

Figure 4.4. Schematic overview of the multilayered diffusion model with drug clearance from the lamina propria and detrusor muscle incorporated. k_E is the elimination rate constant from the bladder wall into systemic circulation (s^{-1}).

Blood flow to the human bladder during filling has been investigated using Doppler ultrasound[11]. As the bladder fills, blood flow steadily increases before slightly dropping once 100 % capacity is achieved. An average blood flow rate over the 0 – 100 % capacity range was used in the model (0.00102 ml s^{-1} g^{-1})[11].

4.2.2.3. Step 3: Incorporating urine dilution

To closer mimic the IDD process, urine production by the kidneys and subsequent dilution of the instilled dose was incorporated into the PK model. Urine moves into the bladder lumen at a specified urine production rate (U_R). Urine accumulation in the bladder is described by the equation

$$V_{BL} = V_{BL}0 + (U_R \times t) \quad (9)$$

where V_{BL} is the volume in the bladder lumen (ml) at time t (min), $V_{BL}0$ is the volume in the bladder lumen at time zero (ml) and U_R is the urine production rate (ml min^{-1}). A constant urine production rate of 1 ml min^{-1} (an accepted normal rate[12]) was used in the model.

4.2.2.4. Step 4: Moving from a 'mass' to 'concentration' - based model

To aid the design process, the STELLA® model was originally built to describe drug movement in terms of mass. However drug concentrations are more valuable when investigating the efficiency of intravesical regimens. Given tissue layer depth was already incorporated within the model, the switch from mass terms enabled the generation of predictive concentration - depth profiles. Concentration terms were generated by normalising the mass of drug in each compartment to the tissue weight of that compartment.

The concentration of drug in each compartment is described by the equation

$$conc_i = \frac{M_i}{W_i} \quad (10)$$

where $conc_i$ is the concentration of drug in the compartment (mg g^{-1}), M_i is the mass of drug in the compartment (mg) and W_i is the compartment tissue weight (g).

4.2.2.5. Step 5: Allowing for multiple intravesical doses

The PK model was initially designed to represent the typical intravesical regimen; that is a single drug instillation voided after a set period of time (typically 1 - 2 h). This type of regimen design is largely empirical. Given the dilution effect urine will have on the instilled dose, a double dosing regimen may be advantageous. Double dosing refers to a secondary instillation of drug administered shortly after voiding of the primary dose. For example, two patients receive a 2 h intravesical regimen:

Patient #1

Patient 1 receives a single instillation of 50 ml drug solution (20 mg ml^{-1}) and is instructed to hold their bladder for 2 h (after which the dose is voided).

Patient #2

Patient 2 receives a single instillation of 50 ml drug solution (20 mg ml^{-1}). In this case the patient is instructed to hold their bladder for 1 h after which the dose is voided. Following a two - minute interlude to allow for dose reconstitution, a second 50 ml dose is instilled (20 mg ml^{-1}). Again the patient is instructed to hold their bladder for 1 h completing the 2 h intravesical treatment. Patient 2 has received two 50 ml doses over the 2 h treatment period.

4.2.2.6. Step 6: Incorporating post - void residual (PVR) volume

Post - void residual (PVR) volume describes the volume of urine remaining in the bladder immediately post - micturition. PVR volume can vary greatly; generally in adults it is close to zero (0.09 - 2.24 ml)[13], however for diagnostic purposes < 50 ml and < 100 ml is considered normal when assessing urinary retention in young and elderly patients respectively[14]. Patients with lower urinary tract symptoms often

exhibit higher PVR values, sometimes > 100 ml[15–17]. Draining post - void residual urine with a catheter has been suggested to improve the efficacy of IDD[18]. However the technique is not commonplace and even when performed may only reduce, rather than completely remove, residual urine[18]. Multiple catheter drains whilst repositioning the catheter and patient are usually required[18].

To account for PVR volume in the bladder lumen, equation 9 was extended to the equation

$$V_{BL} = V_{BL}0 + (U_R \times t) \qquad \text{where,} \qquad V_{BL}0 = V_{Drug} + V_{PVR} \tag{11}$$

where V_{Drug} is the volume of drug solution instilled in the bladder (ml) and V_{PVR} is the PVR volume in the bladder at the point of drug instillation (ml).

4.3. Results and Discussion

Two PK models of IDD have previously been reported. Wientjes *et al* used computer - based PK simulations[19] to suggest an improved dosing strategy for the IDD of MMC[18]. Their model is based on MMC urine PK[20] and bladder wall concentrations[21] determined from *in vivo* IDD studies. Suggested regimen improvements included minimising PVR volume, reducing the urine production rate and increasing the dose from 20 mg to 40 mg. Their model was designed specifically to investigate the IDD of MMC and used a multitude of experimentally determined values specific to the drug (e.g. absorption rate constant, elimination rate constant and relationships between the concentration of drug in the urine and urothelium). More recently Grabnar *et al* developed a kinetic model of IDD to simulate the permeability enhancing effects of chitosan and polycarbophil on pipemidic acid concentrations achieved in the bladder wall[22]. Their model was constructed as an advanced compartmental diffusion model similar to the one described here (Section 4.2.2.1, Figure 4.2), but does not take into consideration the differing partition of the drug between the various tissue layers (K_m, equations 3 and 5).

In contrast to these previous approaches, which were built using high – level coding language, the user - friendly STELLA® model delivers high resolution PK predictions with a far higher degree of flexibility. This allows the rapid generation of a wide range of PK simulations by varying determinants such as the rate of urine production, PVR volume and volume of instillation etc. The graphical capabilities of STELLA® allow simulations to be explored in '*real time*', simultaneously displaying how each part of the model (e.g. bladder lumen volume, drug concentrations in the urothelium) changes with time. This allows for a faster and more thorough understanding of the dynamic processes underlying IDD. Subsequently the STELLA® model allows for the realisation of novel and often counterintuitive dosing strategies, which would not have been elicited using other approaches. Furthermore previously described models have sought to investigate a specific hypothesis for a particular drug. This model was designed to investigate the IDD process as a whole and to be applicable to any drug solution instilled into the bladder.

4.3.1. Validating the model with PYTHON®

To validate the outputs generated by STELLA®, the PK model was simultaneously built using PYTHON™. This was done in collaboration with Yuri Anissimov, an associate professor in mathematical modelling at Griffith University, Brisbane Australia. Dr Anissimov has published extensively in the field of mathematical modelling of biological processes[23–26] and has used multi – compartment diffusion models, such as the one described here, to model the transdermal permeation of drugs[7,27]. PYTHON™ is a widely used, scripting programming language. Whereas STELLA® allows users to design models visually, PYTHON™ uses code to incorporate the many layers of equations necessary to build the model. Considering the different methodology used by these packages to construct the same model, similar outcomes would validate the appropriateness of the underlying approach. To be clear, outputs generated by PYTHON™ do not validate the '*accuracy*' of the model in terms of clinical results predicted *in vivo*; this would require clinical studies. It does however validate that the model has been constructed correctly using the STELLA® software. Steps 1 – 3 of the PK model development were validated with PYTHON™. Further steps represented

interpretations (rather than new coding) of the existing model and subsequently were analysed with STELLA® only.

4.3.1.1. Validating Step 1: Transfer of drug from bladder lumen into the bladder wall

Step 1 design of the PK model was validated by comparing model outputs generated with STELLA® and PYTHON™ (Figure 4.5, Table 4.2). Table 4.1 lists the parameter values input into the model. Early stage model development used arbitrary input values with physiologically relevant values introduced later (4.3.1.4). For all simulations performed, STELLA® and PYTHON™ outputs were identical to 2 decimal places.

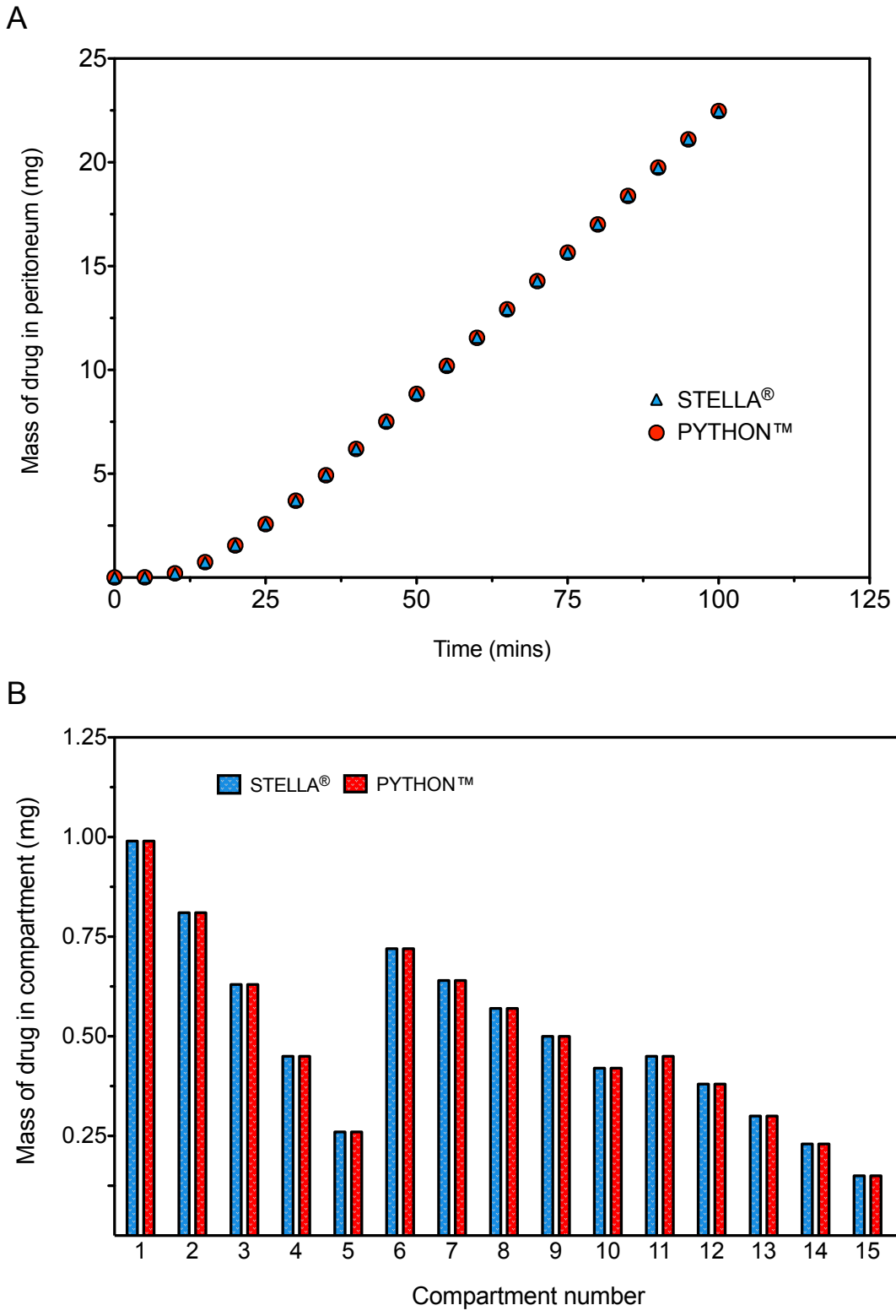

Figure 4.5. A) Mass of drug accumulated in the peritoneum over 100 min. B) Mass of drug accumulated in each compartment of the model after 60 min. STELLA® and PYTHON™ model outputs were identical to 2 decimal places. The increase between compartments 5 and 6 does not represent a decrease in concentration gradient as values represent mass, rather than concentration, of drug.

Bladder lumen		Uro		Uro / LP boundary		LP		LP / DM boundary		DM		DM / Perit boundary	
(C_{BL-1})		**($C_{1-5,\ 5-BL}$)**		**(C_{5-6})**		**($C_{6-10,\ 10-5}$)**		**(C_{10-11})**		**($C_{11-16,\ 16-10}$)**		**(C_{16} - C_{Perit})**	
M_{BL}	1000 mg	Km_1	1	Km_1	1	Km_2	1.5	Km_2	1.5	Km_3	1.5	Km_3	1.5
V_{BL}	50 ml	D_1	1E-07 $cm^2\ s^{-1}$	Km_2	1.5	D_2	1E-06 $cm^2\ s^{-1}$	Km_3	1.5	D_3	1.5E-06 $cm^2\ s^{-1}$	D_3	1.5E-06 $cm^2\ s^{-1}$
SA_{BL}	30 cm^2	h_{BL}	1.67 cm	km_2 / km_1	1.5	h_2	0.02 cm	km_3 / km_2	1	h_3	0.035 cm	h_3	0.035 cm
Km_1	1	h_1	0.01 cm	D_2	1E-06 $cm^2\ s^{-1}$	n_2	5	D_3	1.5E-06 $cm^2\ s^{-1}$	n_3	6	n_3	6
D_1	1E-07 $cm^2\ s^{-1}$	n_1	5	h_1	0.01 cm	h_2 / n_2	0.004 cm	h_2	0.02 cm	h_3 / (n_{3+1})	0.005 cm	h_3 / (n_{3+1})	0.005 cm
h_{BL}	1.67 cm	h_1 / n_1	0.002 cm	n_1	5	$K_{i,i+1}$ or $K_{i+1,i}$	0.0625 s^{-1}	n_2	5	$K_{i,i+1}$ or $K_{i+1,i}$	0.06 s^{-1}	$K_{i,i+1}$	0.06 s^{-1}
h_1	0.01 cm	$K_{i,i+1}$ or $K_{i+1,i}$	0.025 s^{-1}	h_1 / n_1	0.002 cm			h_2 / n_2	0.004 cm				
n_1	5			h_2	0.02 cm			h_3	0.035 cm				
h_1 / n_1	0.002 cm			n_2	5			n_3	6				
K_{BL}	3E-05 s^{-1}			h_2 / n_2	0.004 cm			h_3 / (n_{3+1})	0.005 cm				
				$K_{i,i+1}$	0.1875 s^{-1}			$K_{i,i+1}$	0.075 s^{-1}				

Table 4.1. Parameter values used to validate Step 1 design of the PK model. 'Uro', 'LP', 'DM' and 'Perit' refer to the urothelium, lamina propria, detrusor muscle and peritoneum respectively.

STELLA		PYTHON	

Time (min)	C_{BL}	C_1	C_2	C_3	C_4	C_5	C_6	C_7	C_8	C_9	C_{10}	C_{11}	C_{12}	C_{13}	C_{14}	C_{15}	C_{16}	C_{Perit}
0	0	0	0	0	0	0	0	0	0	0	0	0	0	0	0	0	0	0
0	0	0	0	0	0	0	0	0	0	0	0	0	0	0	0	0	0	0
5	996.846	0.941	0.697	0.473	0.272	0.090	0.202	0.148	0.105	0.072	0.048	0.040	0.026	0.016	0.010	0.006	0.003	0.008
5	996.847	0.940	0.696	0.472	0.271	0.090	0.202	0.148	0.105	0.073	0.048	0.040	0.026	0.017	0.010	0.006	0.003	0.008
10	995.121	0.979	0.766	0.557	0.354	0.157	0.395	0.326	0.265	0.211	0.164	0.161	0.124	0.093	0.065	0.042	0.020	0.198
10	995.121	0.979	0.766	0.557	0.354	0.157	0.395	0.326	0.265	0.211	0.164	0.161	0.124	0.093	0.066	0.042	0.020	0.199
15	993.558	0.989	0.787	0.587	0.389	0.195	0.510	0.439	0.373	0.311	0.254	0.261	0.210	0.163	0.119	0.078	0.039	0.736
15	993.558	0.989	0.787	0.587	0.389	0.195	0.510	0.439	0.373	0.311	0.254	0.261	0.210	0.163	0.119	0.078	0.039	0.737
20	992.062	0.994	0.798	0.604	0.411	0.220	0.584	0.512	0.443	0.377	0.314	0.330	0.270	0.212	0.157	0.104	0.052	1.556
20	992.062	0.994	0.798	0.604	0.411	0.220	0.584	0.512	0.443	0.377	0.314	0.330	0.270	0.212	0.157	0.104	0.052	1.557
25	990.607	0.997	0.805	0.614	0.424	0.236	0.633	0.560	0.489	0.421	0.354	0.375	0.309	0.245	0.182	0.121	0.060	2.569
25	990.607	0.997	0.805	0.614	0.424	0.236	0.632	0.560	0.489	0.421	0.354	0.375	0.309	0.245	0.182	0.121	0.060	2.570
30	989.179	0.998	0.809	0.621	0.433	0.246	0.664	0.591	0.519	0.449	0.380	0.404	0.335	0.266	0.199	0.132	0.066	3.708
30	989.179	0.998	0.809	0.621	0.433	0.246	0.664	0.591	0.519	0.449	0.380	0.404	0.335	0.266	0.199	0.132	0.066	3.709

Table 4.2. Example outputs generated with the STELLA® (red) and PYTHON™ (green) model over 30 min. Data shows drug accumulated (mg) in each compartment over 30 min. STELLA® and PYTHON™ model outputs were identical to 2 decimal places.

4.3.1.2. Validating Step 2: Incorporating drug clearance from the bladder wall

Step 2 was validated by comparing model outputs generated with STELLA® and PYTHON™ (Figure 4.6, Table 4.3). Input parameters are detailed in table 4.1 with the addition of k_{Elim} = 0.00102 s^{-1}. For all simulations performed, STELLA® and PYTHON™ model outputs were identical to 2 decimal places. The incorporation of clearance decreased the amount of drug accumulating in each compartment, exemplified by the peritoneum compartment (Figure 4.6A). Mass balance analysis of the STELLA® model showed all drug in the bladder lumen at time zero is accountable at the end of the simulation (Figure 4.7).

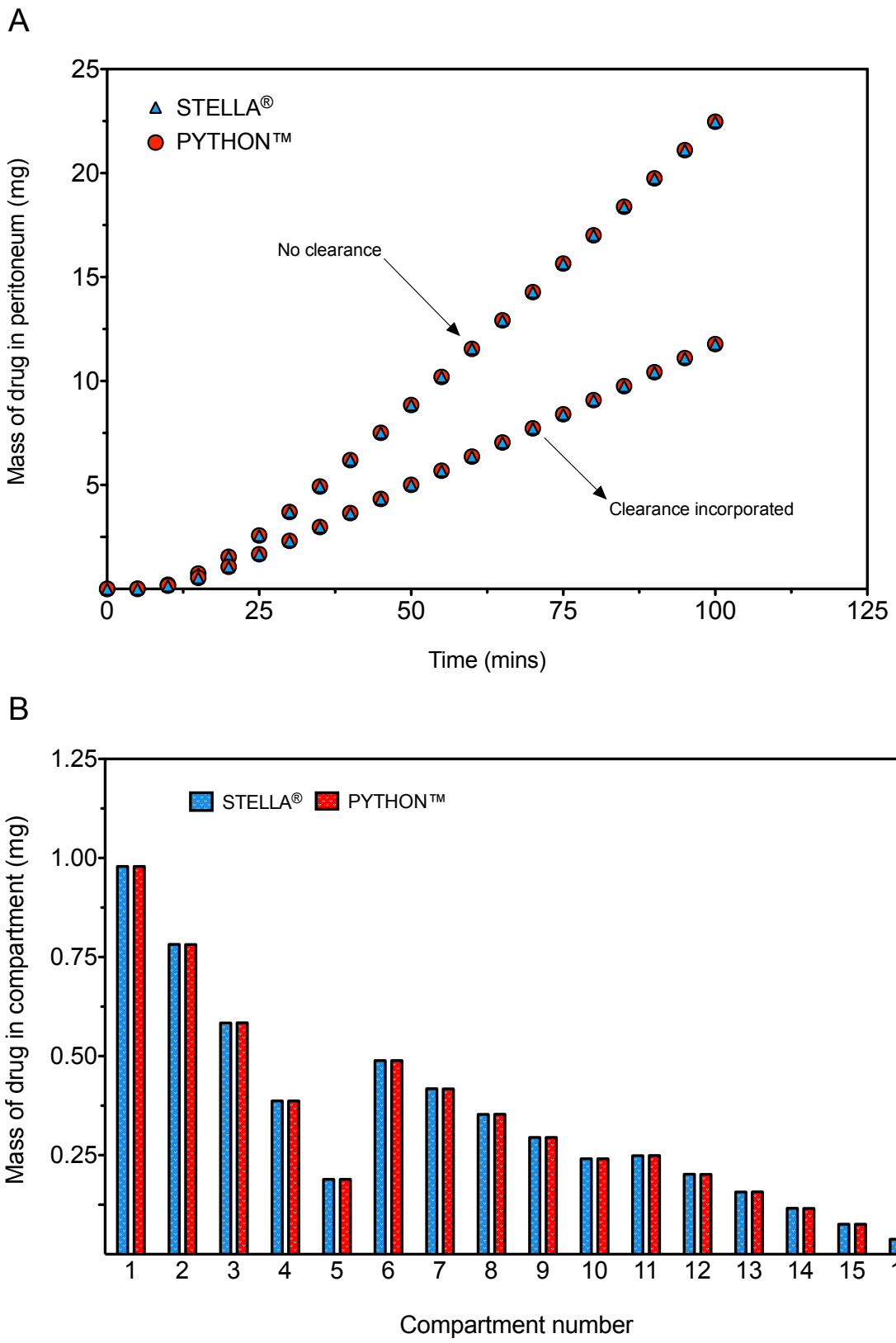

Figure 4.6. A) Mass of drug accumulated in the peritoneum over 100 min with and without the incorporation of drug clearance. B) Mass of drug accumulated in each compartment of the model after 60 min. STELLA® and PYTHON™ model outputs were identical to 2 decimal places.

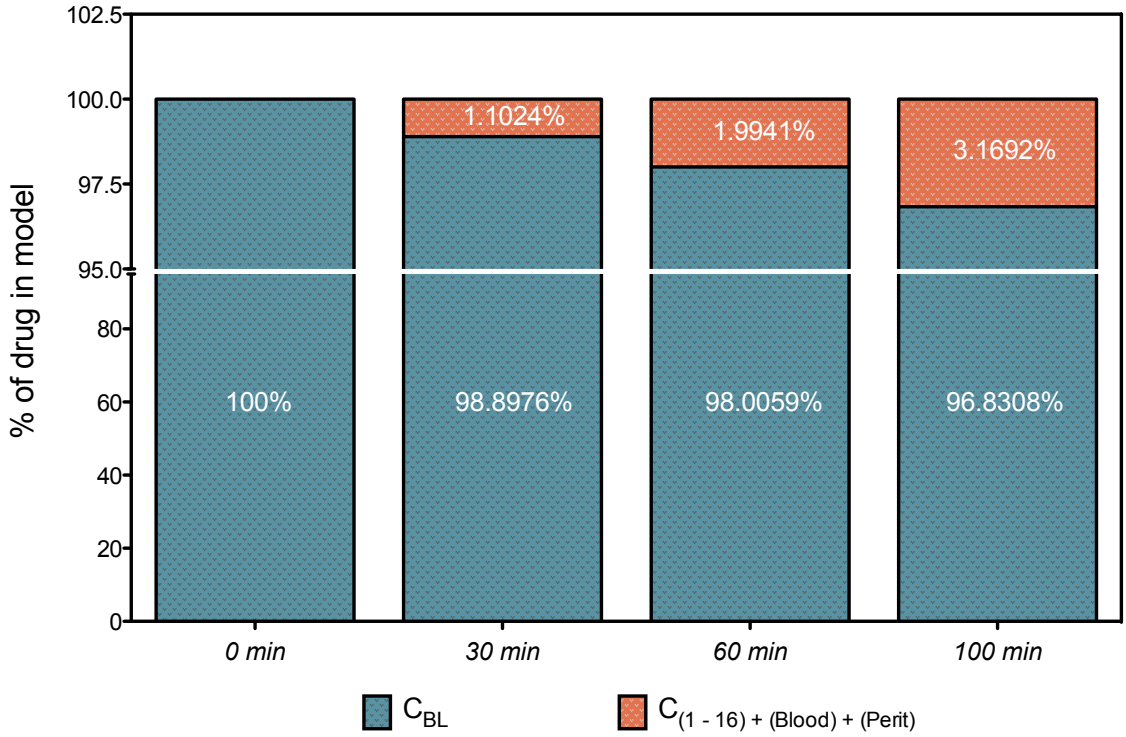

Figure 4.7. Mass balance analysis of the STELLA® model showing 100 % of drug is accountable throughout a 100 min simulation. Input parameters are the same as for figure 4.6. C_{BL} is mass of drug in the bladder lumen and $C_{(1-16)+(Blood)+(Perit)}$ is the sum of the mass of drug in the bladder wall compartments (C_{1-16}), the blood compartment (C_{Blood}) and the peritoneum compartment (C_{Perit}).

STELLA		PYTHON	

Time (min)	C_{BL}	C_1	C_2	C_3	C_4	C_5	C_6	C_7	C_8	C_9	C_{10}	C_{11}	C_{12}	C_{13}	C_{14}	C_{15}	C_{16}	C_{Perit}
0	0	0	0	0	0	0	0	0	0	0	0	0	0	0	0	0	0	0
0	0	0	0	0	0	0	0	0	0	0	0	0	0	0	0	0	0	0
5	996.847	0.940	0.696	0.471	0.270	0.087	0.191	0.137	0.097	0.066	0.043	0.035	0.023	0.014	0.009	0.005	0.002	0.007
5	996.845	0.941	0.696	0.472	0.270	0.087	0.191	0.138	0.097	0.066	0.043	0.035	0.023	0.014	0.009	0.005	0.002	0.007
10	995.115	0.977	0.762	0.551	0.344	0.142	0.348	0.281	0.223	0.174	0.132	0.127	0.097	0.071	0.050	0.031	0.015	0.157
10	995.115	0.977	0.762	0.551	0.344	0.142	0.349	0.281	0.223	0.174	0.132	0.127	0.097	0.071	0.050	0.031	0.015	0.156
15	993.531	0.985	0.778	0.573	0.369	0.167	0.422	0.351	0.290	0.235	0.186	0.188	0.148	0.113	0.082	0.053	0.026	0.536
15	993.530	0.985	0.778	0.573	0.369	0.167	0.422	0.352	0.290	0.235	0.186	0.188	0.148	0.113	0.082	0.053	0.026	0.535
20	991.993	0.987	0.784	0.582	0.380	0.179	0.458	0.387	0.323	0.266	0.215	0.219	0.176	0.136	0.099	0.065	0.032	1.063
20	991.993	0.987	0.784	0.582	0.380	0.179	0.458	0.387	0.323	0.266	0.215	0.220	0.176	0.136	0.099	0.065	0.032	1.063
25	990.478	0.988	0.787	0.586	0.385	0.185	0.475	0.404	0.340	0.282	0.229	0.235	0.189	0.147	0.108	0.071	0.035	1.669
25	990.478	0.988	0.787	0.586	0.385	0.185	0.475	0.404	0.340	0.282	0.229	0.235	0.189	0.147	0.108	0.071	0.035	1.669
30	988.976	0.987	0.787	0.587	0.388	0.188	0.484	0.412	0.348	0.289	0.236	0.243	0.196	0.153	0.112	0.074	0.037	2.314
30	988.976	0.987	0.787	0.587	0.387	0.188	0.484	0.412	0.348	0.289	0.236	0.243	0.196	0.153	0.112	0.074	0.037	2.314

Table 4.3. Example outputs generated with the STELLA® (red) and PYTHON™ (green) model over 30 min. Data shows drug accumulated (mg) in each compartment. STELLA® and PYTHON™ model outputs were identical to 2 decimal places.

4.3.1.3. Validating Step 3: Incorporating urine dilution

Step 3 design was validated by comparing model outputs generated with STELLA® and PYTHON™ (Figure 4.8, Table 4.4). Input parameters are detailed in table 4.1 with the addition of U_R = 1 ml min^{-1}, k_{Elim} = 0.00102 s^{-1} and a change in the bladder surface area from 30 cm^2 to 260 cm^2 (an accurate figure for the human bladder[28], Figure 4.3). For all simulations performed, STELLA® and PYTHON™ model outputs were identical to 2 decimal places (Table 4.4). Urine dilution of the instilled dose reduced the mass of drug accumulating in the peritoneum over time (Figure 4.8).

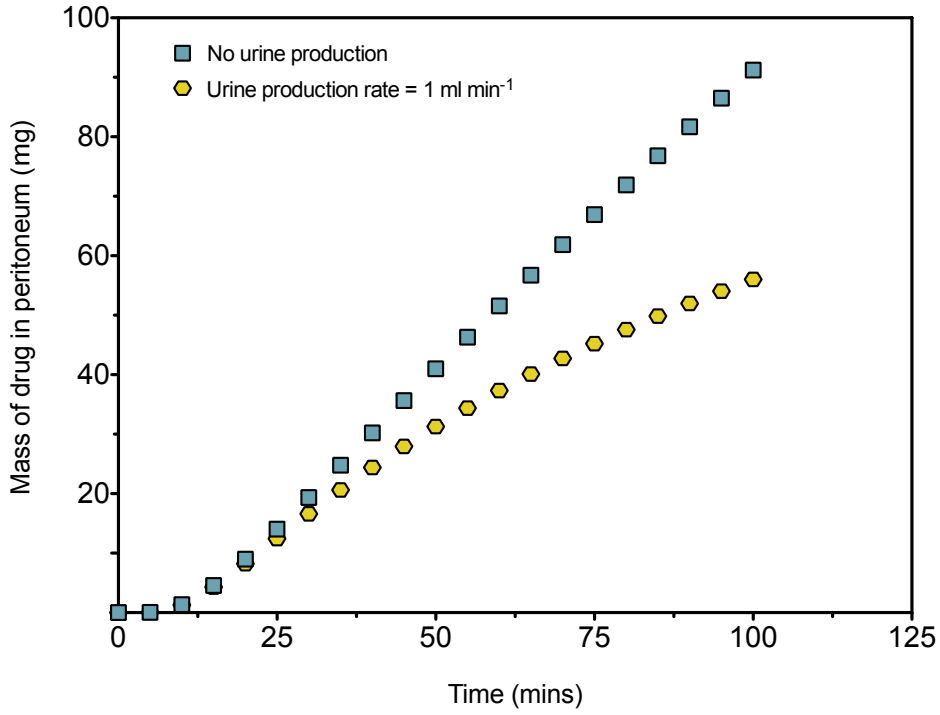

Figure 4.8. Results of STELLA® simulations showing the mass of drug accumulating in the peritoneum compartment over 100 min with and without the incorporation of urine production.

STELLA		PYTHON	

Time (min)	C_{BL}	C_1	C_2	C_3	C_4	C_5	C_6	C_7	C_8	C_9	C_{10}	C_{11}	C_{12}	C_{13}	C_{14}	C_{15}	C_{16}	C_{Perit}
0	0	0	0	0	0	0	0	0	0	0	0	0	0	0	0	0	0	0
0	0	0	0	0	0	0	0	0	0	0	0	0	0	0	0	0	0	0
5	974.639	7.382	5.544	3.797	2.188	0.711	1.575	1.139	0.802	0.548	0.356	0.295	0.191	0.120	0.073	0.041	0.018	0.058
5	974.627	7.385	5.549	3.802	2.192	0.712	1.578	1.140	0.803	0.548	0.356	0.294	0.190	0.120	0.072	0.041	0.018	0.056
10	963.036	6.981	5.543	4.064	2.573	1.090	2.688	2.182	1.744	1.368	1.044	1.014	0.772	0.570	0.400	0.254	0.123	1.291
10	963.028	6.981	5.544	4.065	2.574	1.091	2.690	2.184	1.746	1.370	1.045	1.015	0.773	0.570	0.400	0.254	0.123	1.285
15	953.527	6.441	5.185	3.878	2.540	1.190	3.031	2.549	2.118	1.732	1.385	1.404	1.114	0.855	0.620	0.403	0.198	4.264
15	953.520	6.441	5.185	3.879	2.541	1.190	3.032	2.551	2.120	1.734	1.386	1.406	1.115	0.856	0.620	0.403	0.199	4.259
20	945.080	5.949	4.815	3.633	2.418	1.184	3.057	2.609	2.201	1.830	1.489	1.534	1.235	0.960	0.703	0.461	0.228	8.156
20	945.072	5.949	4.815	3.633	2.418	1.184	3.058	2.610	2.202	1.831	1.490	1.535	1.236	0.960	0.704	0.461	0.228	8.154
25	937.374	5.513	4.472	3.388	2.272	1.136	2.951	2.534	2.153	1.803	1.478	1.533	1.242	0.970	0.714	0.470	0.233	12.331
25	937.366	5.513	4.472	3.388	2.272	1.136	2.952	2.535	2.154	1.803	1.479	1.533	1.242	0.970	0.714	0.470	0.233	12.332
30	930.244	5.129	4.164	3.159	2.126	1.073	2.795	2.407	2.052	1.723	1.418	1.475	1.198	0.938	0.692	0.456	0.226	16.474
30	930.235	5.129	4.164	3.159	2.126	1.073	2.795	2.408	2.052	1.723	1.418	1.475	1.198	0.938	0.692	0.456	0.226	16.476

Table 4.4. Example outputs generated with the STELLA® (red) and PYTHON™ (green) model over 30 min. Data shows drug accumulated (mg) in each compartment. STELLA® and PYTHON™ model outputs were identical to 2 decimal places.

4.3.1.4. Validating Step 4: Moving from a 'mass' to 'concentration' - based model

The introduction of '*concentration*' is simply an interpretation of the existing model (Equation 10) and was therefore investigated using STELLA® only. Further steps in the model development were not validated with PYTHON™ as the underlying model has been shown to work consistently between the two packages. Model simulations were to this point generated using arbitrary input parameters. For completeness, physiologically relevant parameters were input into the model according to table 4.5. Diffusion coefficients[22], partition coefficients[29], tissue layer thickness[9,21,30], total bladder weight[28,31], urine production rate[12] and bladder wall blood flow rate[11] were sourced from the literature. A constant bladder surface area of 260 cm^2 was assumed regardless of intravesical volume. The mass of the different bladder wall layers was calculated from total bladder weight and bladder layer thickness according to the equation

$$W_i = \frac{h_i}{h_{Total}} \times W_{Total} \tag{12}$$

where W_i is the weight of the bladder wall layer (g), h_i is the thickness of the bladder wall layer (cm), h_{Total} is the total thickness of the bladder wall (cm) and W_{Total} is the total weight of the empty bladder (g). It is assumed that the different layers of the bladder wall are of equal density.

Step 4 was investigated with the STELLA® model. Input parameters are detailed in table 4.5. Figure 4.9 shows concentration - depth profiles generated by the model 15, 30, 45 and 60 min post - instillation of the intravesical dose. The profile is representative of those reported in the literature[21] with the highest drug - tissue concentration achieved in the urothelium followed by a relatively sharp decline across the deeper tissue layers.

Bladder lumen		Uro		Uro / LP boundary		LP		LP / DM		DM		DM / Perit boundary	
(C_{BL-1})		**($C_{1-5,\ 5-BL}$)**		**(C_{5-6})**		**($C_{6-10,\ 10-5}$)**		**(C_{10-11})**		**($C_{11-16,\ 16-10}$)**		**(C_{16} - C_{Perit})**	
M_{BL}	1000	Km_1	1	Km_1	1	Km_2	1.5	Km_2	1.5	Km_3	1.5	Km_3	1.5
V_{BL}	50	D_1	1E-07	Km_2	1.5	D_2	1E-06	Km_3	1.5	D_3	2E-06	D_3	2E-06
SA_{BL}	260	h_{BL}	0.192	km_2 / km_1	1.5	h_2	0.10	km_3 / km_2	1	h_3	2.0E-01	h_3	0.20
U_R	1	h_1	0.02	D_2	1E-06	n_2	5	D_3	2E-06	n_3	6	n_3	6
Km_1	1	n_1	5	h_1	0.02	h_2 / n_2	0.02	h_2	0.10	h_3 / (n_{3+1})	0.0286	h_3 / (n_{3+1})	0.0286
D_1	1E-07	h_1 / n_1	0.004	n_1	5	$K_{i,i+1}$ or $K_{i+1,i}$	0.0625	n_2	5	$K_{i,i+1}$ or $K_{i+1,i}$	1.84E-03	$K_{i,i+1}$	1.84E-03
h_{BL}	0.19	$K_{i,i+1}$ or $K_{i+1,i}$	6.25E-03	h_1 / n_1	0.004	K_{Elim}	1.02E-03	h_2 / n_2	0.02	K_{Elim}	1.02E-03		
h_1	0.02	W_{1-5}	0.53	h_2	0.1	W_{6-10}	2.63	h_3	0.2	W_{11-16}	4.38		
n_1	5			n_2	5			n_3	6				
h_1 / n_1	0.004			h_2 / n_2	0.02			h_3 / (n_{3+1})	0.029				
K_{BL}	1E-04			$K_{i,i+1}$	1.88E-02			$K_{i,i+1}$	2.63E-03				
								K_{Elim}	1.02E-03				

Parameter	Description	Units
M_{BL}	Mass of drug in bladder lumen	mg
V_{BL}	Volume of drug in bladder lumen	ml
SA_{BL}	Luminal surface area of the bladder	cm^2
U_R	Urine production rate	ml min^{-1}
Km_{1-3}	Drug partition coefficient	Unitless
D_{1-3}	Drug diffusion coefficient	cm^2 s^{-1}
h_{BL}	Effective thickness of the bladder contents	cm
h_{1-3}	Thickness of tissue layer	cm
n_{1-3}	Number of compartments in tissue layer	Unitless
K_{BL}, $K_{i,i+1}$, $K_{i+1,i}$	Drug transfer coefficient	s^{-1}
W_{1-16}	Weight of tissue layer	g
K_{Elim}	Drug elimination rate constant	s^{-1}

Table 4.5. Parameter values used in Step 4 design of the PK model.

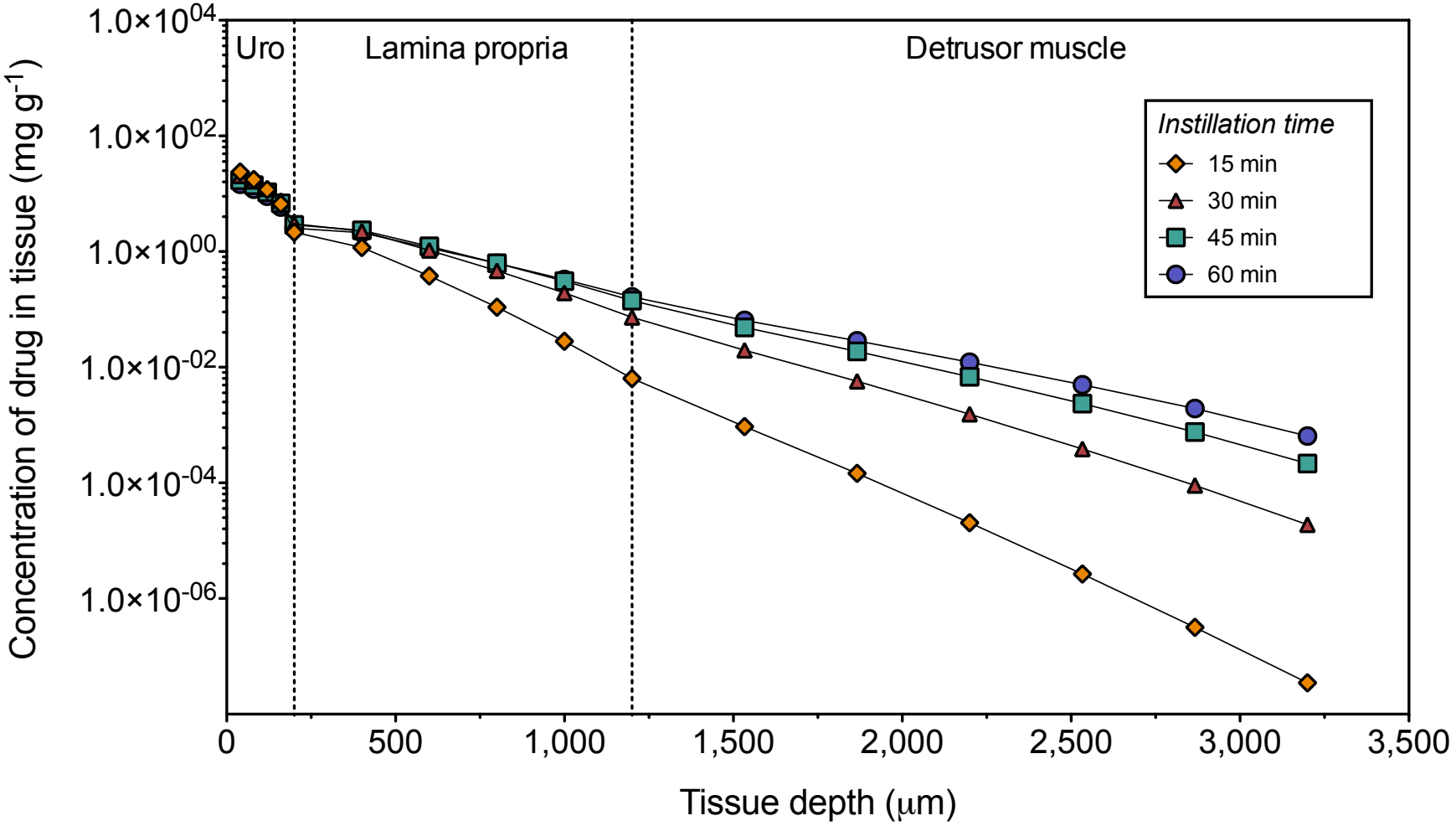

Figure 4.9. Results of STELLA® simulations showing the drug concentration achieved at different tissue depths (concentration - depth profile) at 15, 30, 45 and 60 min post instillation of the intravesical dose.

4.3.1.5. Validating Step 5: Allowing for multiple intravesical doses

To validate the introduction of multiple - dose functionality, the volume and drug concentration in the bladder lumen throughout an example intravesical regimen was investigated (Section 4.2.2.5, Figure 4.10A - B). With the exception of the double dosing technique, all other model inputs were unchanged (Table 4.5). Bladder volume at the end of the 2 h treatment ($V_{BL}2h$) is described by equation 11 (PVR volume is assumed to be 0 ml for both patients).

Patient #1 (single 50 ml drug instillation for 2 h)

$$V_{BL}2h = 50 + (1 \times 120) = 170 \text{ ml}$$

Patient #2 (two 50 ml drug instillations over the 2 h period)

For patient 2, $V_{BL}0$ is replaced with $V_{BL}62$ min, representing the volume in the bladder at the time of the second dose (50 ml drug solution plus 2 ml urine production since voiding of the first dose).

$$V_{BL}2h = 52 + (1 \times 60) = 112 \text{ ml}$$

Simulations show the model is working with respect to final bladder volumes of 170 ml and 112 ml predicted for patient 1 and 2 respectively (Figure 4.10A). This variation in bladder volume translates into higher bladder lumen drug concentrations from 62 min onwards for patient 2 (Figure 4.10B). Bladder lumen drug concentration is described by the equation

$$Lumen_{Conc} = \frac{Lumen_{Mass}}{V_{BL}} \quad (13)$$

where $Lumen_{Conc}$ is the concentration of drug in the bladder lumen (mg ml^{-1}) and $Lumen_{Mass}$ is the mass of drug in the bladder lumen (mg).

The increased luminal drug concentration from 60 – 120 min (for patient 2 as compared to patient 1) would be expected to result in more drug being delivered transurothelially. Consequently, final bladder wall drug concentrations achieved in patient 2 are expected to be higher. To investigate this, bladder tissue concentrations and tissue – drug exposure (AUC) in compartment 3 of the urothelium (100 μm median depth) were compared for the two regimens. AUC values were calculated from tissue drug concentration - time graphs (Figure 4.10C - D) in GraphPad Prism using the trapezoid rule. Over the 2 h treatment period, the double dosing regimen resulted in greater overall exposure of drug to the urothelium; AUC values of 1,028 and 1,305 mg min g^{-1} for the single and double dosing regimens respectively (Figure 4.10C - D). The double dosing technique also resulted in higher final drug urothelial concentrations compared to the standard regimen (Figure 4.10C - D, 9.28 versus 5.51 mg g^{-1} respectively).

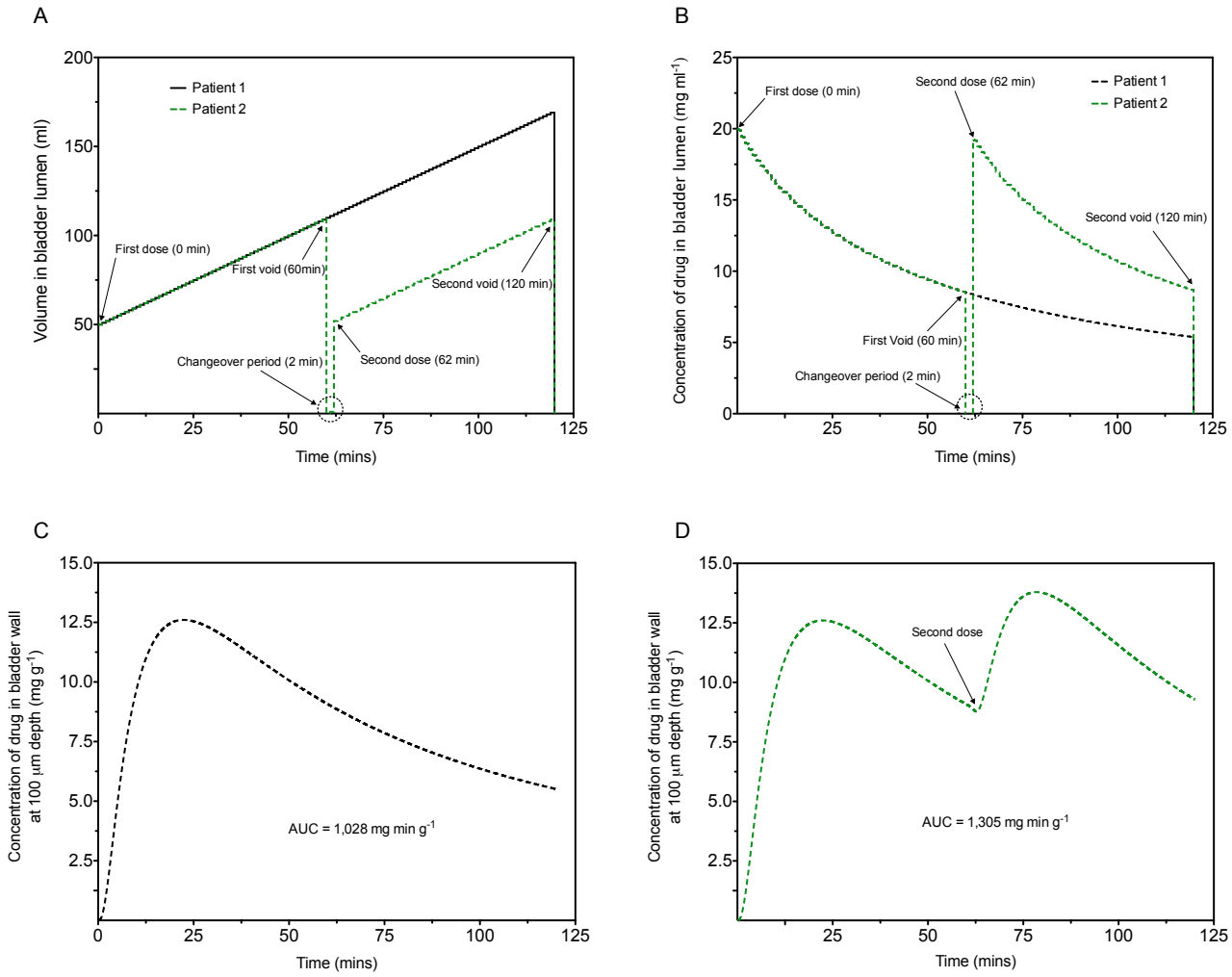

Figure 4.10. Results of STELLA® simulations comparing bladder lumen volume (A), bladder lumen drug concentration (B) and urothelial concentrations at a median depth of 100 μm over a 2 h intravesical regimen for patient 1 (C, standard regimen) and patient 2 (D, double dosing regimen).

4.3.1.6. Validating Step 6: Incorporating post - void residual (PVR) volume

Simulations were performed comparing luminal volume and luminal drug concentration for different PVR volumes (0, 10 and 20 ml) (Figure 4.11). All other parameters were kept constant. Luminal volume at the start of the instillation increased by the value of the PVR volume (Equation 11, Figure 4.11A). Increases in PVR volume decreased the starting luminal drug concentration (Equation 13, Figure 4.11B).

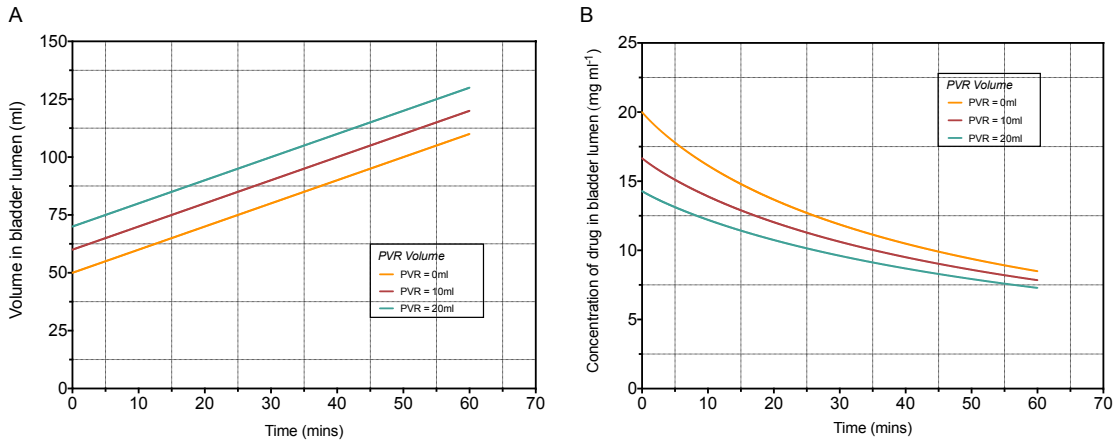

Figure 4.11. Results of STELLA® simulations comparing luminal volume (A) and luminal drug concentration (B) for different PVR volumes (0, 10 and 20 ml).

4.3.2. Investigating the effect of individual variables on the efficacy of intravesical drug delivery

The validated PK model was used to investigate the effect of individual variables on the efficacy of the IDD process. The major limitation cited for IDD is the inability to achieve sufficient drug concentrations in the bladder wall[32]. For the purpose of this exercise, efficacy will be measured on bladder wall drug concentrations achieved and bladder wall drug exposure (AUC). The greater the tissue drug concentration and AUC achieved, the more effective the intravesical regimen. It is however acknowledged that higher drug tissue concentrations may not always be the aim of optimised intravesical regimens.

The range of values considered clinically relevant for the variables associated with an intravesical regimen can vary significantly. A high urine production rate may be

an order of magnitude higher than that of a low one, however a long instillation time is unlikely to be more than 2 or 3 times that of a short one. An approach which multiples all variables by a common factor and then assess individual contribution to the efficacy of the delivery process is unsuitable. Instead variables were investigated within a clinically relevant range. Apart from the variable under investigation, all other variables (model inputs) were kept constant. These baseline variables represent physiologically relevant values as introduced in section 4.3.1.4.

The following variables were investigated: drug diffusion coefficient, concentration of drug instillation, volume of drug instillation, instillation time, urine production rate, and dosing regimen (single versus double dosing).

4.3.2.1. Drug diffusion coefficient (D)

The transurothelial diffusion coefficient (D, $cm^2\ s^{-1}$) represents the ability of a drug to permeate across the urothelium and penetrate into the bladder wall. For an infinite dose (when approximately ≥ 90 – 95 % of the applied dose remains in the donor chamber of the diffusion apparatus during the steady - state period of permeability studies (Section 2.2.5)), transurothelial permeation is described by Fick's first law[33] and the equation

$$J = -D\frac{\Delta C}{\Delta h} \qquad (14)$$

where J is diffusive flux ($mg\ cm^{-2}\ s^{-1}$), D is the transurothelial diffusion coefficient ($cm^2\ s^{-1}$), ΔC is the concentration gradient across the urothelium ($mg\ cm^{-3}$) and Δh is the linear distance travelled (thickness of urothelium, (cm)). D is independent of drug concentration and unique to the drug in question. In contrast to other fields of pharmaceutics such as transdermal delivery, mathematical modelling and *in vitro / ex vivo* transurothelial permeability data is scarce with only two studies reporting D values (both for pipemidic acid)[22,34]. *Ex vivo* transurothelial permeability coefficients (k_P) have been determined for several drugs (Section 2.3.3.2 and 3.3.2.1)[35,36].

k_P is related to D by the equation

$$k_P = \frac{K_m D}{\Delta h} \qquad \text{rearranged to} \qquad D = \frac{k_P \Delta h}{K_m} \tag{15}$$

where k_P is the transurothelial permeability coefficient (cm s^{-1}), Δh is the thickness of the urothelium (cm), and K_m is the partition coefficient of the drug between the urothelium and the donor chamber of the diffusion apparatus[27].

Using equation 15, D values were derived from experimentally determined k_P values (Table 4.6). Owing to the lack of data in the literature, diffusion coefficients for the lamina propria and detrusor muscle were derived from urothelial D values (Table 4.8). The urothelium is the rate - limiting barrier to the movement of drug into the bladder wall[37–39]. It is assumed therefore that diffusion coefficients in the lamina propria and detrusor muscle layers will be greater than that in the urothelium. These assumptions are consistent with results presented by Grabnar *et al* who reported a large increase in diffusion coefficient in the sub - urothelial layers compared to the urothelium[22]. Although not available for all layers of the bladder wall, there are detrusor muscle[29,35] and combined lamina propria / detrusor muscle[22] K_m values for a range of drugs in the literature. These in combination with literature sourced K_m values for similar tissue matrixes, such as the dermis[7] for the lamina propria, allowed good estimation of suitable values for the different layers of the bladder wall (Table 4.8). Based on experimentally determined values (Table 4.6), the effect of varying D values in the range 0.1 – 5.0 x 10^{-07} cm^2 s^{-1} was investigated. An overview of the intravesical regimen is provided in table 4.7 and a complete list of inputs used in the model detailed in table 4.8.

From a clinical standpoint, investigating the ability of a drug to diffuse into the bladder wall is highly relevant. It is common knowledge that the urothelium is a significant barrier to IDD[40]. Additionally clinicians are aware that a drug's physiochemical properties are important to the attainment of therapeutic drug concentrations in target tissues[41]. Early stage screening of drug - like properties is routine in the development of candidate drug molecules[42]. For these reasons a

drug's D value might be considered the principal factor determining whether or not a drug can be successfully delivered intravesically.

Figure 4.13 shows that increasing a drug's D value results in greater drug exposure to each of the bladder wall layers over the course of the treatment regimen (Figure 4.13A - C). Based on the k_P values determined experimentally in this thesis, the comparison between 0.1 and 1.0 x 10^{-07} cm^2 s^{-1} is the most relevant. Concentration - depth profiles show that the increase in D results in higher drug - tissue concentrations at all depths of the bladder wall (Figure 4.12B) and markedly higher exposure of the urothelium (155 % increase in AUC), lamina propria (18,700 % increase) and detrusor muscle (>178 x 10^6 %) to the drug (Figure 4.13A - C). Interestingly, final urothelium concentrations at 60 min (Figure 4.12A, 50.0 % higher when D = 1.0 x 10^{-07} cm^2 s^{-1}) do not accurately represent the increased exposure of the urothelium to the drug over the course of the treatment (Figure 4.13A, 154.5 % increase in AUC). The shape of the tissue concentration - time profile shows the higher D value results in a steeper rise in tissue concentrations and a higher peak concentration in the urothelium (Cmax) (Figure 4.13A); after Cmax is achieved concentrations in the urothelium decline. An explanation may be that the higher D value means more drug permeates into the urothelium subsequently reducing the drug concentration gradient between the bladder lumen and the urothelium as the instillation progresses. As a result drug permeation into the urothelium is superseded by drug clearance from the lower bladder wall layers and final urothelium concentrations are lower than the Cmax. This also explains the counterintuitive observation that final urothelium concentrations with a D value of 5.0 x 10^{-07} cm^2 s^{-1} are actually lower than those with a D value of 1.0 x 10^{-07} cm^2 s^{-1} (Figure 4.12A).

The drug D value is significant to the IDD process. Higher values result in higher drug tissue concentrations and greater exposure of the tissue to the drug. These effects are more pronounced in the deeper bladder wall layers (lamina propria and detrusor muscle) than the urothelium. It may therefore be particularly important to consider a drug's D value when the therapeutic target is located in the lower bladder wall layers e.g. T1 bladder cancer[43].

Drug	k_p (x 10^{-06} cm s^{-1})	D (x 10^{-07} cm^2 s^{-1})
Ketorolac tromethamine	2.63[29]	0.53
Oxybutynin chloride	13.60[36]	2.72
Tamsulosin hydrochloride	0.86[35]	0.17
Terazosin hydrochloride	1.53[35]	0.31
Doxazosin mesylate	5.33[35]	1.1

Table 4.6. Transurothelial diffusion coefficients (D) derived from experimentally determined transurothelial permeability coefficients (k_P) for a range of drugs according to equation 15. Values of 0.02 cm[19] and 1[22,29] were used for urothelium thickness (h) and urothelium partition coefficient (Km) respectively.

Intravesical regimen	
Concentration of drug instillation	1 mg ml^{-1}
Volume of drug instillation	50 ml
Instillation time	60 min
Urine production rate	1 ml min^{-1}
Dosing pattern	Standard, single instillation
Transurothelial diffusion coefficient, D	0.1 – 5.0 x 10^{-07} cm^2 s^{-1}

Table 4.7. Overview of the dosing regimen used to investigate the effect transurothelial diffusion coefficient has on the efficacy of the intravesical delivery process.

Bladder lumen		Uro		Uro / LP boundary		LP		LP / DM boundary		DM		DM / Perit boundary	
(C_{BL-1})		**($C_{1-5,\ 5-BL}$)**		**(C_{5-6})**		**($C_{6-10,\ 10-5}$)**		**(C_{10-11})**		**($C_{11-16,\ 16-10}$)**		**($C_{16-}C_{Perit}$)**	
M_{BL}	50	K_{m1}	1	K_{m1}	1	K_{m2}	1.5	K_{m2}	1.5	K_{m3}	1.5	K_{m3}	1.5
V_{BL}	50	D_1	Variable	K_{m2}	1.5	D_2	D_1 x 10	K_{m3}	1.5	D_3	D_1 x 10	D_3	D_1 x 10
PVR	0	h_{BL}	0.19	K_{m2}/K_{m1}	1.5	h_2	0.1	K_{m3}/K_{m2}	1	h_3	0.2	h_3	0.2
A_{BL}	260	h_1	0.02	D_2	D_1 x 10	n_2	5	D_3	D_1 x 10	n_3	6	n_3	6
U_R	1	n_1	5	h_1	0.02	h_2 / n_2	0.02	h_2	0.1	$h_3/(n_3+1)$	0.0286	$h_3/(n_3+1)$	0.0286
K_{m1}	1	h_1 / n_1	0.004	n_1	5	$k_{i,i+1}$ or $k_{i+1,i}$	Variable	n_2	5	$k_{i,i+1}$ or $k_{i+1,i}$	Variable	$k_{i,i+1}$	Variable
D_1	Variable	$k_{i,i+1}$ or $k_{i+1,i}$	Variable	h_1 / n_1	0.004	K_{Elim}	1.02E-03	h_2 / n_2	0.020	k_{Elim}	1.02E-03		
h_{BL}	0.19	W_{1-5}	0.53	h_2	0.1	W_{6-10}	2.63	h_3	0.2	W_{11-16}	4.38		
h_1	0.02			n_2	5			n_3	6				
n_1	5			h_2 / n_2	0.02			$h_3/(n_3+1)$	0.029				
h_1 / n_1	0.004			$k_{i,i+1}$	Variable			$k_{i,i+1}$	Variable				
k_{BL}	Variable							k_{Elim}	1.02E-03				

Parameter	Description	Units
M_{BL}	Mass of drug in bladder lumen	mg
V_{BL}	Volume of drug in bladder lumen	ml
PVR	Post void residual urine volume	ml
A_{BL}	Luminal surface area of the bladder	cm^2
U_R	Urine production rate	$ml\ min^{-1}$
Km_{1-3}	Drug partition coefficient	Unitless
D_{1-3}	Drug diffusion coefficient	$cm^2\ s^{-1}$
h_{BL}	Effective thickness of the bladder contents	cm
h_{1-3}	Thickness of tissue layer	cm
n_{1-3}	Number of compartments in tissue layer	Unitless
K_{BL}, $K_{i,i+1}$, $K_{i+1,i}$	Drug transfer coefficient	s^{-1}
W_{1-16}	Weight of tissue layer	g
K_{Elim}	Drug elimination rate constant	s^{-1}

Table 4.8. Overview of the PK model inputs used to investigate the effect of transurothelial diffusion coefficient (D). Parameter units are the same as detailed in table 4.5.

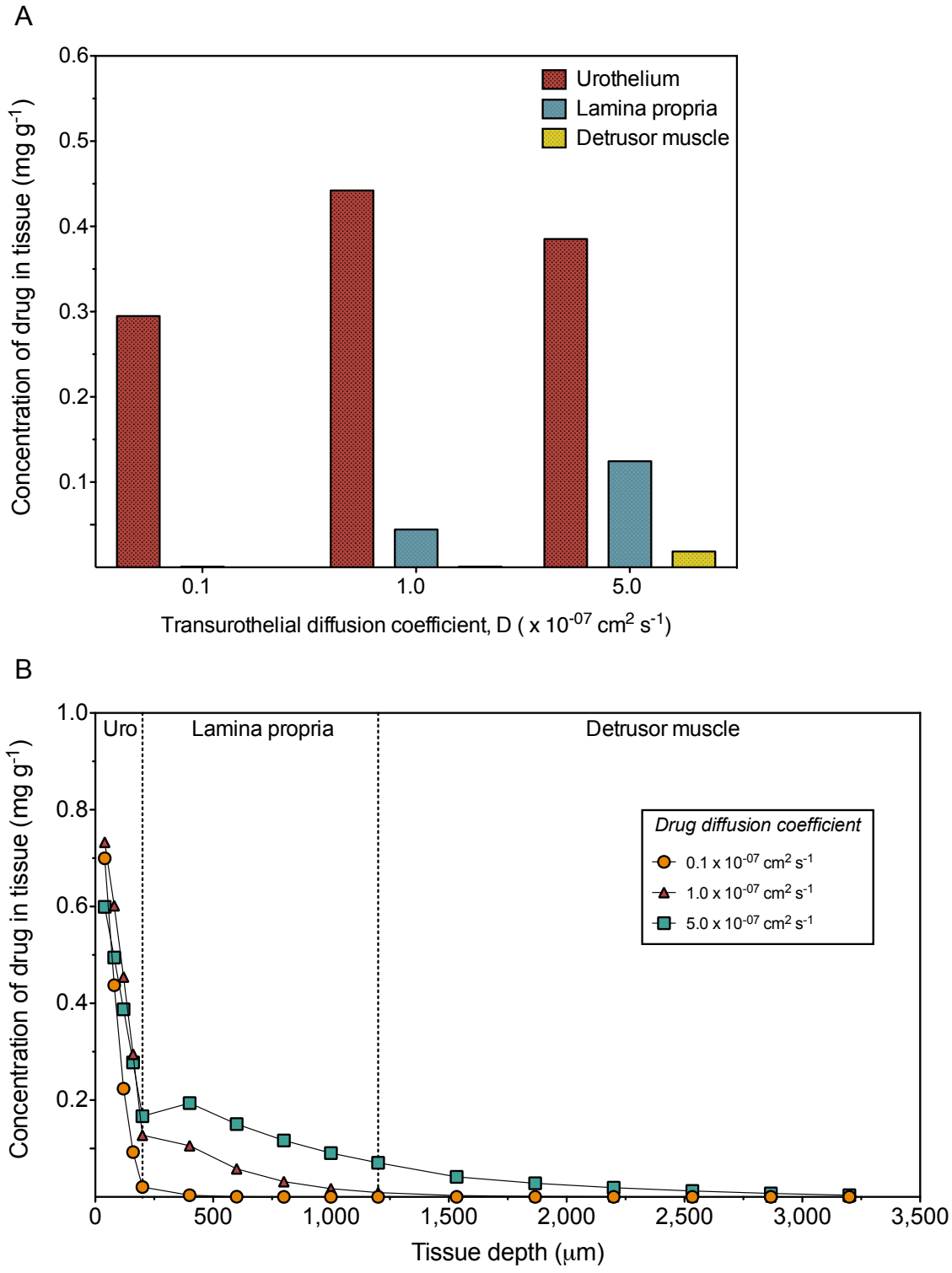

Figure 4.12. Results of PK model simulations showing average drug concentrations in the different layers of the bladder wall (A) and full concentration - depth profiles (B) following 60 min intravesical instillation with drugs of different transurothelial diffusion coefficients (0.1 - 5.0 x 10^{-07} cm^2 s^{-1}).

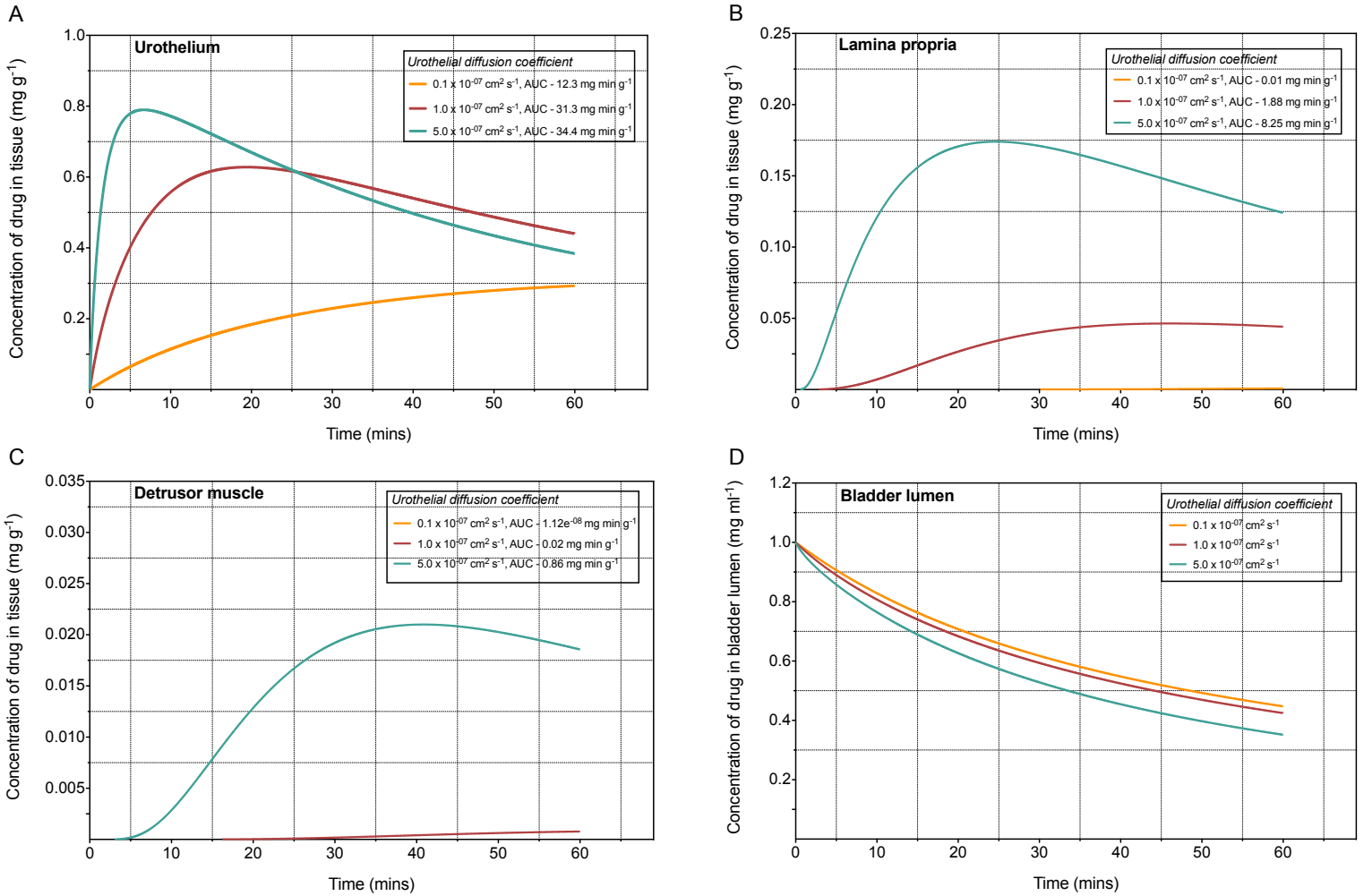

Figure 4.13. Results of PK model simulations showing average drug concentrations in the urothelium (A), lamina propria (B), detrusor muscle (C), and bladder lumen (D) over the course of a 60 min intravesical instillation with drugs of different transurothelial diffusion coefficients (0.1 - 5.0 x 10^{-07} cm^2 s^{-1}).

4.3.2.2. Concentration of drug instillation

In practice, drugs are instilled into the bladder at a range of concentrations. For instance, mitomycin C (MMC) is typically administered at a concentration of 1 mg ml^{-1} [44], whilst oxybutynin at 0.16 mg ml^{-1} [45]. These concentrations are often extrapolated from oral[45] or systemic doses[46] and are not based on bladder wall target concentrations. Furthermore, owing to the limited adverse effects associated with IDD, a range of instillation concentrations for the same drug is not uncommon (oxybutynin has been used clinically in the range 0.05[47] - 1 mg ml^{-1} [48]). On this basis the influence of drug concentrations in the range 0.1 - 10 mg ml^{-1} was investigated. An overview of the intravesical regimen is provided in table 4.9. With the exception of concentration of drug instillation, all other model inputs are consistent with table 4.8.

PK simulations show that drug concentrations achieved throughout the bladder wall are proportional to the concentration of the drug solution instilled (Figure 4.14A). After 60 min, drug tissue concentrations achieved with the 10 mg ml^{-1} solution are ten times higher than those achieved with the 1 mg ml^{-1}, which in turn are ten times higher than those achieved with the 0.1 mg ml^{-1} solution for each layer of the bladder wall (Figure 4.14B). This linear relationship between bladder lumen concentration and bladder wall bioavailability was predictable, given the underlying diffusion equations (Equations 1 - 13). Consequently urothelium, lamina propria and detrusor muscle exposure to drug over the instillation period was proportional to the concentration of drug instillation (Figure 4.15A - C). Dosing concentration has a strong influence on the efficacy of IDD.

Intravesical regimen	
Concentration of drug instillation	0.1 - 10 mg ml^{-1}
Volume of drug instillation	50 ml
Instillation time	60 min
Urine production rate	1 ml min^{-1}
Dosing pattern	Standard, single instillation
Transurothelial diffusion coefficient, D	1.0 x 10^{-07} cm^2 s^{-1}

Table 4.9. Overview of the dosing regimen used to investigate the effect of concentration of drug instillation.

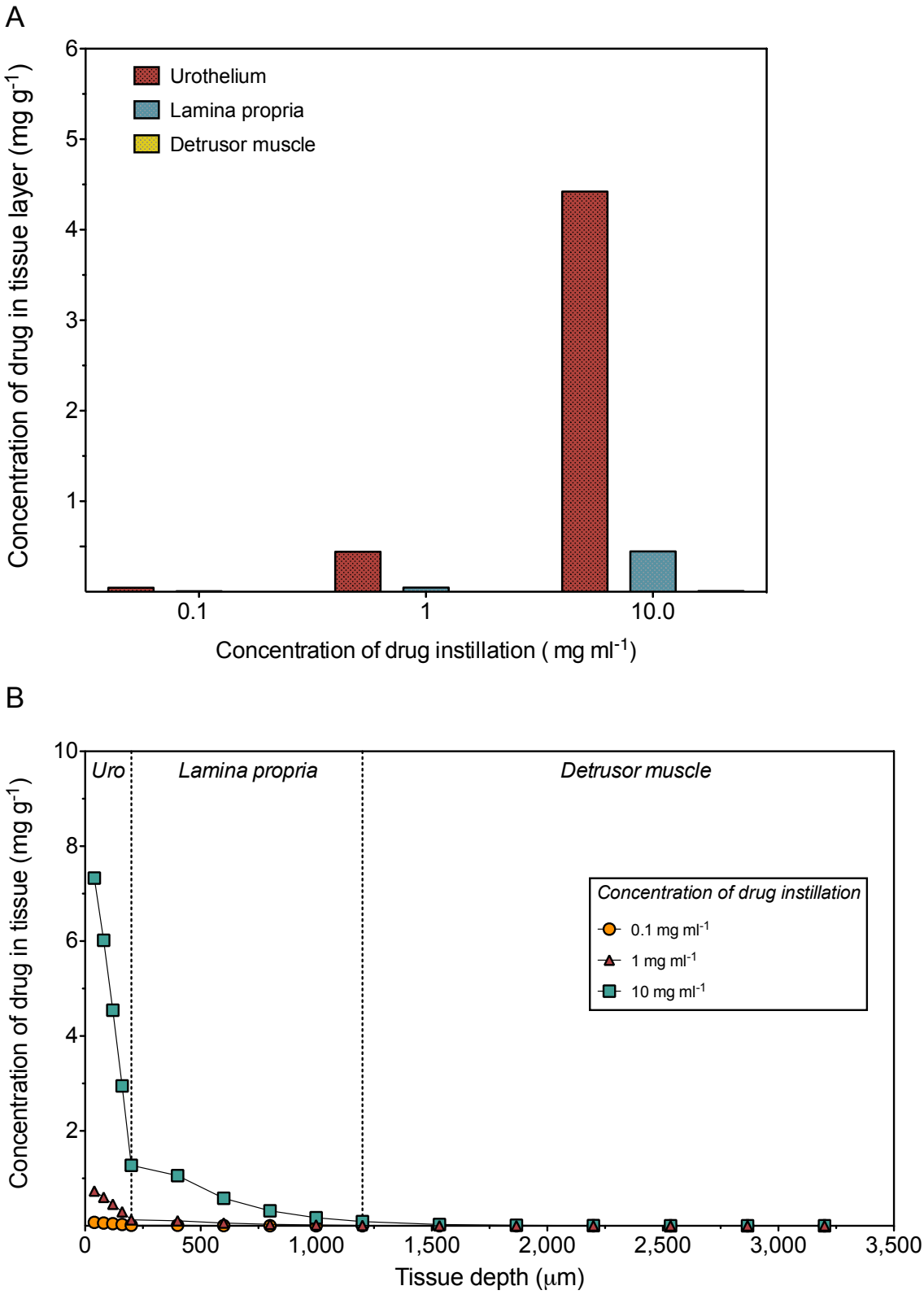

Figure 4.14. Results of PK model simulations showing average drug concentrations in the different layers of the bladder wall (A) and full concentration - depth profiles (B) following 60 min intravesical instillation with different concentrations of drug solution (0.1 - 10 mg ml^{-1}).

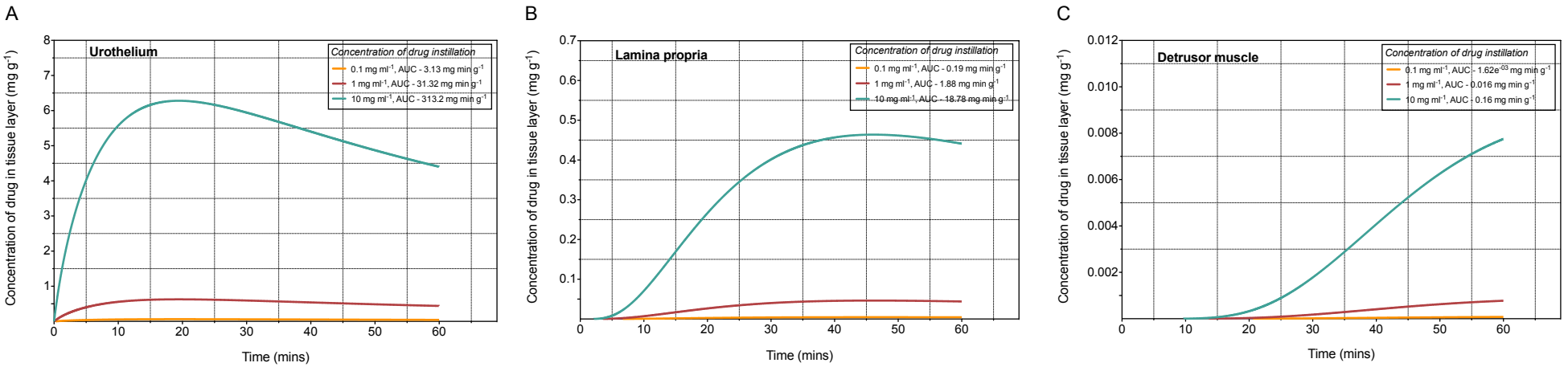

Figure 4.15. Results of PK model simulations showing average drug concentrations in the urothelium (A), lamina propria (B) and detrusor muscle (C) over the course of a 60 min intravesical instillation with different concentrations of drug solution (0.1 - 10 mg ml^{-1}).

4.3.2.3. Volume of drug instillation

Although drug is normally instilled in volumes of 40 - 50 ml[49,50], the literature provides examples from 10 to 100 ml[51,52] and therefore this range was investigated. The human bladder has a maximum capacity of ~800 mls when fully distended although an urge to void initiated at ~300 – 400 mls[8]. A 100 ml instillation may seem like a large volume, however given a urine production rate of 1ml min^{-1} the final bladder volume is well below the normal micturition threshold after 60 min. An overview of the intravesical regimen is provided in table 4.10. With the exception of volume of drug instillation, all other model inputs were consistent with table 4.8.

The volume of drug instillation is often dictated by the solubility of the drug and / or the volume capacity of the bladder. Little consideration is given to the dilution effect urine will have on different volumes of drug instillation. Figure 4.17D shows that despite starting at the same intravesical concentration (1 mg ml^{-1}), the luminal concentration of drug decreases at different rates according the volume of drug solution instilled. The lower the instillation volume, the greater the urine dilution effect and the faster the luminal drug concentration decreases. Drug concentrations achieved in the bladder wall are proportional to the concentration of the drug in the bladder lumen (Figure 4.14 - 15). Consequently the greater the initial volume of drug instillation, or more accurately the wider the differential between the volume of instillation and the rate of urine production, the higher the drug concentration achieved at each depth of the bladder wall (Figure 4.16B). Increasing the volume of drug instillation from 10 ml to 50 ml resulted in a 216.3 % increase in the final urothelial drug concentration after 60 min (Figure 4.16A). Once the drug instillation exceeds a certain volume, further increases have a lesser effect on bladder wall drug concentrations as the dilution effect of urine is negated. Increasing the volume of instilled drug solution from 50 ml to 100 ml resulted in a much lower 35.9 % increase in the final urothelial concentration of drug after 60 min (Figure 4.16A).

Intravesical regimen	
Concentration of drug instillation	1 mg ml^{-1}
Volume of drug instillation	10 - 100 ml
Instillation time	60 min
Urine production rate	1 ml min^{-1}
Dosing pattern	Standard, single instillation
Transurothelial diffusion coefficient, D	1.0 x 10^{-07} cm^2 s^{-1}

Table 4.10. Overview of the dosing regimen used to investigate the effect of instilled drug volume.

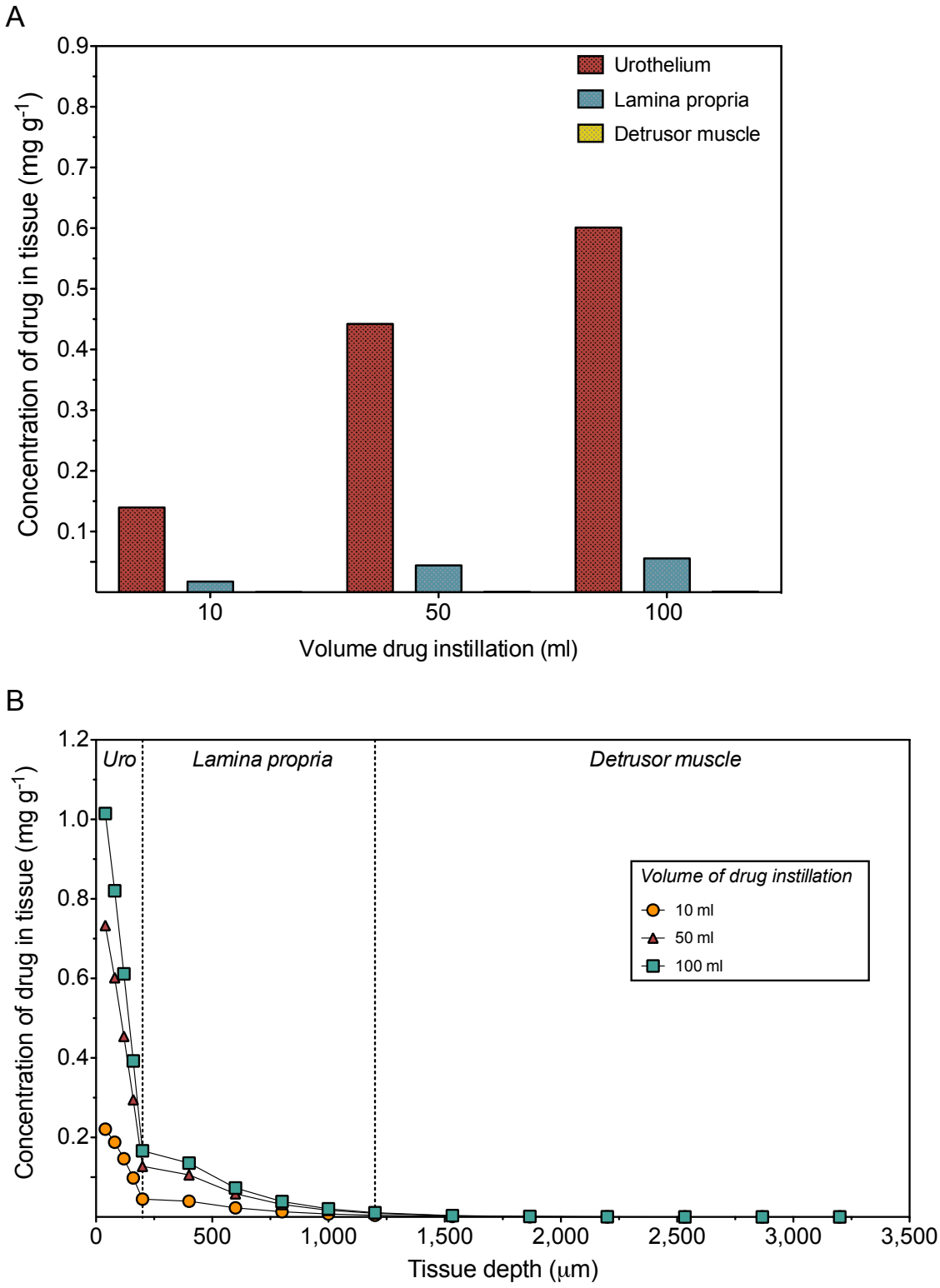

Figure 4.16. Results of PK model simulations showing average drug concentrations in the different layers of the bladder wall (A) and full concentration - depth profiles (B) following 60 min intravesical instillation with different volumes of instilled drug solution (10 - 100 ml).

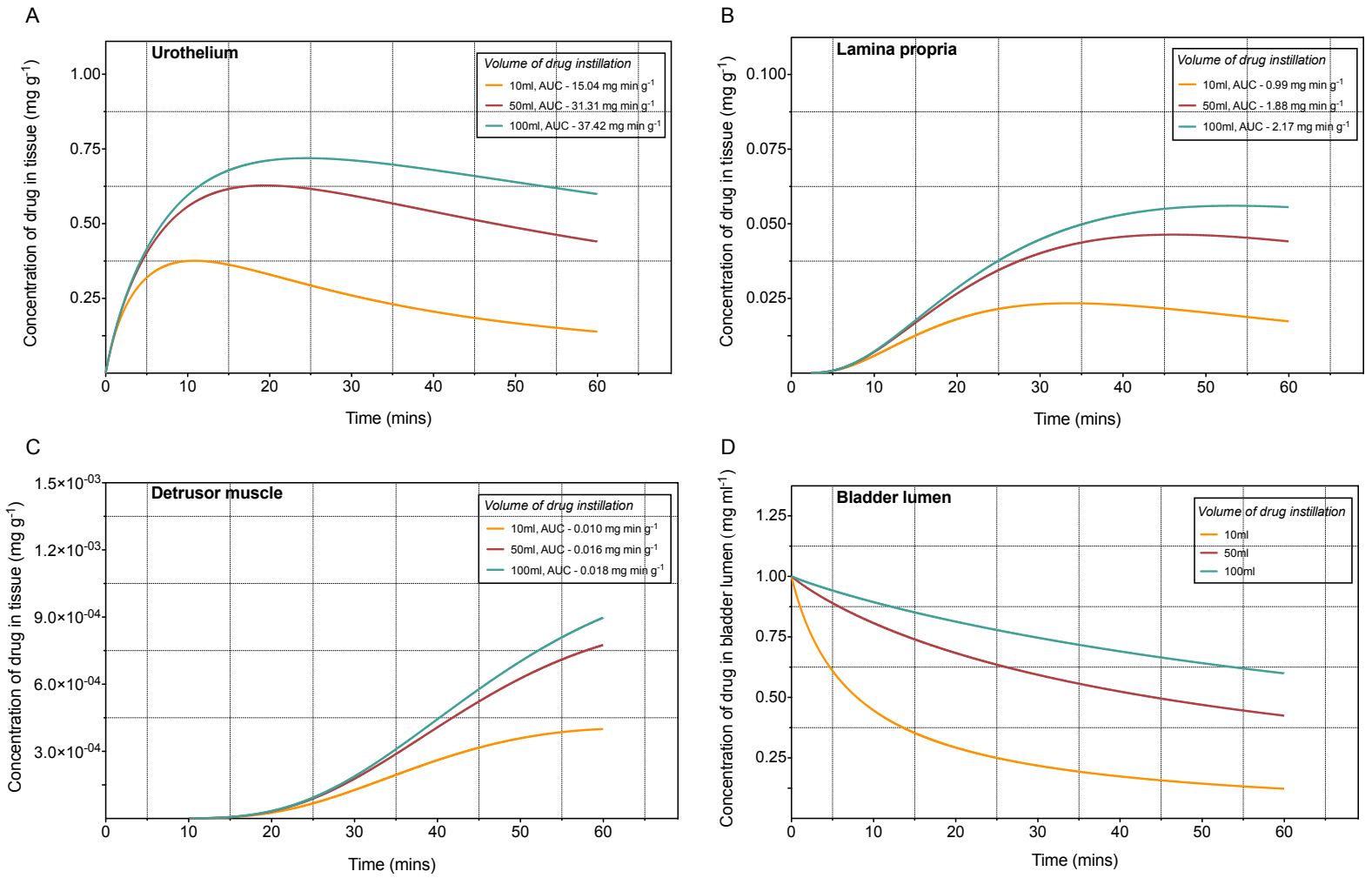

Figure 4.17. Results of PK model simulations showing average drug concentrations in the urothelium (A), lamina propria (B), detrusor muscle (C), and bladder lumen (D) over the course of a 60 min intravesical instillation with different volumes of drug solution (10 - 100 ml).

4.3.2.3.a. Solving the ideal volume of intravesical instillation

It follows that for any given urine production rate, micturition threshold and suggested intravesical treatment length, there must be an ideal volume of drug instillation for the drug in question (V_{Ideal}) that maximises the concentration of drug achieved in the bladder wall. A volume below V_{Ideal} will result in excessive dilution of the luminal drug concentration (Figure 4.17D), whilst a volume above V_{Ideal} will result in the micturition threshold being reached prematurely. V_{Ideal} would be independent of drug concentration and apply to any concentration of a drug as long as urine production rate, micturition threshold and intravesical treatment length are fixed. V_{Ideal} was investigated by calculating urothelium – drug exposure (AUC) over the instillation period. The AUC was then plotted against volume of drug instillation to illicit V_{Ideal} (Figure 4.18). V_{Ideal} was investigated for a 1 h and 2 h intravesical regimen (Table 4.11, Figure 4.18). All other model inputs were consistent with table 4.8.

Maximising urothelium drug exposure can be described as 'instillation time limiting' or 'micturition threshold limiting'. PK simulations demonstrated that, regardless of the concentration of drug instilled, a V_{Ideal} of 140 ml and 87.5 ml was predicted for the 1 h and 2 h regimens respectively (Figure 4.18). In the case of the 1 h instillation the V_{Ideal} corresponds to the maximum volume of drug that can be instilled when taking into consideration the instillation time and assumed micturition threshold of 200 ml. For the 2 h regimen this was not the case and a V_{Ideal} of 87.5 ml, 7.5 ml greater than the maximum volume of drug that should be instilled following the assumption of the 1 h regimen, was calculated. In this example it is more effective to instil 87.5 ml for a shorter period of time (110 min, AUC = 1,233 mg min g^{-1}) than it is to instil 80 ml for the full 2 h (AUC = 1,228 mg min g^{-1}).

V_{Ideal} is unique to the drug (permeability characteristics), patient (micturition threshold and urine production rate) and regimen (instillation time) under investigation. Figure 4.18 shows that minor changes in the regimen (1 h versus 2 h) lead to significant variation in V_{Ideal}. The concept of there being an optimal volume for a given instillation is not considered in practice, rather the same

volume of drug would be instilled for both regimens. This leads to suboptimal dosing (using a 140 ml instillation for the 2 h regimen results in a 37 % decrease in the AUC achieved (Figure 4.18)) and potentially a reduced therapeutic effect compared to the V_{Ideal} of 87.5 ml. Although calculated based on drug exposure to the urothelium in this example, V_{Ideal} can be calculated based on maximum tissue concentration using the same modelling technique.

Intravesical regimen	
Concentration of drug instillation	1 – 20 mg ml^{-1}
Volume of drug instillation	25 - 200 ml
Instillation time	1 h / 2 h or micturition threshold reached
Urine production rate	1 ml min^{-1}
Dosing pattern	Standard, single instillation
Transurothelial diffusion coefficient, D	1.0 x 10^{-07} cm^2 s^{-1}
Micturition threshold	200 ml

Table 4.11. Overview of the dosing regimen used to investigate V_{Ideal}.

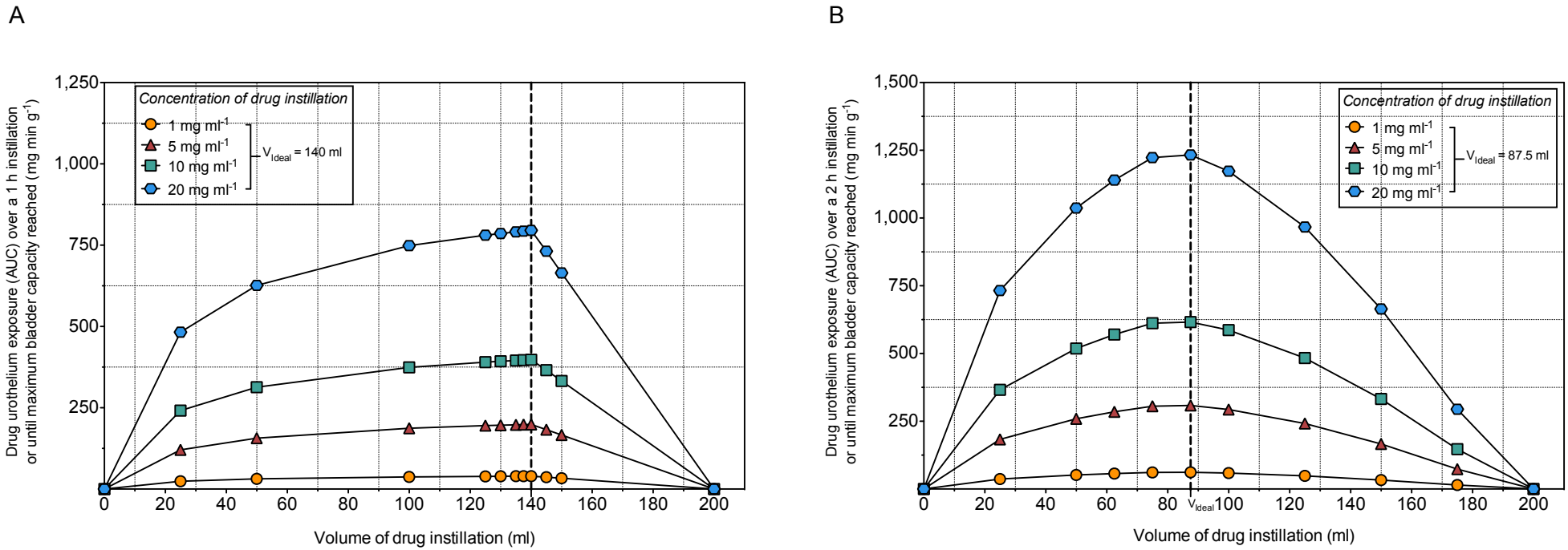

Figure 4.18. Total exposure of urothelium to drug (AUC) for the 1 h (A) and 2 h (B) regimen or at the micturition threshold following instillation with 1, 5, 10 and 20 mg ml^{-1} drug solution (volume of drug instillation varied). For all concentrations of drug instillation the maximum AUC was achieved with an instillation volume of 140 ml and 87.5 ml for the 1 h and 2 h regimens respectively.

4.3.2.4. Instillation time

Instillation time refers to the time difference between the point of instillation and the point at which the instilled dose is voided. Interestingly, regardless of the therapy, recommended instillation times are usually 1 h. The recommended instillation time for MMC is 1 h[53]. Similarly intravesical gemcitabine is retained for 1 h[54] as is intravesical oxybutynin[55,56]. There are examples where instillations are retained for shorter periods of time such as DMSO (30 - 40 min)[57]. Intravesical Bacillus Calmette – Guérin (BCG) is a notable exception with a longer instillation time of 2 h[58]. Based on this information the effect of varying instillation time between 30 and 90 min was investigated. An overview of the intravesical regimen is provided in table 4.12. With the exception of instillation time, all other model inputs are consistent with table 4.8.

Results from PK simulations show that prolonging instillation time increases the bladder wall drug exposure for all tissue layers (Figure 4.20A - C). Owing to the narrow range of realistic instillation times, variations in AUC are not as significant as they are for other variables such as instillation concentration (Section 4.3.2.2, Figure 4.15). Interestingly final drug concentrations in the urothelium and lamina propria are higher after 30 min than they are after 90 min (Figure 4.19A). The prolonged instillation time results in increased dilution of the instilled dose, which in turn means the permeation rate of drug into the urothelium, and hence the lamina propria, is superseded by drug clearance from the bladder wall (tissue concentration - time curve plateaus and declines (Figure 4.20A - B). Although cumulative exposure continues to increase in these layers, drug tissue concentration decreases. This observation is counterintuitive and not something that is considered clinically; patients are often told to hold the instillation for as long as possible. There may be scenarios where a longer instillation time is of no additional clinical benefit. For example if the aim of this intravesical regimen was to reach therapeutic concentrations in the urothelium and the disease - specific IC_{50} for the drug is 0.45 mg g^{-1}, a therapeutic tissue concentration is established after 6 min but is lost by 58 min (Figure 4.21). After this point the concentration of drug in the urothelium is sub - therapeutic and of no clinical benefit. The 60 min instillation is equally as effective as the longer 90 min regimen but is more efficient

(e.g. less clinic time and resources) and less uncomfortable for the patient. This may not be the case for the detrusor muscle where after 90 min drug concentrations are only just beginning to plateau and have not yet started to decline (Figure 4.20C). It is important therefore when designing the length of an instillation to consider the drugs site of action in the bladder wall and the target concentrations desired.

Intravesical regimen	
Concentration of drug instillation	1 mg ml^{-1}
Volume of drug instillation	50 ml
Instillation time	30 - 90 min
Urine production rate	1 ml min^{-1}
Dosing pattern	Standard, single instillation
Transurothelial diffusion coefficient, D	1.0×10^{-07} cm^2 s^{-1}

Table 4.12. Overview of the dosing regimen used to investigate the effect of instillation time.

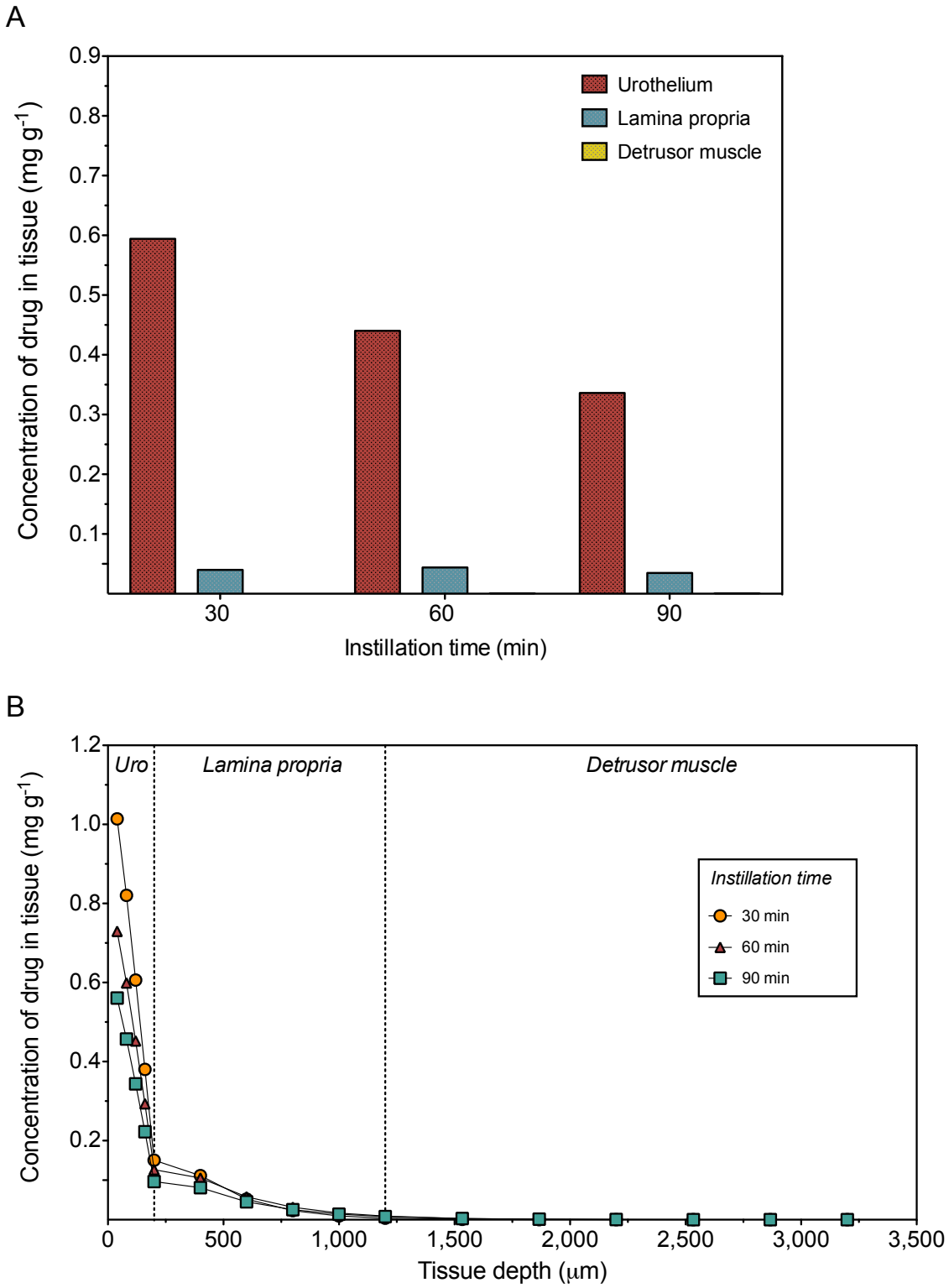

Figure 4.19. Results of PK model simulations showing average drug concentrations in the different layers of the bladder wall (A) and full concentration - depth profiles (B) following 30, 60 and 90 min instillation time.

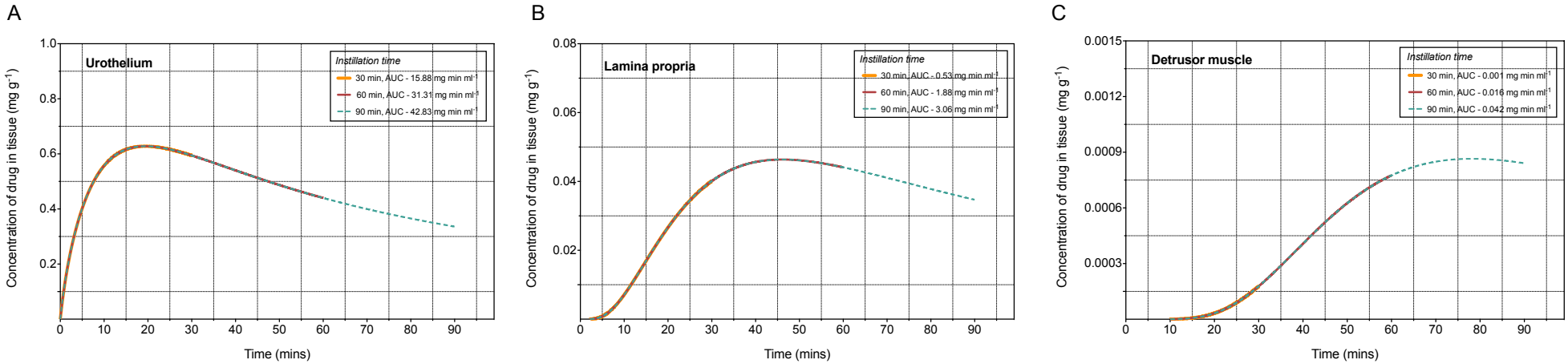

Figure 4.20. Results of PK model simulations showing average drug concentrations in the urothelium (A), lamina propria (B) and detrusor muscle (C) over the course of a 30 (orange), 60 (red) and 90 min (green) instillation.

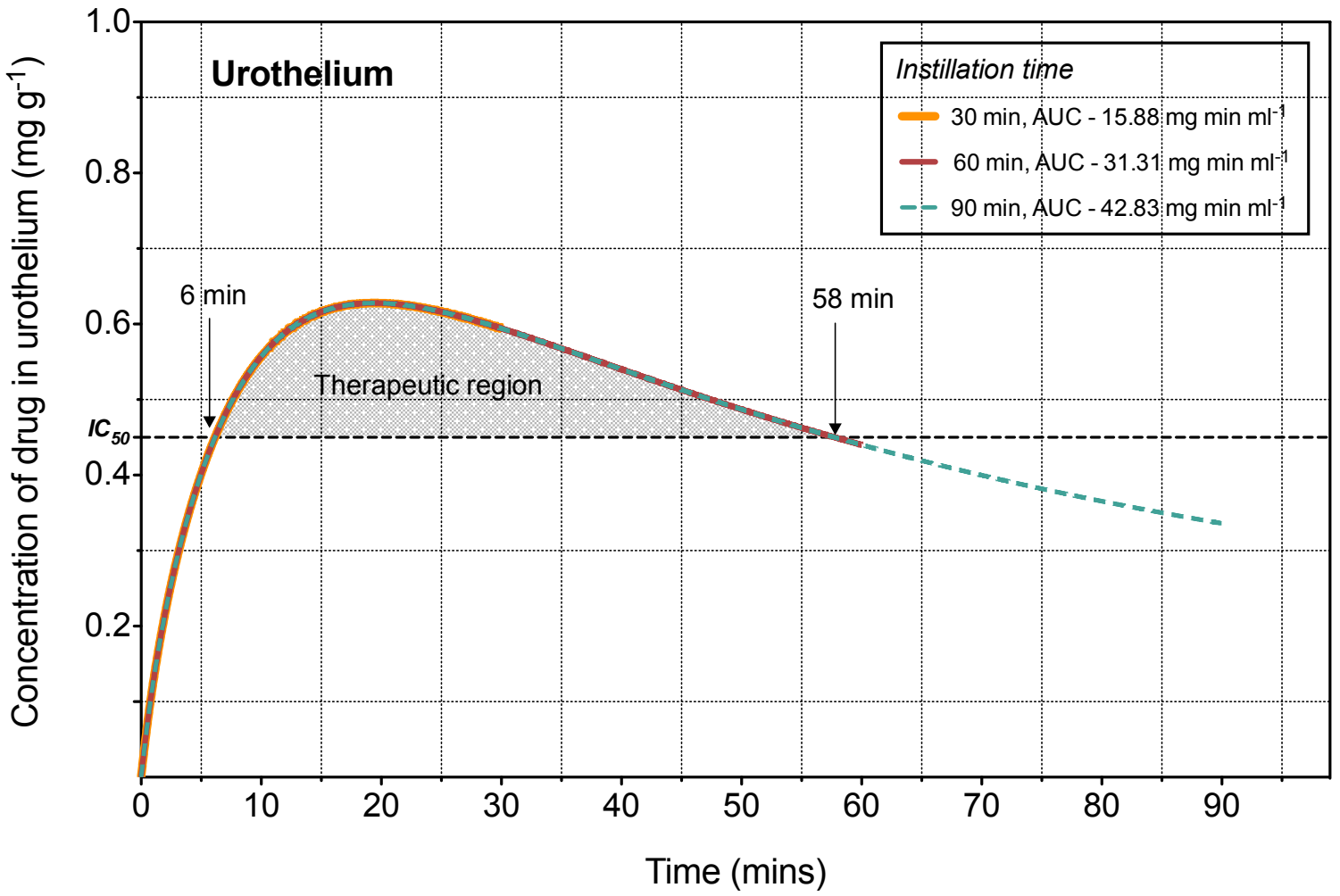

Figure 4.21. Results of PK model simulations showing average drug concentrations in the urothelium over the course of a 30, 60 and 90 min instillation period. Exposure of the urothelium to therapeutic drug concentrations is shaded grey (IC_{50} – 0.45 mg g^{-1}).

4.3.2.5. Urine production rate

A commonly cited limitation of IDD is the continual dilution of the instilled dose by urine[32]. Although often stated as ~ 1 ml min^{-1} [12,59], adult urine production rate varies widely and can be as high as 20 ml min^{-1} [60]. Considering this, a urine production rate range of 1 - 10 ml min^{-1} was investigated. An overview of the intravesical regimen is provided in table 4.13. With the exception of urine production rate, all other model inputs are consistent with table 4.8.

In contrast to other variables such as volume of instillation (Section 4.3.2.3) or instillation time (Section 4.3.2.4), urine production rate is difficult to alter. Some specialist clinics advise patients to fast the morning of their treatment[53] and this has been shown to reduce urine production rate by ~30 %[61]. Additionally a single 200 μg dose of desmopressin 1 h before treatment has been shown to reduce urine production rate by ~50 %[61], although this is not currently recommended.

Figure 4.22B shows that as urine production rate increases, tissue drug concentrations at each depth of the bladder wall decrease. The same is true for bladder tissue drug exposure over the course of the instillation period (Figure 4.23A - C). This results from the decrease in luminal drug concentration caused by urine dilution (Figure 4.23D). Increasing the urine production rate from 1 to 5 ml min^{-1} results in a 64.6 % reduction in AUC for the urothelium (Figure 4.23A) and a 47.7 % reduction in the final tissue concentration achieved at the end of the instillation period (Figure 4.22A). PK predictions confirm the important role that urine production rate plays in the efficacy of IDD.

Intravesical regimen	
Concentration of drug instillation	1 mg ml^{-1}
Volume of drug instillation	50 ml
Instillation time	60 min
Urine production rate	1 - 10 ml min^{-1}
Dosing pattern	Standard, single instillation
Transurothelial diffusion coefficient, D	1.0 x 10^{-07} cm^2 s^{-1}

Table 4.13. Overview of the dosing regimen used to investigate the effect of urine production rate.

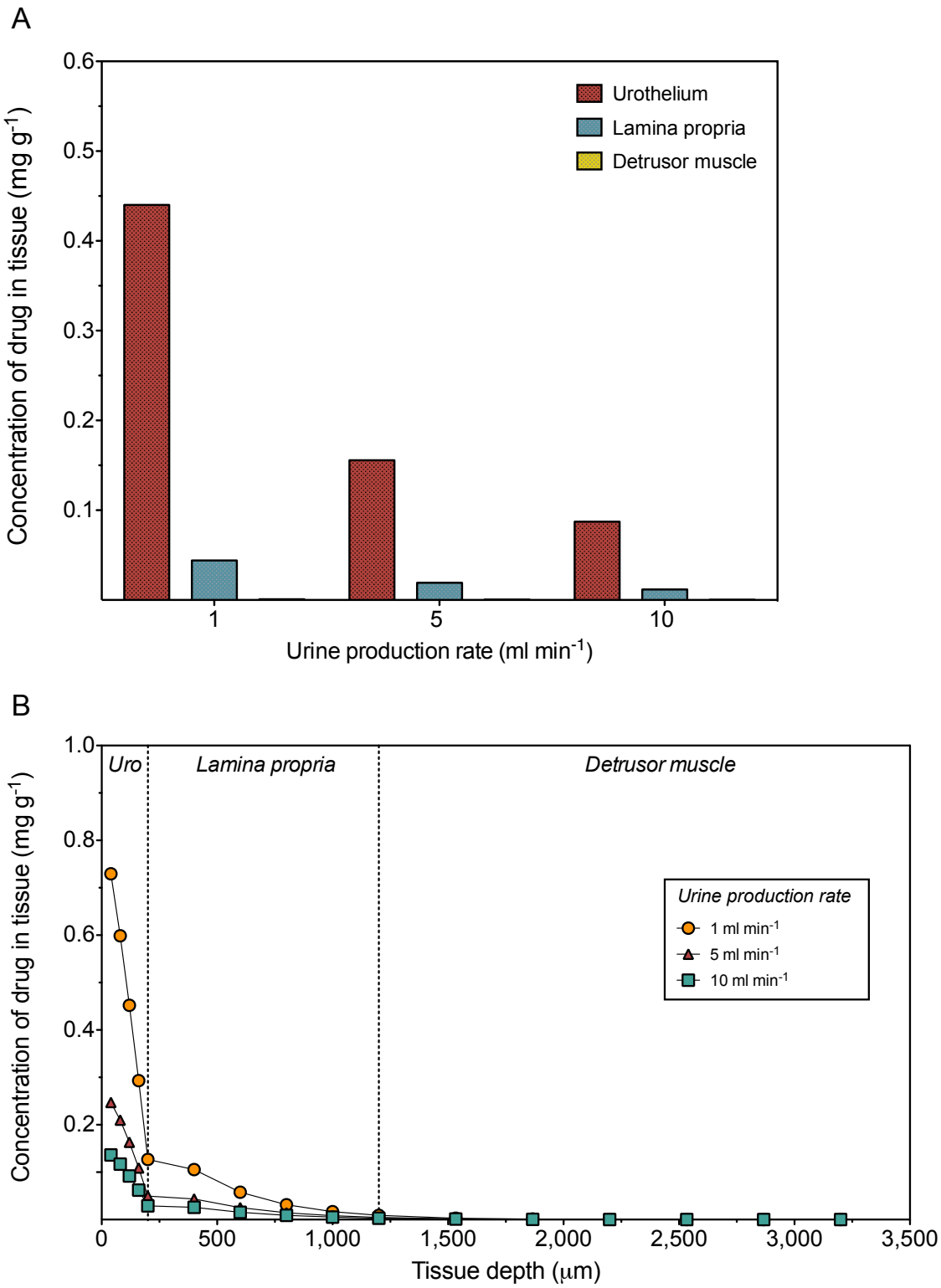

Figure 4.22. Results of PK model simulations showing average drug concentrations in the different layers of the bladder wall (A) and full concentration - depth profiles (B) following 60 min intravesical instillation with a urine production rate of 1, 5 and 10 ml min^{-1}.

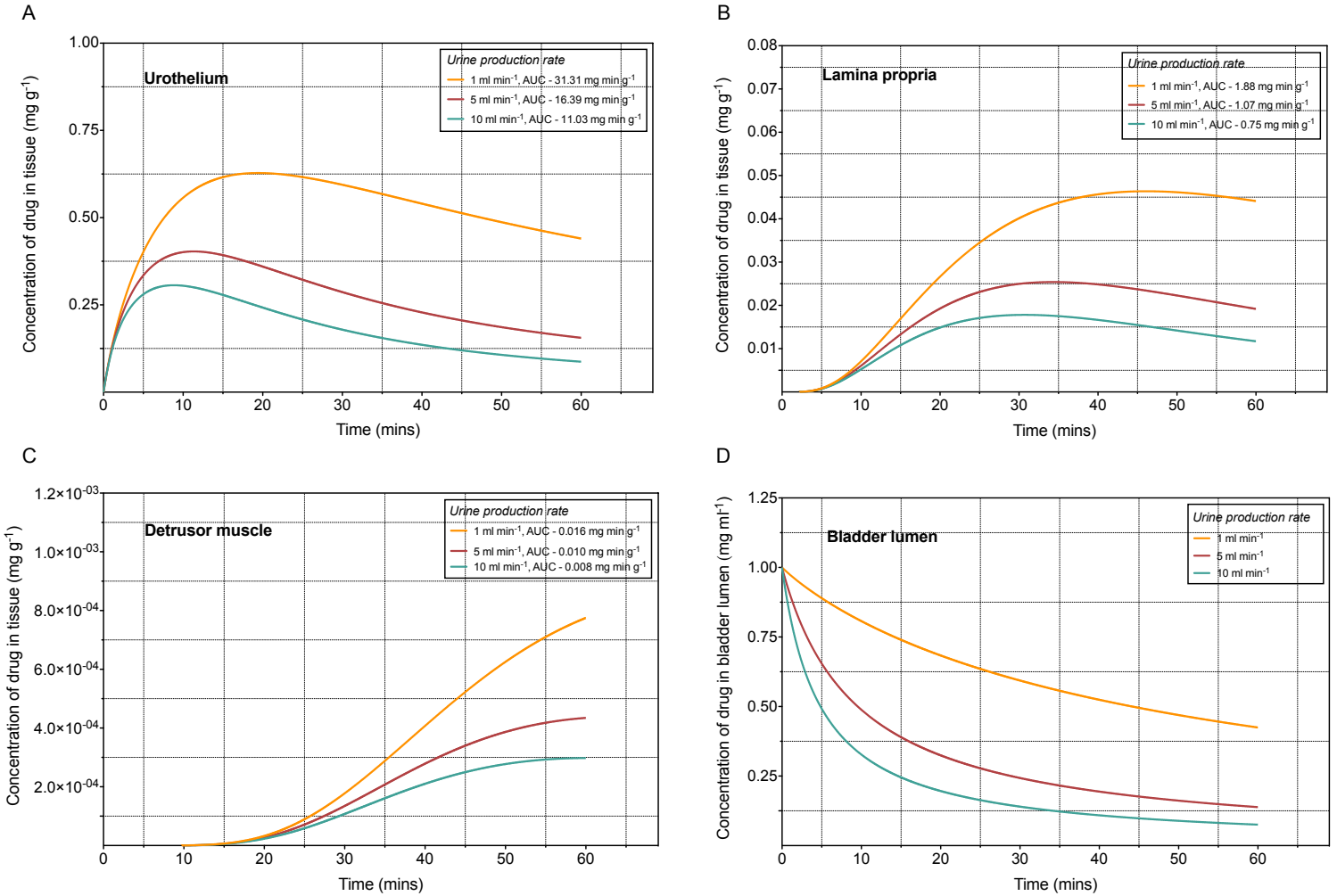

Figure 4.23. Results of PK model simulations showing average drug concentrations in the urothelium (A), lamina propria (B), detrusor muscle (C), and bladder lumen (D) over the course of a 60 min intravesical instillation with a urine production rate of 1, 5 or 10 ml min^{-1}.

4.3.2.6. Dosing regimen: Single versus double dosing

Double dosing is a novel concept that refers to the instillation of a second dose immediately after voiding of the primary dose (Section 4.2.2.5). From a practical standpoint the concept is simple and feasible. The catheter would be left *in situ* after the first instillation and a second pre - prepared dose administered halfway through the treatment regimen following first dose voiding. The catheter is then removed following instillation of the second dose. Double dosing is perhaps most applicable to longer instillation regimens such as the 2 h treatment period used for BCG[62]. Two instillations over the 120 min treatment period (with a 2 min change over period) were compared to a standard single instillation. An overview of the intravesical regimen is provided in table 4.14. With the exception of dosing pattern, all other model inputs are consistent with table 4.8.

Concentration - depth profiles show that the double dosing strategy results in higher drug concentrations throughout the bladder wall at the end of the treatment period (Figure 4.24B). After 60 min, increases in bladder lumen drug concentration (Figure 4.25A) lead to a 27.2 % increase in the overall exposure of the urothelium to drug (Figure 4.25B) and a 66.6 % increase in the final urothelial drug concentration (Figure 4.24A).

Intravesical regimen	
Concentration of drug instillation	1 mg ml^{-1}
Volume of drug instillation	50 ml
Instillation time	120 min
Urine production rate	1 ml min^{-1}
Dosing pattern	Double dosing. Two 60 min instillations over the 120 min treatment period
Transurothelial diffusion coefficient, D	1.0 x 10^{-07} cm^2 s^{-1}

Table 4.14. Overview of the dosing regimen used to investigate the effect of double dosing.

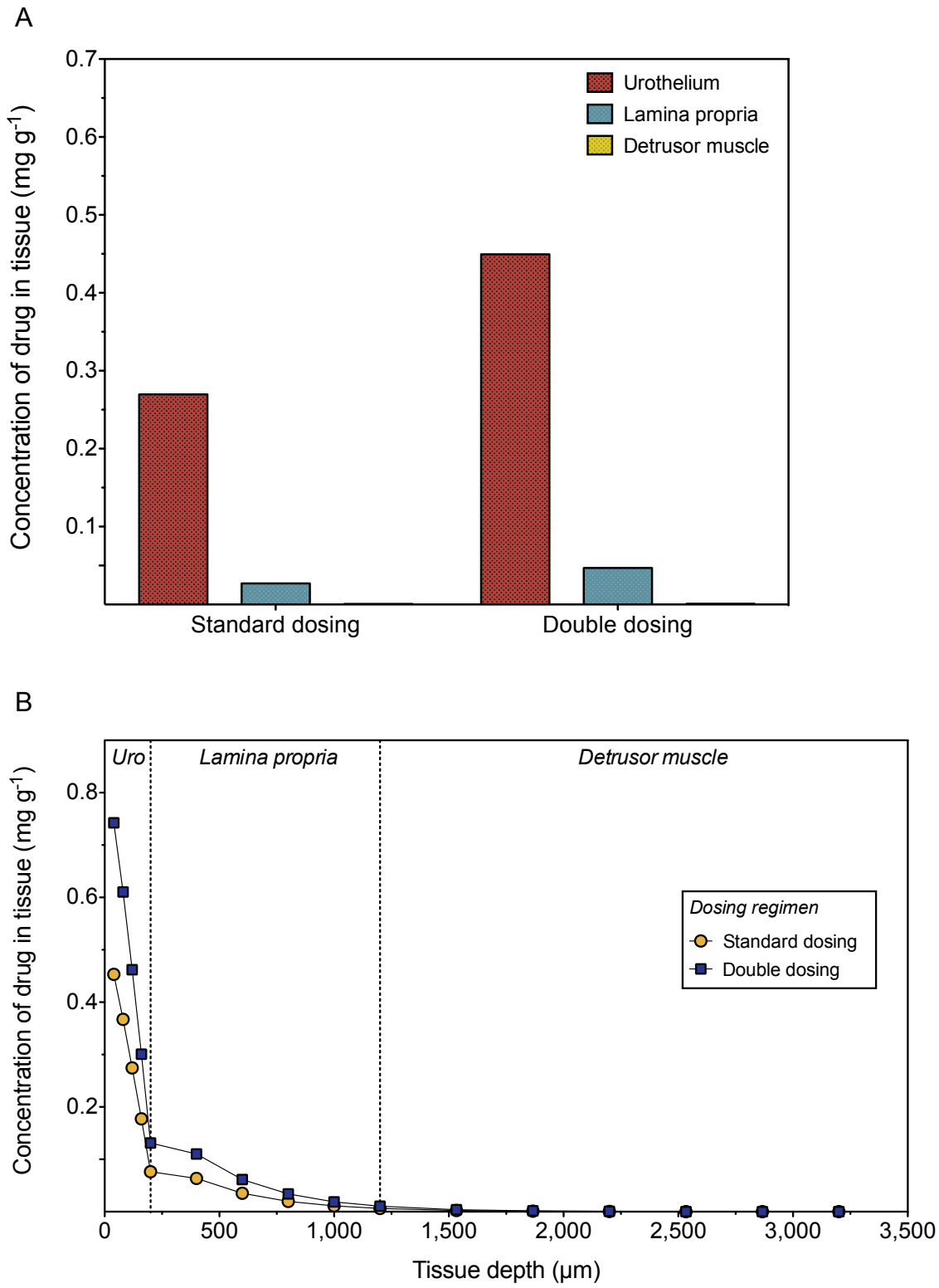

Figure 4.24. Results of PK model simulations showing average drug concentrations in the different layers of the bladder wall (A) and full concentration - depth profiles (B) following a 2 h standard and double dosing regimen.

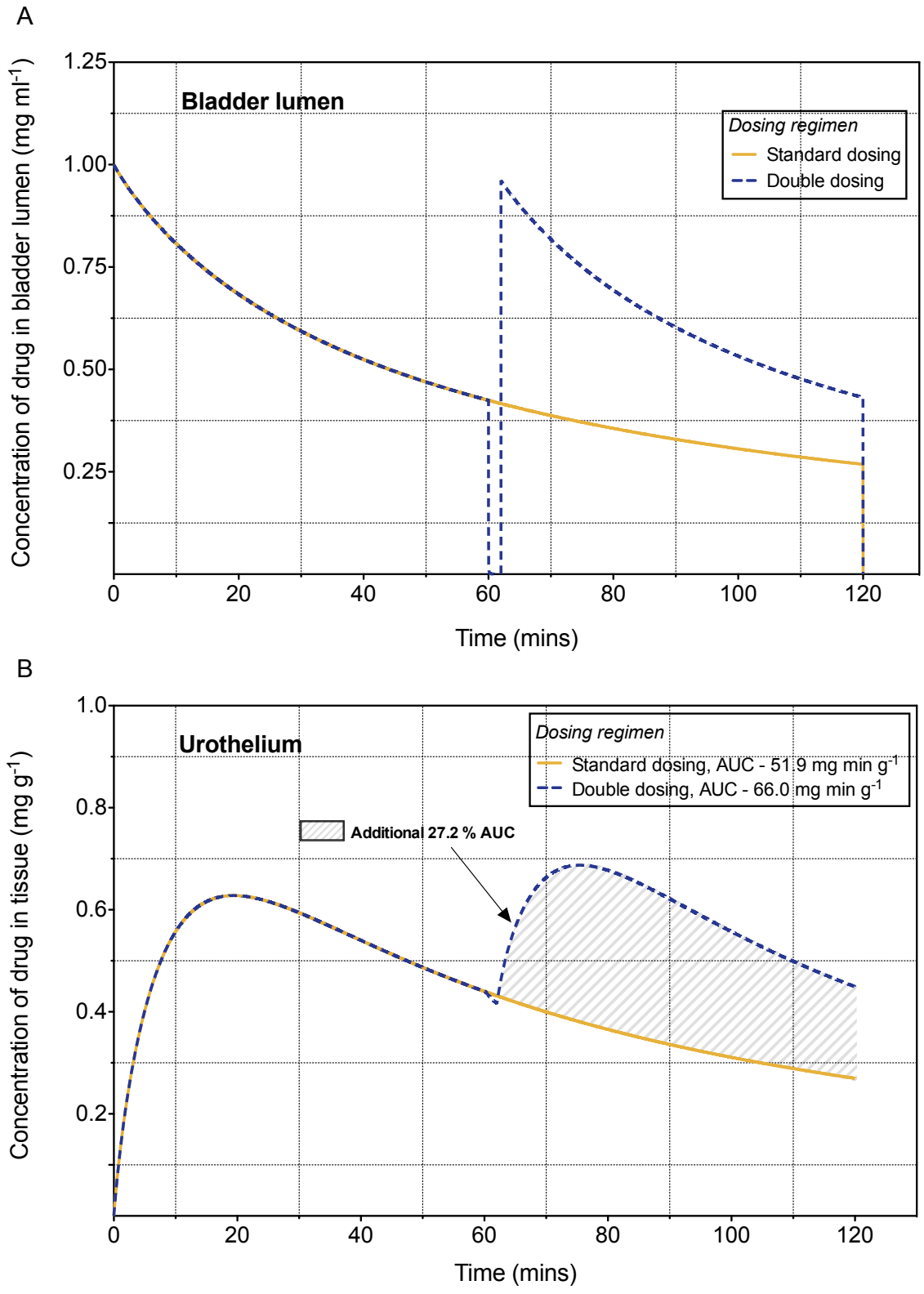

Figure 4.25. Results of PK model simulations showing bladder lumen concentrations (A) and average drug concentrations in the urothelium (B) over the course of a 2 h standard (gold) or double dosing (blue) regimen.

4.3.3. Using the PK model to optimise an IDD regimen

Having investigated the key physiological / clinical variables associated with IDD, the possible advantages such modelling could have in the clinical setting was explored. Using a study sourced from the literature, the PK model was used to optimise an intravesical regimen.

Beiko *et al* conducted a double - blind randomised controlled trial assessing the safety and efficacy of intravesical agents in reducing ureteral stent - related discomfort (SRD) (Section 2.1.1)[63]. One of the drugs investigated was oxybutynin. The reported / estimated parameters of the study and the suggested optimised regimen are listed in table 4.15. Other model inputs such as bladder blood flow rate and drug partition coefficients in the different layers of the bladder wall are reported in table 4.8. These parameters were kept constant between the reported and optimised IDD regimens.

Three adjustments were made; the single 120 min instillation was changed to two 60 min instillations (double dosing); urine production rate was reduced by 30 % from 2 ml min^{-1} to 1.4 ml min^{-1} by asking the patient to fast on the morning of their treatment[61]; finally using V_{Ideal} theory, the volume of instillation was increased from 9 ml to 115 ml. The concentration of drug instillation was not altered.

Increasing the instilled drug volume, reducing urine output and using the double dosing technique resulted in markedly higher luminal drug concentrations throughout the treatment period (Figure 4.26A). As a result the optimised regimen significantly increased oxybutynin concentrations achieved at all depths of the bladder wall (Figure 4.27B). Final drug concentrations in the urothelium, lamina propria and detrusor muscle were increased by 1,967 %, 1,757 % and 1,329 % respectively after instillation of the optimised regimen. Maximum drug concentrations in the urothelium, lamina propria and detrusor muscle were increased by 116 %, 253 % and 307 % (Figure 4.26B - D). Over the treatment period, drug exposure (AUC) of the urothelium, lamina propria and detrusor muscle was greatly increased (Figure 4.26B - D). Changes to the reported intravesical regimen are simple and practically easy to implement. The treatment

duration was not altered, neither was the formulation or concentration of the instilled drug solution. Requesting patients to abstain from fluids (and omitting diuretic doses if applicable) is already recommended by some clinics[64]. The optimisation of the regimen reported by Beiko *et al* is a good example of the flexibility and potential usefulness of the PK model. It also serves to highlight the empirical nature of IDD regimen design to date. Improving the design of IDD regimens by implementing changes highlighted by the model should lead to improved clinical outcomes and importantly maximise the potential of this delivery route.

	Regimen reported by Beiko *et al*	Regimen optimised using PK model
Concentration of drug instillation	1.1 mg ml^{-1}, reported	1.1 mg ml^{-1}, reported
Volume of drug instillation	9 ml, reported	115 ml, calculated as V_{Ideal}
Instillation time	120 min, rounded from a reported 117.8 min	120 min, rounded from a reported 117.8 min
Urine production rate	2 ml min^{-1}, estimated from reported voided volumes	1.4 ml min^{-1}, 30 % reduction achieved by morning fasting
Dosing pattern	One single 9 ml instillation over the treatment period	Two 115 ml instillations over the treatment period
Transurothelial diffusion coefficient, D	2.72 x 10^{-07} cm^2 s^{-1}, determined *ex vivo* (Table 4.6)	2.72 x 10^{-07} cm^2 s^{-1}, determined *ex vivo* (Table 4.6)

Table 4.15. Intravesical parameters used to compare the original and optimised oxybutynin instillation reported by Beiko *et al*[63].

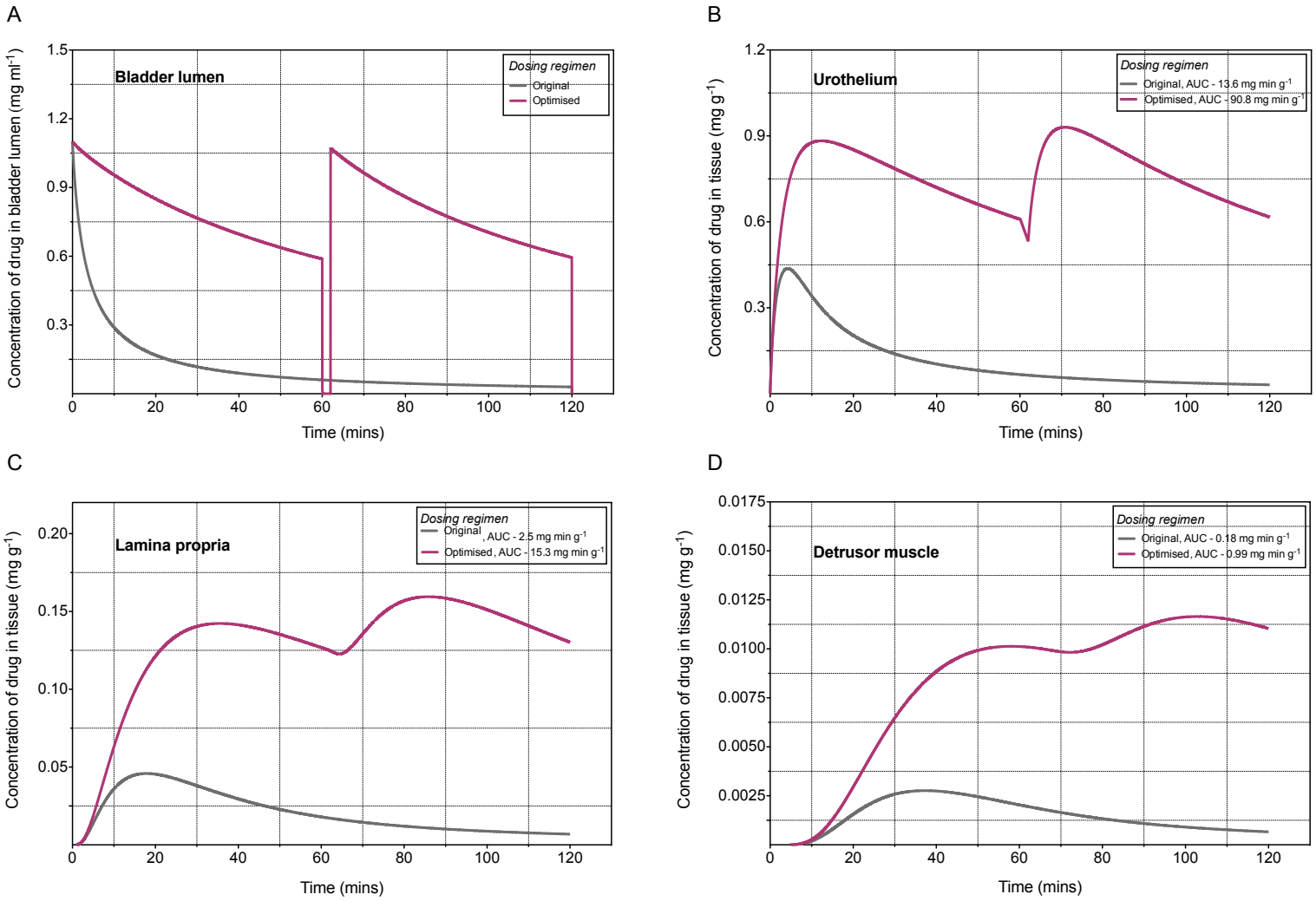

Figure 4.26. Results of PK model simulations showing average drug concentrations in the bladder lumen (A), urothelium (B), lamina propria (C), and detrusor muscle (D) over the course of a 2 h instillation with the original (grey) and optimised (pink) intravesical regimen.

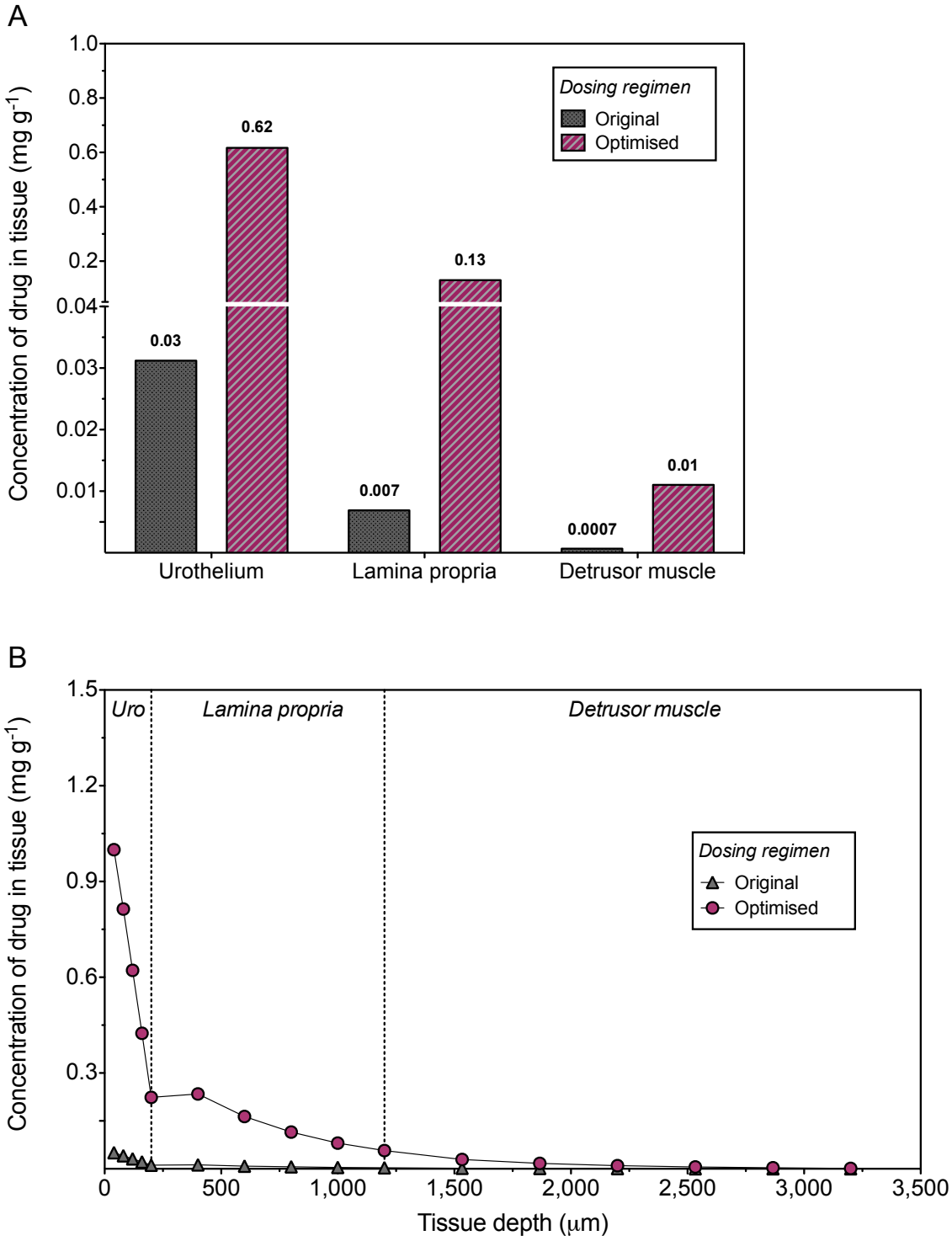

Figure 4.27. Results of PK model simulations showing average drug concentrations in the different layers of the bladder wall (A) and full concentration - depth profiles (B) following a 2 h instillation with the original (grey) and optimised (pink) IDD regimen.

4.4. Conclusions

A PK model of IDD has been developed. The model is highly flexible, allowing key variables to be altered in order to explore their role in the IDD process. Novel modelling techniques and dosing concepts such as V_{Ideal} and double dosing have been identified and their usefulness investigated. Additionally, counterintuitive realisations, such as the marginal benefits associated with extending instillation time, have been elicited. The model has many potential applications including but not limited to the design of future IDD regimens and the optimisation of existing ones and may be valuable to investigators wishing to explore different permutations of IDD dosing regimens in the future.

4.5. Reference List

1. iSEESYSTEMS. Frequently asked questions about STELLA [Internet]. iSEE systems. 2013 [cited 2013 Oct 25]. Available from: http://www.iseesystems.com/community/support/FAQs.aspx#0

2. Washington C, Washington N, Wilson CG. Pharmacokinetic modelling using Stella on the Apple Macintosh. 1st ed. New York: Ellis. Horwood; 1990. 115 p.

3. Salem AH, Noreddin AM. Moxifloxacin in lower respiratory tract infections: in silico simulation of different bacterial resistance and drug exposure scenarios. J Chemother. 2014 Apr;26(2):80–5.

4. Kambayashi A, Blume H, Dressman J. Understanding the in vivo performance of enteric coated tablets using an in vitro-in silico-in vivo approach: Case example diclofenac. Eur J Pharm Biopharm. 2013 Nov;85(3 Pt B):1337–47.

5. Ranta V-P, Laavola M, Toropainen E, Vellonen K-S, Talvitie A, Urtti A. Ocular pharmacokinetic modeling using corneal absorption and desorption rates from in vitro permeation experiments with cultured corneal epithelial cells. Pharm Res. 2003 Sep;20(9):1409–16.

6. Grass GM, Lee VH. A model to predict aqueous humor and plasma pharmacokinetics of ocularly applied drugs. Invest Ophthalmol Vis Sci. 1993 Jun;34(7):2251–9.

7. Anissimov YG, Roberts MS. Modelling dermal drug distribution after topical application in human. Pharm Res. 2011 Sep;28(9):2119–29.

8. Tortora GJ, Derrickson BH. Principles of Anatomy and Physiology. 12th ed. John Wiley & Sons; 2008.

9. Hakenberg OW, Linne C, Manseck A, Wirth MP. Bladder wall thickness in normal adults and men with mild lower urinary tract symptoms and benign prostatic enlargement. Neurourol Urodyn. 2000;19(5):585–93.

10. Miodoński AJ, Litwin JA. Microvascular architecture of the human urinary bladder wall: a corrosion casting study. Anat Rec. 1999 Mar;254(3):375–81.

11. Kershen RT, Azadzoi KM, Siroky MB. Blood flow, pressure and compliance in the male human bladder. J Urol. 2002 Jul;168(1):121–5.

12. Helms JR. Urinalysis and Renal Clearance. Mathematics for Medical and Clinical Laboratory Professionals. 1st ed. Cengage Learning; 2008. p. 193–202.

13. Lee M. Basic Skills in Interpreting Laboratory Data, 5th edition. ASHP; 2013. 1124 p.

14. Shenot PJ. Urinary retention [Internet]. Merck manual online. 2013. Available from: http://www.merckmanuals.com/professional/genitourinary_disorders/voiding_disorders/urinary_retention.html

15. Kelly CE. Evaluation of Voiding Dysfunction and Measurement of Bladder Volume. Rev Urol. 2004;6(Suppl 1):S32–7.

16. Milleman M, Langenstroer P, Guralnick ML. Post-void residual urine volume in women with overactive bladder symptoms. J Urol. 2004 Nov;172(5 Pt 1):1911–4.

17. Mombelli G, Picozzi S, Messina G, Truffelli D, Marenghi C, Maffi G, et al. Free uroflowmetry versus "Do-It-Yourself" uroflowmetry in the assessment of patients with lower urinary tract symptoms. Int Urol Nephrol. 2014 May 18;

18. Au JL-S, Badalament RA, Wientjes MG, Young DC, Warner JA, Venema PL, et al. Methods to Improve Efficacy of Intravesical Mitomycin C: Results of a Randomized Phase III Trial. J Natl Cancer Inst. 2001 Apr 18;93(8):597–604.

19. Wientjes MG, Badalament RA, Au JL. Use of pharmacologic data and computer simulations to design an efficacy trial of intravesical mitomycin C therapy for superficial bladder cancer. Cancer Chemother Pharmacol. 1993;32(4):255–62.

20. Dalton JT, Wientjes MG, Badalament RA, Drago JR, Au JLS. Pharmacokinetics of intravesical mitomycin C in superficial bladder cancer patients. Cancer Res. 1991;51(19):5144.

21. Wientjes MG, Badalament RA, Wang RC, Hassan F, Au JL. Penetration of mitomycin C in human bladder. Cancer Res. 1993;53(14):3314.

22. Grabnar I, Bogataj M, Belic A, Logar V, Karba R, Mrhar A. Kinetic model of drug distribution in the urinary bladder wall following intravesical instillation. Int J Pharm. 2006 Sep 28;322(1-2):52–9.

23. Anissimov YG. Mathematical models for skin toxicology. Expert Opin Drug Metab Toxicol. 2014 Apr;10(4):551–60.

24. Roberts MS, Anissimov YG. Modeling of hepatic elimination and organ distribution kinetics with the extended convection-dispersion model. J Pharmacokinet Biopharm. 1999 Aug;27(4):343–82.

25. Anissimov YG, Roberts MS. Diffusion modeling of percutaneous absorption kinetics. 1. Effects of flow rate, receptor sampling rate, and viable epidermal resistance for a constant donor concentration. J Pharm Sci. 1999 Nov;88(11):1201–9.

26. Anissimov YG, Jepps OG, Dancik Y, Roberts MS. Mathematical and pharmacokinetic modelling of epidermal and dermal transport processes. Adv Drug Deliv Rev. 2013 Feb;65(2):169–90.

27. Yuri G. Anissimov. Mathematical Models for Different Exposure Conditions. Dermal Absorption and Toxicity Assessment [Internet]. Informa Healthcare; 2007 [cited 2015 Feb 20]. p. 271–86. Available from: http://informahealthcare.com/doi/abs/10.3109/9780849375927.014

28. Chalana V, Dudycha S, Yuk J-T, McMorrow G. Automatic Measurement of Ultrasound-Estimated Bladder Weight (UEBW) from Three-Dimensional Ultrasound. Rev Urol. 2005;7(Suppl 6):S22–8.

29. Williams NA, Bowen JL, Al-Jayyoussi G, Gumbleton M, Allender CJ, Li J, et al. An ex vivo investigation into the transurothelial permeability and bladder wall

distribution of the nonsteroidal anti-inflammatory ketorolac. Mol Pharm. 2014 Mar 3;11(3):673–82.

30. Oelke M, Höfner K, Jonas U, Ubbink D, de la Rosette J, Wijkstra H. Ultrasound measurement of detrusor wall thickness in healthy adults. Neurourol Urodyn. 2006;25(4):308–17; discussion 318.

31. Kanyilmaz S, Calis FA, Cinar Y, Akkoc Y. Bladder wall thickness and ultrasound estimated bladder weight in healthy adults with portative ultrasound device. J Res Med Sci. 2013 Feb;18(2):103–6.

32. GuhaSarkar S, Banerjee R. Intravesical drug delivery: Challenges, current status, opportunities and novel strategies. J Controlled Release. 2010 Dec 1;148(2):147–59.

33. Fick A. Über diffusion. Ann Phys. 1855;94(1):59–86.

34. Grabnar I, Bogataj M, Mrhar A. Influence of chitosan and polycarbophil on permeation of a model hydrophilic drug into the urinary bladder wall. Int J Pharm. 2003;256(1-2):167–73.

35. Williams N, Allender C, Bowen J, Gumbleton M, Joshi H, Harrah T, et al. An ex vivo investigation into the viability of delivering α-blockers locally for ureteral stent-related discomfort. J Urol. 2013 Apr;189(4):Supplement Page e850.

36. Williams NA, Lee KM, Bowen JL, Gumbleton M, Allender CJ, Harrah T, et al. Investigating detrusor muscle concentrations of oxybutynin after intravesical delivery in an ex vivo porcine model. J Pharm Sci. 2015 Apr;

37. Walker BE. Electron microscopic observations on transitional epithelium of the mouse urinary bladder. J Ultrastruct Res. 1960 Jun;3(4):345–61.

38. Peter S. The junctional connections between the cells of the urinary bladder in the rat. Cell Tissue Res. 1978;187(3):439–48.

39. Lewis SA, Eaton DC, Diamond JM. The mechanism of Na+ transport by rabbit urinary bladder. J Membr Biol. 1976 Aug 27;28(1):41–70.

40. Weintraub MD, Li QQ, Agarwal PK. Advances in intravesical therapy for the treatment of non-muscle invasive bladder cancer (Review). Mol Clin Oncol. 2014 Sep;2(5):656–60.

41. Lin JH, Lu AY. Role of pharmacokinetics and metabolism in drug discovery and development. Pharmacol Rev. 1997 Dec;49(4):403–49.

42. Dennis M. Absorption processes. In: Sammes P, Talor J, editors. Comprehensive medicinal chemistry. Oxford, UK: Pergamon; 1990. p. 1–44.

43. Ho PL, Williams SB, Kamat AM. Immune therapies in non-muscle invasive bladder cancer. Curr Treat Options Oncol. 2015 Feb;16(2):315.

44. Shelley MD, Mason MD, Kynaston H. Intravesical therapy for superficial bladder cancer: a systematic review of randomised trials and meta-analyses. Cancer Treat Rev. 2010 May;36(3):195–205.

45. Lose G, Nørgaard JP. Intravesical oxybutynin for treating incontinence resulting from an overactive detrusor. BJU Int. 2001 Jun;87(9):767–73.

46. Van Nieuwkoop C, den Exter PL, Elzevier HW, den Hartigh J, van Dissel JT. Intravesical gentamicin for recurrent urinary tract infection in patients with intermittent bladder catheterisation. Int J Antimicrob Agents. 2010 Dec;36(6):485–90.

47. Di Stasi SM, Giannantoni A, Vespasiani G, Navarra P, Capelli G, Massoud R, et al. Intravesical electromotive administration of oxybutynin in patients with detrusor hyperreflexia unresponsive to standard anticholinergic regimens. J Urol. 2001;165(2):491–8.

48. Krause P, Fuhr U, Schnitker J, Albrecht U, Stein R, Rubenwolf P. Pharmacokinetics of intravesical versus oral oxybutynin in healthy adults: results of an open label, randomized, prospective clinical study. J Urol. 2013 Nov;190(5):1791–7.

49. Kuroda M, Niijima T, Kotake T, Akaza H, Hinotsu S, 6th Trial of the Japanese Urological Cancer Research Group. Effect of prophylactic treatment with intravesical epirubicin on recurrence of superficial bladder cancer - The 6th

Trial of the Japanese Urological Cancer Research Group (JUCRG): a randomized trial of intravesical epirubicin at dose of 20mg/40ml, 30mg/40ml, 40mg/40ml. Eur Urol. 2004 May;45(5):600–5.

50. Oosterlinck W, Kirkali Z, Sylvester R, da Silva FC, Busch C, Algaba F, et al. Sequential intravesical chemoimmunotherapy with mitomycin C and bacillus Calmette-Guérin and with bacillus Calmette-Guérin alone in patients with carcinoma in situ of the urinary bladder: results of an EORTC genito-urinary group randomized phase 2 trial (30993). Eur Urol. 2011 Mar;59(3):438–46.

51. Mizunaga M, Miyata M, Kaneko S, Yachiku S, Chiba K. Intravesical instillation of oxybutynin hydrochloride therapy for patients with a neuropathic bladder. Paraplegia. 1994 Jan;32(1):25–9.

52. Apostolidis A, Gonzales GE, Fowler CJ. Effect of intravesical resiniferatoxin (RTX) on lower urinary tract symptoms, urodynamic parameters, and quality of life of patients with urodynamic increased bladder sensation. Eur Urol. 2006;50(6):1299–305.

53. Thiruchelvam N. Intravesical mitomycin C chemotherapy: patient information [Internet]. Addenbrooke's hospital, Intravesical mitomycin C chemotherapy: procedure-specific information. 2014. Available from: http://www.cuh.org.uk/sites/default/files/publications/PIN2048_intravesical_chemotherapy_Mitomycin.pdf

54. Witjes JA, van der Heijden AG, Vriesema JLJ, Peters GJ, Laan A, Schalken JA. Intravesical gemcitabine: a phase 1 and pharmacokinetic study. Eur Urol. 2004 Feb;45(2):182–6.

55. Mizunaga M, Miyata M, Kaneko S, Taniguchi N, Yachiku S, Chiba K, et al. Intravesical oxybutynin hydrochloride in the treatment of urge incontinence in the elderly. Nihon Hinyōkika Gakkai Zasshi. 1996 Jun;87(6):923–7.

56. Singh G, Thomas DG. Intravesical oxybutynin in patients with posterior rhizotomies and sacral anterior root stimulators. Neurourol Urodyn. 1995;14(1):65–71.

57. Thiruchelvam N. Intravesical DMSO: patient information [Internet]. Addenbrooke's hospital, Intravesical DMSO: procedure-specific information. 2014. Available from: http://www.cuh.org.uk/sites/default/files/publications/PIN2051_intravesical_instillation_of_DMSO.pdf

58. Thiruchelvam N. Intravesical immunotherapy: patient information [Internet]. Addenbrooke's hospital, Intravesical immunotherapy: procedure-specific information. 2014. Available from: http://www.cuh.org.uk/sites/default/files/publications/PIN2049_intravesical_immunotherapy.pdf

59. Hankins J, Intravenous Nurses Society. Intravenous therapy: clinical principles and practice. Philadelphia: Saunders; 1995.

60. Fallis WM. Indwelling Foley Catheters Is the Current Design a Source of Erroneous Measurement of Urine Output? Crit Care Nurse. 2005 Apr 1;25(2):44–51.

61. Cliff AM, Heatherwick B, Scoble J, Parr NJ. The effect of fasting or desmopressin before treatment on the concentration of mitomycin C during intravesical administration. BJU Int. 2000;86(6):644–7.

62. Alliance Pharmaceuticals Ltd. SPC: ImmuCyst® 81mg powder for intravesical suspension [Internet]. 2014 [cited 2015 Mar 1]. Available from: https://www.medicines.org.uk/emc/medicine/7779

63. Beiko D, Watterson J, Knudsen B, others. A double-blinded prospective randomized controlled trial assessing the safety and efficacy of intravesical agents for ureteral stent symptoms following extracorporeal shockwave lithotripsy. J Endourol. 2004;18(8):723–30.

64. Australia and New Zealand Urological Nurses Society. Clinical Guidelines: Instillation of Intravesical Solutions [Internet]. White T, editor. 2012 [cited 2015 Mar 3]. Available from: http://www.anzuns.org/wp-content/uploads/2011/12/ANZUNS-Clinical-Guidelines-Intravesical-Instillations-20121.pdf

Chapter Five: Comparison of Upper and Lower Urinary Tract Permeability to Mitomycin C

5.1. Introduction

Urothelial carcinoma is the fourth most common tumour type and can occur in the lower (bladder) or upper (ureter and kidney) urinary tract[1–3]. Bladder cancer accounts for 90 – 95 % of all urothelial carcinomas[1–3], whilst those originating in the upper urinary tract (UTUC) represent 5 – 10 %[4,5]. Although rare, the incidence of UTUC has increased over the last three decades and now stands at ~ 2 cases per 100,000 person - years[6]. Owing to restricted symptomology, disease is commonly advanced at diagnosis. Consequently prognosis is poor with an overall 5 - year survival rate of < 50 %[7]. Although the urinary tract is lined by one continuous urothelium, UTUC exhibit a different pathology to urothelial carcinoma of the bladder; most importantly UTUC are significantly more aggressive and invasive[8].

Regardless of tumour location, European Association of Urology (EAU) guidelines state the gold standard treatment for UTUC is radical nephroureterectomy (RNU), that is surgical removal of the kidney and ureter[3]. For certain patients, endoscopic management has emerged as a new treatment option and in 2009 it accounted for > 10 % of all UTUC surgical interventions in England[7]. This conservative approach allows preservation of the kidney, whilst sparing the patient the complications and morbidity associated with major surgery[3]. Endoscopic cases fall into two distinct groups; those for whom endoscopic treatment is imperative and those for which it is elective. Imperative indications include renal insufficiency, solitary kidney, bilateral UTUC and those patients for whom major surgery is unsuitable[3,8,9]. Elective indications are stringent (Figure 5.1) and are limited to highly specific, low - grade tumours in patients whose contralateral kidney is functioning normally[3].

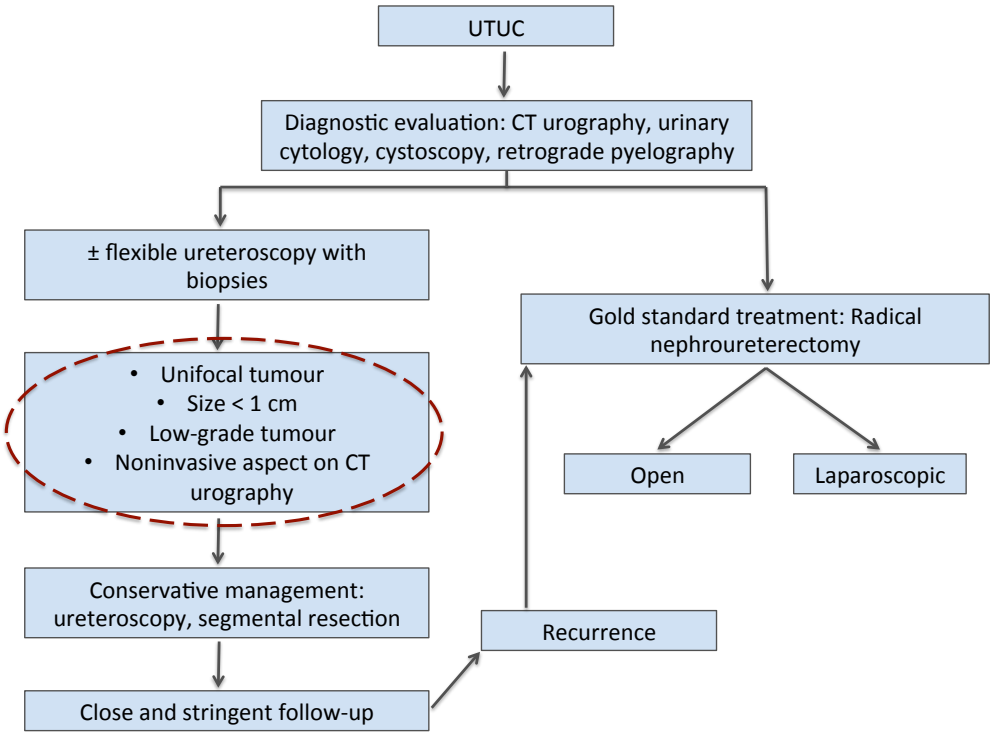

Figure 5.1. Overview of the EAU UTUC treatment pathway[3]. Strict tumour characteristics must be met for an elective endoscopic approach to be considered (circled red).

Although no randomised controlled trials comparing endoscopic management with RNU have been performed, a systematic review of oncological outcomes suggested that, for specific favourable low - grade UTUC elective cases, endoscopic management can yield effective oncological control and renal preservation[9]. This is supported by comparable 5 - year disease specific survival between immediate RNU and endoscopic management[9,10]. Unfortunately these benefits come at the expense of unfavourable tumour progression and recurrence[9], with one study reporting recurrence in 68 % of the cohort[10].

It has been proposed that recurrence after endoscopic management may be reduced by post - operative, adjuvant topical administration of chemotherapeutic agents such as mitomycin C (MMC)[10–13] or Bacillus Calmette - Guérin (BCG)[14–18]. The rationale behind this stems from the established efficacy of these agents in the management of bladder cancer[19,20]. There are three main techniques used to deliver drugs to the upper urinary tract: Firstly, drug can be delivered in an antegrade fashion percutaneously via a nephrostomy tube. This delivery method is often used following percutaneous resection when access is already available. Secondly, drug can be administered in a retrograde manner using an open - ended ureteric catheter; this technique is favoured after ureteroscopic ablation[3,9]. Thirdly, although less - common, drug can be administered intravesically through an indwelling double - J stent. This technique relies on vesicoureteral reflux of the drug solution from the bladder up into the ureter and renal pelvis[21]. The renal pelvis is the central, hollow structure of the kidney where urine collects prior to passage down the ureter (Figure 5.2).

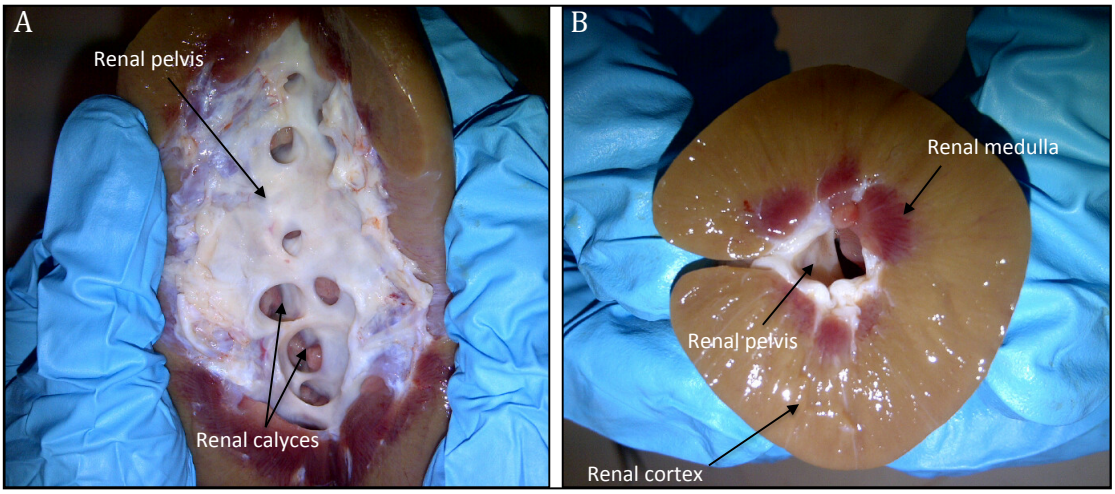

Figure 5.2. Bird's – eye view (A) and cross – sectional tunnel view (B) of the renal pelvis from an *ex vivo* porcine kidney. Urine moves from the medulla through the renal calyces to the renal pelvis. From the renal pelvis urine passes down the ureter to the bladder.

The efficacy of topical chemotherapy in UTUC is not proven. The poor quality of the studies (small, retrospective studies with limited follow up and no control arms) prevents results from demonstrating unequivocal benefit[3,9]. If topical drug delivery is to be of benefit in reducing the recurrence of UTUC, then efficacious concentrations of drug must be achieved in the target tissue[9].

The urothelium forms a continual lining of the renal pelvis, ureter, bladder and proximal urethra[22]. Currently, the accepted dogma is that urothelial permeability is consistent throughout the urinary tract. This is largely based on the assumption that histologically the urothelium is unchanged in the upper and lower urinary tract[23]. To date, no study has sought to investigate the relative permeability of the bladder, ureter and renal pelvis urothelium. However evidence suggests that despite apparent histological homology, protein expression on the surface of the urothelial umbrella cells is not consistent[24,25]. Given the important role the umbrella cells play in maintaining barrier function, we hypothesise that this may give rise to varying transurothelial permeation at these distinct locations. This chapter investigated the relative permeability and drug - tissue concentrations achieved in the bladder, ureter and kidney following topical instillation with MMC.

5.1.1. Aims and Objectives of Chapter Five

To aim of this chapter was to investigate the relative permeability of the upper and lower urinary tract urothelium to MMC.

The key objectives were:

1. To topically instill a single concentration of MMC to isolated *ex vivo* porcine bladder, ureter and kidney.

2. To construct concentration - depth profiles of MMC in the different urinary tract tissues.

3. To normalise the total amount of permeated drug to the surface area of urothelium and investigate the relative permeability of the upper and lower urinary tract to MMC.

5.2. Materials and Methods

5.2.1. Materials

All chemicals were purchased from Sigma - Aldrich, Poole, UK and were used as received unless otherwise stated. All organic solvents were of HPLC grade and were obtained from Fisher Scientific, Loughborough, UK unless otherwise stated.

5.2.2. Topical instillation of MMC to isolated porcine bladder, ureter and kidney

En bloc porcine urinary tracts, from pigs weighing 70 - 90 kg, were obtained fresh from a local abattoir as described (Section 2.2.5). Working in a shallow bed of Krebs, excess perivesical fat was trimmed and the bladder, ureters and kidneys dissected out. Ureters (~ 10 cm) were dissected out so as to leave ~ 2 cm attached to the bladder and kidney. Organs were rinsed with saline to remove any residual urine and then filled using an open - ended ureteral catheter (Section 3.2.5) with MMC solution (1 mg ml^{-1} in normal saline) (mitomycin - C 40 mg powder for solution for injection, Prostrakan, UK). The bladder, kidney and ureter were filled through the urethra, ureteral orifice and directly into the ureter respectively. Since the volume of the renal pelvis is variable, pre - experimental test instillations with methylene blue (1 mg ml^{-1} in normal saline) were carried out to ensure adequate contact with the renal pelvis urothelium was achieved. Post - instillation, entry orifices were sutured and the organs submerged in oxygenated Krebs maintained at 37 °C in a waterbath for 60 min (Section 3.2.5). Four experiments, each representing a different *ex vivo* porcine urinary tract, were performed.

5.2.3. Investigating total permeation of MMC into the bladder, ureter and kidney wall: Preliminary studies

Following 60 min instillation, organs were removed, emptied and opened with a single vertical incision. To remove surface - adsorbed drug the urothelium was thoroughly rinsed with saline. Tissue samples from areas of drug contact (observed due to purple staining conferred by MMC) were excised and their apparent surface area measured. For kidney samples the renal pelvis was isolated from the underlying cortex by cutting along the natural plane of the tissue with a scalpel (Figure 5.3). The separated cortex was then cut in half representing cortex proximal and distal to the renal pelvis. For all tissues, samples were weighed, homogenised and the drug extracted in 1 ml of mobile phase as described (Section 2.2.6.1). Extracted drug was quantified using HPLC (Section 5.2.3.1). Average drug concentrations were calculated by dividing the total amount of drug recovered by the total weight of tissue. Transurothelial permeation was calculated by normalising the total amount of drug extracted from the tissue to the surface area of the tissue sample.

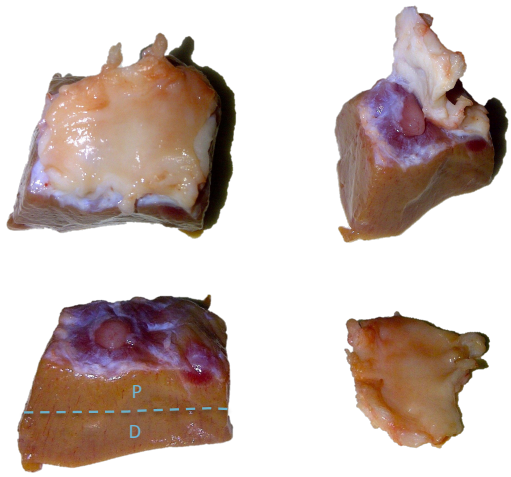

Figure 5.3. Stepwise dissection (left to right) of the renal pelvis wall (white) from the underlying renal cortex (brown). The renal cortex was subsequently cut in half representing tissue proximal (P) and distal (D) to the renal pelvis.

5.2.3.1. Analysis of MMC

MMC was analysed by HPLC (Section 2.2.2). The mobile phase consisted of 80 % 5 mM phosphate buffer (pH 7) : 20 % ACN, with UV detection at 365 nm. The injection volume was 20 μl and flow rate 1ml min^{-1}.

5.2.4. Investigating the distribution of MMC into the bladder, ureter and kidney wall: Concentration - depth studies

Following 60 min instillation, organs were removed, instilled drug emptied and tissue samples taken as described (Section 5.2.3). In this instance the renal pelvis was not isolated from the underlying renal cortex. Tissue samples were immediately snap frozen and the tissue sectioned using a cryostat (Section 2.2.6.1). Samples were serially sectioned parallel to the urothelial surface at 50 μm thickness and sections collected in pre - weighed 1.5 ml eppendorf tubes. Two 50 μm tissue sections between 0 and 100 μm were grouped for analysis, as were the two 50 μm sections between 100 and 200 μm. Groups of six 50 μm tissue sections between 200 and 1,400 μm and groups of twelve 50 μm tissue sections between 1,400 and 7,400 μm were also grouped. MMC was extracted and quantified using HPLC (Section 5.2.3.1). Average drug concentrations at different tissue depths were calculated as described (Section 2.2.7.2). Transurothelial permeation was calculated by normalising the total amount of drug extracted from all tissue sections to the surface area of the tissue sample.

5.2.4.1. Validating extraction of MMC

Deionised water (0.5 ml) was added to the tissue homogenate of sectioned urinary tract tissue (previously extracted according to Section 5.2.3). Samples were then immediately vortexed, centrifuged and the supernatant discarded. Ethyl acetate (0.25 ml) was added to the homogenate and MMC extracted for 24 h with 10 min sonication per sample. Samples were then centrifuged and the supernatant isolated for analysis by HPLC (Section 5.2.3.1).

5.2.4.2. Quantifying tissue layers depths of the ureter, bladder and kidney wall

Samples of ureter, bladder and kidney were taken from porcine urinary tracts excised immediately post - sacrifice on site at the abattoir. Samples were fixed,

sectioned and stained with Masson's trichrome prior to examination by light microscopy (Section 3.2.6). The mean depths of the different tissue layers for the ureter, bladder and kidney were measured directly from photomicrographs using NIS - Elements Basic Research imaging software (Nikon Instruments Europe B.V, Amsterdam, Netherlands).

5.2.5. Statistical analysis

All statistical analyses were performed using GraphPad Prism version 6.0c (GraphPad Software, Inc, San Diego, California, USA). For all comparisons, one – way ANOVA with Tukey's post – hoc test for multiple comparisons was used.

5.3. Results and Discussion

5.3.1. Investigating total permeation of MMC into the bladder, ureter and kidney wall: Preliminary studies

Using a ureteral catheter, 1 mg ml^{-1} MMC was instilled into isolated porcine bladder, ureter and kidney. Owing to natural intra - species variation, urinary organs varied in size and subsequently the volume of MMC instilled varied (Table 5.1). Pre - experimental test instillations with methylene blue showed filling of the kidney through the ureteral orifice resulted in complete exposure of the renal pelvis urothelium (Figure 5.4). Coincidently, MMC stained the urothelium purple making it easy to identify tissue areas exposed to drug solution (Figure 5.5).

Prelim Studies	Organ	Weight (g)	Size (cm)	Instillation (ml)
Urinary tract 1	Bladder	37.3	Whole	12
	Ureters	2.2 / 3.4	10.6 / 10.6	2 / 2
	Kidneys	109.3 / 108.1	Whole	7 / 7
Urinary tract 2	Bladder	23.4	Whole	10
	Ureters	2.9 / 2.7	12 / 13	4 / 4
	Kidneys	128.5 / 119.3	Whole	15 / 12
Urinary tract 3	Bladder	35.2	Whole	10
	Ureters	2.2 / 2.5	12 / 13	2.5 / 3
	Kidneys	106.4 / 104.2	Whole	5 / 6
Urinary tract 4	Bladder	35.9	Whole	14
	Ureters	2.1 / 1.7	13.4 / 13	3.5 / 3.5
	Kidneys	71.8 / 75.8	Whole	4 / 4

Table 5.1. Individual organ dimensions and volumes of MMC instilled in each of the four *ex vivo* porcine urinary tracts. ('Prelim' – preliminary).

Figure 5.4. Porcine kidney instilled through the ureteral orifice with methylene blue (1 mg ml^{-1}) using an open - ended ureteral catheter. The technique resulted in complete exposure of the renal pelvis urothelium to the instilled solution.

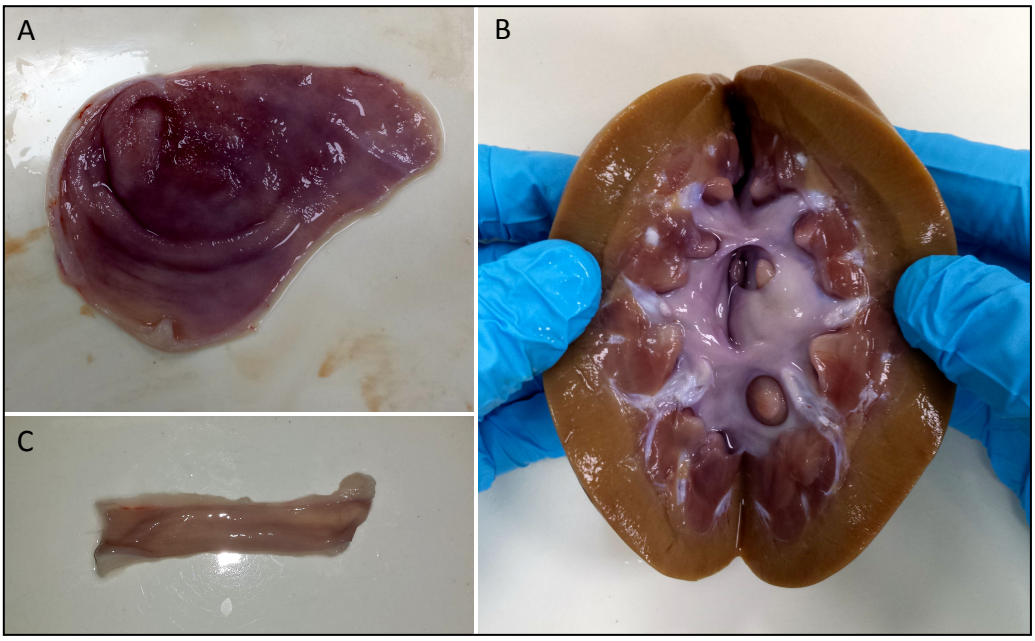

Figure 5.5. *Ex vivo* porcine bladder (A), kidney (B) and ureter (C) following 60 min instillation with MMC (1 mg ml^{-1}). Purple staining of the tissue urothelium enables easy identification of the areas of drug contact.

5.3.1.1. Analysis of MMC

HPLC analysis of MMC produced sharp, near - symmetrical peaks that eluted at a stable retention time (Figure 5.7). Analyte quantitation was calculated using an external standard solution (section 2.3.3.1) ranging in concentration from 0.01 to 10 μg ml^{-1}. Calibration curves were run in triplicate and showed high linearity (R^2 value = 0.9999) across the expected analyte concentration range (Figure 5.6). The LLOD and LLOQ was 0.003 and 0.01 μg ml^{-1} respectively, with good sensitivity shown in homogenised urinary tract tissue (Figure 5.7D - E).

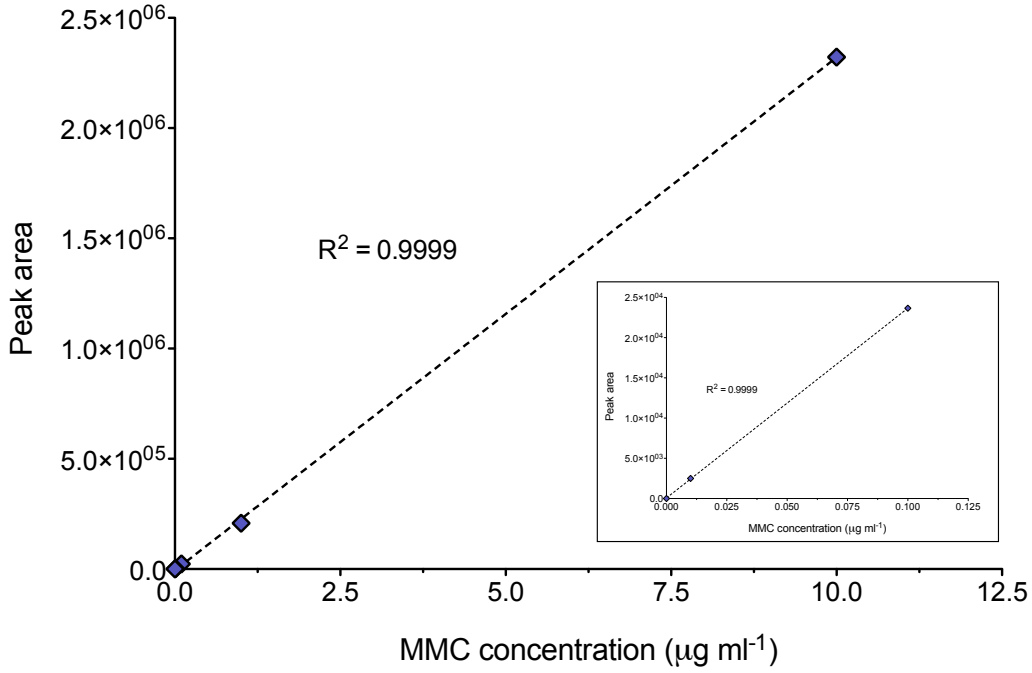

Figure 5.6. External standard calibration curve used in the HPLC analysis of MMC. Inset, a clearer plot of the calibration values between 0 and 0.1 μg ml^{-1}.

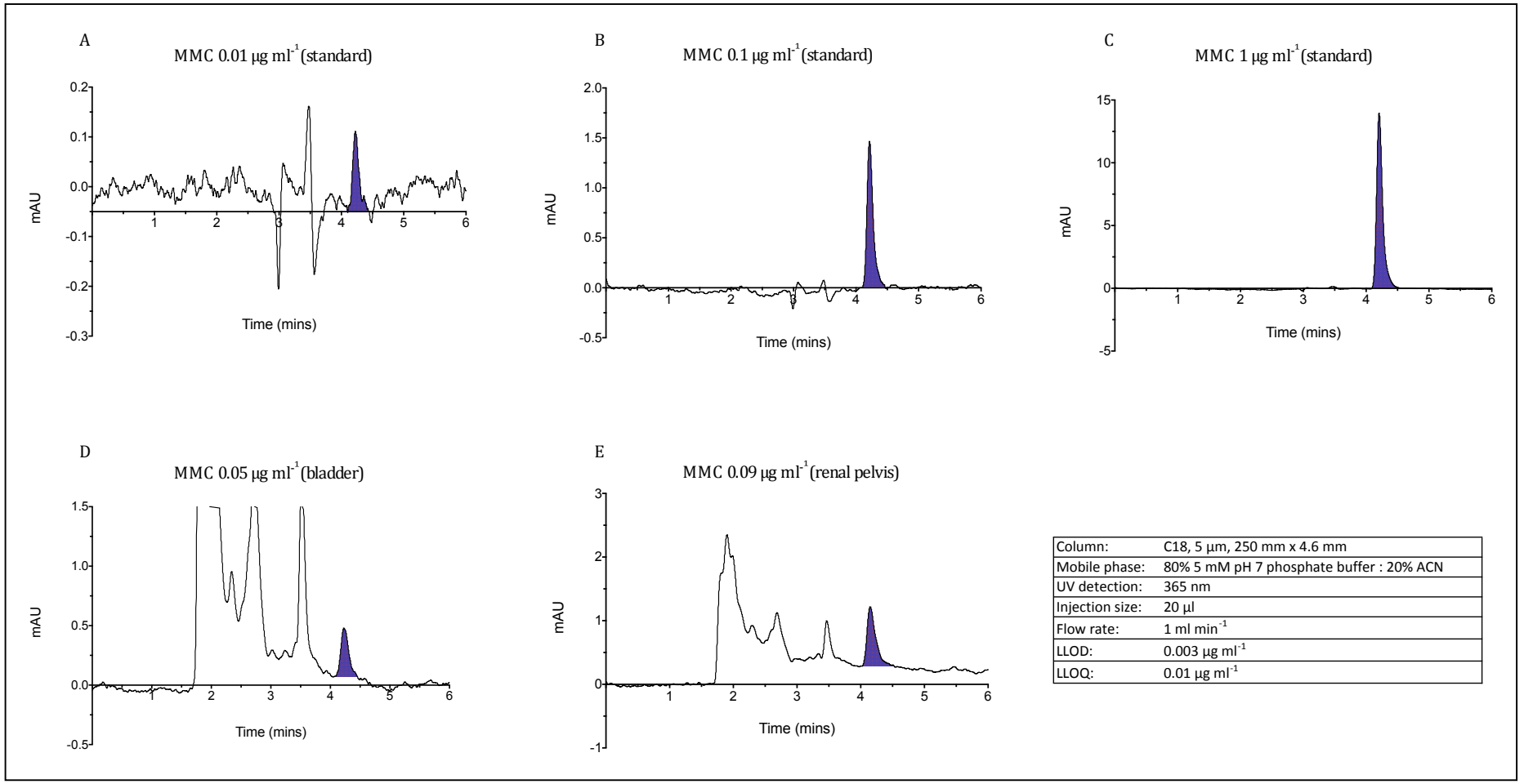

Figure 5.7. Example HPLC chromatograms showing the analysis of MMC calibration standards (A - C) and drug recovered from bladder (D) and kidney (E) tissue samples near the LLOQ.

Considering the large variation in thickness of the bladder, ureter and kidney, drug recovered from the tissue was normalised to surface area allowing a more accurate comparison of permeation. For the kidney, amounts of MMC recovered from the renal cortex were frequently below the LLOQ and as such permeation represents drug recovered from the renal pelvis only. Interestingly, after 60 min, permeation of MMC across ureteral urothelium (4.29 $\mu g\ cm^{-2}$) was significantly greater than bladder urothelium (0.66 $\mu g\ cm^{-2}$) or kidney urothelium (0.84 $\mu g\ cm^{-2}$) ($p < 0.001$) (Figure 5.8B). There was no significant difference between permeation across the kidney and bladder urothelium ($p > 0.05$). This pattern of increased ureteral permeability was observed consistently in each of the four urinary tracts investigated (Figure 5.8A). When expressing drug recovered as a total concentration per weight of the tissue, concentrations of MMC in the ureter (20.44 $\mu g\ g^{-1}$) were significantly greater than that of the bladder (1.07 $\mu g\ g^{-1}$) or kidney (5.32 $\mu g\ g^{-1}$) ($p < 0.001$ and 0.05 respectively) (Figure 5.9B). MMC tissue concentrations in the kidney were markedly higher than those in the bladder for three of the four urinary tracts investigated (Figure 5.9A), however overall this was not statistically significant ($p > 0.05$). As was the case with transurothelial permeation, the pattern of increased ureteral MMC concentrations was consistent across the four urinary tracts investigated (Figure 5.9A).

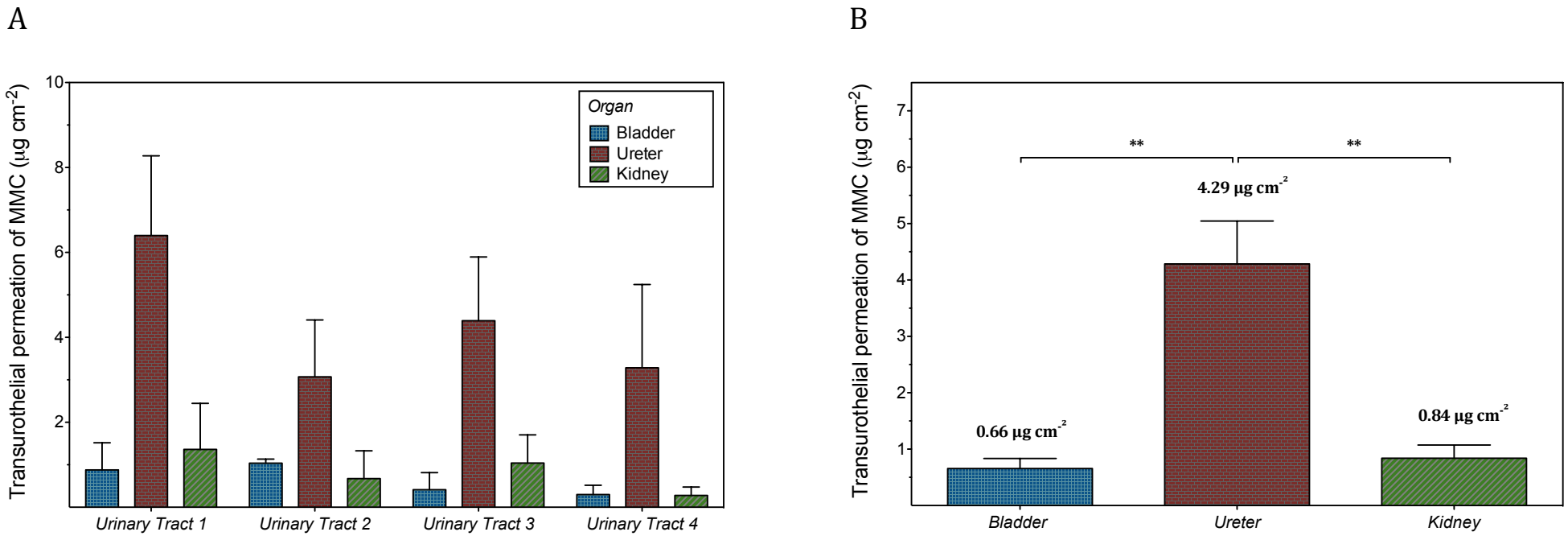

Figure 5.8. A) Transurothelial permeation of MMC into urinary tract tissue following 60 min instillation of 1 mg ml^{-1} MMC for each of the four urinary tracts investigated. For each urinary tract, bars show mean ± SD of all the raw data (tissue samples analysed per urinary tract: bladder (n = 5), ureter (n = 10), kidney (n = 6). B) Average transurothelial permeation of MMC into urinary tract tissue following 60 min instillation of 1 mg ml^{-1} MMC. (n = 4 urinary tracts ± SEM, ** p < 0.01 for the ureter versus the bladder and the ureter versus the kidney, calculated by one – way ANOVA with Tukey's post – hoc test for multiple comparisons).

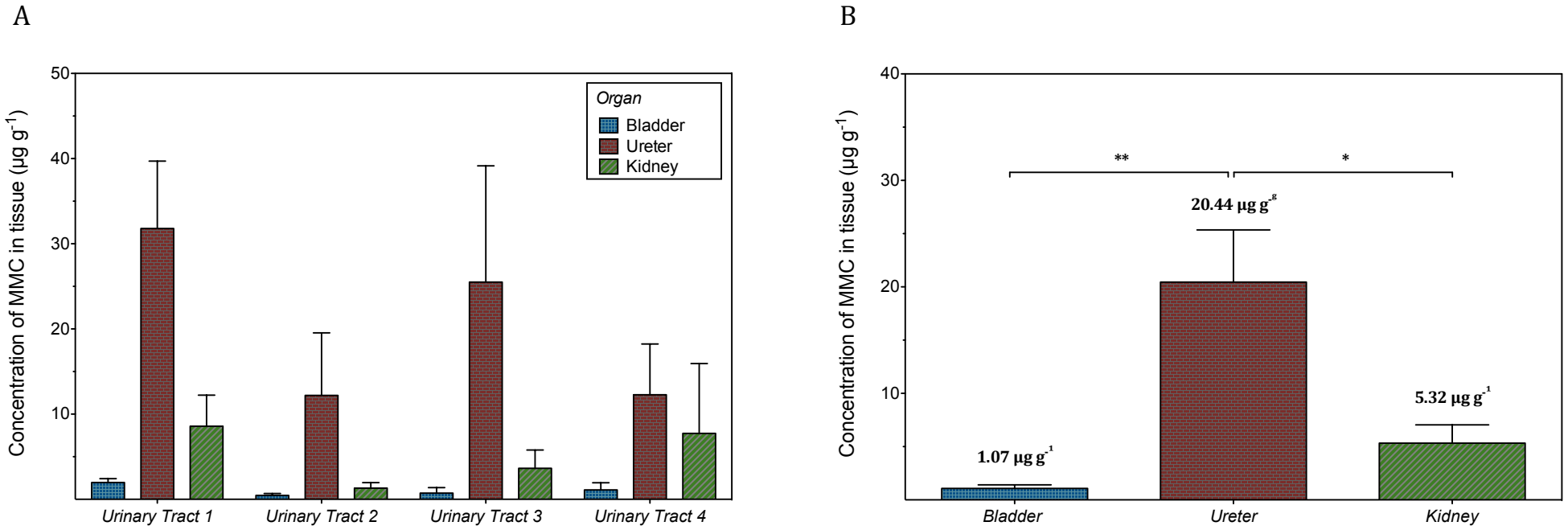

Figure 5.9. A) Drug – tissue concentrations achieved in urinary tract tissue following 60 min instillation of 1 mg ml^{-1} MMC for each of the four urinary tracts investigated. For each urinary tract, bars show mean ± SD of all the raw data (tissue samples analysed per urinary tract: bladder (n = 5), ureter (n = 10), kidney (n = 6). B) Average drug – tissue concentrations achieved in urinary tract tissue following 60 min instillation of 1 mg ml^{-1} MMC. (n = 4 urinary tracts ± SEM, ** p < 0.01 for the ureter versus the bladder, * p < 0.05 for the ureter versus the kidney, calculated by one – way ANOVA with Tukey's post – hoc test for multiple comparisons).

5.3.1.2. Quantifying tissue layers depths of the ureter, bladder and kidney wall

Although the relative thickness of tissue layers within the bladder wall is well established, the upper urinary tract is less well characterised. Sections of tissue were stained with Masson's trichrome (Figure 5.10) and tissue layer depths measured directly from photomicrographs using NIS - Elements imaging software (Figure 5.10D). Measurements (calculated as the distance between the top and base of the layer) were taken across the whole of the micrograph and the mean thickness of the tissue layers determined (Table 5.2).

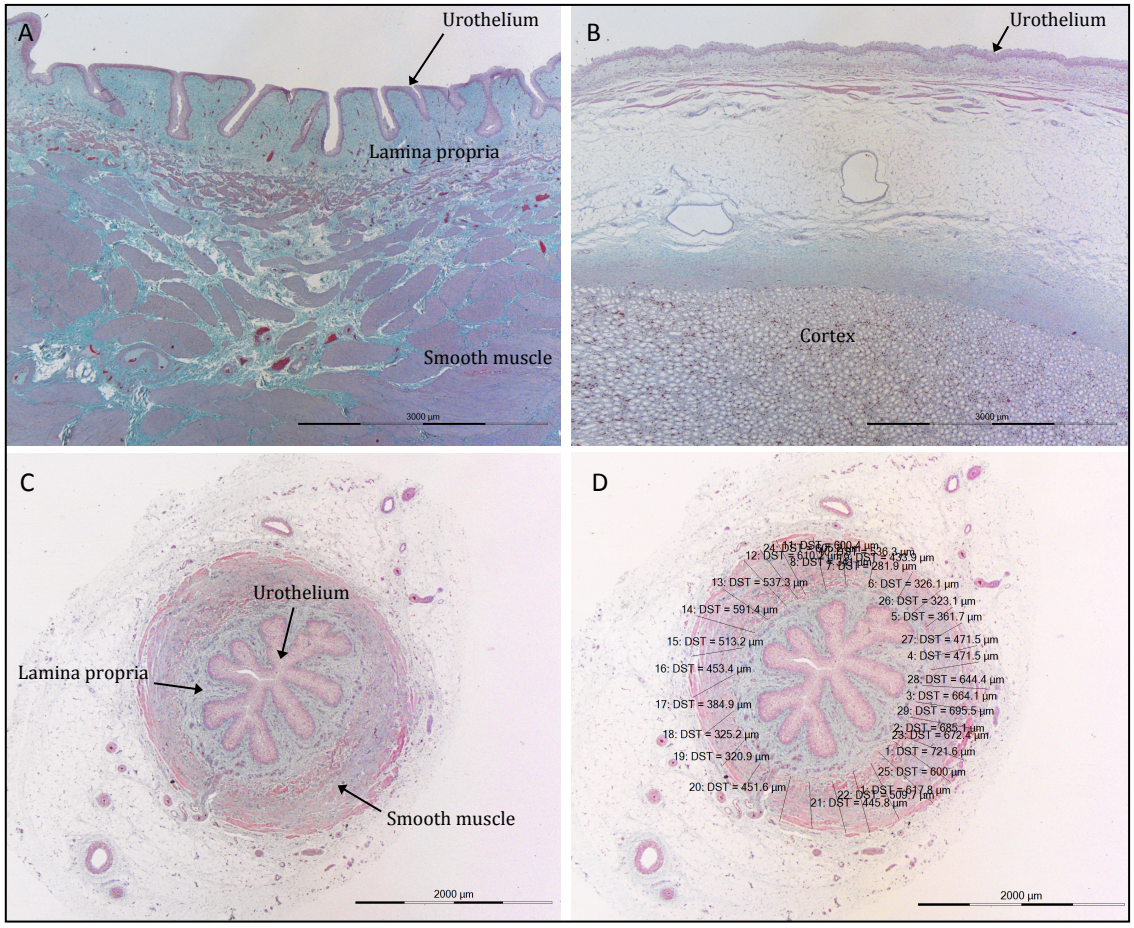

Figure 5.10. Photomicrographs of bladder (A), kidney (B) and ureter (C - D) sections stained with Masson's trichrome. All samples were taken from a single *ex vivo* porcine urinary tract. Example of ureteral smooth muscle layer measurements calculated with NIS - Elements imaging software (D).

Organ	*Thickness of tissue layer (µm)*					
	Urothelium	Lamina propria	Smooth muscle	Cortex	Adventitia	Whole wall
Ureter	186.9	355.8	652.9	*N/A*	1,104.1	2,299.7
Bladder	182.6	1,252.0	3,433.8	*N/A*	357.9	5,226.3
Kidney	176.5	*N/A*	*N/A*	5,635.4	*N/A*	9,282.1

Table 5.2. Tissue layer measurements for *ex vivo* porcine ureter, bladder and kidney. Values represent mean of 20 measurements for each layer from 2 whole porcine urinary tracts.

5.3.2. Investigating the distribution of MMC into the bladder, ureter and kidney wall: Concentration - depth studies

Preliminary studies looked only at total MMC permeated (Figure 5.8), treating the urothelium, lamina propria and detrusor muscle as a single compartment. Consequently results report average concentrations across the whole of the tissue wall (Figure 5.9B). When comparing drug penetration into tissues of differing thickness, average drug concentrations can misrepresent the data. The bladder wall is considerably thicker than the ureteral wall (Table 5.2); consequently areas deep in the bladder wall (where drug may not have not reached) will drive down the average tissue concentration expressed as microgram per gram of tissue. To extend and improve upon these preliminary studies, concentration - depth profiles were constructed to more closely examine MMC permeation and concentrations achieved in the different layers of the urinary tract tissues (Figure 5.11A and 5.12).

Again the volume of MMC instilled varied (Table 5.3), however organ weights, dimensions and instillation volumes were similar to the preliminary study (Table 5.1).

CDP Studies	Organ	Weight (g)	Size (cm)	Instillation (ml)
Urinary tract 1	Bladder	26.32	Whole	16.5
	Ureters	0.87 / 1.13	5 / 6	1 / 1.9
	Kidneys	147.5 / 151.5	Whole	8.5 / 9.5
Urinary tract 2	Bladder	29.13	Whole	17
	Ureters	1.64 / 2.22	10 / 10	1.8 / 2.0
	Kidneys	104.94 / 103.86	Whole	7.1 / 10.9
Urinary tract 3	Bladder	40.56	Whole	24.3
	Ureters	2.24 / 2.31	10 / 10	2.25 / 2.75
	Kidneys	159.5 / 143.9	Whole	14 / 14.5
Urinary tract 4	Bladder	32.9	Whole	26
	Ureters	2.2 / 2.3	10 / 10	2 / 3.3
	Kidneys	145.2 / 144.5	Whole	11 / 16.25

Table 5.3. Individual organ dimensions and volumes of MMC instilled in each of the four *ex vivo* porcine urinary tracts. ('CDP', concentration – depth profile).

Figure 5.11A shows average concentration - depth profiles for MMC in the different urinary tract tissues. Profiles resembled those constructed for other molecules in this thesis (Sections 2.3.3.2, 3.3.2.2) with drug concentrations highest in the superficial (urothelial) tissue sections, followed by a comparatively steep decline in concentration as tissue depth increased. Average concentrations of MMC in the ureter and kidney were markedly higher than those achieved in the bladder at all tissue depths investigated (Figure 5.11A). This was the case in each of the four urinary tracts investigated (Figure 5.12). Variation in the relative proportion and composition of tissue layers of the upper and lower urinary tract makes comparison of drug concentrations in the lamina propria and detrusor muscle difficult. The urothelium of the upper and lower porcine urinary tract however is of a similar thickness (Table 5.2). Urothelial MMC concentrations (calculated at 150 μm tissue depth) were > 6.5 fold higher in the ureter and kidney compared to the bladder (Figure 5.11B, $p < 0.01$).

To validate the MMC extraction protocol, a second extraction in ethyl acetate was carried out on samples from each tissue type (two 50 μm sections between 100 and 200 μm tissue depth for each of the four urinary tracts). Prior to the addition of ethyl acetate, a washing step was included to remove any adsorbed MMC from the surface of the tissue homogenate. MMC is highly soluble in ethyl acetate and the solvent has been used to extract MMC from bladder tissue by other groups[26]. For all tissue sections the amount of MMC extracted in the secondary step was

below the LLOD, suggesting complete extraction of MMC had been achieved in the analytical extraction.

MMC permeation across ureteral urothelium (9.07 μg cm^{-2}) was significantly greater than that across bladder urothelium (0.94 μg cm^{-2}, $p < 0.001$, Figure 5.11C). Transurothelial permeation across kidney urothelium (3.61 μg cm^{-2}) was greater than bladder urothelium (~ 4 fold higher) however this was not statistically significant ($p = 0.086$, Figure 5.11C). Ureteral permeation was significantly greater than kidney urothelium ($p < 0.01$, Figure 5.11C) and at tissue depths beyond 350 μm MMC concentrations in the ureter were greater than those in the kidney (Figure 5.11A, 5.12). Although results from the concentration - depth study yielded higher transurothelial permeation results that those in the preliminary studies, the pattern of the ureter exhibiting significantly increased MMC permeability remained consistent.

Bladder wall concentrations are similar to those reported by other groups[26] (Figure 5.13A), especially when comparing median bladder wall concentrations (4.3 versus 5.6 μg g^{-1} in the urothelium for this data and that reported by Wientjes *et al* respectively, Figure 5.13B). However owing to differences in experimental design it is not reasonable to make direct comparisons. Unfortunately, no previous study has sought to investigate MMC concentrations achieved in the upper urinary tract following local delivery and therefore no ureteral or renal pelvis values are available with which compare. Indeed, this is the first study to compare urothelial permeability between the upper and lower urinary tract for any molecule.

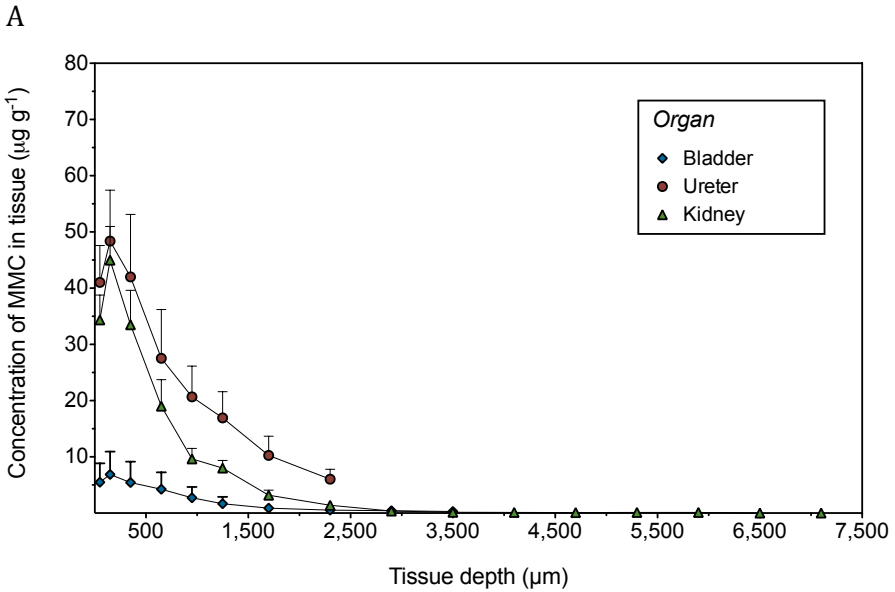

Figure 5.11. A) Average concentration - depth profiles of MMC in *ex vivo* porcine bladder, ureter and kidney wall following 60 min instillation of 1 mg ml^{-1} MMC. B) Average urothelium concentrations (calculated at 150 µm depth) following 60 min instillation of 1 mg ml^{-1} MMC (p < 0.01 for the ureter and kidney versus the bladder, calculated by one - way ANOVA with Tukey's post – hoc test for multiple comparisons). C) Transurothelial permeation of MMC in *ex vivo* porcine bladder, ureter and kidney wall following 60 min instillation of 1 mg ml^{-1} MMC (*** p < 0.001 for the ureter versus the bladder, ** p < 0.01 for the ureter versus the kidney, calculated by one - way ANOVA with Tukey's post – hoc test for multiple comparisons). (For all figures, n = 4 urinary tracts ± SEM).**

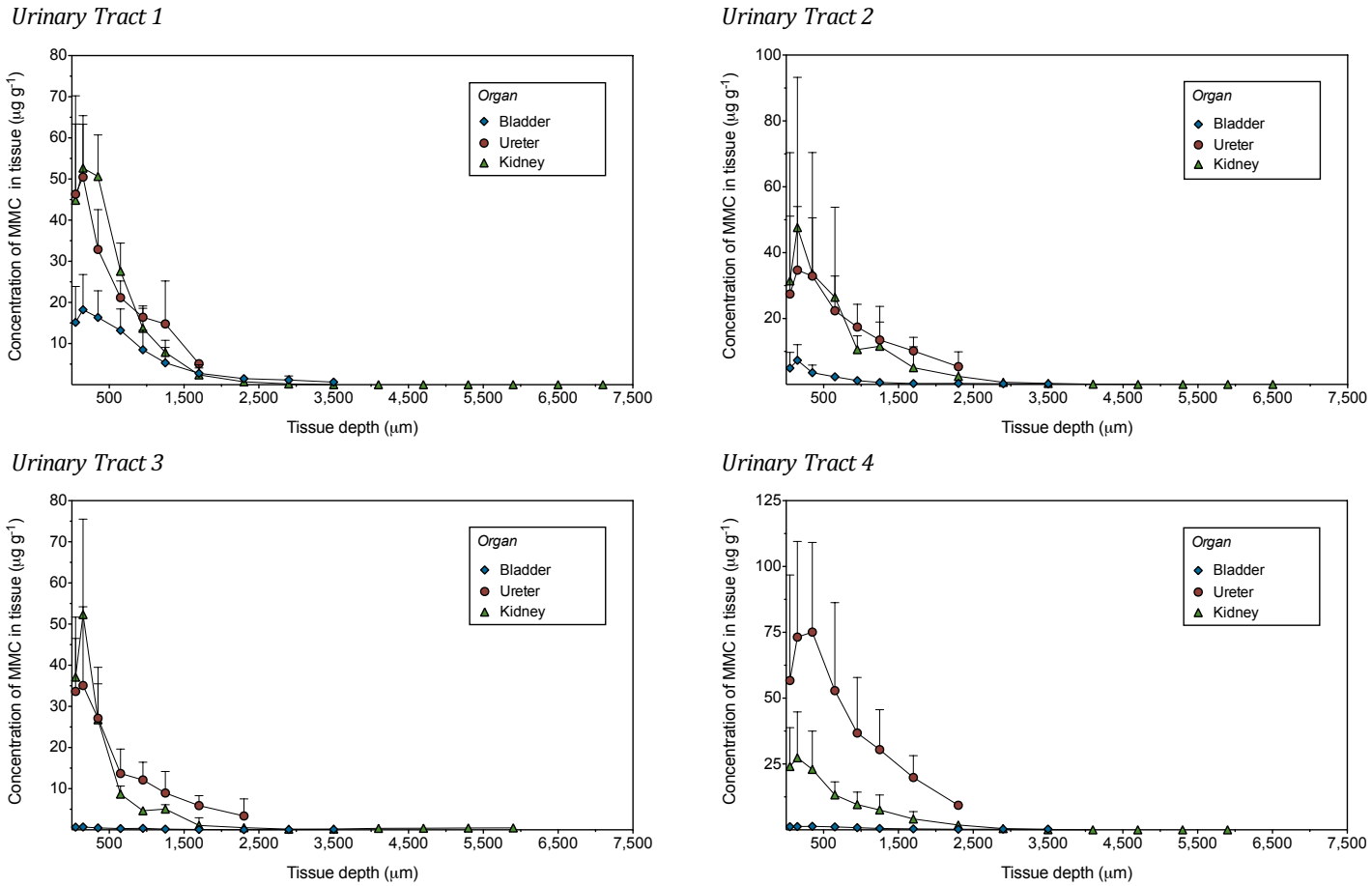

Figure 5.12. Concentration - depth profiles for each of the four urinary tracts investigated, showing drug concentrations achieved in *ex vivo* porcine bladder, ureter and kidney wall following 60 min instillation of 1 mg ml^{-1} MMC. Symbols show mean ± SD of all raw data (tissue samples analysed, n = 'Urinary Tract 1': 6 bladder, 5 ureter and 5 kidney replicates, 'Urinary Tract 2': 5 bladder, 8 ureter and 5 kidney replicates, 'Urinary Tract 3': 4 bladder, 8 ureter and 3 kidney replicates and 'Urinary Tract 4': 6 bladder, 4 ureter and 5 kidney replicates respectively).

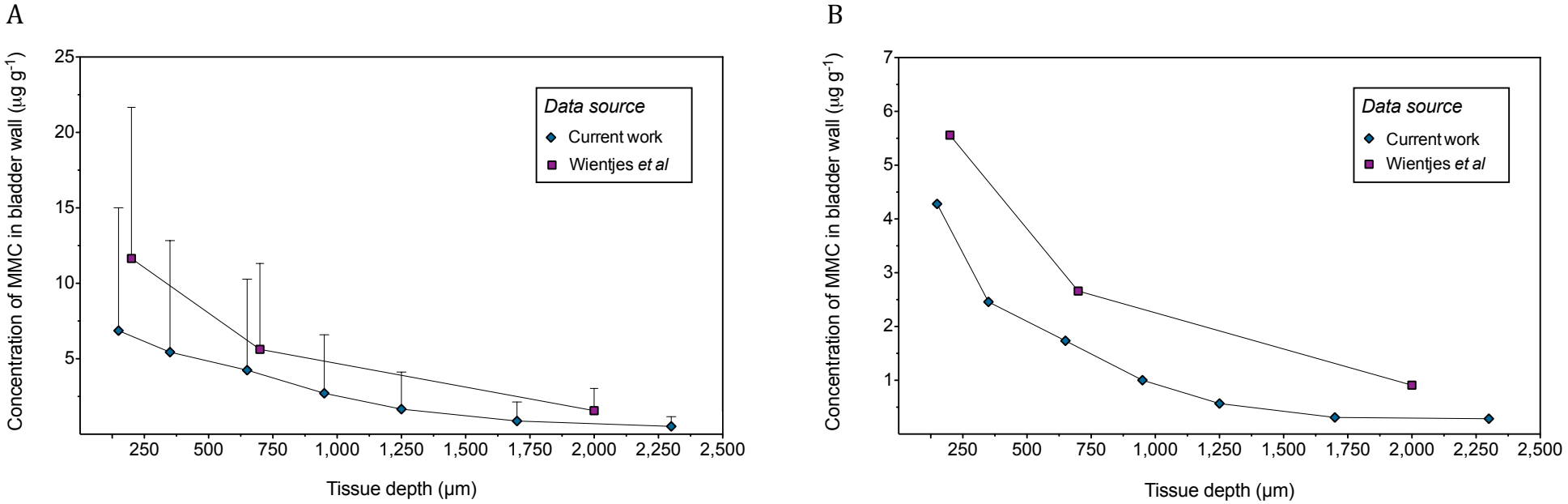

Figure 5.13. Comparison of MMC concentration - depth profiles in bladder wall from this study (blue symbols, 60 min instillation of 1 mg ml^{-1} MMC to *ex vivo* porcine bladder) and that of Wientjes *et al*[26] (purple symbols, 60 - 120 min instillation of 0.5 mg ml^{-1} MMC to *in vivo* human bladder). Figure A shows mean values ± SD and figure B shows median values from the same data. (n = 4 bladders ± SD and 7 bladders ± SD for this work and that of Wientjes *et al* respectively).

The greater permeability of porcine ureter might be explained by the relative uroplakin (UP) content of the different regions of the urinary tract[24]. It was generally believed that the upper and lower urinary tracts were lined by one homogenous urothelium[24]. Urothelia at these different regions are morphologically similar in terms of thickness and were presumed to perform a similar barrier function[23]. Indeed, histology of the *ex vivo* porcine urinary tract showed no discernable difference in the thickness of the urothelium of the upper or lower urinary tract (Table 5.2). However recently it has been shown that, based on ultrastructure and UP content, the urothelium of the mammalian urinary tract can be divided into at least three different cell lineages: renal pelvis / ureter, bladder / trigone and proximal urethra[24]. Immunofluorescence and transmission electron microscopy of bovine urothelium indicates urothelial cells of the bladder contain more UP than those of the ureter[24]. Immunoblotting analysis of these isolated urothelia indicated the bladder UP content to be ~ 10 times higher than that of the ureter[24]. Additionally, immunoblot analysis of bovine urothelia cultured *in vitro* showed the bladder to contain ~ 10 times more UP than either the ureter or renal pelvis. When maintained under identical *in vitro* conditions, bovine urothelia from the bladder and ureter exhibited very different proliferative potential and formed morphologically distinct colonies[24]. Conversely, *in vitro* cultured urothelia from the renal pelvis showed indistinguishable growth potential from that of the ureter. Preliminary work by the same group suggested the concept of urothelial heterogeneity also extended to monkey and human[24].

Following on from this work Riedel *et al* showed that, with respect to UP composition, urothelial heterogeneity was indeed more prominent in umbrella cells of the human ureter than those of the bladder[25] (the renal pelvis was not investigated). Immunohistochemical staining revealed that 15 of the 18 ureters investigated possessed a significant subpopulation of ureteral umbrella cells lacking UPIII and UPIb. The authors concluded that the UPIII / UPIb pair may in fact be completely absent from the ureters. In comparison, only 2 of the 10 bladder samples investigated lacked UPIII and UP1B and both of these samples were taken from the ureteral orifice or its immediate surrounding; suggesting the urothelium may have been of ureteral origin. UPIII is integral to the formation of an effective urothelial barrier[24,27]. UPIII knockout mice exhibit a more permeable urothelium

demonstrated by the increased penetration of methylene blue into umbrella cells and a higher transurothelial permeability to water and urea[27,28]. Similar to findings in the human ureter, UPIII knockout mice exhibit reduced production of the UPIII partner protein UPIb. It is possible the lack of the UPIII / UPIb pair in the human ureter might render human ureteral urothelium more permeable than that of the bladder. Interestingly the authors also found that umbrella cell - associated cytokeratin 20, an additional marker of urothelial differentiation[29], showed a more extended expression among umbrella cells of the bladder than among those of the ureter. Evidence therefore suggests that mammalian ureteral urothelium is less differentiated than that of the bladder. Although the UP content of the human renal pelvis was not investigated, bovine data[24] and evidence that the renal pelvis and ureter are from the same cell lineage suggests it may exhibit a similar heterogeneity and increased permeability. Although preliminary studies found no discernable difference between the permeability of the renal pelvis and bladder (Figure 5.8B), more detailed concentration – depth analysis found the renal pelvis to be consistently more permeable than the bladder, although statistical significance was not achieved ($p = 0.086$, Figure 5.11C). The reason for the disparity between the results is unclear; it is possible that drug extraction from the kidney was more complete in the concentration – depth study owing to the thinness of the sectioned tissue. This would also explain the higher transurothelial permeation results determined versus the preliminary study. Although the mammalian renal pelvis and ureter are now believed to originate from the same cell lineage, results from this work suggest the two tissues may be different in terms of their permeability to MMC. In both preliminary and concentration – depth studies, the ureter was significantly more permeable than the renal pelvis, suggesting an underlying difference in barrier function.

It should be pointed out that UP expression studies have not been carried out in the pig. Urothelial heterogeneity is suggested to be an explanation for the results observed in this study based on results from other mammalian species in the literature as discussed. Furthermore pigs are established and well characterised models of the human urinary tract[30–32], exhibiting similar physiology[33–35], tissue structure and composition to that of humans[36–38].

5.4. Conclusions

Ex vivo porcine ureter is significantly more permeable to MMC than bladder urothelium and consequently higher MMC tissue concentrations can be achieved after topical application. The renal pelvis was also found to be consistently more permeable than the bladder, although significance was not demonstrated. The data presented in this chapter correlates with the theory that the mammalian ureter represents a different cell lineage to the bladder and that it is innately more permeable. A less differentiated urothelium may have no major functional consequences for the ureter as, in comparison to the bladder, upper tract urothelia have less barrier requirements (lower intraluminal pressure, less distension and storage requirements) and therefore the presence of fully functional UPs may not be essential[25]. However there may be distinct advantages when considering the topical administration of drug to the upper urinary tract. Increased urothelial permeability to chemotherapeutics such as MMC would potentially allow higher drug concentrations to be achieved in the ureteral wall. Unfortunately, unlike urothelial carcinoma of the bladder[39–42], to our knowledge MMC concentrations necessary to effectively treat UTUC have not been established. Nonetheless, if delivered to the upper urinary tract in an effective manner, the increased permeability of the ureter and renal pelvis could have important ramifications for the conservative treatment of UTUC.

5.4.1. Future Studies

Suggestions for future studies include:

- Immunohistochemical analysis of porcine urinary tract to determine UP content
- Comparing upper and lower urinary tract permeability to MMC in human tissue.
- Further investigations to ascertain whether the urothelium of the renal pelvis is more permeable than that of the bladder to MMC.
- Additional studies to investigate whether this pattern of increased upper tract permeability is seen for other clinically relevant molecules such as BCG[17].
- Investigating the homogeneity of the GAG layer throughout upper and lower urinary tract urothelia. The GAG layer is crucial to the barrier function of the urothelium (1.1.2.1.c)[43,44], however no groups have investigated its relative distribution at the different anatomical sites of the urinary tract.

5.5. Reference List

1. Ploeg M, Aben KKH, Kiemeney LA. The present and future burden of urinary bladder cancer in the world. World J Urol. 2009 Jun;27(3):289–93.

2. Rouprêt M, Zigeuner R, Palou J, Boehle A, Kaasinen E, Sylvester R, et al. European guidelines for the diagnosis and management of upper urinary tract urothelial cell carcinomas: 2011 update. Eur Urol. 2011 Apr;59(4):584–94.

3. Rouprêt M, Babjuk M, Compérat E, Zigeuner R, Sylvester R, Burger M, et al. European Guidelines on Upper Tract Urothelial Carcinomas: 2013 Update. Eur Urol. 2013 Mar 19;

4. Munoz JJ, Ellison LM. Upper tract urothelial neoplasms: incidence and survival during the last 2 decades. J Urol. 2000 Nov;164(5):1523–5.

5. Siegel R, Naishadham D, Jemal A. Cancer statistics, 2013. CA Cancer J Clin. 2013 Jan;63(1):11–30.

6. Raman JD, Messer J, Sielatycki JA, Hollenbeak CS. Incidence and survival of patients with carcinoma of the ureter and renal pelvis in the USA, 1973-2005. BJU Int. 2011 Apr;107(7):1059–64.

7. Eylert MF, Hounsome L, Verne J, Bahl A, Jefferies ER, Persad RA. Prognosis is deteriorating for upper tract urothelial cancer: data for England 1985-2010. BJU Int. 2013 Jul;112(2):E107–13.

8. Stewart GD, Bariol SV, Grigor KM, Tolley DA, McNeill SA. A comparison of the pathology of transitional cell carcinoma of the bladder and upper urinary tract. BJU Int. 2005 Apr;95(6):791–3.

9. Cutress ML, Stewart GD, Zakikhani P, Phipps S, Thomas BG, Tolley DA. Ureteroscopic and percutaneous management of upper tract urothelial carcinoma (UTUC): systematic review. BJU Int. 2012 Sep;110(5):614–28.

10. Cutress ML, Stewart GD, Wells-Cole S, Phipps S, Thomas BG, Tolley DA. Long-term endoscopic management of upper tract urothelial carcinoma: 20-year single-centre experience. BJU Int. 2012 Dec;110(11):1608–17.

11. Patel A, Fuchs GJ. New techniques for the administration of topical adjuvant therapy after endoscopic ablation of upper urinary tract transitional cell carcinoma. J Urol. 1998 Jan;159(1):71–5.

12. Keeley FX Jr, Bagley DH. Adjuvant mitomycin C following endoscopic treatment of upper tract transitional cell carcinoma. J Urol. 1997 Dec;158(6):2074–7.

13. Eastham JA, Huffman JL. Technique of mitomycin C instillation in the treatment of upper urinary tract urothelial tumors. J Urol. 1993 Aug;150(2 Pt 1):324–5.

14. Palou J, Piovesan LF, Huguet J, Salvador J, Vicente J, Villavicencio H. Percutaneous nephroscopic management of upper urinary tract transitional cell carcinoma: recurrence and long-term followup. J Urol. 2004 Jul;172(1):66–9.

15. Chen GL, Bagley DH. Ureteroscopic management of upper tract transitional cell carcinoma in patients with normal contralateral kidneys. J Urol. 2000 Oct;164(4):1173–6.

16. Martínez-Piñeiro JA, García Matres MJ, Martínez-Piñeiro L. Endourological treatment of upper tract urothelial carcinomas: analysis of a series of 59 tumors. J Urol. 1996 Aug;156(2 Pt 1):377–85.

17. Giannarini G, Kessler TM, Birkhäuser FD, Thalmann GN, Studer UE. Antegrade perfusion with bacillus Calmette-Guérin in patients with non-muscle-invasive urothelial carcinoma of the upper urinary tract: who may benefit? Eur Urol. 2011 Nov;60(5):955–60.

18. Clark PE, Streem SB, Geisinger MA. 13-year experience with percutaneous management of upper tract transitional cell carcinoma. J Urol. 1999 Mar;161(3):772–5; discussion 775–6.

19. Williams SK, Hoenig DM, Ghavamian R, Soloway M. Intravesical therapy for bladder cancer. Expert Opin Pharmacother. 2010 Apr;11(6):947–58.

20. Shelley MD, Mason MD, Kynaston H. Intravesical therapy for superficial bladder cancer: a systematic review of randomised trials and meta-analyses. Cancer Treat Rev. 2010 May;36(3):195–205.

21. Pollard ME, Levinson AW, Shapiro EY, Cha DY, Small AC, Mohamed NE, et al. Comparison of 3 Upper Tract Anticarcinogenic Agent Delivery Techniques in an Ex Vivo Porcine Model. Urology. 2013 Oct 16;

22. Wu X-R. Urothelial tumorigenesis: a tale of divergent pathways. Nat Rev Cancer. 2005 Sep;5(9):713–25.

23. Hicks RM. The fine structure of the transitional epithelium of rat ureter. J Cell Biol. 1965;26(1):25.

24. Liang F-X, Bosland MC, Huang H, Romih R, Baptiste S, Deng F-M, et al. Cellular basis of urothelial squamous metaplasia. J Cell Biol. 2005 Dec 5;171(5):835–44.

25. Riedel I, Liang F-X, Deng F-M, Tu L, Kreibich G, Wu X-R, et al. Urothelial umbrella cells of human ureter are heterogeneous with respect to their uroplakin composition: different degrees of urothelial maturity in ureter and bladder? Eur J Cell Biol. 2005 Mar;84(2-3):393–405.

26. Wientjes MG, Badalament RA, Wang RC, Hassan F, Au JL. Penetration of mitomycin C in human bladder. Cancer Res. 1993;53(14):3314.

27. Hu P, Deng FM, Liang FX, Hu CM, Auerbach AB, Shapiro E, et al. Ablation of uroplakin III gene results in small urothelial plaques, urothelial leakage, and vesicoureteral reflux. J Cell Biol. 2000 Nov 27;151(5):961–72.

28. Hu P, Meyers S, Liang F-X, Deng F-M, Kachar B, Zeidel ML, et al. Role of membrane proteins in permeability barrier function: uroplakin ablation elevates urothelial permeability. Am J Physiol Renal Physiol. 2002 Dec;283(6):F1200–7.

29. Moll R, Löwe A, Laufer J, Franke WW. Cytokeratin 20 in human carcinomas. A new histodiagnostic marker detected by monoclonal antibodies. Am J Pathol. 1992 Feb;140(2):427–47.

30. Tscholl R, Tettamanti F, Zingg E. Ileal substitute of ureter with reflux-plasty by terminal intussusception of bowel: animal experiments and clinical experience. Urology. 1977 Apr;9(4):385–9.

31. Coolsaet BL, van Mastrigt R, van Duyl WA, van Rees Vellinga F. Some influences of the contractile element on the visco-elastic properties of bladder wall strips. Eur Urol. 1978;4(6):450–6.

32. Van Mastrigt R, Griffiths DJ. Contractility of the urinary bladder. Urol Int. 1979;34(6):410–20.

33. Crowe R, Burnstock G. A histochemical and immunohistochemical study of the autonomic innervation of the lower urinary tract of the female pig. Is the pig a good model for the human bladder and urethra? J Urol. 1989 Feb;141(2):414–22.

34. Bridgewater M, MacNeil H, Brading A. Regulation of tone in pig urethral smooth muscle. J Urol. 1993;150(1):223–8.

35. Sibley G. An experimental model of detrusor instability in the obstructed pig. Br J Urol. 1985;57(3):292–8.

36. Dixon JS, Gosling JA. Histology and fine structure of the muscularis mucosae of the human urinary bladder. J Anat. 1983 Mar;136(Pt 2):265–71.

37. Teufl F, Dammann F, Wehrmann M. In vitro study of morphology of the bladder wall using MR tomography at 1.0 Tesla: correlation with histology. RöFo. 1997 May;166(5):406–10.

38. Narumi Y, Kadota T, Inoue E, Kuriyama K, Horinouchi T, Kasai K, et al. Bladder wall morphology: in vitro MR imaging-histopathologic correlation. Radiology. 1993 Apr;187(1):151–5.

39. Schmittgen TD, Wientjes MG, Badalament RA, Au JL. Pharmacodynamics of mitomycin C in cultured human bladder tumors. Cancer Res. 1991 Aug 1;51(15):3849–56.

40. Xu BH, Gupta V, Singh SV. Mechanism of differential sensitivity of human bladder cancer cells to mitomycin C and its analogue. Br J Cancer. 1994 Feb;69(2):242–6.

41. Schmittgen TD, Weaver JM, Badalament RA, Wientjes MG, Klein EA, Young DC, et al. Correlation of human bladder tumor histoculture proliferation and sensitivity to mitomycin C with tumor pathobiology. J Urol. 1994 Nov;152(5 Pt 1):1632–6.

42. Yen WC, Schmittgen T, Au JL. Different pH dependency of mitomycin C activity in monolayer and three-dimensional cultures. Pharm Res. 1996 Dec;13(12):1887–91.

43. Lilly JD, Parsons CL. Bladder surface glycosaminoglycans is a human epithelial permeability barrier. Surg Gynecol Obstet. 1990 Dec;171(6):493–6.

44. Parsons CL, Boychuk D, Jones S, Hurst R, Callahan H. Bladder surface glycosaminoglycans: an epithelial permeability barrier. J Urol. 1990 Jan;143(1):139–42.

Chapter Six: General Discussion

6.1. General Overview of Thesis

Intravesical drug delivery (IDD) offers a unique opportunity to target pathology of the lower urinary tract. High concentrations of drug can be delivered directly to the bladder with minimal systemic absorption and significantly improved adverse effect profiles compared to alternative administration routes[1]. Despite its advantages, IDD has several inherent limitations including the low permeability of the urothelium[2], the continual dilution of the instilled dose by urine and the limited capacity of the bladder and hence low residence time of the dose[3]. IDD has been used successfully to manage a wide range of conditions such as bladder cancer[4], interstitial cystitis / painful bladder syndrome[5] and overactive bladder (OAB)[6] and continues to be investigated for novel indications[7]. Despite this the majority of IDD regimens remain empirically designed and as a result its potential largely unfulfilled.

When researching this project it became apparent that there was limited information available in the literature regarding bladder wall drug concentrations achieved following IDD. Although there were many IDD clinical studies, there was no information detailing desired target tissue concentrations in the bladder wall. There continues to be very few groups working in this field. Such shortcomings underpinned the motivation for Boston Scientific Corporation (BSC) to instigate this research project. BSCs ketorolac – eluting ureteral stent (Lexington™) unexpectedly failed to meet its primary clinical endpoint[8], despite preliminary IDD studies showing the agent was effective in the management of ureteral stent – related discomfort[9]. It was theorised that drug release from the stent was likely insufficient to establish effective target tissue concentrations. Subsequently BSC decided a bottom – up approach to investigate the viability of delivering ketorolac locally to the urinary tract was necessary. The original aims of this project were to investigate the local delivery of ketorolac to the urinary tract, determine drug release characteristics from the Lexington™ stent and investigate / suggest improved techniques for stent formulation.

Chapter two of this thesis focused on the development of an *ex vivo* porcine model to investigate the transurothelial permeability and bladder wall distribution of

drugs after their local application to the urothelium. This research group had limited experience in the urology area and subsequently new experimental techniques and procedures were devised. This provided many challenges including: how to obtain and efficiently transport the porcine tissue, how to ensure and evaluate that the barrier function of urothelium was maintained during experimental conditions, how to generate drug permeability parameters, how to investigate drug distribution in the bladder wall and how to extract and analyse low concentrations of drug in complex tissue medium. *Ex vivo* porcine tissue was chosen owing to the history of pigs being used as animal models in urology[10]. A wide range of techniques were used to validate the integrity of the urothelial barrier including: investigating markers of permeation, measuring transepithelial resistance (TEER) and examining the urothelial surface using scanning electron microscopy (SEM). In line with similar work carried out in the transdermal field, early transurothelial permeation studies were performed on isolated bladder mucosa (urothelium and lamina propria). Ideally, isolated urothelium would be the tissue of choice, however owing to the thickness of the urothelium (~ 200 μm) and the delicate nature of the single layer of umbrella cells, this was not feasible. The mucosal protocol was then superseded by a simpler technique that used full thickness bladder wall followed by washing of the urothelial surface. Using this technique any remaining surface - adsorbed drug was within error of the amount of drug extracted from the tissue. It also negated the need to manipulate and potentially damage the urothelium that was necessary to isolate the mucosa. This then lead to further experimental development focused on drug extraction and analysis from the bladder wall. Extracting and quantifying drug in tissue medium is inherently more complicated and challenging than doing so in 'clean' environments such as saline or Krebs. Potential problems include incomplete drug extraction and interfering peaks / reduced sensitivity during HPLC – UV analysis. Consequently significant time and effort went into the design and optimisation of HPLC methods during this thesis. At this time a concentration – depth profiling technique was optimised that allowed the determination of drug concentrations throughout the bladder wall. Although this technique had been reported in the literature, it had only been used by a small number of groups and was new to this research group. Mimicking the dosing concentration of ketorolac shown to be clinically effective *in vivo,* concentration – depth profiles were generated in the

bladder wall and compared to literature sourced IC_{50} values. Results suggested intravesical ketorolac would result in efficacious target concentrations in the bladder wall[11]. Considering this, it is likely that the Lexington™ stent failed owing to poor drug release from the device rather than an incorrect choice of drug. Follow up studies planned to investigate different techniques of drug – stent loading and determine drug release profiles over the course of stent use.

Approximately one year into this project the focus of BSC's research and development division shifted and drug release studies from the Lexington™ stent were postponed. The overarching aim of this project evolved to focus on investigating the transurothelial delivery of clinically relevant molecules and developing strategies to maximise the potential of IDD.

In chapter three *ex vivo* work was extended to include a whole bladder setup allowing the incorporation of urine dilution. This was the first time urine production had been incorporated into *ex vivo* IDD studies. Artificial urine was added to the bladder at a physiological rate and concentration – depth profiles determined following the IDD of oxybutynin. A significant challenge in this work concerned the analysis of oxybutynin. Originally HPLC was used as the detection method, however oxybutynin has a poor chromophore and shows maximum absorbance at 210 nm[12]. At this wavelength there is significant interference from other molecules in homogenised tissue and consequently UV detection was unsuitable for sensitive quantification[12]. Consequently oxybutynin was measured by HPLC – MS, which significantly increased the sensitivity at which the drug could be quantified (LLOQ of 3 ng ml^{-1} compared to ~ 250 ng ml^{-1} using HPLC – UV detection).

Intravesical oxybutynin is highly efficacious in the management of OAB in patients refractory to oral treatment[13] and is used extensively for this indication[14]. Despite this, the mechanism of action (MOA) is unclear. Originally believed to act by directly inhibiting M_3 muscarinic receptors in the detrusor muscle, there is now significant evidence that antimuscarinics activate muscarinic receptors at the urothelial and / or suburothelial level to modulate the afferent arc of the micturition cycle[15]. *Ex vivo* studies showed that despite permeating the urothelium at a high rate in comparison to ketorolac, oxybutynin concentrations achieved in

the detrusor muscle were significantly lower than reported IC_{50} values suggesting target concentrations achieved post – IDD would not be sufficient to directly inhibit detrusor contraction. Unfortunately this work did not concomitantly investigate detrusor muscle contractility with drug concentrations achieved in the bladder wall. This was a real shame and had it been feasible would have contributed to the impact of this work. Looking forward, the incorporation of concomitant pharmacology studies, whether performed in - house or in collaboration with partners, is essential to eliciting the MOA in studies such as these.

Chapter four documented the design of a computer – based pharmacokinetic (PK) model of IDD. Originally the model was designed to incorporate drug clearance from the bladder wall into the *ex vivo* studies. However it became clear that the usefulness of the model was actually its ability to compare the efficacy of different IDD regimens. It was evident from the literature that the majority of regimens were designed without consideration of the variables associated with IDD such as instillation volume, concentration or length. The model provided a platform for these variables to be investigated. The model was built using STELLA® which allows mathematical models to be designed diagrammatically rather than by high – level programming code. This work was in part assisted by Yuri Anissimov, a mathematician who has published extensively in the field of mathematical modelling of biological processes[16–20]. This collaboration was initiated after the original design of the PK model. It was deemed important to consult the expertise of a mathematician who is at the forefront of this niche area of research. Yuri was able assist with the choice of the underlying diffusion equations and validate outputs generated by the STELLA® model using PYTHON™, a widely used programming language. Using the model, the key variables associated with IDD were investigated and their contribution to the efficacy of the IDD process evaluated. To demonstrate the usefulness of the model an IDD regimen from the literature was optimised using techniques highlighted by the model and significant improvements predicted. Currently the value of the model lies not in its ability to predict *in vivo* bladder concentrations achieved after IDD, but rather to highlight comparative differences between regimens and dosing variables. In the future, validation of the models ability to predict *in vivo* bladder wall concentrations could

only be achieved through *in vivo* pig studies. Urine concentrations however could be validated clinically using patient urine samples from IDD regimens.

The final chapter of this thesis extended transurothelial permeability studies to the upper urinary tract. In addition to treating urothelial carcinoma of the bladder, topical mitomycin C (MMC) is suggested to be efficacious in reducing the recurrence of upper tract urothelial carcinoma (UTUC)[21–24]. Interestingly despite evidence that protein expression on the surface of the urothelial umbrella cells is not consistent[25,26], no groups had previously investigated the hypothesis that urothelium barrier function differs at these distinct locations. *Ex vivo* studies showed conclusively that the urothelium of the ureter was significantly more permeable to MMC than the bladder and that urothelial concentrations achieved in the upper urinary tract were significantly higher. The reasoning for this disparity might be explained by the relative distribution and density of uroplakin plaques in the upper and lower porcine urinary tract as has been shown in other mammals. This research is particularly interesting as a more permeable urothelium may provide higher target tissue concentrations after local delivery and subsequently a significant opportunity to manage UTUC conservatively. Ideally future work would mirror these studies in human tissue, however owing to the ethical approval necessary and the limited supply of whole urinary tract organs this is extremely unlikely. *In vivo* studies in large mammals such as pigs require substantial resources, however if feasible they would be an exciting next step in which to take this research.

The bladder offers a unique opportunity for the local delivery of therapies. It is one of a small number of organs that can conveniently and minimally invasively be accessed. IDD is seemingly well placed as a method for delivering high concentrations of drug directly to the bladder and has been used to manage a wide range of bladder conditions. It was therefore surprising to discover that very little was known about the permeability and tissue distribution of drugs following topical application. Whereas other significant barriers to drug delivery, such as the stratum corneum and blood brain barrier, had been extensively studied, information on the urothelium was extremely limited. This project originally set out to evaluate the potential of drug eluting ureteral stents for delivering drugs

out to evaluate the potential of drug eluting ureteral stents for delivering drugs directly to the urinary tract. However it soon became clear that rational device design, in particular drug loading and release rates, was hampered by the paucity of information defining the urothelial barrier. Therefore the project naturally evolved to explore the fundamental issues of transurothelial permeability and drug distribution following topical delivery. From here several novel *ex vivo* and *in silico* methods were developed to investigate IDD. These techniques can be used to rationally inform on the design of new, or optimisation of existing, IDD regimens and in doing so maximise the potential of what remains a poorly understood drug delivery technique.

6.2. Reference List

1. GuhaSarkar S, Banerjee R. Intravesical drug delivery: Challenges, current status, opportunities and novel strategies. J Control Release. 2010 Dec 1;148(2):147–59.

2. Lewis SA. Everything you wanted to know about the bladder epithelium but were afraid to ask. Am J Physiol Renal Physiol. 2000;278(6):F867.

3. Hsu C-C, Chuang Y-C, Chancellor MB. Intravesical drug delivery for dysfunctional bladder. Int J Urol. 2013 Jun;20(6):552–62.

4. Shen Z, Shen T, Wientjes MG, O'Donnell MA, Au JL. Intravesical treatments of bladder cancer: review. Pharm Res. 2008;25(7):1500–10.

5. Matsuoka PK, Haddad JM, Pacetta AM, Baracat EC. Intravesical treatment of painful bladder syndrome: a systematic review and meta-analysis. Int Urogynecol J. 2012 Sep;23(9):1147–53.

6. Evans RJ. Intravesical therapy for overactive bladder. Curr Urol Rep. 2005 Nov;6(6):429–33.

7. Rajaganapathy BR, Janicki JJ, Levanovich P, Tyagi P, Hafron J, Chancellor MB, et al. Intravesical Liposomal Tacrolimus Protects Against Radiation Cystitis Induced by 3-Beam Targeted Bladder Radiation. J Urol. 2015 Mar 31;

8. Krambeck AE, Walsh RS, Denstedt JD, Preminger GM, Li J, Evans JC, et al. A novel drug eluting ureteral stent: a prospective, randomized, multicenter clinical trial to evaluate the safety and effectiveness of a ketorolac loaded ureteral stent. J Urol. 2010;183(3):1037–43.

9. Beiko D, Watterson J, Knudsen B, others. A double-blinded prospective randomized controlled trial assessing the safety and efficacy of intravesical agents for ureteral stent symptoms following extracorporeal shockwave lithotripsy. J Endourol. 2004;18(8):723–30.

10. Crowe R, Burnstock G. A histochemical and immunohistochemical study of the autonomic innervation of the lower urinary tract of the female pig. Is the pig a

good model for the human bladder and urethra? J Urol. 1989 Feb;141(2):414–22.

11. Williams NA, Bowen JL, Al-Jayyoussi G, Gumbleton M, Allender CJ, Li J, et al. An ex vivo investigation into the transurothelial permeability and bladder wall distribution of the nonsteroidal anti-inflammatory ketorolac. Mol Pharm. 2014 Mar 3;11(3):673–82.

12. Khire A, Vavia P. Electron capture detection of oxybutynin in plasma: precolumn derivatization approach and application to a pharmacokinetic study. Analytical Methods. 2014;6(5):1455.

13. Mizunaga M, Miyata M, Kaneko S, Yachiku S, Chiba K. Intravesical instillation of oxybutynin hydrochloride therapy for patients with a neuropathic bladder. Paraplegia. 1994 Jan;32(1):25–9.

14. Weese DL, Roskamp DA, Leach GE, Zimmern PE. Intravesical oxybutynin chloride: experience with 42 patients. Urology. 1993 Jun;41(6):527–30.

15. Mansfield KJ. Muscarinic Receptor Antagonists, the Overactive Bladder and Efficacy against Urinary Urgency. Clin Med Insights. 2010;(2):471–80.

16. Anissimov YG. Mathematical models for skin toxicology. Expert Opin Drug Metab Toxicol. 2014 Apr;10(4):551–60.

17. Yuri G. Anissimov. Mathematical Models for Different Exposure Conditions. Dermal Absorption and Toxicity Assessment [Internet]. Informa Healthcare; 2007 [cited 2015 Feb 20]. p. 271–86. Available from: http://informahealthcare.com/doi/abs/10.3109/9780849375927.014

18. Roberts MS, Anissimov YG. Modeling of hepatic elimination and organ distribution kinetics with the extended convection-dispersion model. J Pharmacokinet Biopharm. 1999 Aug;27(4):343–82.

19. Anissimov YG, Roberts MS. Diffusion modeling of percutaneous absorption kinetics. 1. Effects of flow rate, receptor sampling rate, and viable epidermal resistance for a constant donor concentration. J Pharm Sci. 1999 Nov;88(11):1201–9.

20. Anissimov YG, Jepps OG, Dancik Y, Roberts MS. Mathematical and pharmacokinetic modelling of epidermal and dermal transport processes. Adv Drug Deliv Rev. 2013 Feb;65(2):169–90.

21. Cutress ML, Stewart GD, Wells-Cole S, Phipps S, Thomas BG, Tolley DA. Long-term endoscopic management of upper tract urothelial carcinoma: 20-year single-centre experience. BJU Int. 2012 Dec;110(11):1608–17.

22. Patel A, Fuchs GJ. New techniques for the administration of topical adjuvant therapy after endoscopic ablation of upper urinary tract transitional cell carcinoma. J Urol. 1998 Jan;159(1):71–5.

23. Keeley FX Jr, Bagley DH. Adjuvant mitomycin C following endoscopic treatment of upper tract transitional cell carcinoma. J Urol. 1997 Dec;158(6):2074–7.

24. Eastham JA, Huffman JL. Technique of mitomycin C instillation in the treatment of upper urinary tract urothelial tumors. J Urol. 1993 Aug;150(2 Pt 1):324–5.

25. Liang F-X, Bosland MC, Huang H, Romih R, Baptiste S, Deng F-M, et al. Cellular basis of urothelial squamous metaplasia. J Cell Biol. 2005 Dec 5;171(5):835–44.

26. Riedel I, Liang F-X, Deng F-M, Tu L, Kreibich G, Wu X-R, et al. Urothelial umbrella cells of human ureter are heterogeneous with respect to their uroplakin composition: different degrees of urothelial maturity in ureter and bladder? Eur J Cell Biol. 2005 Mar;84(2-3):393–405.